SD 75-SA-0012

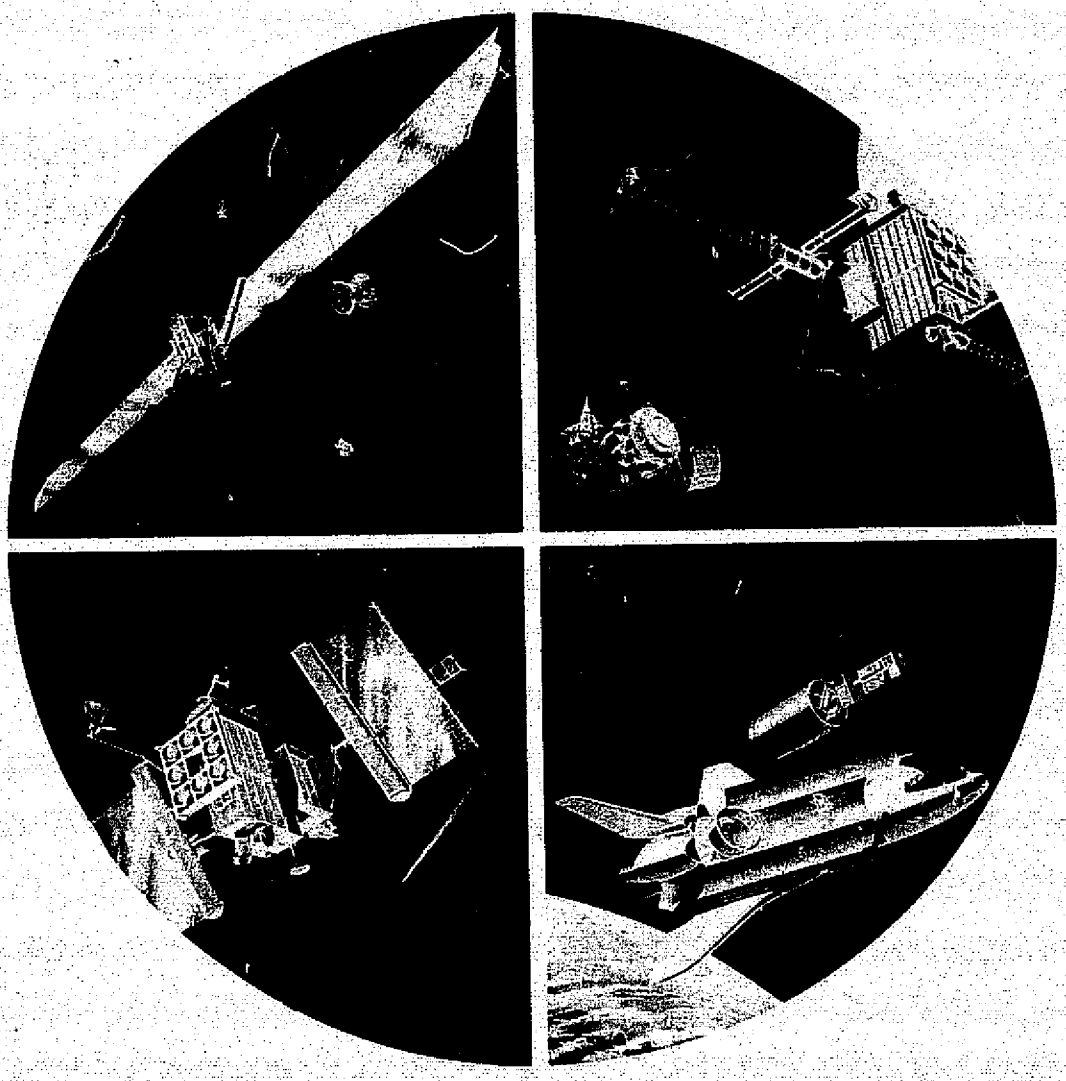

Solar Electric Propulsion System Thermal Analysis

FINAL REPORT

Contract NAS8-30542

February 28, 1975

Space Division
Rockwell International

FOREWORD

This report is submitted by the Space Division of Rockwell International Corporation to the National Aeronautics and Space Administration's George C. Marshall Space Flight Center, Huntsville, Alabama, in accordance with NASA Contract NAS8-30542.

Contract NAS8-30542 authorized an analytical investigation of various thermal control concepts which are applicable to the Solar Electric Propulsion Stage (SEPS). The performance period for this study was December 27, 1973 through February 27, 1975. The results of the study are presented in this report.

Technical coordination of the contract activities was provided by Mr. D. Moss of the Astronautics, Propulsion and Thermodynamics Division at MSFC. The study was conducted by Mr. L. E. Ruttner, SS&A, Flight Technology, Aerothermo Group, as Study Manager. Technical assistance was provided by Mr. J. P. Wright and Mr. R. L. Swanson of the SS&A's, Aerothermo Group.

The author also wishes to acknowledge the contributions of Messrs. T. W. Tysor, Jr., and C. L. Watkins.

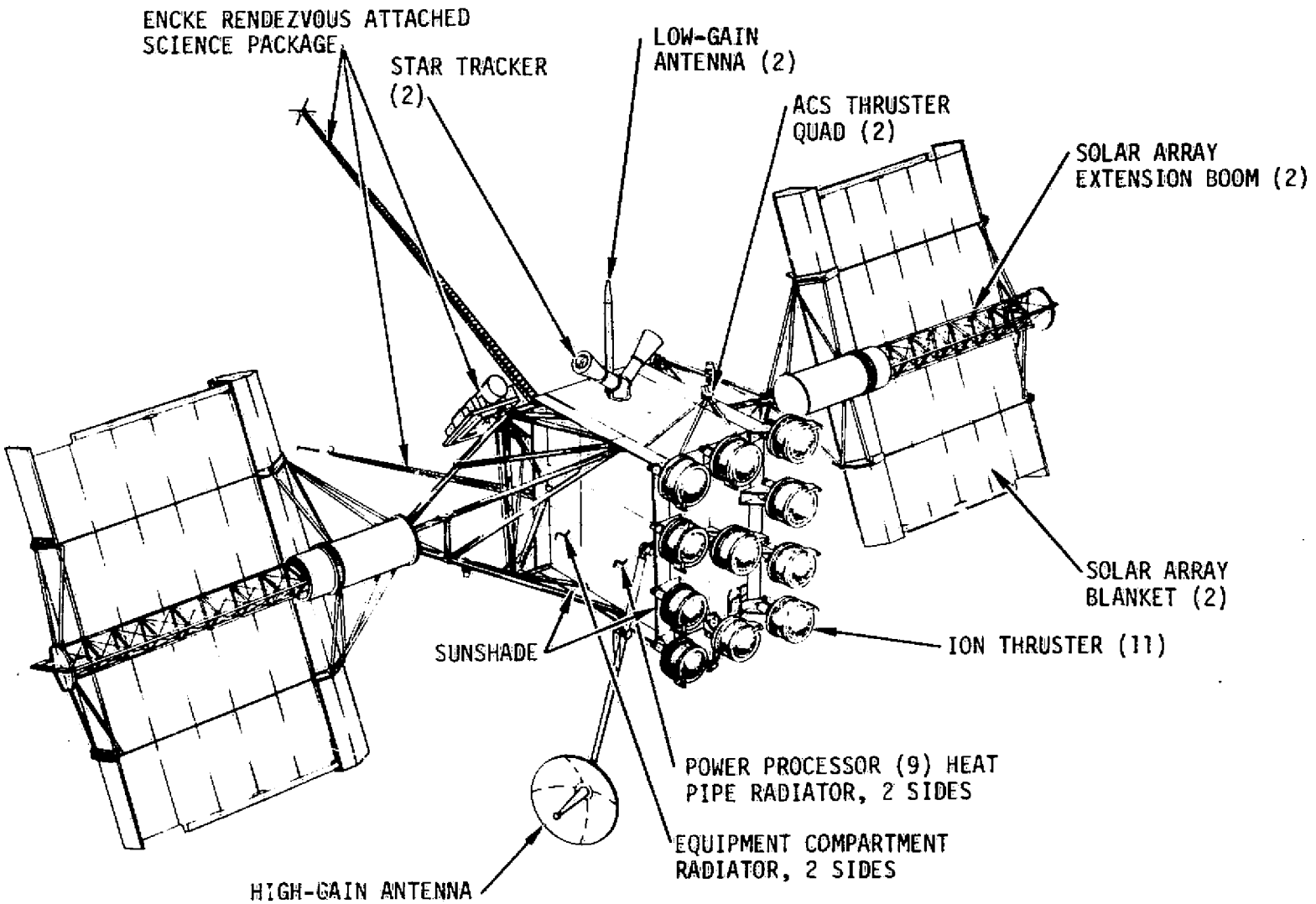

TYPICAL SEPS PLANETARY CONFIGURATION

NOMENCLATURE

A	Area
C	Thermal Conductance
°C	Degree Centigrade
cm	Centimeter
EC	Equipment Compartment
F	Configuration Factor
°F	Degree Fahrenheit
h	Heat Transfer Coefficient
K	Thermal Conductivity
°K	Degree Kelvin
L, ℓ, x	Length
PP	Power Processor
M	Meter
Q, $\dot{Q}$	Heat Load
AU	Astronomical Unit
R	Thermal Resistance
°R	Degree Rankine
S	Solar Constant
T	Temperature
V	Volume
W	Width/Watts
α	Absorptivity
Δ	Differences between Values
ϵ	Emissivity
δ	Density
σ	Stephan-Boltzman Constant
θ	Angle
η	Efficiency

Subscripts

e	Evaporator
eff	Effective
I	Interface
L	Louver
0	Outside, ambient
pp	Power Processor
R	Radiator
s	Solar; Sink
SA	Solar Array
sp	Space
T	Total
V	Vapor
λ	Wave Length

CONTENTS

ILLUSTRATIONS

TABLES

PRECEDING PAGE BLANK NOT FILMED

INTRODUCTION AND SUMMARY

Solar electric propulsion have evolved over the last decade from a promising experimental technique to a practical technology whose elements have reached an advanced state of engineering development. Recent improvements in ion thruster and power processor (PP) efficiency and advances in lightweight, high power solar arrays have contributed significantly to this evolution.

Solar electric propulsion offers operational advantages of high specific impulse, high propellant density, flexibility in launch and target approach conditions, as well as maneuvering capability for stationkeeping and attitude control during rendezvous or in orbit. The use of solar electric propulsion makes economically possible a spectrum of high-energy missions such as Encke Rendezvous, Close Solar Probe, Saturn Orbiter, Mercury Orbiter and geosynchronous missions.

These varied mission profiles result in a broad spectrum of thermal control system requirements. Factors such as vehicle orientation, internal heat loads, and solar distance must be considered. The temperatures of various elements and surfaces can be expected to vary throughout a given mission (particularly with passive or semi-passive control). Since electronic component reliability is highly temperature dependent, the thermal control system must provide acceptable average temperatures over each mission as well as control of maximum and minimum temperatures.

This Final Report presents the results of the work performed under contract NAS8-30542 entitled "Solar Electric Propulsion Stage Thermal Analysis". The purpose of the study was a) evaluate different thermal control elements applicable to the SEPS; b) develop and analyze thermal control concepts, c) evaluate and make recommendations(s) of the concept best applicable to SEPS and d) identify follow-on efforts, such as development and experimental programs to be performed, for future studies.

In the study special emphasis was placed on the Power Processor and Equipment Compartment thermal control system. Several thermal control concepts were developed and analyzed. After evaluating each concept based on performance, simplicity, reliability and weight, one was selected and recommended to be used on SEPS.

The study is divided into four parts:

1. Evaluation of thermal control elements
2. Definition of boundary conditions
3. Thermal Analysis
4. Evaluation of thermal control concepts and recommendations.

1.0 THERMAL CONTROL TECHNOLOGY

To provide a detailed analysis of thermal control considerations on the Solar Electric Propulsion Stage (SEPS) and to remain within the constraints of Contract NAS8-30542 Exhibit "A", Thermal Subsystem Design Approach, passive and semi-passive thermal control elements applicable to SEPS have been surveyed. These elements are:

- Louvers
- Multilayer Insulation (MLI)
- Thermal Control Coatings
- Conduction Interfaces
- Heat Pipes

Louvers

Thermal control louvers are used to vary the effective radiative properties of a baseplate radiator as a function of local temperature. This is accomplished by regulating the position of radiation barriers relative to the baseplate.

Louvers can be classified by configuration, blade description, and actuator type. Two basic configurations have been flown: 1) a series of small blades which rotate to an open position normal to the baseplate, and 2) a cruciform structure which rotates within a plane to expose a high emissivity section of the baseplate. Blades have ranged from a thin (10 mil) sheet of polished aluminum to hollow structures of formed aluminum foil to frames covered with multilayer insulation.

Bimetallic and fluid actuation systems have been developed and flown to provide temperature-sensitive control of blade position. The former system relies on the differential expansion of a bimetallic spring to rotate either one or two blades as a function of spring temperature. The spring and baseplate are thermally coupled by radiation only. Fluid systems use either bulk liquid thermal expansion or increase in vapor pressure with temperature within a closed volume bellows or piston to provide actuation force. A mechanical linkage

connects the bellows to all blades of the system. Coupling between the baseplate and sensor device is conductive.

Bimetallic actuated louvers have been used for thermal control in many spacecraft. In most applications louvers have been oriented such that they are protected from direct solar radiation by shades, dust covers or spacecraft orientation. The use of a protective device might limit the heat rejection capability. Limiting the spacecraft orientation permits a design exclusive of solar input and high blade temperature problems without affecting the heat rejection capability. Both analytical and experimental results are available for louvers. Figure 1-1 presents a typical louver effective emittance versus blade angle for a louver system. Values range from 0.028 for blades closed to 0.798 for blades open. Figures 1-2 and 1-3 demonstrate effective absorptance vs sun angle for blade angles from 0° to 90° in 10° increments.

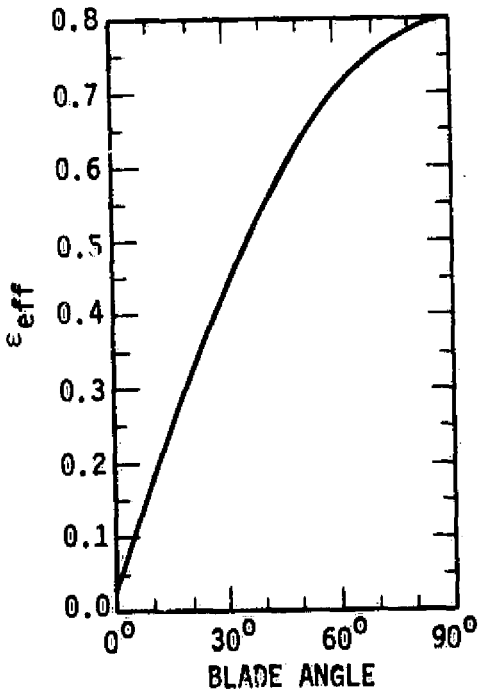

Figure 1-1. Effective Emittance vs Blade Angle

Reference 9

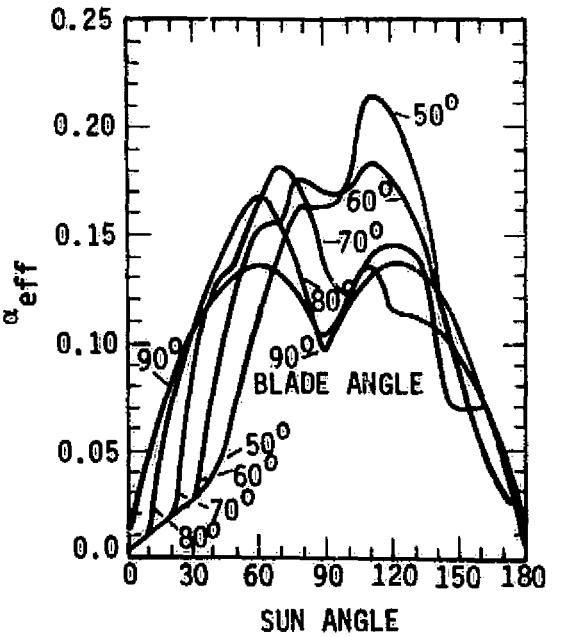

Figure 1-2. Effective Absorptance vs Sun Angle

Reference 9

A comparison of three different louver analyses is shown on Figure 1-4. The heat rejection capability of a louver system with blades fully open and a baseplate temperature of 294°K (21°C), is plotted for: a diffuse blade, specular base system; a diffuse base, specular blade system and the all specular system. It is evident from the figure that the all specular louver system is capable of greater heat rejection in the solar environment. Figures 1-5 to 1-7 present data obtained from the ATS-F & G spacecraft louver tests. Figure 1-8 presents the effect of white paint on blade temperatures, while Figure 1-9 demonstrates the effect of the white paint on louver effective emittance (ε_{eff}). Additional louver performance data are presented in Figure 1-10 thru 1-12 for the Poineer and for an improved louver system.

For the Pioneer louver system, the baseplate was coated with "Cat-a-lac" white paint (ε = .85) and the louver blade facing the baseplate was bare aluminum (ε = .04). For the improved louver system the baseplate was coated with S13-G white paint (ε = .88) while the louver blade was beryllium coated on both sides with vacuum deposited aluminum (ε = .03). Figure 1-11 compares different spacecraft louvers. Figure 1-12 demonstrates that the improved system can accommodate more 16 fold change in thermal load compared to a 5 fold change for the Poineer System .

Additional louver performance data are available in the literature From the data presented here it can be concluded that the majority of spacecraft thermal control requirements can be satisfied by existing flight proven louvers. Furthermore, the all specular louver system is superior to other systems. White paint applied to the blades can be used to control blade temperatures within acceptable limits without significantly affecting system performance. Finally, louver characteristics can be adequately predicted thereby eliminating much of the costly solar simulation testing (if necessary).

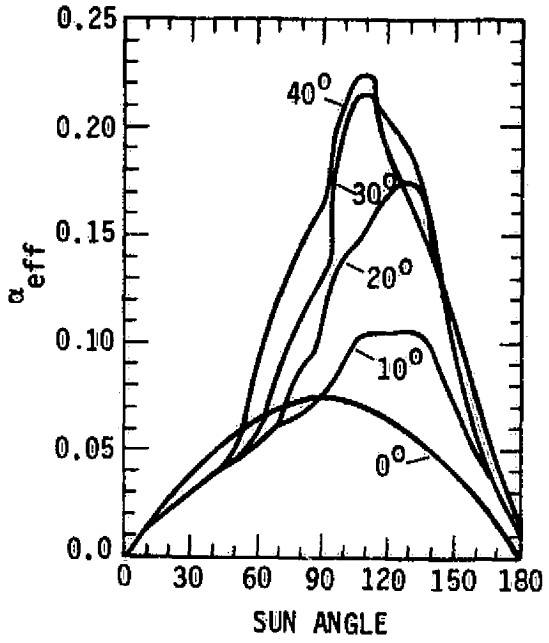

Figure 1-3. Effective Absorptance vs Sun Angle

Reference 9

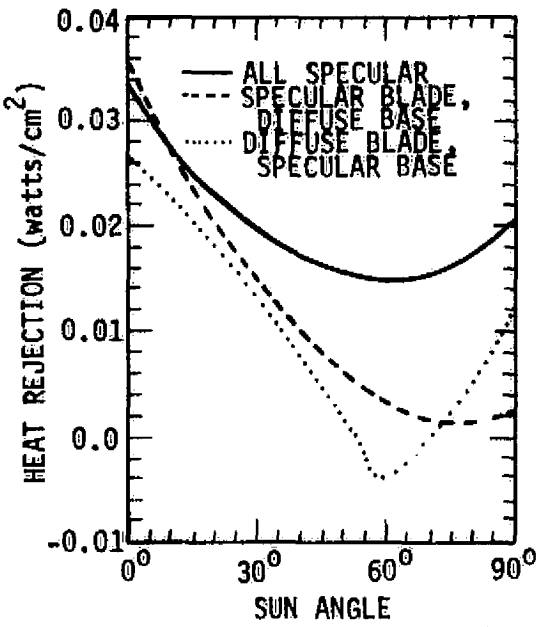

Figure 1-4. Heat Rejection Capability Comparison-Blade Angle = 90° (open Base Temperature = 294°K

Reference 9

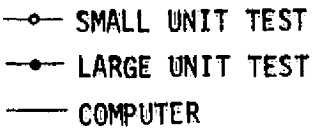

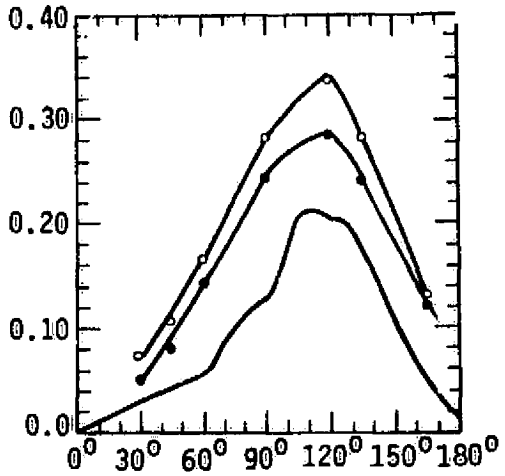

Figure 1-5. Effective Absorptance vs Sun Angle Blade Angle = 30°

Reference 9

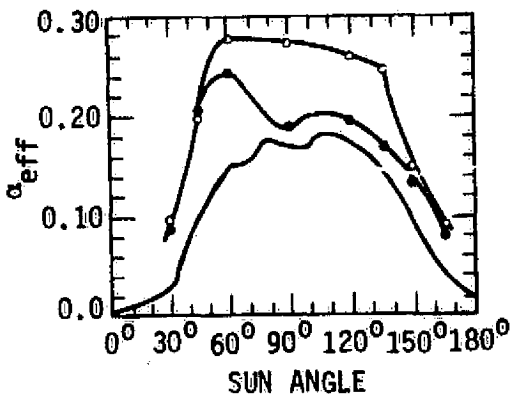

Figure 1-6. Effective Absorptance vs Sun Angle Blade Angle = 60°

Reference 9

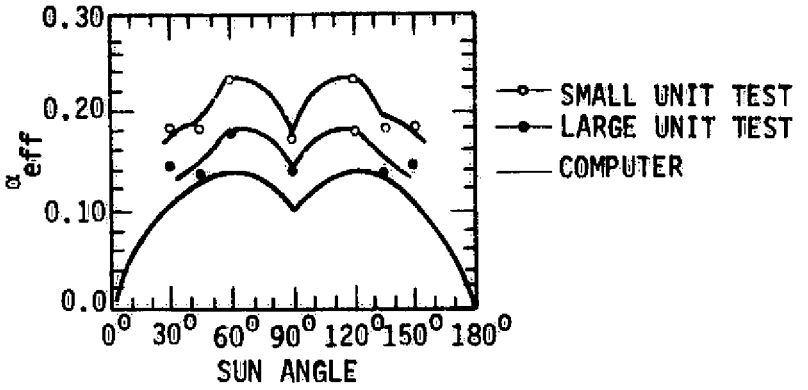

Figure 1-7. Effective Absorptance vs Sun Angle Blade Angle = 90°

Reference 9

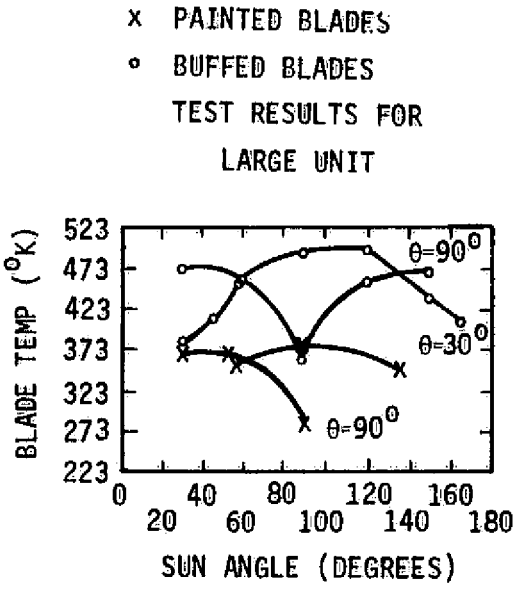

Figure 1-8. Effects of Paint on Blade Temperature

Reference 9

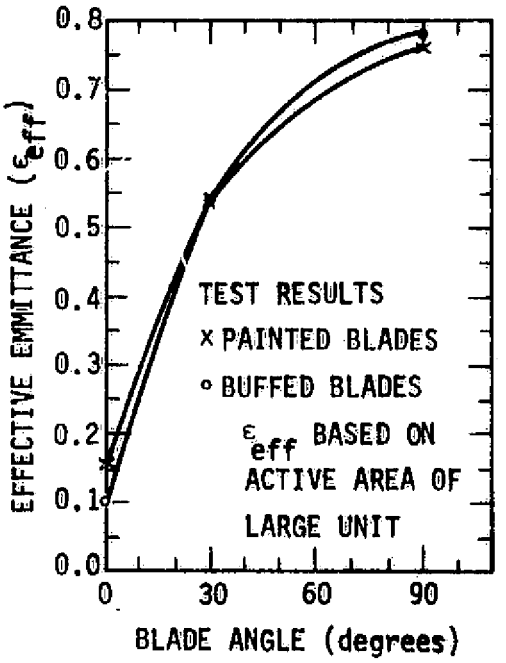

Figure 1-9 Effects of Paint on Effective Emittance

Reference 9

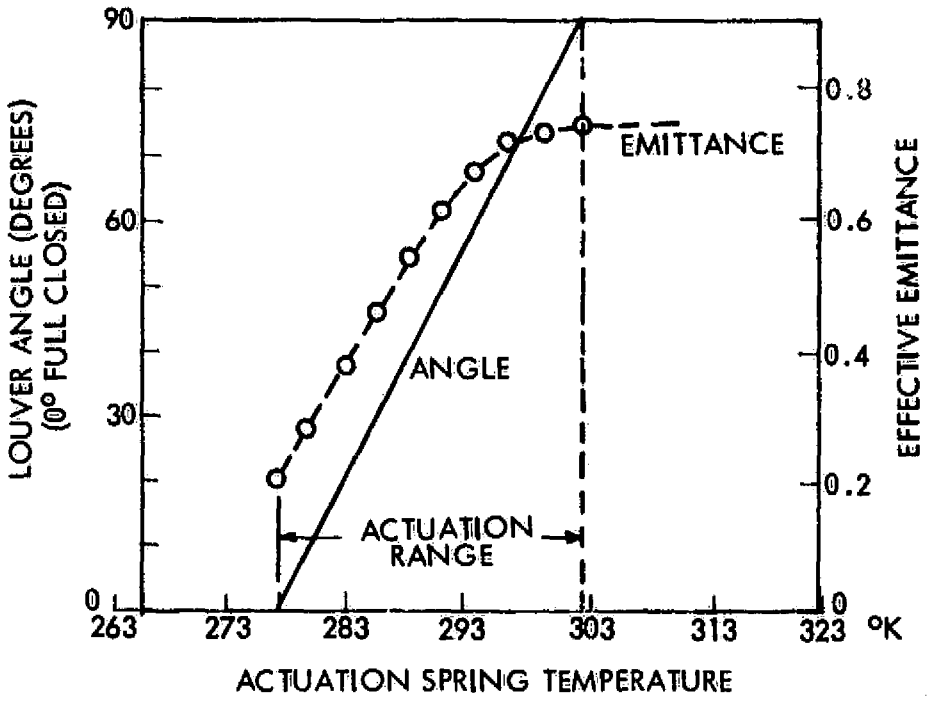

Figure 1-10. Angular Response of Pioneer Louvers to Temperature

Reference 10

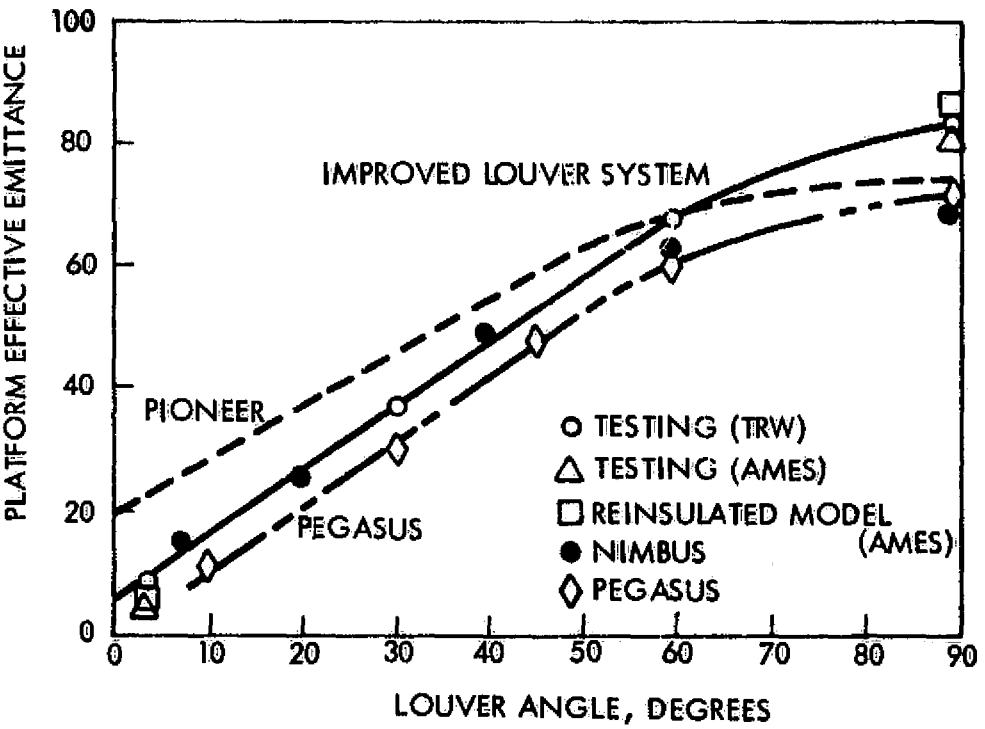

Figure 1-11. Improved Louver System Thermal Performance

Reference 10

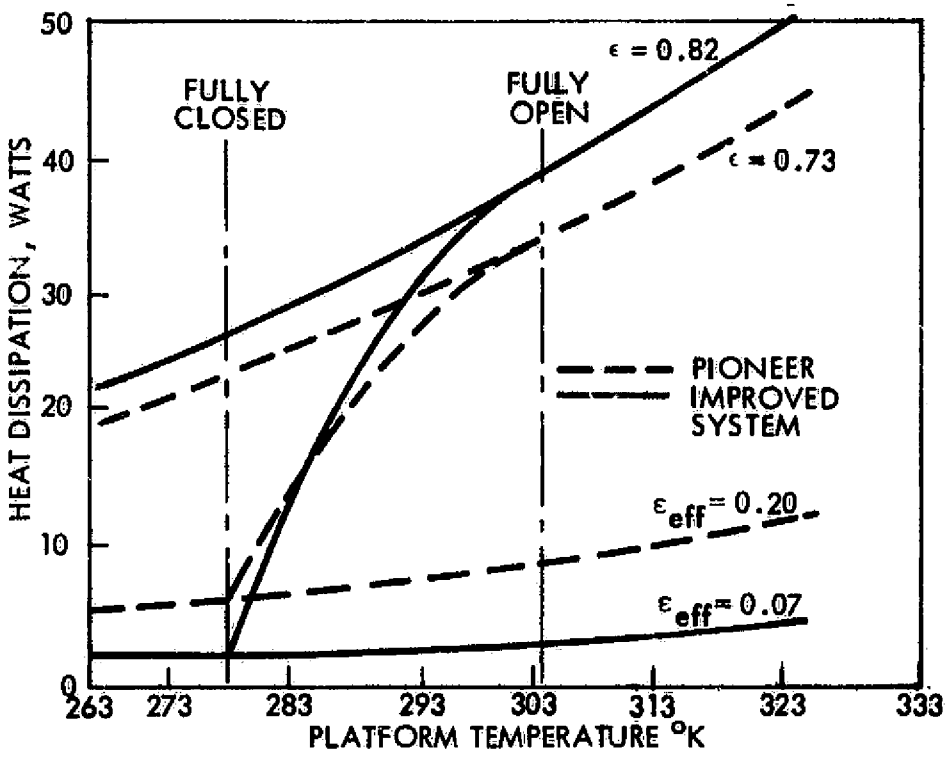

Figure 1-12. Heat Dissipation Versus Platform Temperature

Reference 10

Failure of an entire louver system will occur when all of the blades fail to respond to temperature changes within the control range. This condition is more likely in gang-actuated systems than in systems with individual blade actuation. A bearing failure for one blade of the ganged system will prevent movement of other blades and cause system failure. The single blade failure will generally cause only slightly degraded performance in an individual activation system.

Credible failure points in a louver assembly are: 1) actuator (bellows or bimetallic element), 2) louver springs, 3) linkage bearings or fatigue points, 4) blade shaft bearings or flex pivots.

Assessment of the overall system reliability involves manipulation of four quantities: 1) failure rates, 2) operational time, 3) number of units per system, and 4) number of allowable failures per system. Since items 2, 3 and 4 depend on specific design and analysis, reliability figures are not presented here. Suffice it to say that total reliability figures of .99 or better can be obtained (on paper) for either type of actuation system. Table 1-1 indicates failure rates for louver system components. Table 1-2 describes several louver systems flown.

Component	Failures/10^6 hours
Bellows	.09
Bimetallic elements	.01
Louver springs	.05
Bearings	.02
Flex pivots	.02

Table 1-1. Failure Rates for Louver System Components

TABLE 1-2.

LOUVERS

ACTUATOR TYPE	BLADE DESCRIPTION	FUNCTIONAL TEMP. RANGE (°K)	EMISSIVITY RANGE	FLOWN ON	WEIGHT $\frac{Kg}{M^2}$	DESIGN LIFE (YRS.)	UNIT SIZE M^2	PERFOR-MANCE	COMMENTS
Bellows	Al. form wrapped with 15 layers of al. mylar	292 - 300	.15-.65	Nimbus	.635	.5	.074	Good	Fluid (Freon-114) actuated. No failures in 64 systems flown to date.
Bi-metallic	Polished Alum.	Typically 297 - 308	.06-.61	OAO Pegasus Nimbus	.307	1.0	0.2, 0.21	Satis-factory	Internal systems (radiate to vehicle skin).
Bi-metallic	20 mil polished alum.	(none given)	.08-.72	Mariner II	.36		.12	Satis-factory	
Bi-metallic	10 mil polished alum.	286 - 300	.12-.76	Mariner C	.164		.15		
Bi-metallic	Rect. cross-section of 3 mil al. foil	278 - 303	.20-.73	Pioneer			.37		Annular system. ϵ range can be improved to .07-.82

Reference 19

Multilayer Insulation

A multilayer insulation (MLI) consists of many layers of radiation-reflecting shields separated by low-conductivity spacers. This assembly is placed perpendicular to the flow of heat. Each reflective layer is a thin polymeric film which is metalized on one or both sides enabling the layer to reflect a large percentage of the radiation it receives from a warmer surface. The radiation shields are separated from each other to reduce the heat transferred from shield to shield by solid conduction. Typical separation techniques are to crinkle each layer, to provide continuous spacers, or to provide point contact. The gas in the space between the shields is vented to low pressure to decrease convection and conduction by gas molecules. Table 1-3 summarizes the thermophysical properties of MLI component metals, substrate films, and spacer materials.

MLI systems have been used in a wide variety of applications ranging from cryogenic storage tanks to complex spacecraft. However, most of the recent research efforts have concentrated on improved thermal performance on cryogenic propellant storage tanks. Table 1-4 summarizes the thermophysical properties of different MLI composites. The leading candidates based on thermal performance, weight, and ease-of-manufacturing criteria are DAM/Superfloc, DAM/Silk Net, and SAM/Embossed. These systems use aluminized mylar for the reflective shield and the spacer technique noted. Current research effort is concentrated on development of goldized Kapton MLI systems for Space Shuttle applications. The chief reasons for the effort are elimination of the moisture reaction with aluminum during ground operations and reentry, improved thermal performance with a lower shield emittance, and capability to withstand higher operating temperatures The leading goldized Kapton MLI systems are DGK/Superfloc, DKG/Silk Net, and SKG/Embossed.

The thermal performance of any given MLI design depends upon the following variables:

Table 1-3. Thermophysical Properties of MLI Materials

Material	Density ρ $\left(\frac{g}{cm^3}\right)$	Specific Heat C_p $\left(\frac{cal}{g\ ^oK}\right)$	Thermal Conductivity K $\left(\frac{W}{^oK\ cm}\right)$	Weight/Area* Nominal Thickness $\left(\frac{g}{cm^3}\right)$	Lateral Conduction Kt $\left(\frac{W}{^oC} X\ 10^6\right)$
Aluminum	2.71	0.208	2.02	0.008*	6.06*
Gold	19.32	0.030	3.88	0.58*	11.66*
Mylar	1.38	0.315	0.0015	0.91**	0.95**
Kapton	1.49	0.260	0.00155	0.95**	0.98**
Nylon net	0.44	No Data	No Data	1.37	No Data
Dacron net	0.38	No Data	No Data	0.63	No Data
Silk net	0.44	No Data	No Data	0.68	No Data
Dexiglas	1.99	No Data	No Data	1.56	No Data
Tissuglas	2.24	No Data	No Data	1.66	No Data

*Gold and aluminum thickness = 300 angstroms
**Mylar and Kapton thickness = 0.00025 inch

Table 1-4. Thermophysical Properties of MLI Composites

Material Designation or Tradename	Nominal Layer Density N $\left(\frac{\text{layers}}{\text{cm}}\right)$	Shield Emittance ϵ	Nominal Blanket Density ρ $\left(\frac{\text{g}}{\text{cm}^3}\right)$	Nominal Blanket Effective Thermal Conduction $10^5 \times K_{eff}$ $\left(\frac{\text{W}}{^\circ\text{C}}\right)$	Effective Emittance $10^3 \times \epsilon_{eff}$ 20-Shield Blanket	Nominal Blanket Weight (20 layers) $\left(\frac{\text{g}}{\text{cm}^2}\right)$	Source
SAM-crinkled	26	0.038/.36	0.014	1.37	3.04	0.011	National Research
SAM-embossed (NARSAM)	24	0.045/.36	.022	1.74	2.90	0.019	Rockwell
DAM-Superfloc	12	0.026/.040	.016	1.32	1.35	0.027	Convair
DAM-nylon net	32	0.026	0.054	.9	2.45	0.034	Open[**]
DAM-dacron net	No data available						Open
DAM-silk net	20	0.026	0.045	1.32	2.25	0.046	Open
DAM-Dexigles	24	0.035	0.059	1.48	3.0	0.05	Lockheed
DAM-Tissuglas	40	0.035	0.052	.74	2.5	0.026	Lockheed
DAM-foam (GAC-4)	15	0.035	0.04	3.16	4.1	0.054	Goodyear
DAM-foam (GAC-9)	22	0.035	.027	1.58	2.95	0.024	Goodyear
DGM-dacron net	26	0.029	No data				Open
DGM-silk net	20	0.022	0.045	0.84	1.40	0.022	Open
DGK-dacron net	26	0.027	0.042	0.54	1.20	0.032	Open
DGK-silk net	No data available						Open
DGK-Superfloc	12	0.027	0.016	0.72	0.74	0.027	Convair
DGK-Nomex net	No data available						
SGK-embossed	32	0.037/.47	.03	.65	2.6	0.02	Rockwell

[*]Include 2% open (perforated) area K ≅ 1.424×10^{-5} W/°K when not pen ated

[**]Open implies more than one source

DAM - Double Aluminized Mylar
SMA - Single Aluminized Mylar
DGK - Double Goldized Kapton
SGK - Single Goldized Kapton
DGM - Double Goldized Mylar

1. Number of layers
2. Surface optical properties
3. Layer density
4. Penetrations and methods of attachment
5. Type and number of joints
6. Type of installation in the vicinity of corners and penetrations
7. Size and number of vent holes

Effective emittance and effective thermal conductivity are two measures of thermal performance commonly used to compare MLI systems. Effective emittance (ε_{eff}) is used in connection with high-temperature applications, such as unmanned spacecraft and science scan platforms where radiation is the primary heat transfer mode. Effective thermal conductivity (K_{eff}) is used in connection with low-temperature calorimeter and cryogenic tank applications where radiation and conduction heat transfer modes are equally important in MLI blanket design and installation. For the SEPS study, ε_{eff} will be the performance measure.

Figure 1-13 shows MLI thermal performance for various applications based upon effective emittance and size of blanket. The performance levels can be separated into three categories according to density of discontinuities:

1. Calorimeters and cryogenic tanks have few discontinuities, and near ideal performance is achievable.
2. Most unmanned spacecft and propulsion systems have a moderate number of discontinuities.
3. Science scan platform and highly complex spacecraft have many discontinuities.

The vertical bars are uncertainty bands believed to be representative of more recent cases. The results of Figure 1-13 show that control of discontinuity heat transfer is a crucial spacecraft design problem.

The Rockwell Space Division has recent experience building MLI systems and installing them on cryogenic tanks, unmanned spacecraft, and complex science scan platforms.

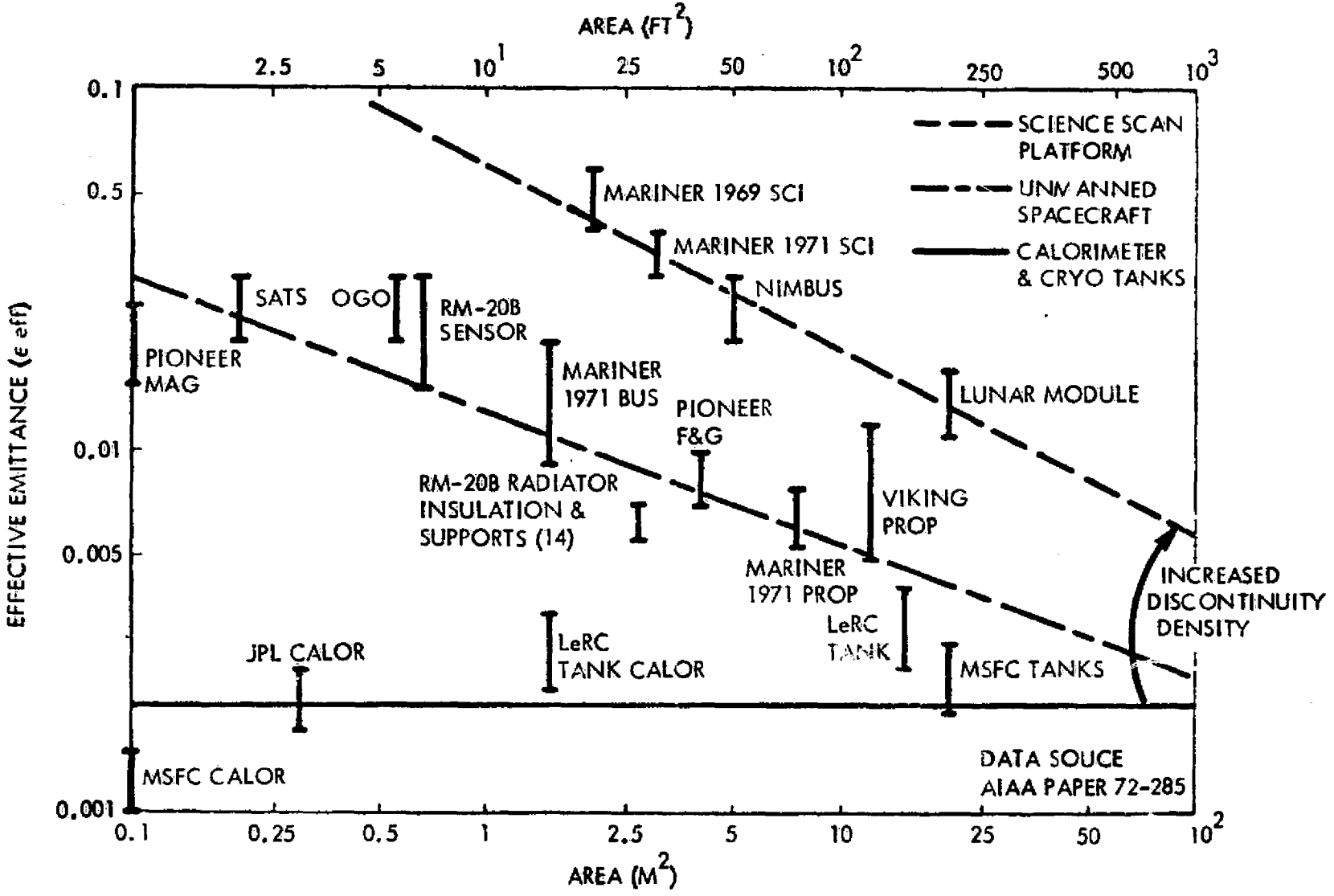

Figure 1-13. Historical Data for MLI Performance Vs Area

The type of multi-layer insulation predominantly used at Rockwell on sensors and spacecraft is NARSAM, a 1/4-mil-thick mylar, aluminized on one side and embossed with a pattern which gives it a natural lay of 60 layers per inch. This proprietary MLI (Rockwell Material Specification MB0135-034) has specific advantages when applied to surfaces with complex contours, multiple discontinuities, or requiring deployable or compressible insulation. The use of an embossment pattern rather than a spacer gives the insulation a high degree of compressibility with a low spring rate. The return to original height is 100 percent within the range of loads normally experienced. This allows the insulation to be folded and stowed in a compressed condition and deployed in orbit. The lack of spacers also reduces fabrication time and allows more complex configurations with smaller pieces. The single aluminized surface reduces the insulation conductivity parallel to the layers by one-half, compared to the double aluminized surface, and therefore reduces the thermal effect of discontinuities and support posts. The embossing pattern also allows the individual sheets to stretch a small amount to allow for thermal contraction without ripping at support post holes. The embossing pattern is a random pattern of small peaks which will not allow nesting of sheets, and provides a repeatable stack height. The insulation remains flexible and the embossment effective from liquid helium temperatures to 344°K.

A low temperature heat rejection radiator for the RM-20B infrared sensing system was satisfactorily isolated from the ambient temperature spacecraft using the NARSAM MLI. Thermal vacuum tests documented in Reference 18 showed effective emittance values ranging from 0.0055 to 0.007. This range of values characterizes a complete thermal isolation system including insulation, shields and radiator structural supports. As can be seen on Figure 1-13, the thermal performance achieved for the RM-20B radiator insulation system is somewhat superior to other systems representative of its size and discontinuity category. The performance comparison is conservative in that the area of the shields was also including for purposes of locating the RM-20B radiator data on Figure 1-13. Based on the actual

radiator area of 1.3 square meters, it can be seen that the RM-20B radiator insulation emittance is significantly lower than comparable systems.

In another application a large cryogenic tank was insulated with NARSAM for NASA-MSFC. The predicted ε_{eff} is 0.005 for this installation and includes the effects of vent holes, attach posts, joints, a plumbing penetration, and instrument leads. Full-scale performance testing has not been completed. However, subscale testing does provide confidence that acceptable performance levels can be achieved.

All MLI systems require penetrations and other discontinuities in an actual cryogenic tank or spacecraft installation. The Space Division experience in the above applications suggests the following techniques and procedures for reducing discontinuity heat transfer.

All MLI systems require some method of attachment of the blanket to the spacecraft. A common method is to use posts. This procedure requires that oversize holes be cut into the blanket to accommodate the post. The Space Division uses low-conductivity, high-strength hollow fiberglass posts to minimize thermal performance degradation of the MLI blanket. Additionally, radiation in the annular space of the oversize hole is reduced by interposing MLI washers every five layers.

Large MLI blankets installed on plane and cylindrical surfaces and smaller blankets installed on double-curved surfaces, such as a sphere, require the joining of two blanket sections together for an efficient design. Numerous joint configurations have been investigated. Thermally, overlap joints are most efficient. Figure 1-14 shows MLI thermal performance for two recent Mariner flight blankets tested on a calorimeter based upon effective emittance and length of blanket overlap. The longer the overlap, the lower is ε_{eff}. Figure 1-14 also shows the same thermal performance based upon local percentage increase in ε_{eff}. Based upon this result, Space Division MLI blankets are designed to employ a 20-centimeter (eight-inch) minimum overlap for thermal efficiency. In addition, the Space Division builds MLI blankets in five-layer modules.

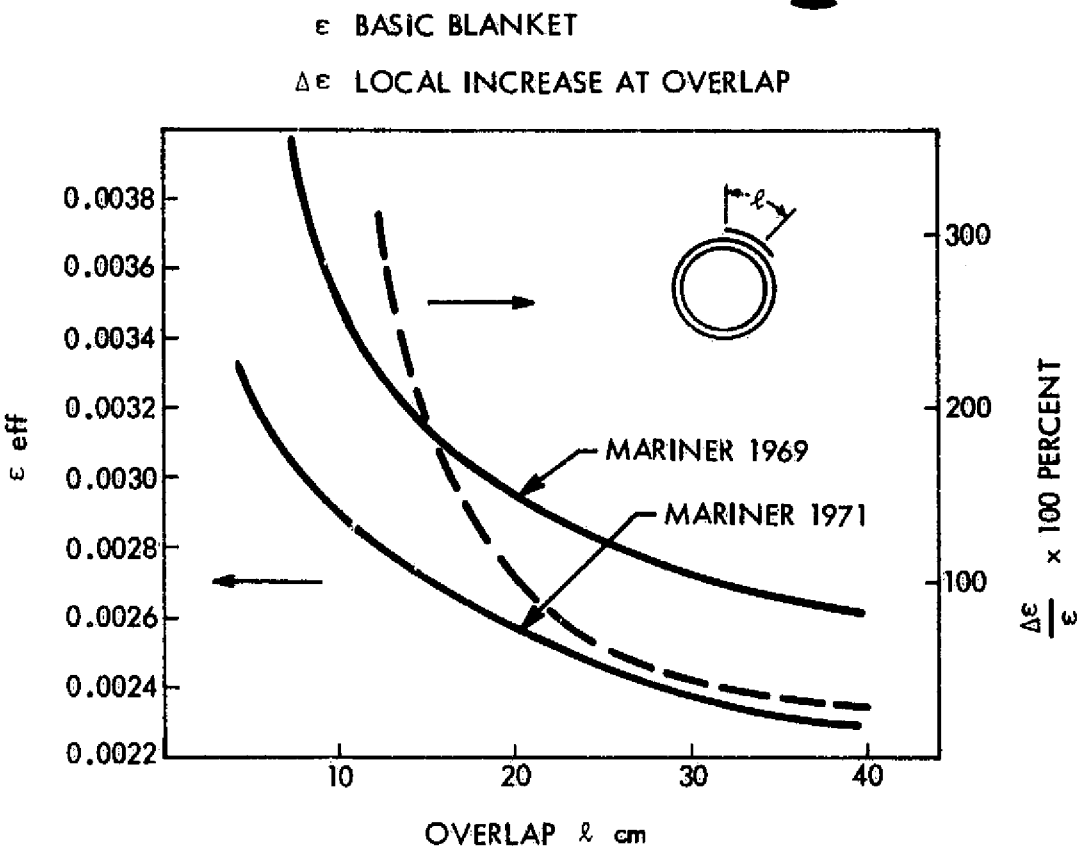

Figure 1-14. MLI Performance Versus Overlap

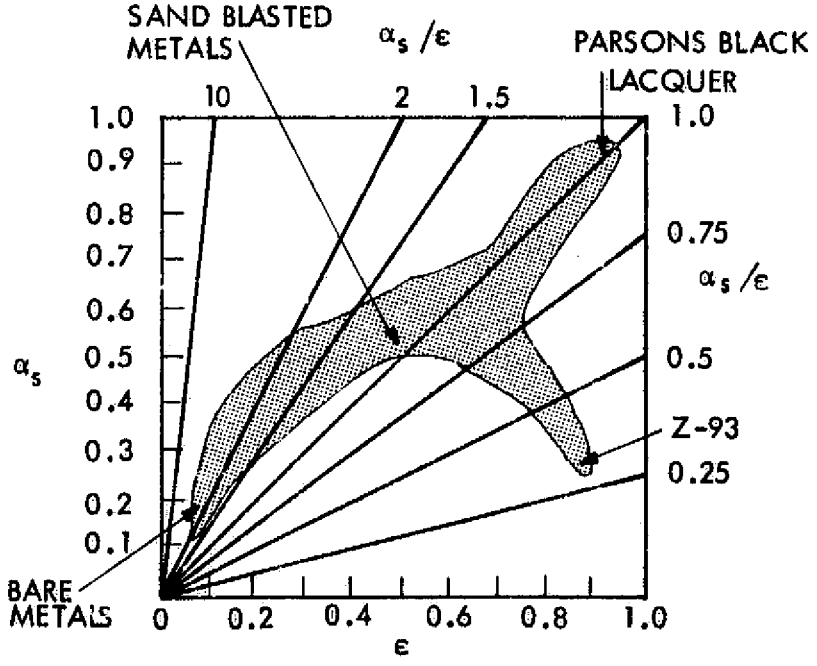

Figure 1-15. Available Range of Optical Properties

This procedure allows for joints to be staggered, which further increases MLI blanket thermal performance.

Broadside venting is needed during the launch-ascent phase of a space mission to evacuate the MLI blanket rapidly and to reduce potential blanket damage due to pressure stresses at MLI attach points. Typically, each layer is perforated with small vent holes, and the vent area is one-to-two-percent of total blanket area. This practice degrades thermal performance since radiation is transmitted directly through the vent holes, which are thermally black ($\varepsilon = 1.0$). Space Division tests and analyses indicate that the apparent emittance of a single metalized layer and the radiation component of effective emittance are increased proportionately by the vent area. For example, if the apparent emittance is 0.045 for an unperforated shield, then the apparent emittance of a perforated shield with two-percent vent holes will be approximately 0.065 (an increase of 40 percent in MLI blanket effective emittance compared to a nonperforated blanket). Some additional venting studies and tests are needed to optimize blanket design.

Thermal Control Coatings

Thermal control coatings are coatings and surface finishes with desired values of solar absorptance (α_s) and emittance (ε). They are used for spacecraft thermal control by selective absorption and emission of visible and infrared radiation. The classification of the various optical surfaces and the process by which they can be obtained are given in Table 1-5. Of these, solar reflection is the most important for spacecraft application since it is desirable to minimize the effects of the variable solar environment on temperature surfaces. Table 1-6 indicates maximum temperatures for different coating groups.

A wide range of optical properties is currently attainable. For example, solar reflectors have been developed with α_s/ε as low as 0.09, while solar absorbers have been developed with α_s/ε exceeding 10. However, only a limited selection of these coatings (represented by the shaded area in Figure 1-15) are stable under long-term exposure to ultraviolet radiation, prelaunch handling, and ascent heating and

Table 1-5. Methods of Obtaining Various Types of Surfaces

Optical Type of Surface	α_s	ϵ_T	Polished Metals	As-Received Metals	Sandblasted Metals	Vacuum Metallics	Vacuum Nonmetallics	Conversion Coatings	Plated Coatings	Metallic Paints	Nonmetallic Paints	Vitreous Enamel	Inorganic Bonded	Transparent Conversion	Transparent Nonpigmented Paints
Total absorber	0.9	0.9	--	--	--	--	--	X	--	--	X	X	X	X	X
Median IR absorber	0.9	0.5	--	--	--	--	X	X	--	--	--	--	--	X	X
Solar absorber	0.9	0.1	--	--	--	X	X	--	X	--	--	--	--	--	--
Median solar absorber	0.5	0.9	--	--	--	--	--	X	--	--	X	X	X	X	X
Medium	0.5	0.5	--	--	X	--	X	X	--	X	--	--	X	X	X
Median solar absorber	0.5	0.1	X	X	X	X	X	--	X	--	--	--	--	--	--
Solar reflector	0.1	0.9	--	--	--	--	--	X	--	--	X	X	X	X	X
Median IR reflector	0.1	0.5	--	--	--	--	X	X	--	X	--	--	--	X	X
Total reflector	0.1	0.1	X	X	--	X	X	--	--	--	--	--	--	--	--

TABLE 1-6

MAXIMUM TEMPERATURES FOR COATING GROUPS

Description	T Max., °K
Bare Metal	N/A
Paint	
Urethane Vehicle	340
Epoxy Vehicle	420
Silicone-alkyd Vehicle	620
Silicone Vehicle	700
Chemical Surface Finish	
Alodine (Conversion coating)	480
Anodize	810
Flame, Plasma Spray	810
Tapes	
Aluminized mylar	370
Series Emittance	700
Optical Solar Reflector (OSR)	590

are applicable to large areas. Paints represent the major source of these coatings since paints can easily be applied to large and complex shaped structures with a high degree of reproducibility and reliability. Many white paints degrade in the space environment. However, research and development have produced some inorganic pigments which have been experimentally shown to be relatively stable to ultravoilet radiation.

Two basic conclusions can be drawn from the vast quantity of experimental data:

1. In general, continued exposure of paints to ultravoilet radiation in a vacuum increases α_s until some saturation value is reached. The total increase in α_s is usually dependent on the operating temperature as well as the exposure time.
2. Results from experiments flown in the solar wind show considerably more degradation than those flown in a near-earth environment and those tested in the laboratory.

The most reliable data, to date, appears to be the results of the experiments flown on OSO-II, OSO-III, Pegasus, Lunar Orbiter IV, and Mariner V. These data are summarized in Table 1-7. The most promising coatings are Z-93 and OSR. The effect of ultravoilet radiation on the solar absorptance of other relatively stable coatings are shown in Figure 1-16. Complex surfaces (conventional, radiative coatings applied to a repetitive set of surface projections, such as grooves, fins, ridges, etc.) may be used to produce desired directional radiative properties. One obvious application of complex surfaces is to limit the visibility between two surfaces on the space station, i.e., solar panels and a radiator. Several complex surfaces have been designed and tested. Some of the results of this program are shown in Figure 1-17.

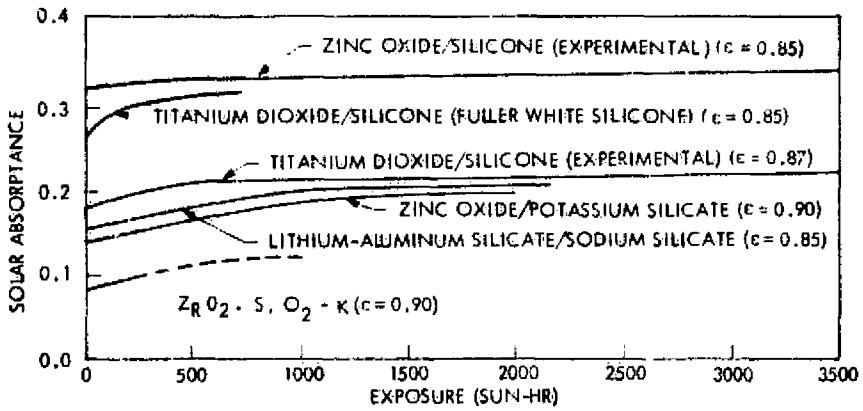

Figure 1-16. Solar Absorptance Versus Ultraviolet Exposure at 300°K

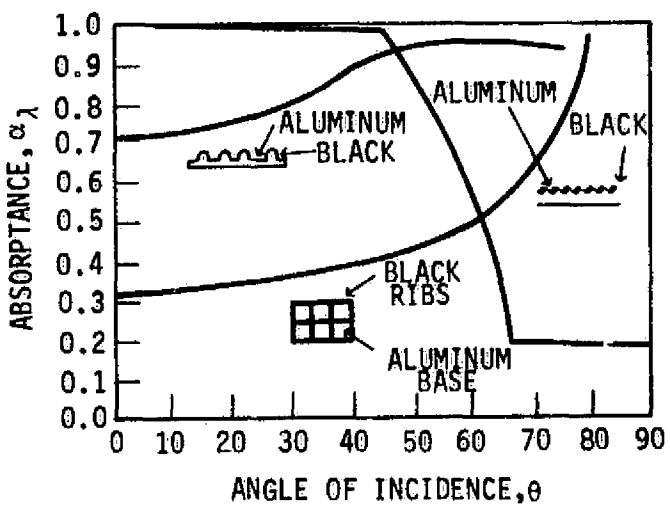

Figure 1-17. Directional Spectral Absorptance Versus Angle of Incidence

Table 1-7. Coating Degradation in Space Environment

COATING	ϵ	α_S*		ESH‡	FINAL α_S** (SOLAR WIND)
		INITIAL	FINAL		
ZINC OXIDE/POTASSIUM SILICATE (Z-93)	0.90	0.17	0.18	7500	0.32
ZINC OXIDE/SILICONE (S-13)	0.81	0.19	0.34	2400	0.40
TREATED ZINC OXIDE/SILICONE (S-13G)	0.88	0.23	0.31	7500	0.34
OPTICAL SOLAR REFLECTOR FUSED SILICA/SILVER	0.76	0.05	0.05	7500	--
COBALT OXIDE	0.07	0.72	0.63	7500	--
METHYL SILICONE	0.81	0.22	0.33	2700	--
PARSON'S BLACK LACQUER	0.96	0.98	0.68	7500	--
V GROOVE	0.91	0.98	0.98	7500	--

*TEMPERATURE OF COATING LESS THAN 0C
**MARINER DATA
‡EQUIVALENT SUN HOURS

Reference 2

Conduction Interfaces

Interface conductance refers to the conduction of heat between two surfaces held in physical contact by mechanical means. The surface interface consists of a finite discontinuity between the two surfaces with a few points of material contact. The modes of heat transfer between the two surfaces to be considered are (1), solid conduction through the true contact area, (2) gaseous, molecular, or other conduction through the interstitial fluid of filler, and (3) thermal radiation.

The four major variables affecting contact resistance are surface material, surface finish, interface pressure, and the presence or absence of some liquid or gas in the interface. The optimum interface model is one where no discontinuity of material exists at the interface. Up to some practical limit, this is approached by increasing the interface pressure, which tends to flatten the material high points and reduce the interface thermal resistance (i.e., it tends to increase conductance). Another technique for reducing interface resistance is to add an interstitial material at the interface. This material should have the characteristic of flowing into the interface surface hills and valleys, replacing the air or vacuum in the voids. The use of an interface material requires that this material be thin enough that the decrease in interface contact resistance offsets the rise in resistance through the interface material. Typical filler materials used in installing electronic equipment and components are silicone greases, thin silicone rubbers, and soft metals such as indium. Preliminary design thermal contact resistance guidelines are shown in Table 1-8. Figure 1-18 demonstrates the conductance of an alumumum-aluminum joint with and without joint filler materials as a function of apparent pressure.

More recent development in investigating conduction interfaces for different materials are summarized in Figures 1-19 and 1-20 demonstrating thermal contact conductance for vacuum - (2×10^{-4} Torr) conditions without and with interface materials.

Table 1-8. Preliminary Design Thermal Contact Resistances

Description	Environmental Pressure	Approximate * Interface Pressure $\frac{10^{-5}\ dyne}{cm^2}$	R_i $\frac{°C\ cm^2}{watt}$
Small stud-mounted components (such as stud-mounted transistors)	Sea level	3447.5	0.32
		344.75	3.22
	High vacuum	3447.5	0.52
		344.75	5.16
Mounting feet of equipment with contact areas of about 6.45 cm^2	Sea level	689.5	3.22
		69	6.45
	High vacuum	689.5	12.9
		69	32.26
Large-surface contact areas	Sea level	69	6.45
		6.9	19.36
	High vacuum	69	45.16
		6.9	129.0

* Pressure varies over footprint depending on bolt pattern, etc.

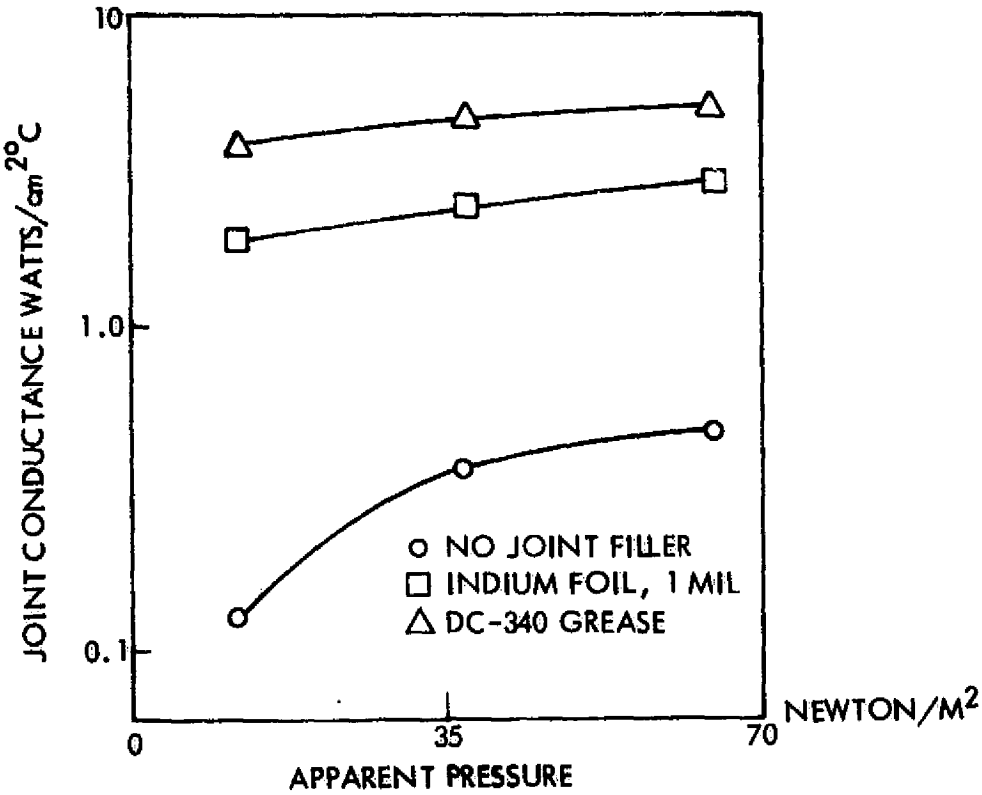

Figure 1-18. Aluminum Joint Conductance Versus Pressure

Reference 12

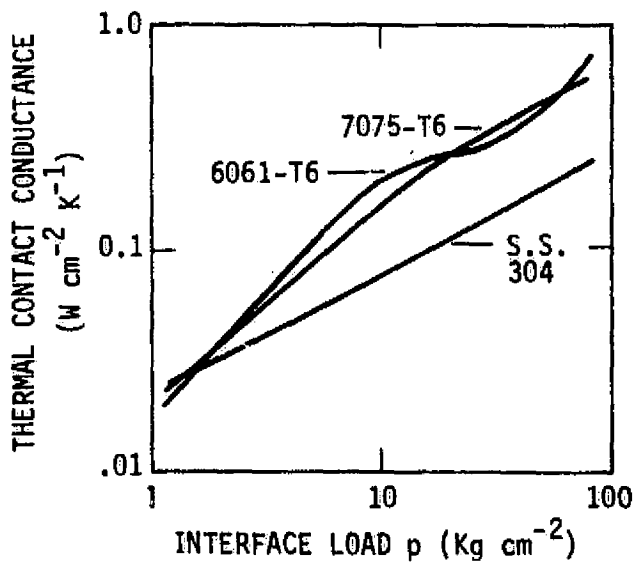

Figure 1-19. Thermal Contact Conductance in Vacuum - No Interface Materials

Reference 13

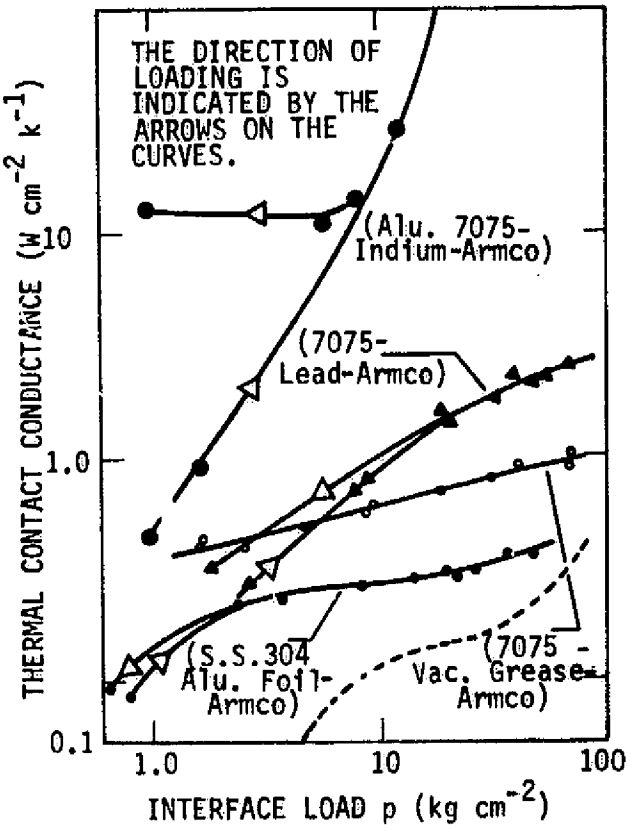

Figure 1-20. Thermal Contact Conductance in Vacuum with Interface Materials

Reference 13

Heat Pipes

The heat pipe is a unique high-flux heat transport device which uses the evaporation, condensation, and surface tension of a working fluid to give it an effective thermal conductance many times that of copper. The major operating characteristics of a heat pipe are (1) near isothermal operation over a length of several feet, (2) thermal transformer operation, where heat is added over a large area at low flux, (3) thermal power flattenting where large cariations in input heat flux causes very little temperature variation, and (4) temperature control, where a constant temperature may be maintained for large variations in heat transfer rate along the heat pipe.

By using various working fluids, heat pipes can be designed to operate from cryogenic temperatures to higher temperatures, limited only by materials technology. Generally, heat pipes are built from circular cross-section tubes, although pipes of practically any shape can be built, including flexible types.

The ability of a heat pipe to transport energy is related to the rate at which heat can be conducted from the heat source to the fluid, the rate at which the fluid can be circulated within the heat pipe, and the rate at which energy can be extracted from the condensing vapor at the heat sink. The limiting factor affecting the rate at which the fluid and vapor can be circulated are the capillary pumping limit (wicking limit), the sonic limit, and the entrainment limit.

In a zero-gravity field, the maximum heat transport capability of a heat pipe can be expressed in terms of its length and a liquid transport factor which combines the pertinent fluid properties, the capillary pumping radius, the flow permeability of the wick structure, and the wick flow area. Figure 1-21 shows this factor for several fluids as a function of temperature of the heat pipe. The wicking factor is frequently a useful parameter. It relates the capillary pumping power of the wick (which is a function of the effective diameter of the pores) versus the frictional flow area afforded by the wick structure. A number of wick designs have been developed that theoretically have large pumping capability while maintaining a low flow resistance. For example, such designs can employ composite wick structures such as those shown on Figure 1-22.

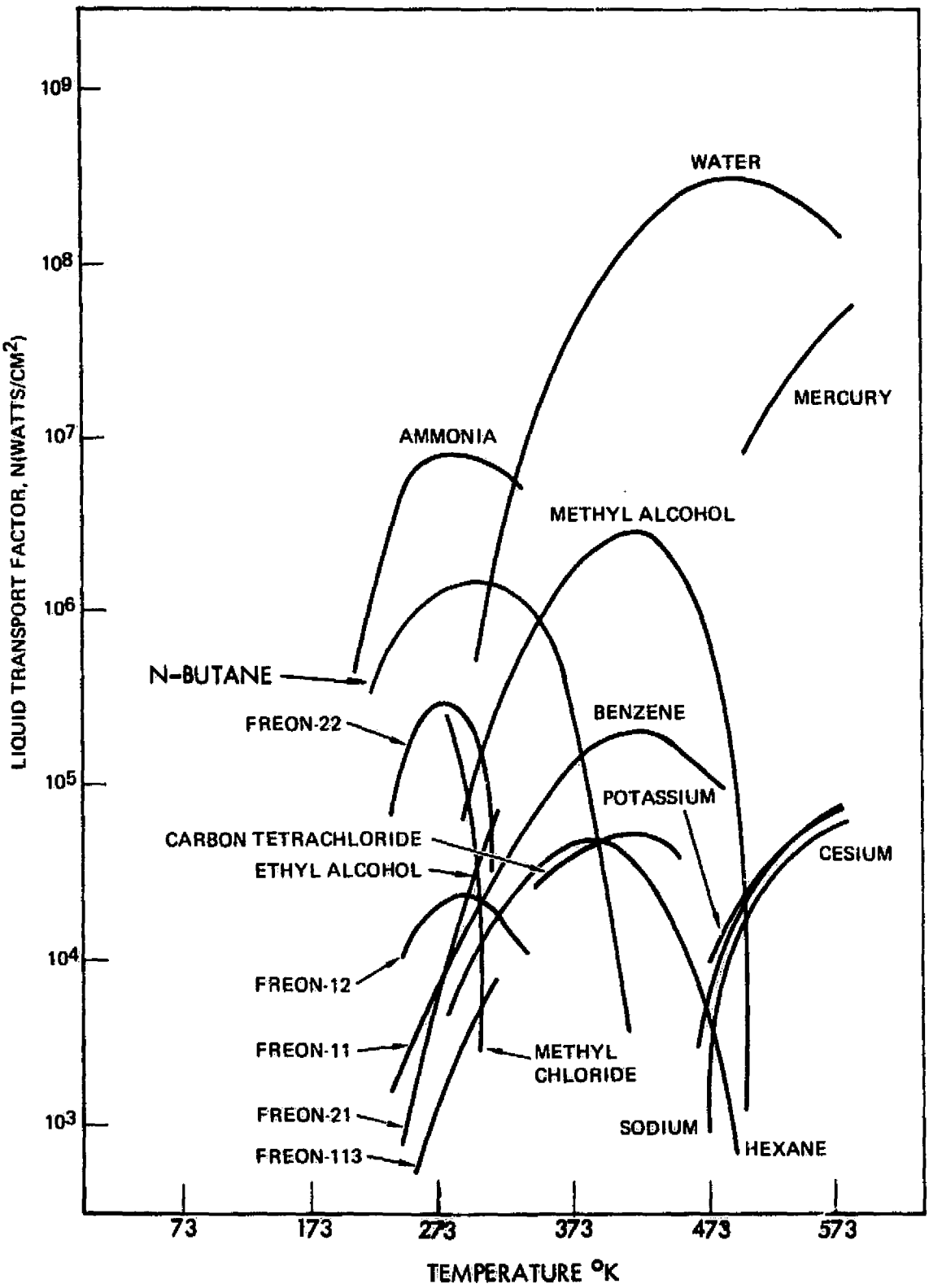

Figure 1-21. Liquid Transport Factor for Various Fluids

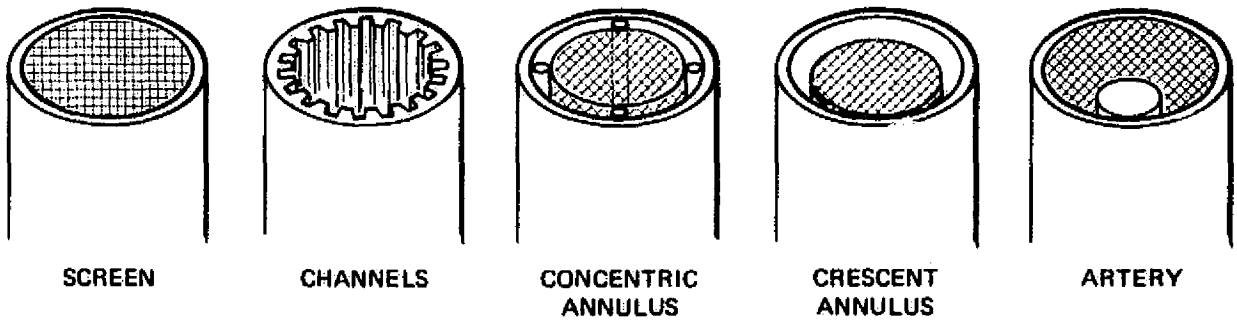

Figure 1-22. Heat Pipe Wick Designs

Besides the standard heat pipe, the variable conductance heat pipe (VCHP) is widely used. This kind of pipe maintains a nearly constant internal temperature level when fluctuations of the heat load into the pipe occur. To accomplish this, a non-condensing gas is added to the working fluid. The principle of non-condensible gas control is the formation of a gas plug at the condenser end of the pipe which acts as a diffusion barrier to the flowing vapor. The gas plug tends to shut-off that portion of the condenser which it fills, leading to an axial temperature gradient along the heat pipe as shown on Figure 1-23. By varying the length of this gas plug, one varies the active condenser area and, hence, the heat rejection properties of the system.

A feature which makes non-condensible gas control particularly attractive is that the basic heat pipe (Figure 1-23) accomplishes this variation in the condenser area passively. By introducing a fixed mass of gas into the system shown, it occupies a certain portion of the condenser section, depending on the operating temperature of the pipe's active region and the environmental conditions. If the operating temperature increases, the vapor pressure of the working fluid increases. This compresses the non-condensible gas into a smaller volume, thus providing a greater active condenser area. On the other hand, if the operating temperature falls, the vapor pressure of the working fluid falls and the fixed mass of gas expands to a greater volume, thus blocking a larger portion of the condenser. The net effect is to provide a passively controlled variable condenser area which increases or decreases with the heat pipe temperature. As a

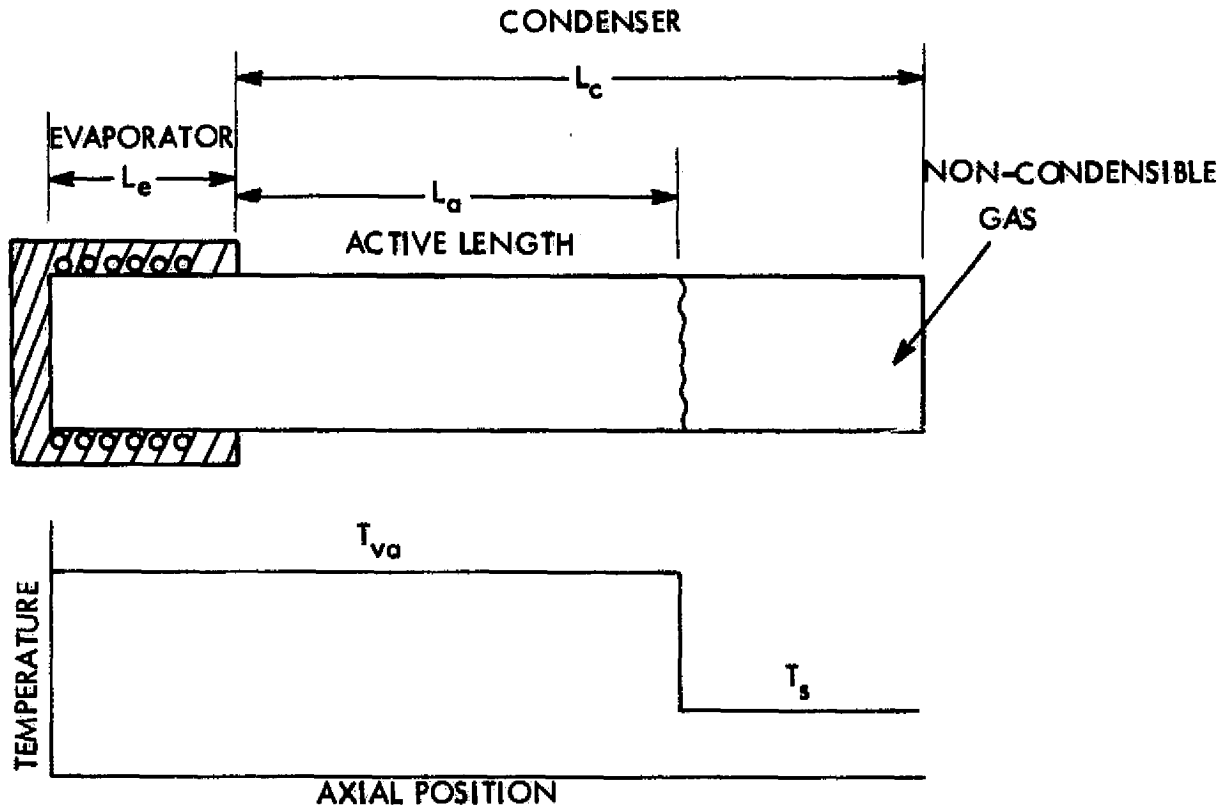

Figure 1-23. Definition of an Analytical Model for a Gas Loaded Heat Pipe

consequence, this reduces the temperature response of the active zone to variations in the heat input rate on environmental (sink) conditions.

To achieve high control sensitivity, the active condenser length L_a (Figure 1-23) should be a very strong function of the operating temperature. This in turn requires that the active condenser length be a strong function of the system total pressure. Since motion of the vapor-gas interface reflects compression of the gas inventory, it follows that to minimize the sensitivity of the active condenser length to the total pressure it is desirable to minimize the relative compression of gas necessary to move the interface. A convenient method for accomplishing this is to provide a large gas storage volume outside the range of vapor-gas interface travel; i.e., a gas reservoir. The application of the gas reservoir on a gas controlled heat pipe is shown schematically with temperature distribution on Figure 1-24. The reservoir can be either a) wicked ("cold reservoir") or b) non-wicked ("hot reservoir").

The presence of a wick in a closed system guarantees that saturation conditions exist provided, of course, that the temperature is not above the critical point of the fluid. The saturated vapor in the reservoir is in equilibrium at the reservoir temperature. At maximum condition, the vapor in the reservoir reduces the volume available for gas storage. However, at the minimum condition, the saturated vapor reduces the amount of gas required to fill the reservoir and therefore reduces the storage requirements.

The non-wicked reservoir is thermally coupled to either the heat pipe evaporator or the heat source. The reservoir is non-wicked to avoid saturation conditions at temperatures equal to or greater than the heat pipe vapor temperature. Saturation conditions would, of course, prevent gas storage in the reservoir. Because there is no interconnection between the heat pipe wick and the reservoir, any fluid from the heat pipe that is accumulated in the reservoir, due to spillage and diffusion, must diffuse back out during start up. This can result in relatively long start up times (e.g., several hours) for this type of system.

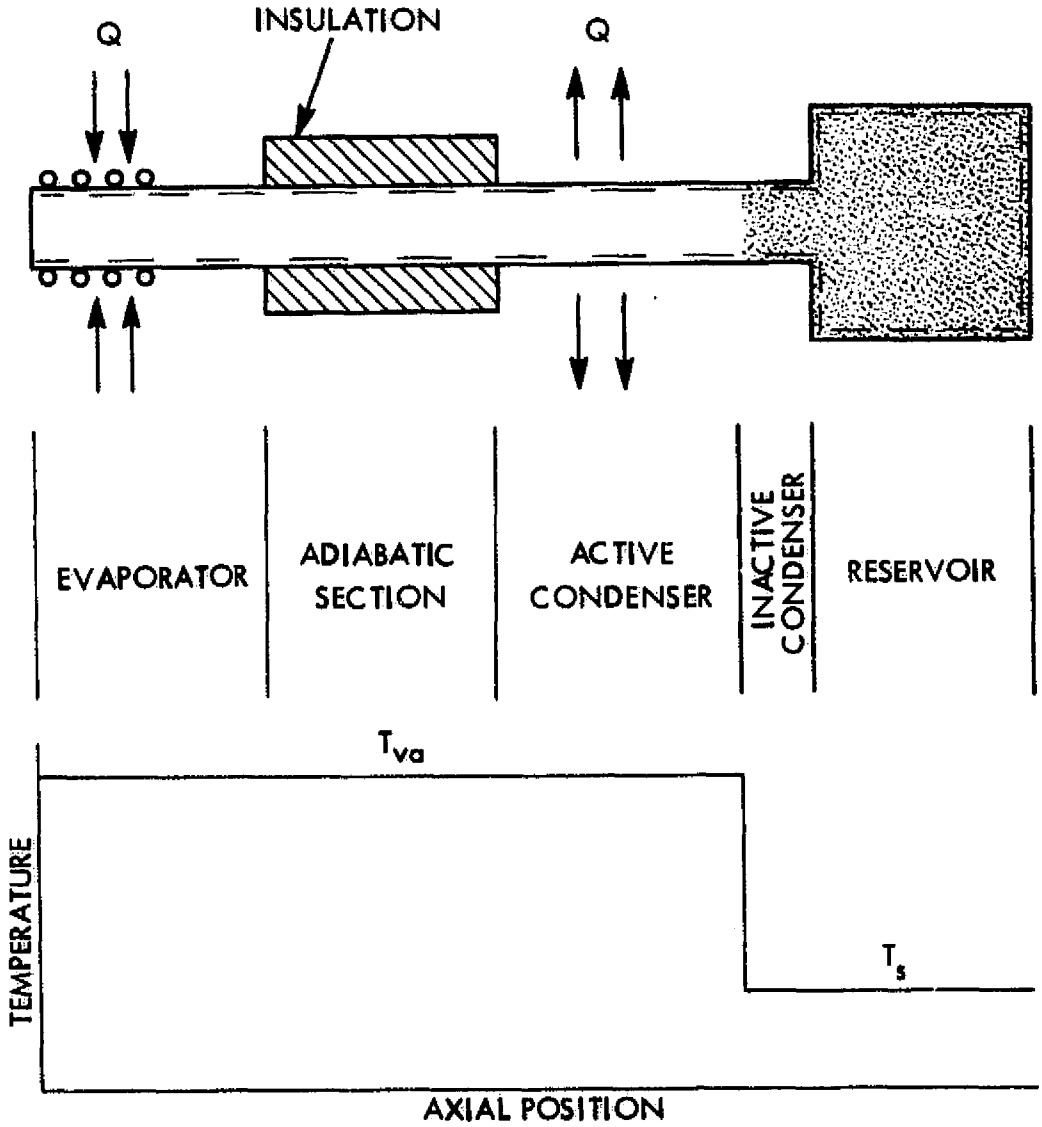

Figure 1-24. Schematic Diagram and Temperature Distribution of a Cold Wicked Reservoir Gas Controlled Heat Pipe

Figures 1-25 thru 1-27 present performance data calculated for standard heat pipes having length of 1.10M with an evaporation and condenser length of 0.1M. These figures give indications of how different wick designs can influence (increase/decrease) heat pipe heat transport. Figure 1-28 and 1-29 present performance curves for variable conductance heat pipes with wicked (cold reservoirs). They can be used for servicing the reservoir where the range of sink temperatures is specified.

For most wick designs the temperature drops through the walls and wicks are dominating and the temperature drop along the vapor is small. In Figures 1-25 thru 1-29 the range for which the temperature drop along the vapor is less than 1% of the total temperature drop is indicated by a solid line; the remaining range is indicated by a dotted line.

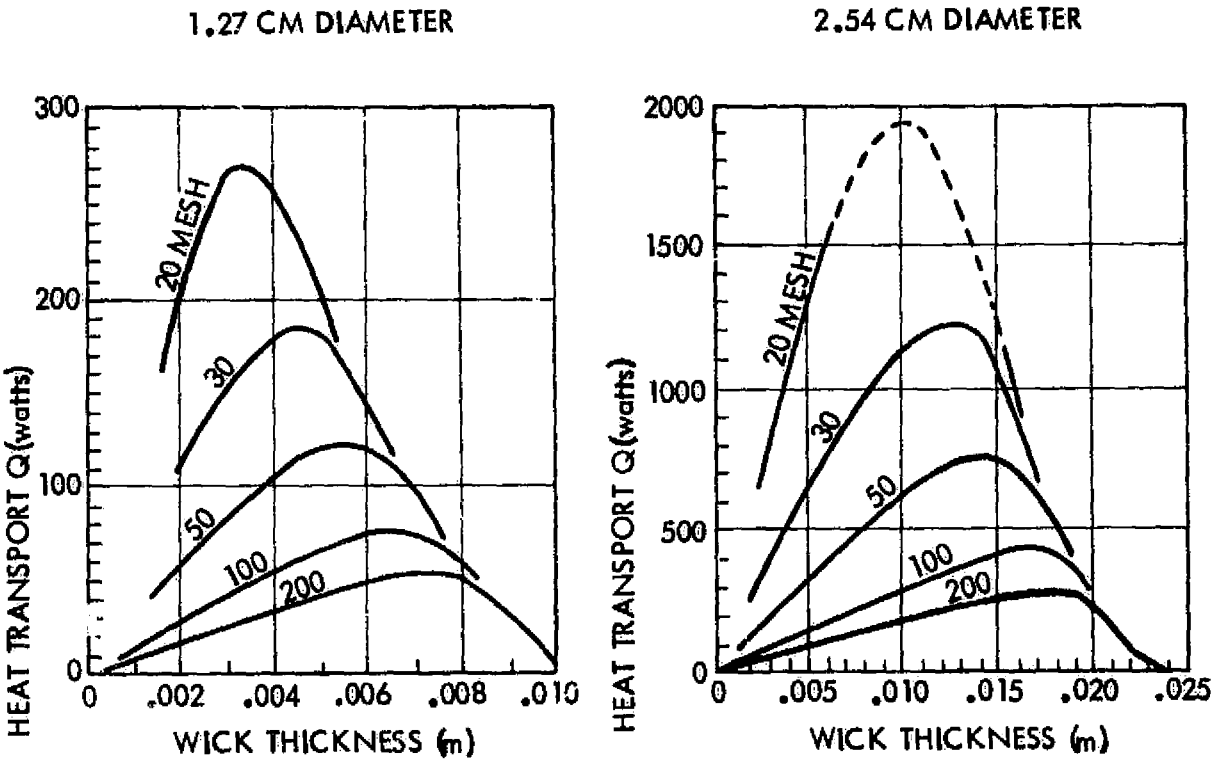

AXIAL HEAT TRANSPORT

TEMPERATURE:	373°K	WORKING FLUID:	WATER
CONTAINER MATERIAL:	COPPER	WICK MATERIAL:	COPPER

Figure 1-25. Porous Slab Wick

Reference 8

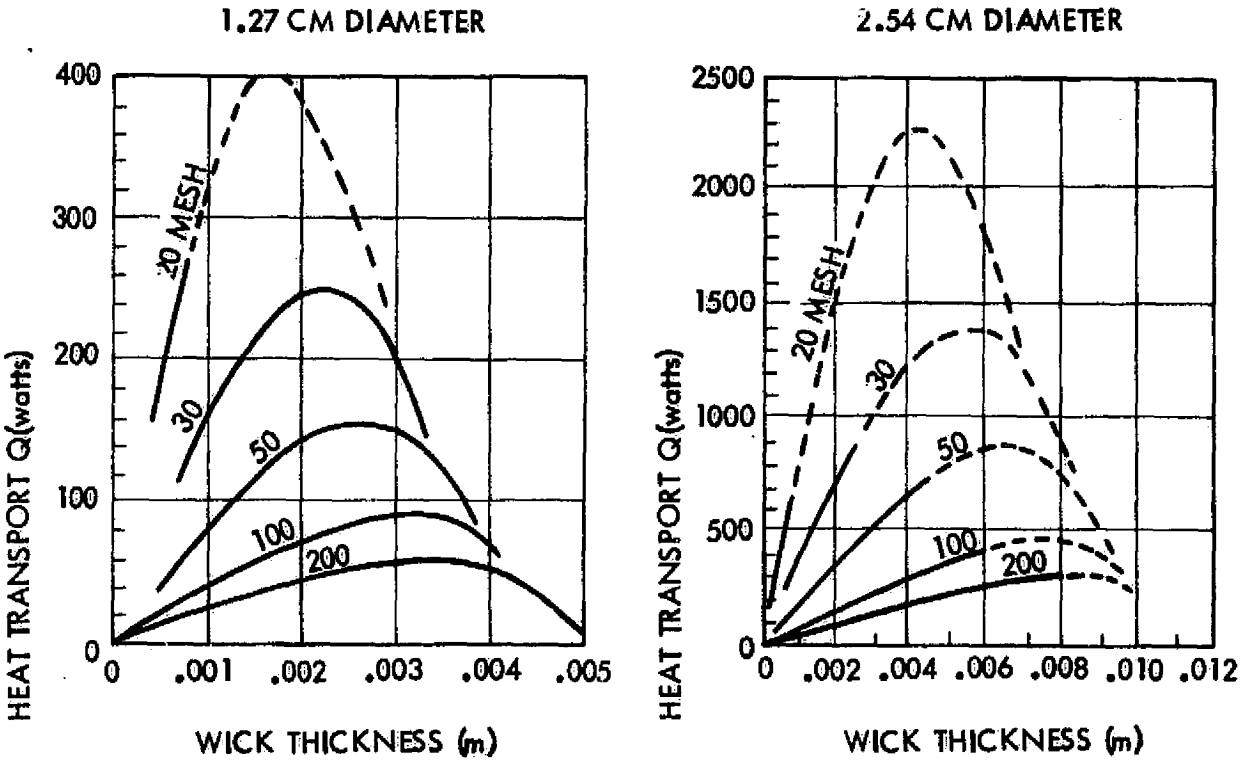

AXIAL HEAT TRANSPORT

TEMPERATURE: 373°K WORKING FLUID: WATER

CONTAINER MATERIAL: COPPER WICK MATERIAL: COPPER

Figure 1-26. Circumferential Screen Wick

Reference 8

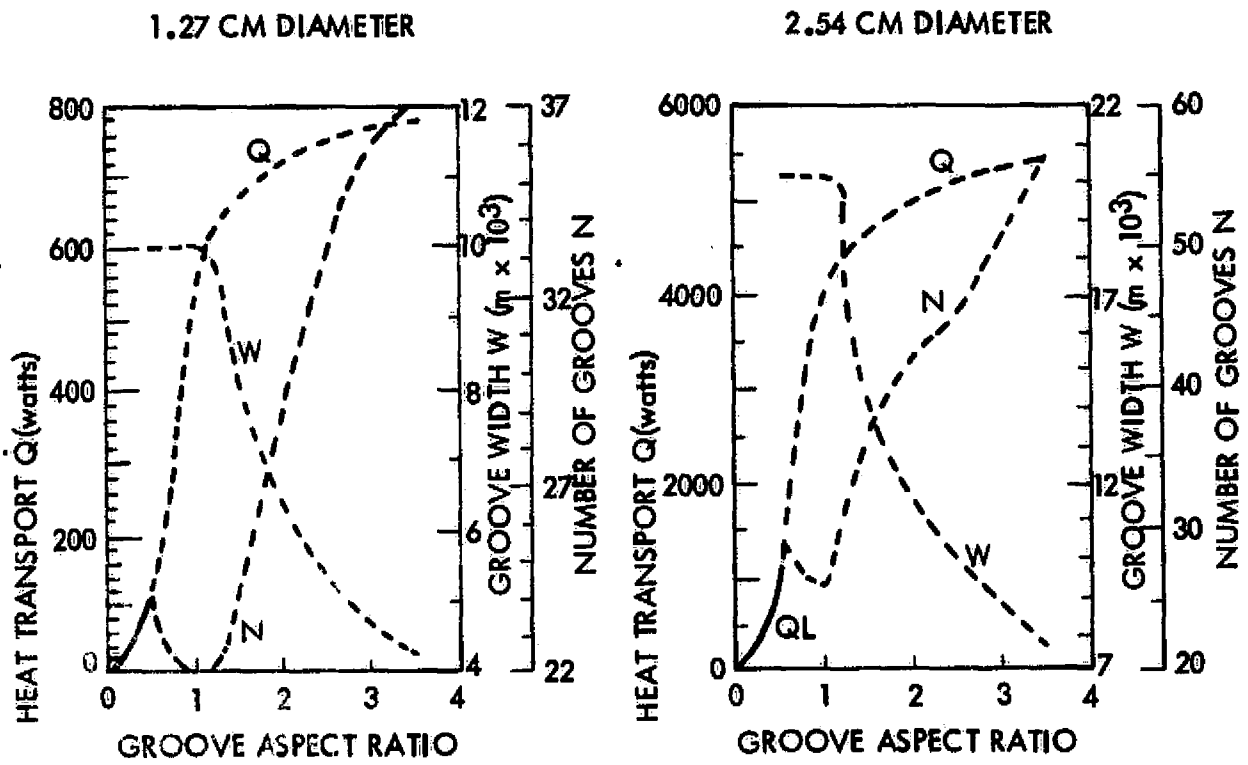

HEAT PIPE
AXIAL HEAT TRANSPORT, GROOVE WIDTH AND NUMBER OF GROOVES

TEMPERATURE: 373°K WORKING FLUID: WATER CONTAINER MATERIAL: COPPER

Figure 1-27. Axially Grooved Heat Pipe
Reference 8

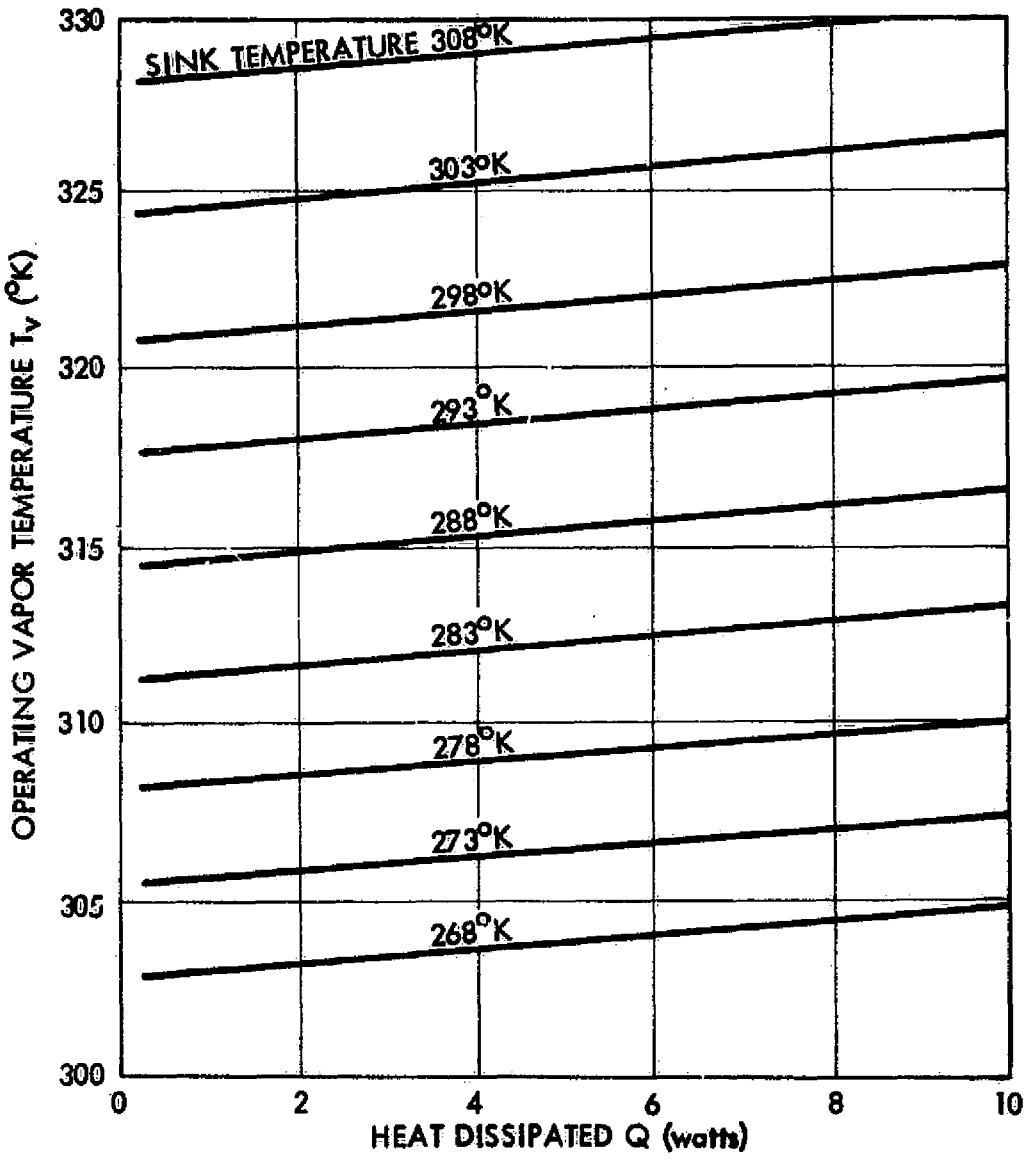

NOMINAL VAPOR TEMPERATURE: 318°K
RANGE OF SINK TEMPERATURES: 268° TO 308°K
WORKING FLUID: AMMONIA

Figure 1-28. Performance of VCHP with Cold Wicked Reservoir Vapor Temperature versus Heat Load

Reference 8

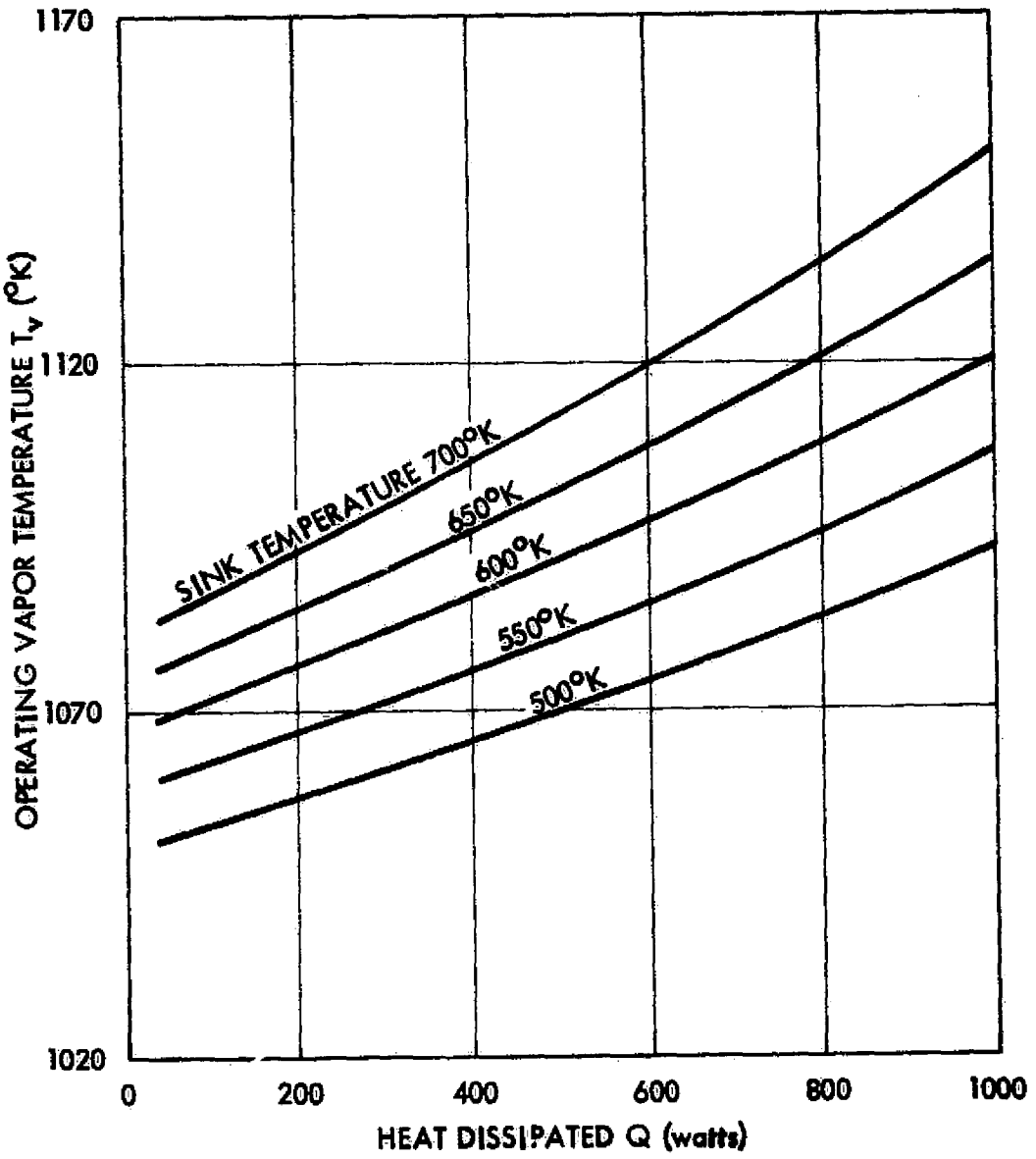

NOMINAL VAPOR TEMPERATURE:	1100°K
RANGE OF SINK TEMPERATURES:	500° TO 700°K
WORKING FLUID:	SODIUM

Figure 1-29. Performance of VCHP with Cold Wicked Reservoir Vapor Temperature versus Heat Load

Reference 8

2.0 BOUNDARY CONDITION DEFINITION

Thermal Environment

The principal boundary conditions for the thermal analysis include component temperature limits, solar heating loads and design configurations.

Both external and internal thermal sources determine the SEPS environment. Solar heating represents the major source of external heating with secondary heating from planetary bodies (i.e., earth). The SEPS missions can be grouped into four classes: outbound, inbound, combined outbound/inbound and earth orbital. Although variations occur between missions in a given class, the major differences occur between classes. During the different development stages of the SEPS program several of the previously planned missions, as tabulated in NAS 8-30592 Statement of Work (Table 3) have been omitted or changed and new missions have been added. At present the following missions are planned: 1) Comet (Encke) rendezvous 2) Astroid (Metis) rendezvous 3) out of the Ecliptic 4) Mercury Orbiter 5) Saturn Orbiter and 6) Jupiter Orbiter. The reference mission characteristics are shown on Figures 2-1 thru 2-6 indicating power profiles and solar distances as a function of flight time. Figure 2-7 demonstrates the variation of the solar constant as a function of the distance from the sun.

The temperature limits of the different SEPS components are shown in Table 2-1.

In analyzing the different missions it was concluded that the Mercury Orbiter mission will impose the highest environmental (solar) load on the SEPS at the end of the mission when it will reach 0.38 AU distance from the sun.

From the planned missions both the Saturn Orbiter and the Jupiter Orbiter will go to 5.0 AU solar distance. By analyzing the Mercury Orbiter and the Saturn or Jupiter Orbiter missions maximum and minimum temperatures will be obtained to select the proper radiator areas to meet all requirements. For additional temperatures and radiator size for a 926 KM altitude low earth orbit mission will also be evaluated.

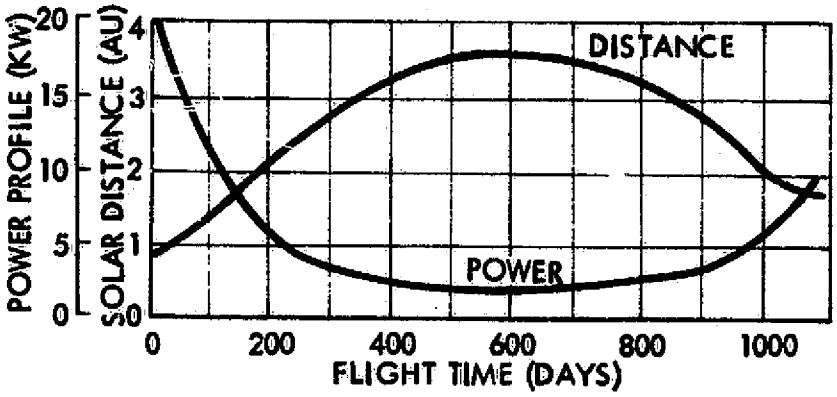

Figure 2-1. Encke Rendezvous

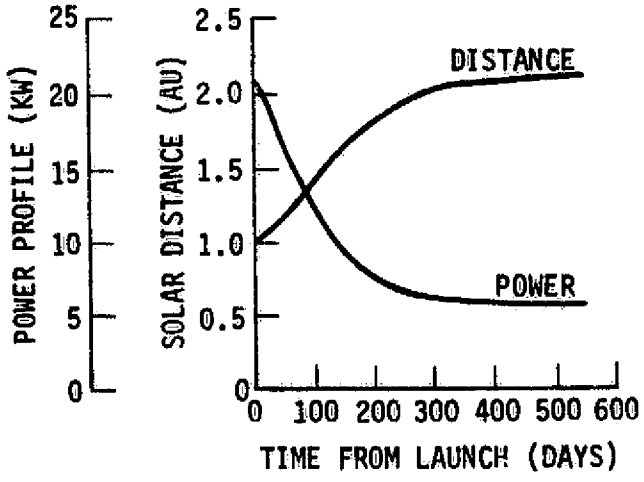

Figure 2-2. Metis Rendezvous Reference 16

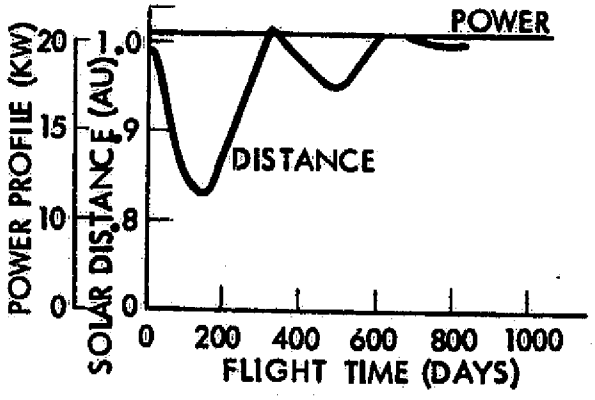

Figure 2-3. Out of Ecliptic
Reference 16

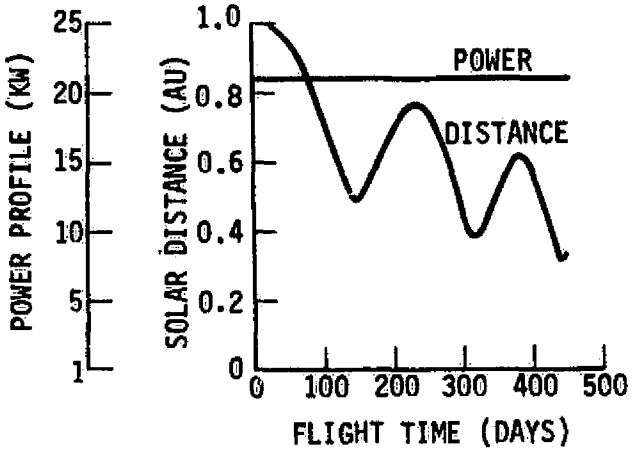

Figure 2-4. Mercury Orbiter
Reference 16

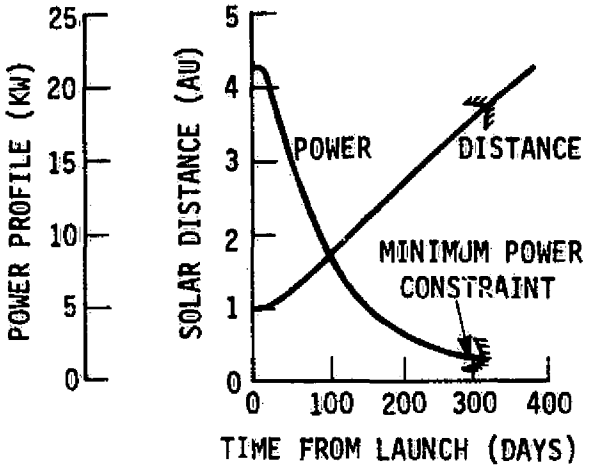

Figure 2-5. Saturn Orbiter
Reference 16

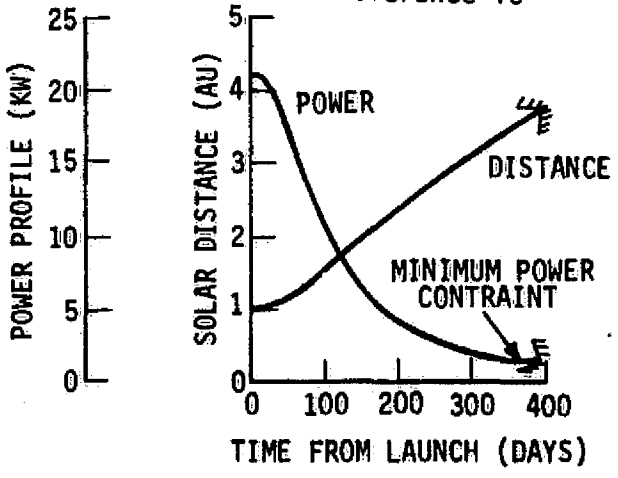

Figure 2-6. Jupiter Orbiter
Reference 16

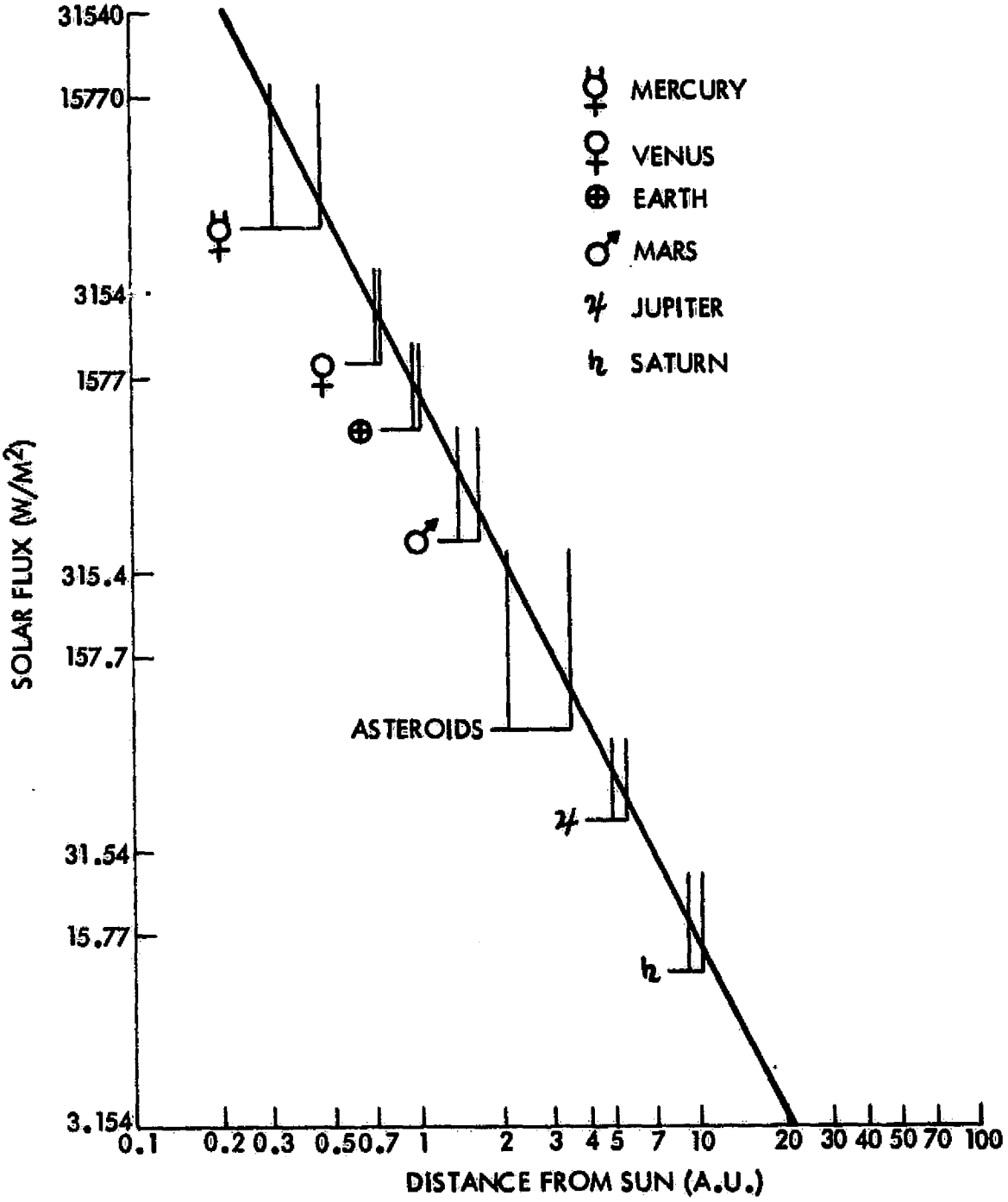

Figure 2-7. Variation of Solar Constant with Distance From Sun

Table 2-1 Temperature Limits of SEPS Components

System and Component	Temperature Limits (°K)			
	Operational		Survival	
	Maximum	Minimum	Maximum	Minimum
Attitude Control				
Star sensors	323	263	348	238
Gyro assembly	358	273	398	218
Sun sensors	328	273	337	238
ACS electronics	338	66	358	255
RCS thrusters (valve)	323	278	323	268
RCS thrusters (nozzle)	1373	278	1373	268
RCS tank, lines, etc.	323	278	323	268
Approach guidance				
Sensor	308	298	348	218
Gimbals	353	253	353	253
Command and data				
Computer	353	218	398	218
Data processor	328	253	348	243
Recorder	313	263	328	253
Communications				
Telemetry modulator	328	253	348	243
Command detector	328	253	348	243
S-band receiver	328	253	348	243
S-band transmitter	328	253	348	243
S-band power amplifier	328	253	348	243
X-band transmitter	328	253	348	243
X-band amplifier	328	253	348	243
CU	328	253	348	243
Power				
Array	413	118	413	118
Regulators	338	273	348	258
Battery	298	273	313	263
Thrust				
Mercury tank	338	255	373	243
Thrusters	533	253	533	253
Power conditioners	323	258	373	223

Configuration Studies

The SEPS configuration design is strongly influenced by several factors such as thermal control considerations, packaging factors (i.e. solar array dimensions), thruster plume clearance, payload geometry, etc.

The two major elements requiring thermal control in the SEPS are the Power Processors (PP's) and Equipment Compartment (EC). For the first phase of the study program the PP thermal control concept was based on the PP design developed originally by Hughes Research Laboratories (HRL), as will be described in detail later, and several SEPS concept design options have been evaluated using louvers as thermal control device. Several of these SEPS design concepts are shown in Figure 2-8.

In September 1974 the Advanced System Technology (ATS) Thrust Subsystem Design Review was held at NASA Lewis Research Center (LeRC). There LeRC indicated that the PP thermal control concept using both heat pipes and louvers provides packaging, performance, weight, reliability and cost advantages over the existing baseline (HRL) concept using louvers only. The key difference, in addition to the heat pipes, was the packaging of the PP electronics. While the original HRL concept spaced the electronic components over a large radiator area to distribute the heat, the proposed concept concentrated the electronics into a smaller package and utilized heat pipes to transport the heat to a separate radiator. This smaller electronics package design was selected by the AST Committee as the new PP baseline. However, the specific design of the thermal control system was left open for further studies. Representative configurations for the HRL and new PP concepts (using heat pipes) are shown on Figure 2-9 and 2-10 respectively.

Power Processor Thermal Control

The baseline SEPS with a 21-kW propulsion power uses up to seven 3-kW PP's simultaneously. Although the PP's are highly efficient (about 90 percent), the heat generated by the seven units total over 2000 watts. Efficient rejection of this heat is one of the key problems. The other problem is to maintain efficiently the non-operating PP's and spare PP's above the minimum allowable temperature.

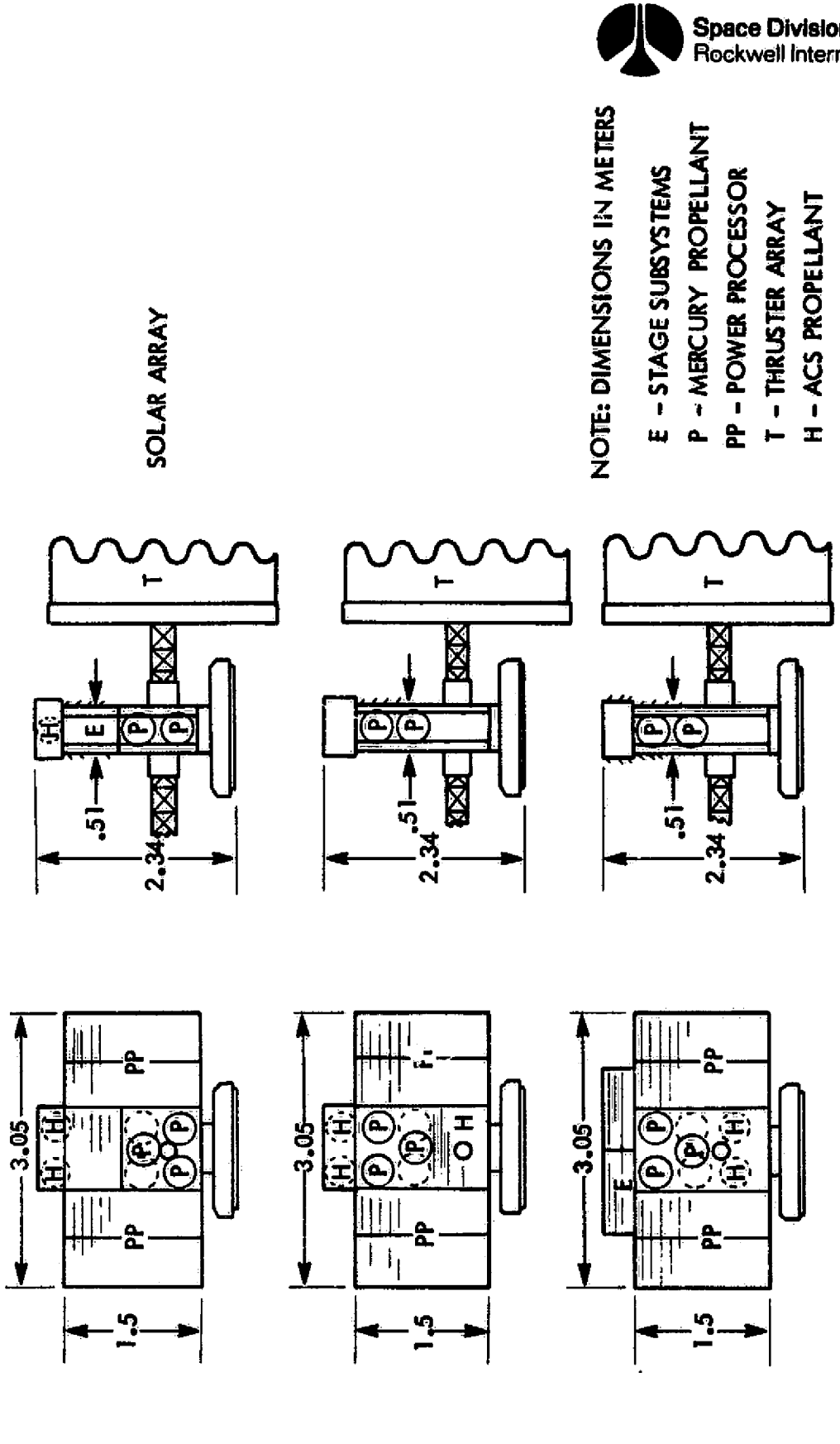

Figure 2-8. SEPS Concept Design Options

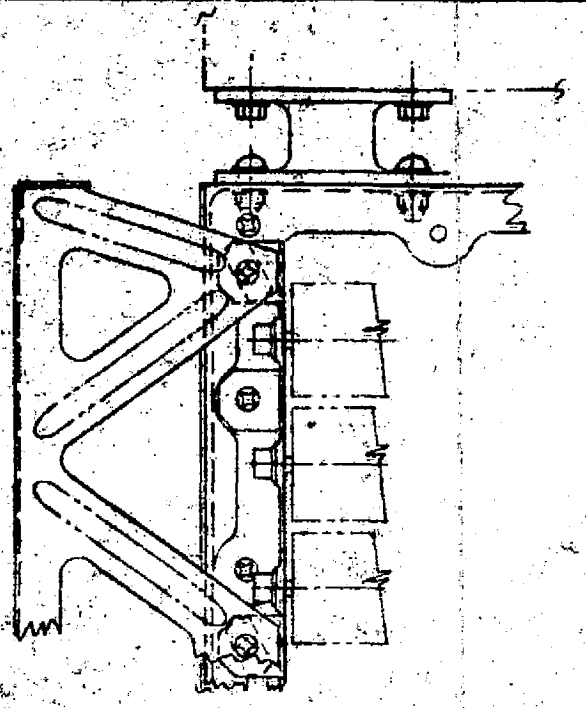

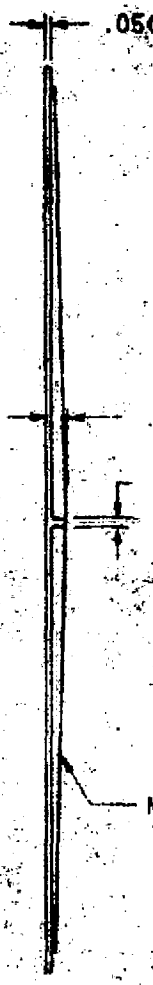

SECT G - G
SCALE: 1/1

LOUVER SUPPORT

.60 TYP

.50

LOUVER SUPPORT IS ATTACHED WITH THE SAME FASTENERS AS MODULE PLATES

8-32 SCREWS &
MINIATURE NUTPLATES
13 PLACES

LOUVERS

NSULATION SUPPORT—
YPICAL 2 PLACES
N FREE EDGES OF
P.C. ASSEMBLY)

MOUNTING FRAME

VIEW H - H
SCALE: 1/1

ORIGINAL PAGE IS
OF POOR QUALITY

FOLDOUT FRAME

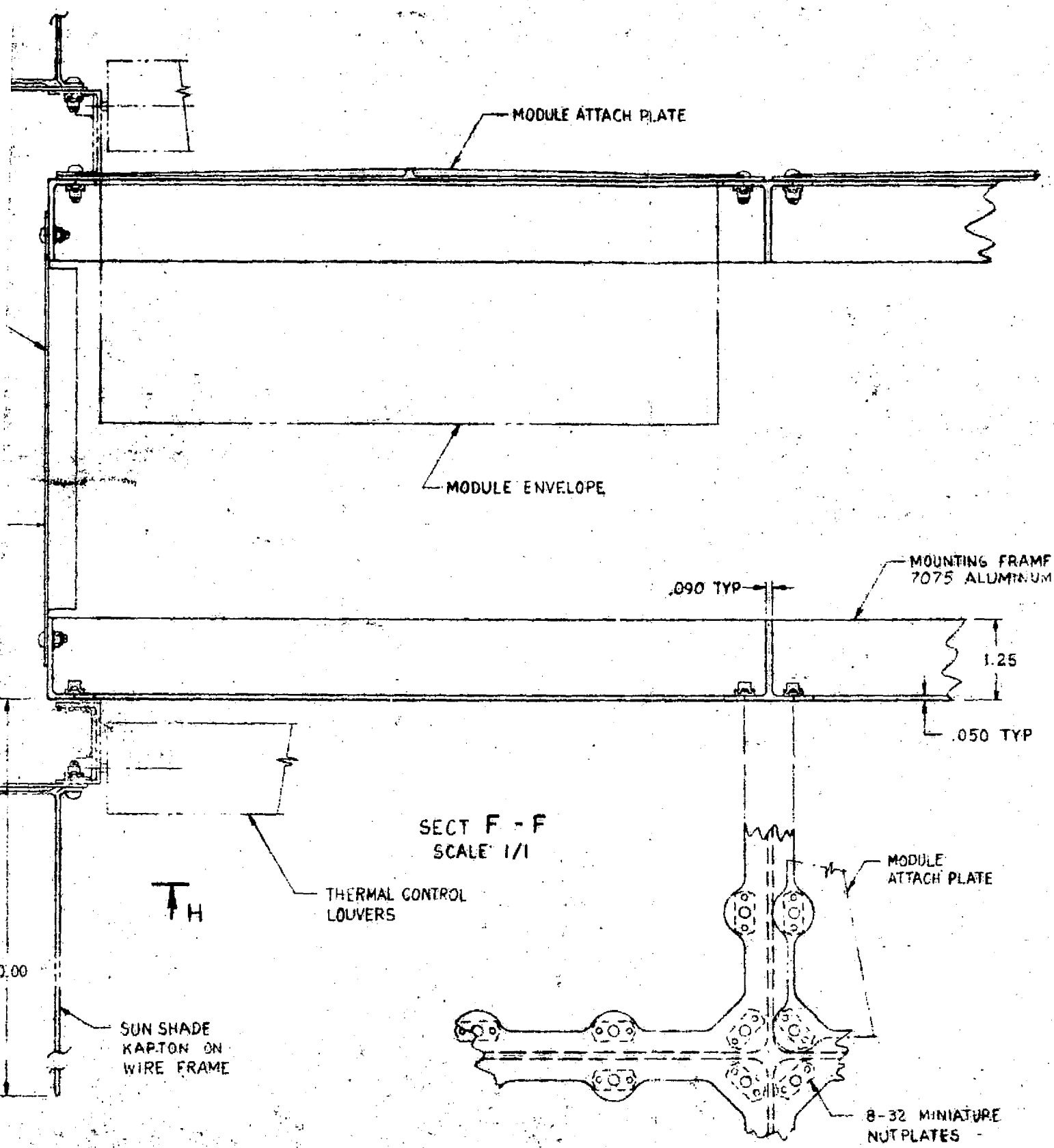

FOLDOUT FRAME

2

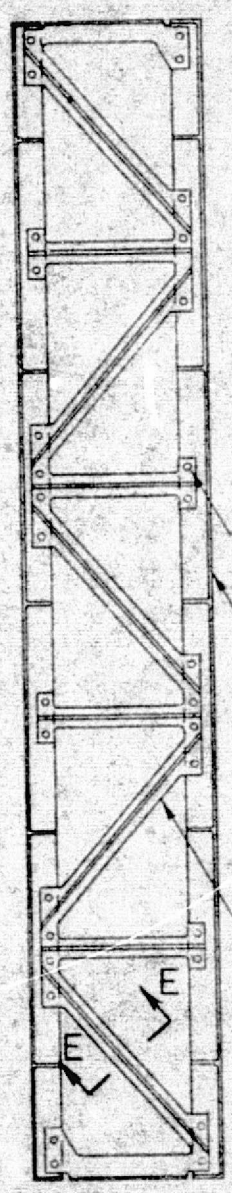

VIEW D - D

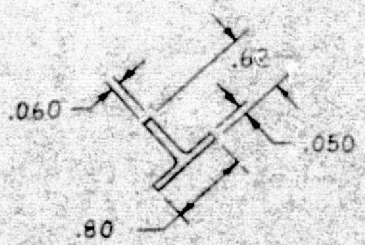

SECT E - E
SCALE: 1/1

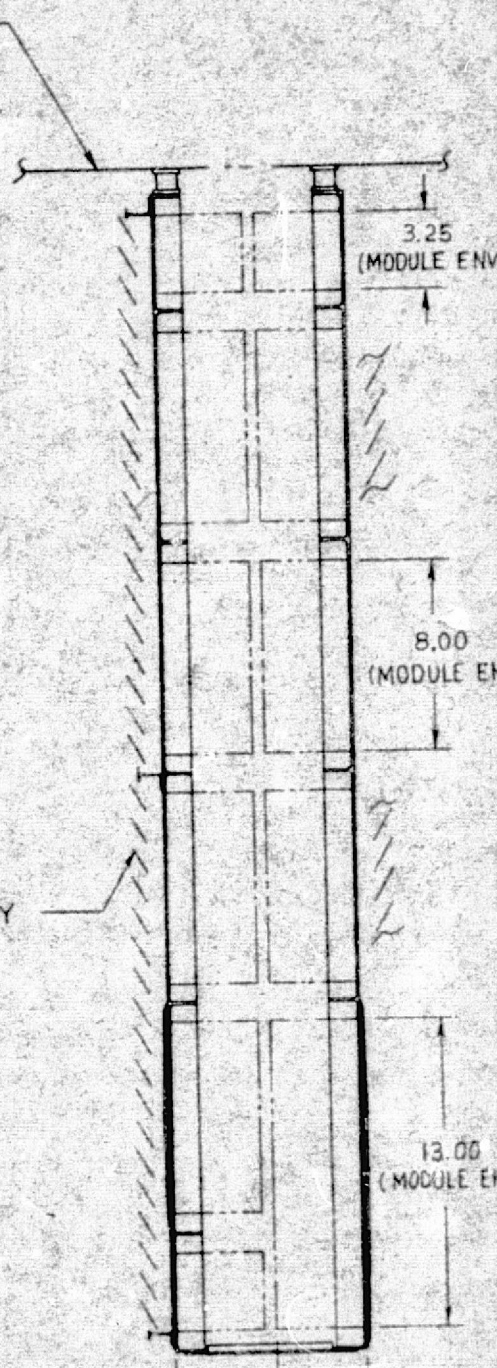

SECT C - C

FOLDOUT FRAME

3

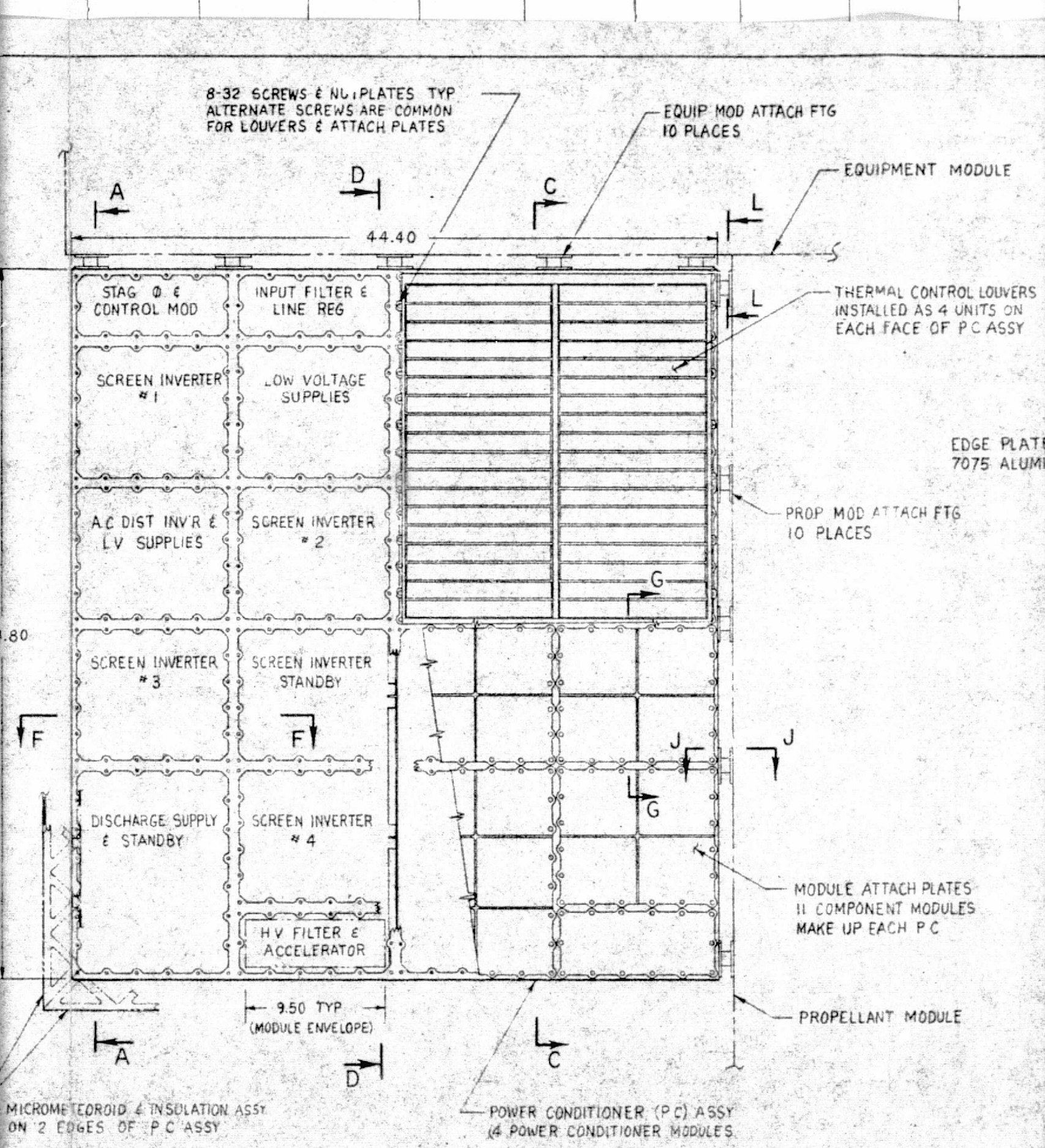

OLDOUT FRAME

4

VIEW OF FACE OF POWER CONDITIONER ASSY

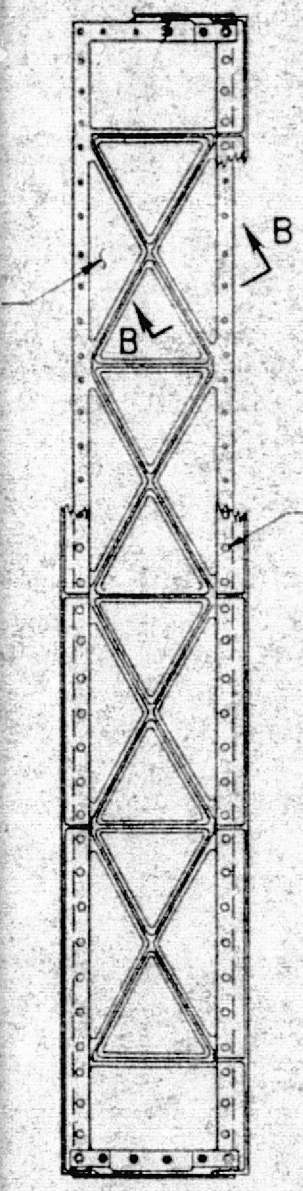

VIEW A-A
OF EDGE PLATE TWO PLACES
EXPOSED EDGES OF P.C ASSY

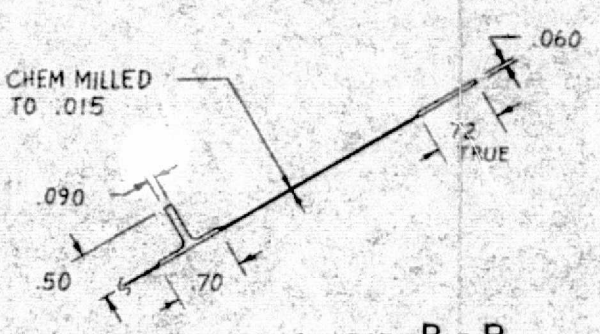

SECT B - B
SCALE: 1/1

CORNER TIE
7075 ALUMINUM

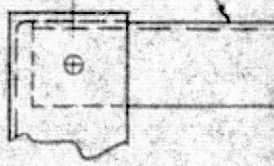

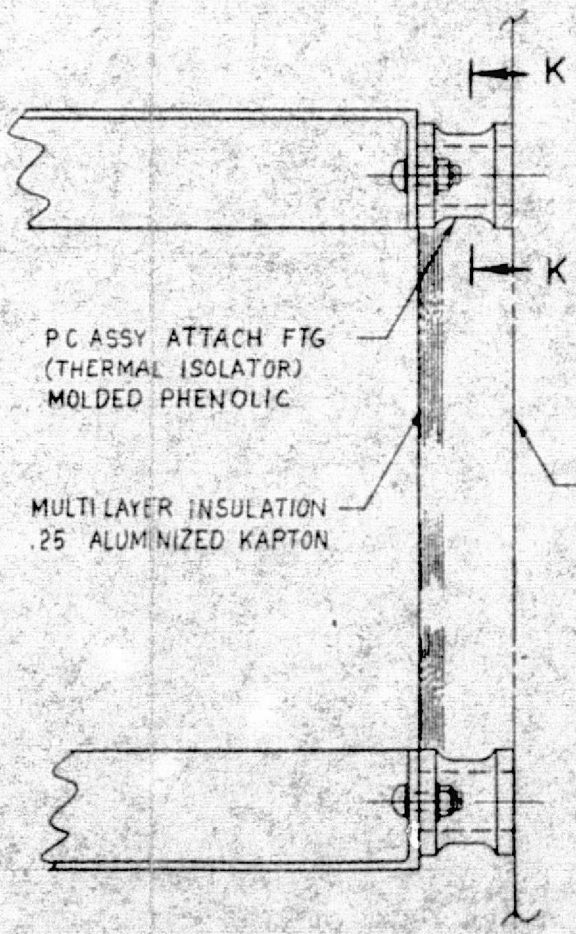

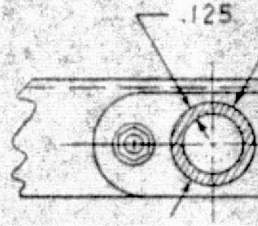

VIEW K
SCALE:

SECT J - J
SCALE: 1/1
TYP FOR ATTACHMENT OF P C ASSY TO EQUIP & PROPELLANT MODULES

FOLDOUT FRAME
5

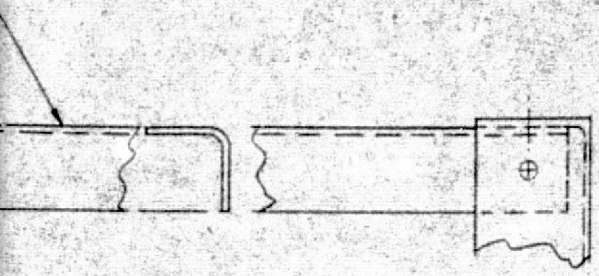

VIEW L - L
SCALE: 1/1
(ATTACH FTGS NOT SHOWN)

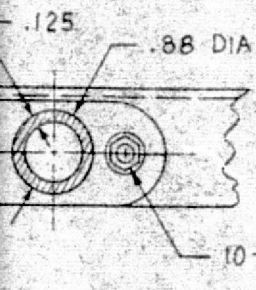

IEW K - K
CALE: 1/1

ULE

FOLDOUT FRAME

6

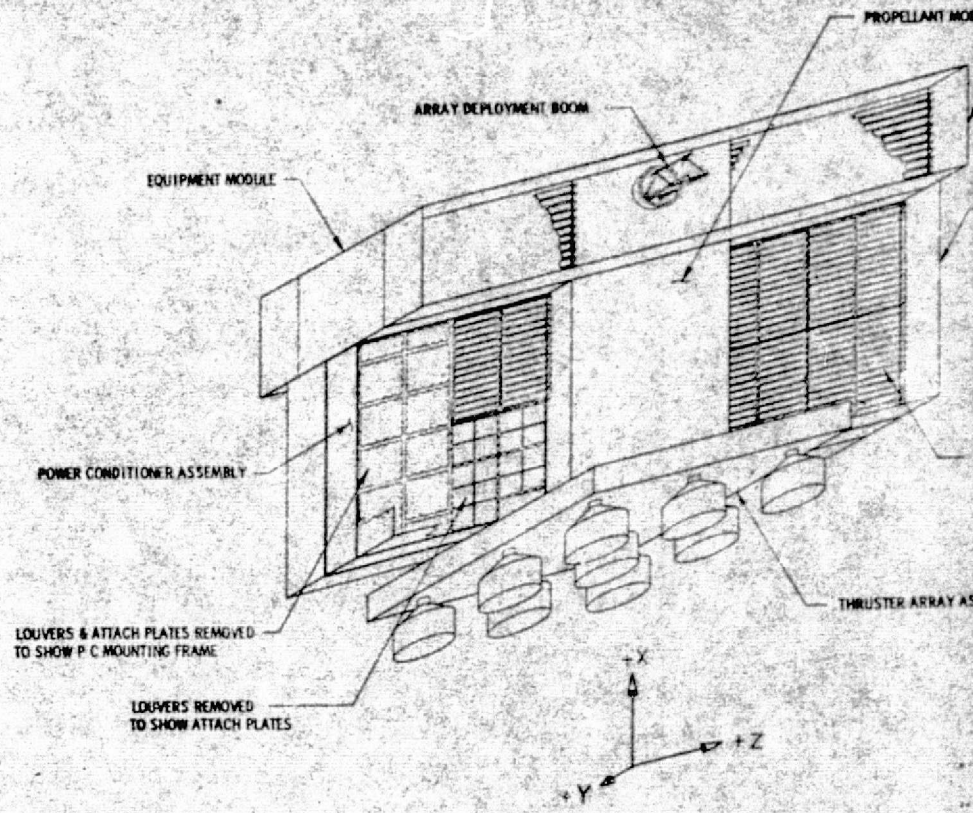

FOLDOUT FRAME

7

FIGURE

SCALE 1/4 UNLESS NOTED	DRN DON THOMP DATE 3-13-74 MODEL	ROCKWELL INTERNATIONAL CORPORATION SPACE DIVISION [illegible] BOULEVARD, DOWNEY, CALIFORNIA

POWER CONDITIONER ASSY -
SEPS (THERMAL ANALYSIS)

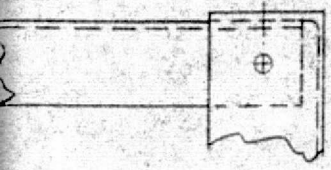

HOWN)

32 SCREWS & NUTS

AME

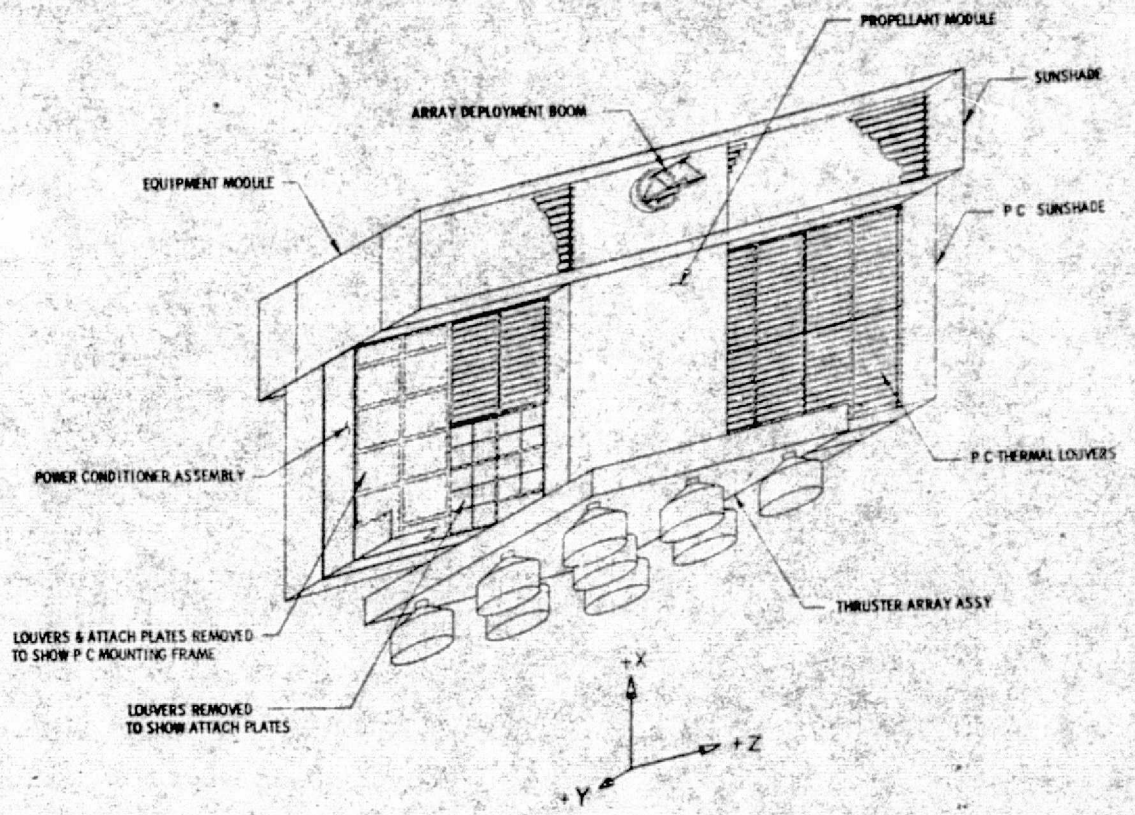

FOLDOUT FRAME

7

FIGURE 2-9 SHT 1

SCALE 1/4 MODIFIED	BY DON THOMP DATE 3-15-74 MODEL	ROCKWELL INTERNATIONAL CORPORATION SPACE DIVISION 12214 LAKEWOOD BOULEVARD DOWNEY, CALIFORNIA	
POWER CONDITIONER ASSY - SEPS (THERMAL ANALYSIS)			3091-1

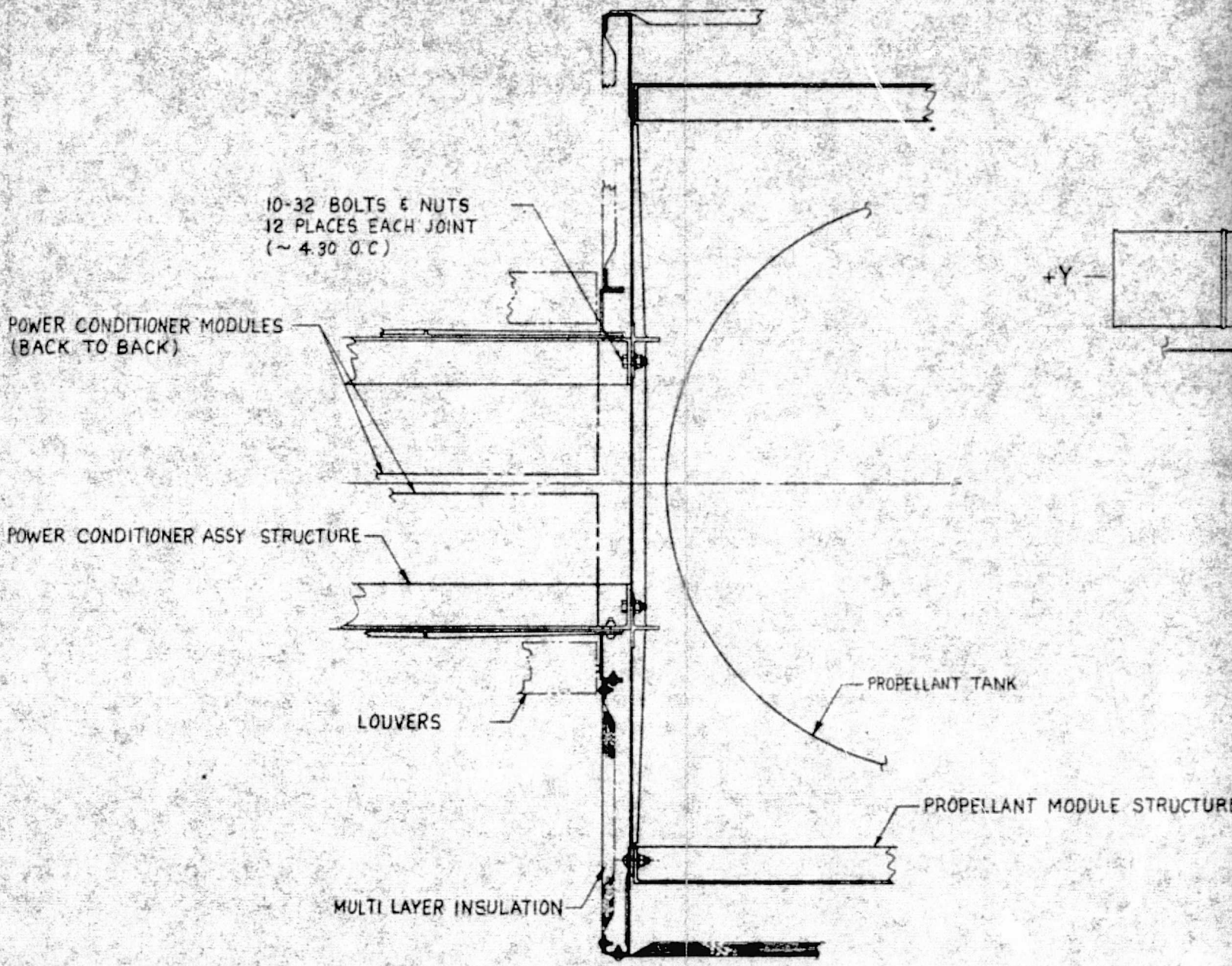

FOLDOUT FRAME

1

VIEW A - A
SCALE 1/2

TER

PLOYMENT MAST

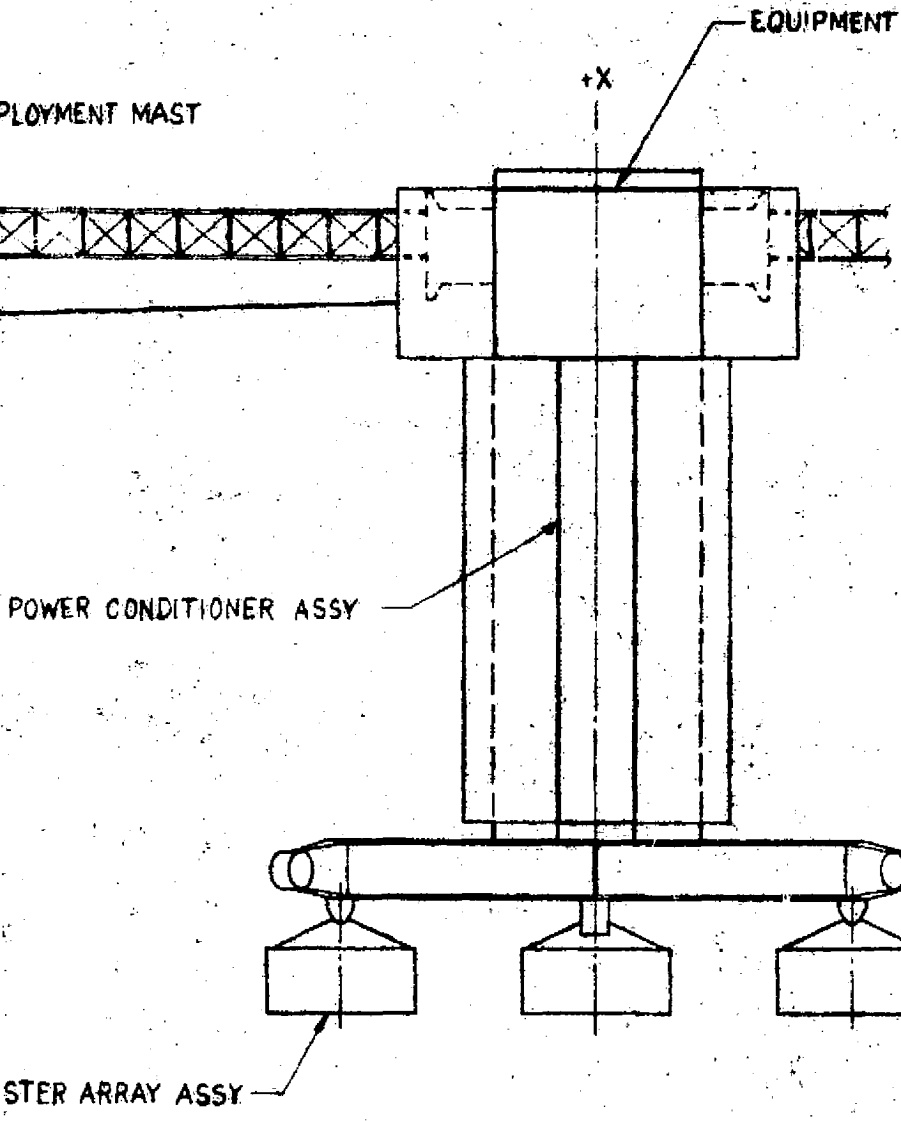

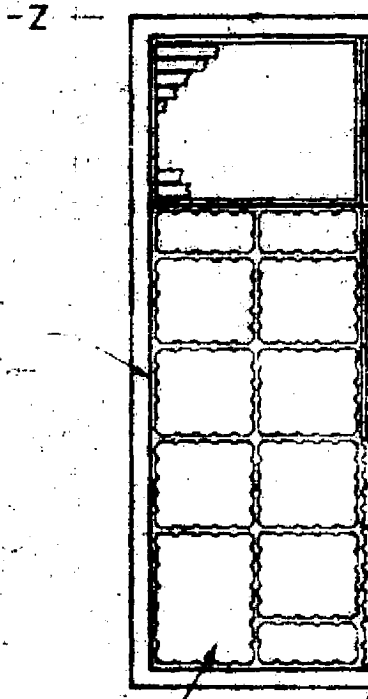

FOLDOUT FRAME

2

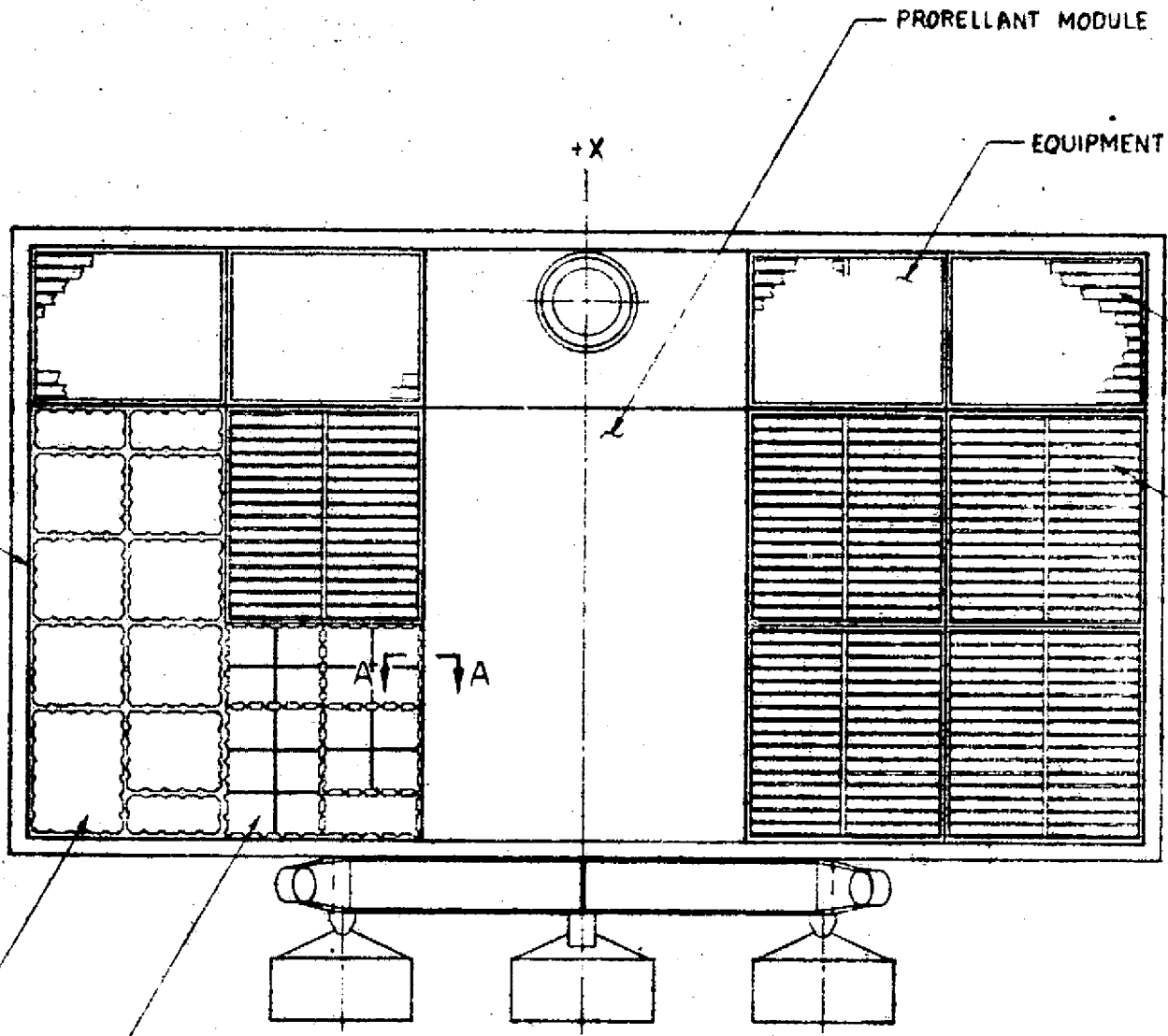

FOLDOUT FRAME

FOLDOUT FRAME

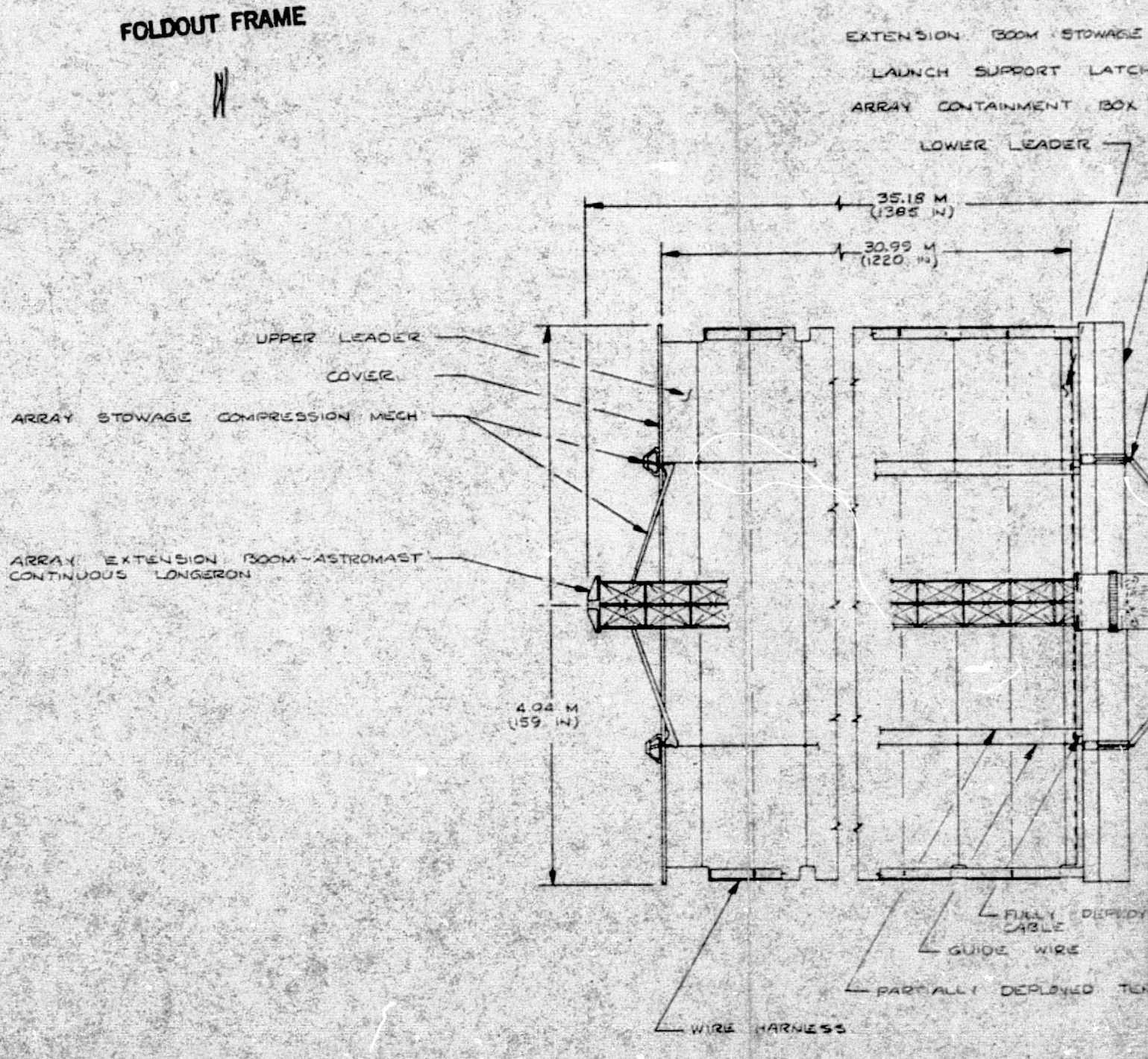

FOLDOUT FRAME

2

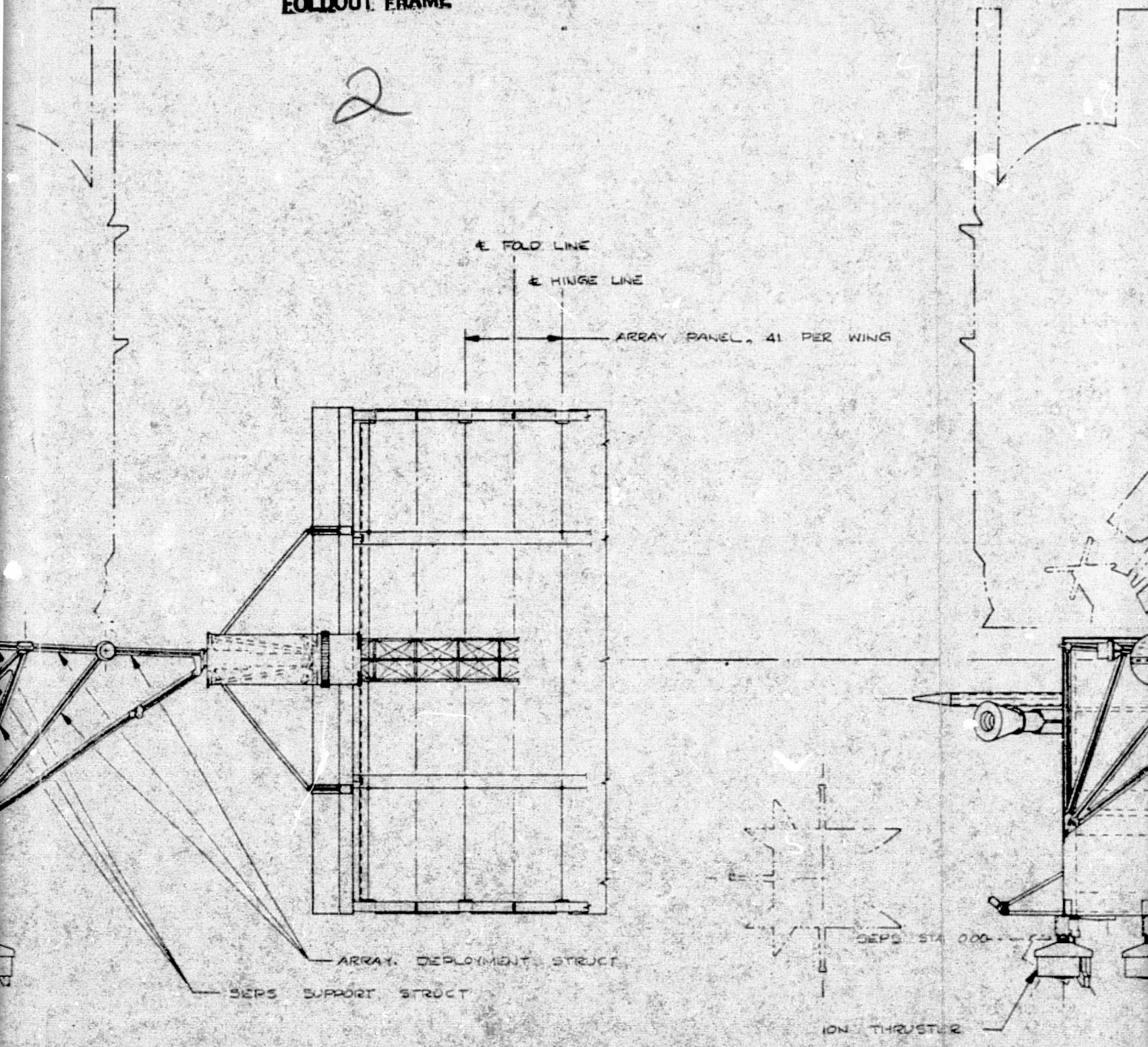

FOLDOUT FRAME

3

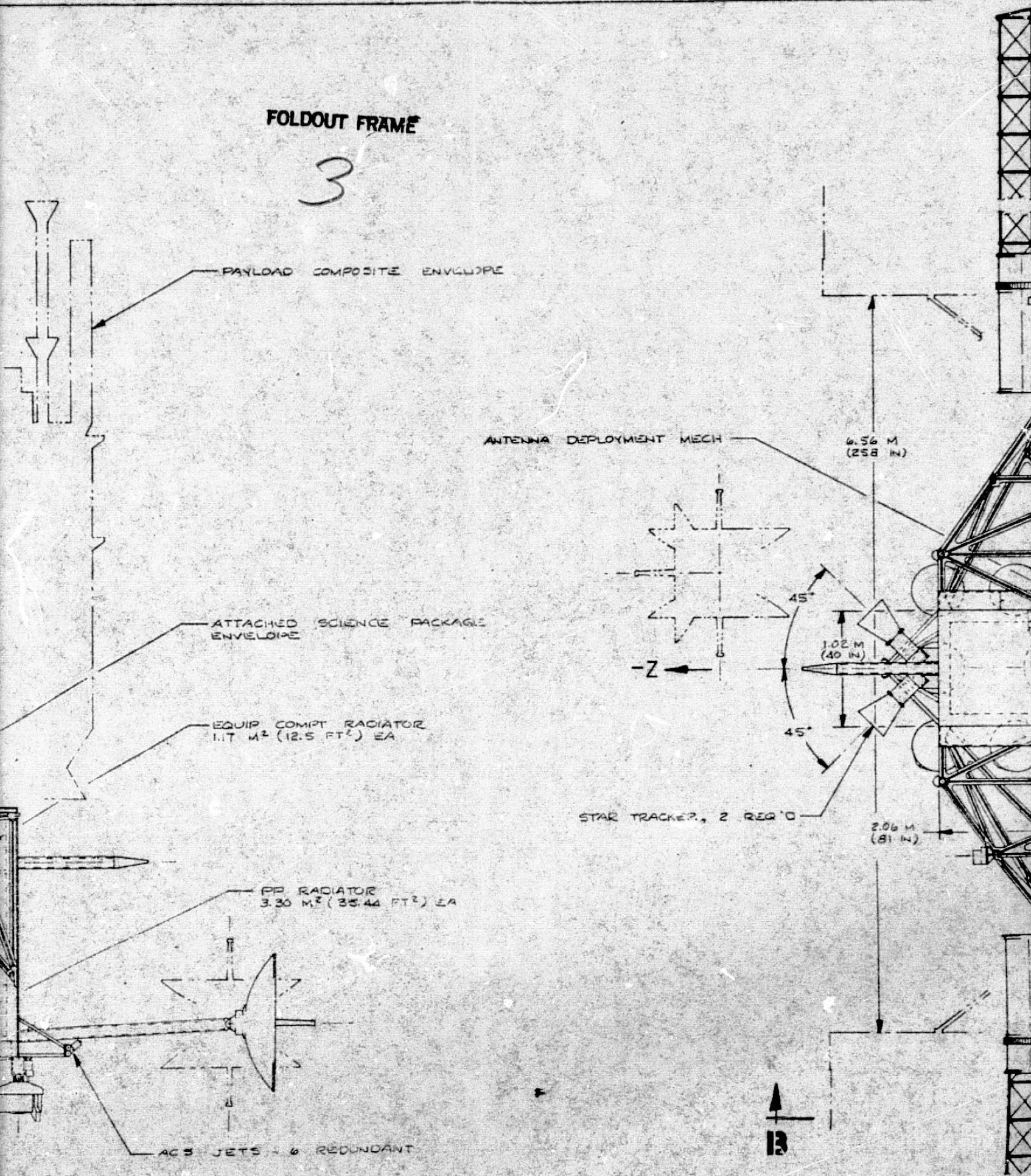

FOLDOUT FRAME

4

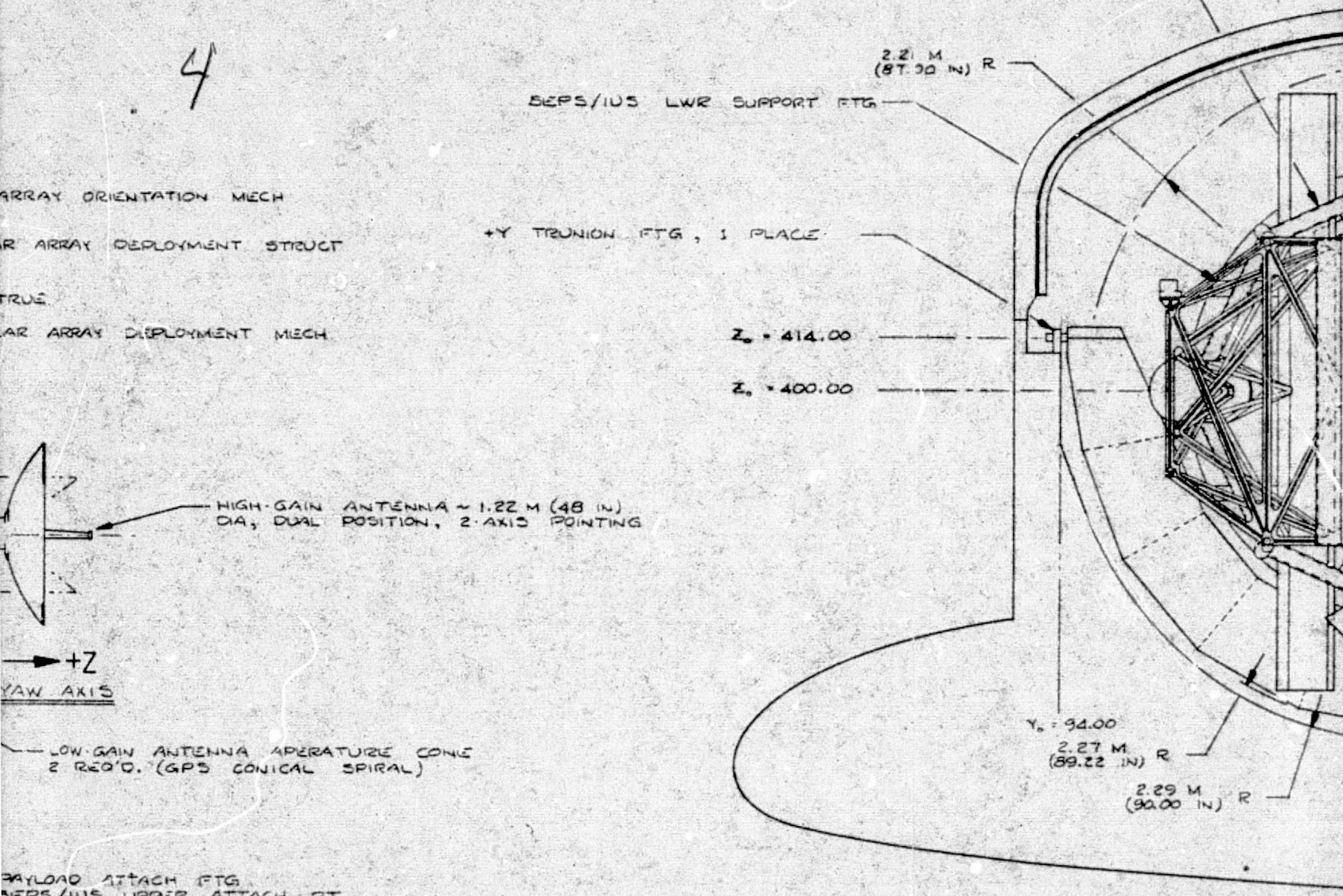

ARRAY ORIENTATION MECH

R ARRAY DEPLOYMENT STRUCT

TRUE

AR ARRAY DEPLOYMENT MECH

HIGH-GAIN ANTENNA ~ 1.22 M (48 IN) DIA, DUAL POSITION, 2-AXIS POINTING

+Z

YAW AXIS

LOW-GAIN ANTENNA APERATURE CONE 2 REQ'D. (GPS CONICAL SPIRAL)

PAYLOAD ATTACH FTG
SEPS/IUS UPPER ATTACH PT

SECTIO

FOLDOUT FRAME

5

URATION SCALE 1/20

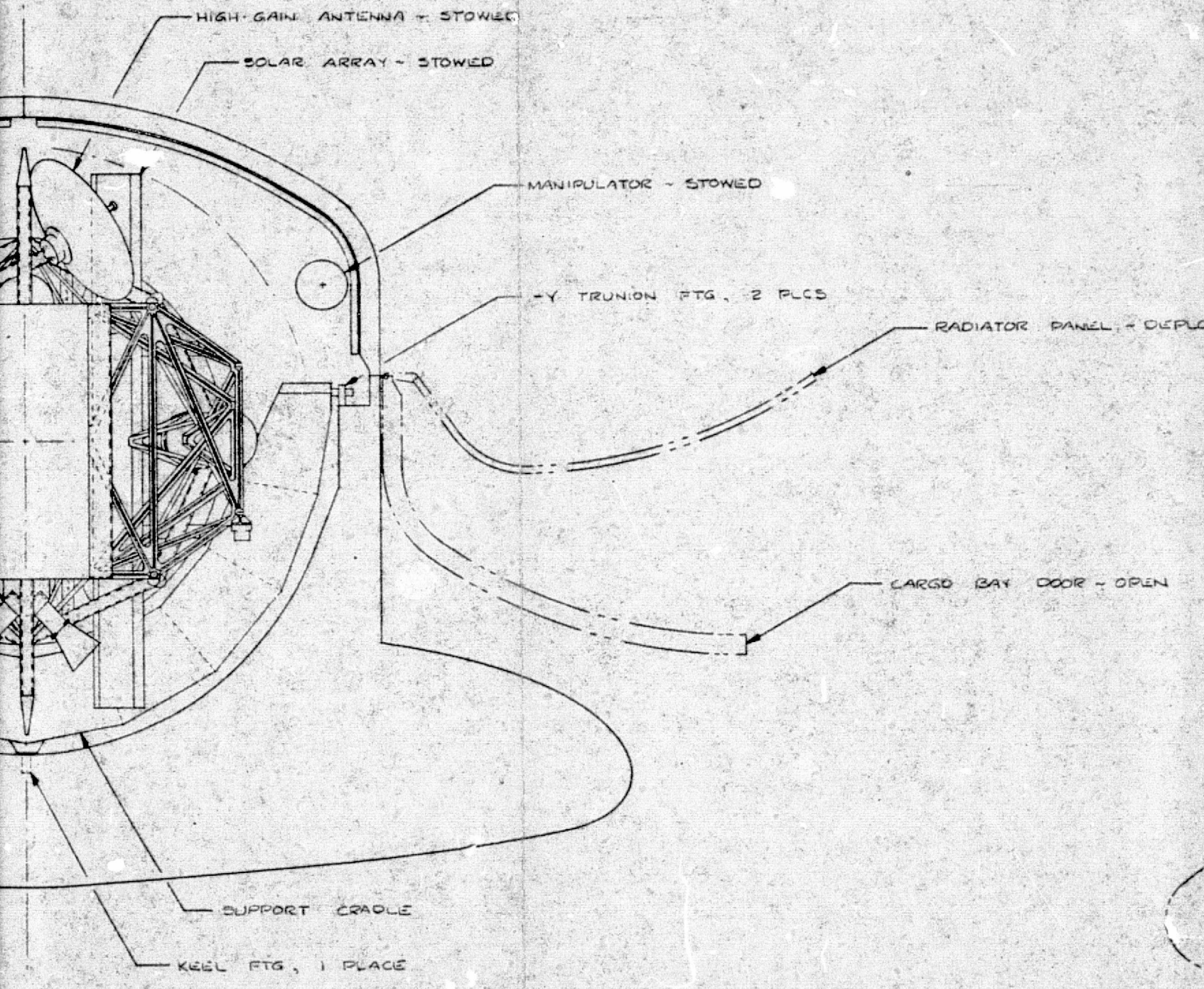

A-A SCALE 1/20

FOLDOUT FRAME

LOYED

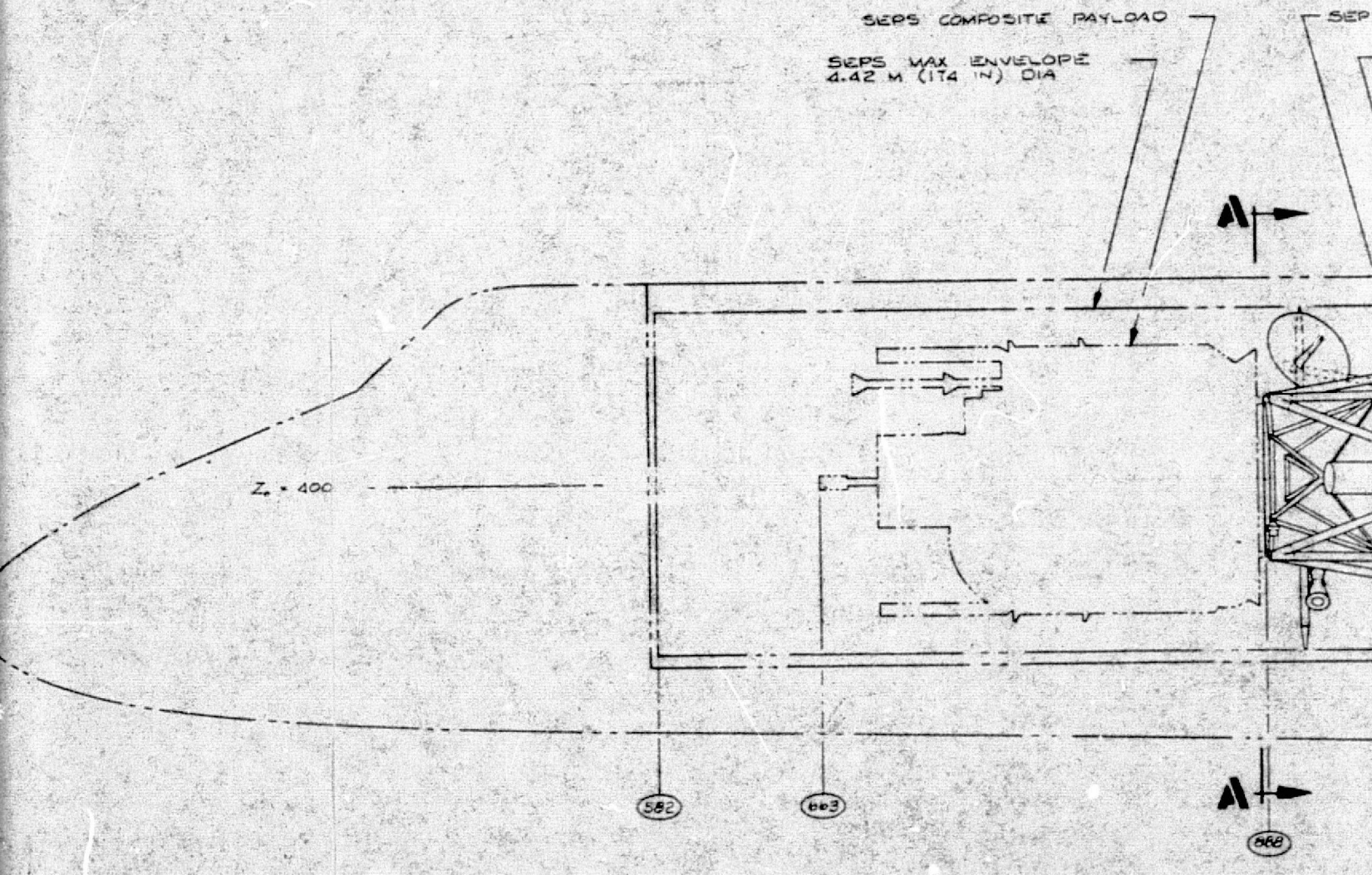

FOLDOUT FRAME

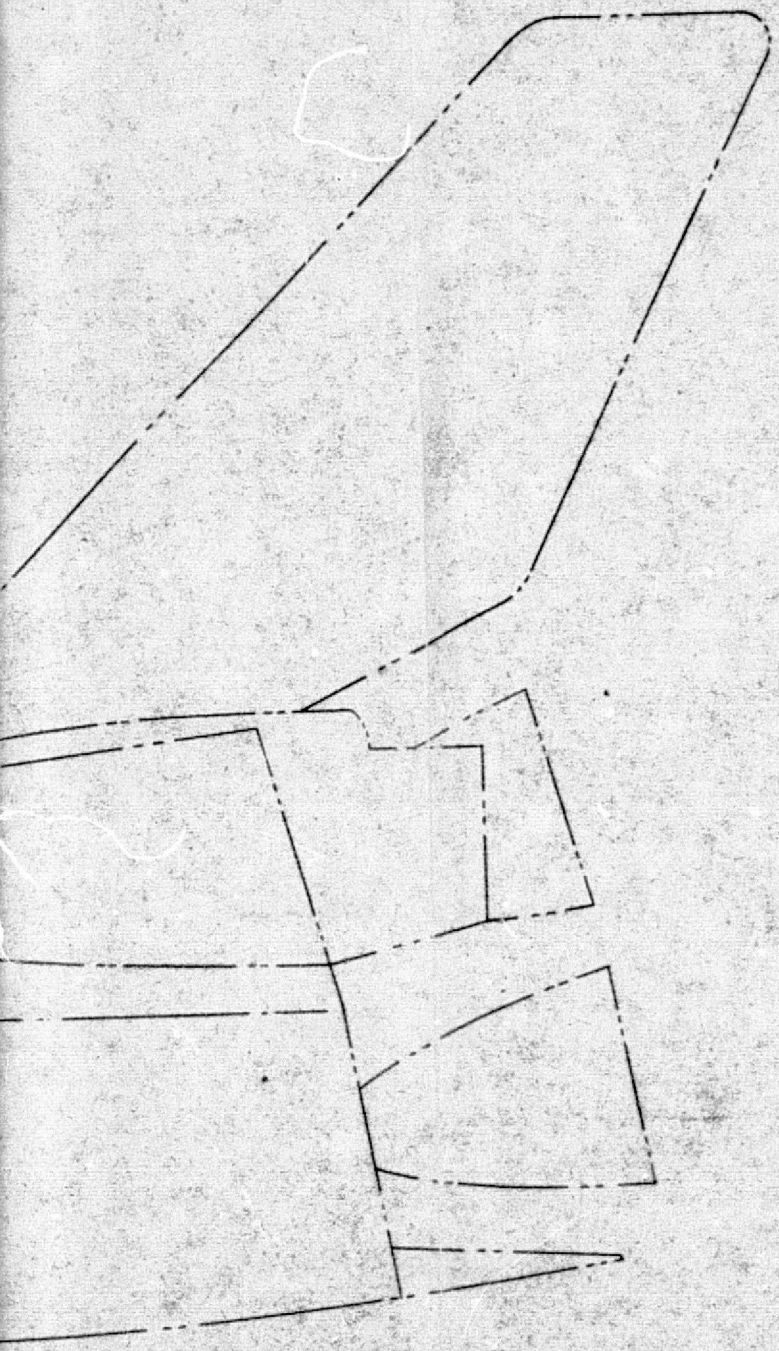

FOLDOUT FRAME

8

FIGURE 2-10 SHT 1

SCALE AS NOTED	BY KURTKINS DATE 2-6-74 MODEL	ROCKWELL INTERNATIONAL CORPORATION SPACE DIVISION 12214 LAKEWOOD BOULEVARD, DOWNEY, CALIFORNIA	2375-13 SHT 1 OF 2

BASELINE PLANETARY SEPS CONFIGURATION
EVOLUTIONARY SEPS STUDY

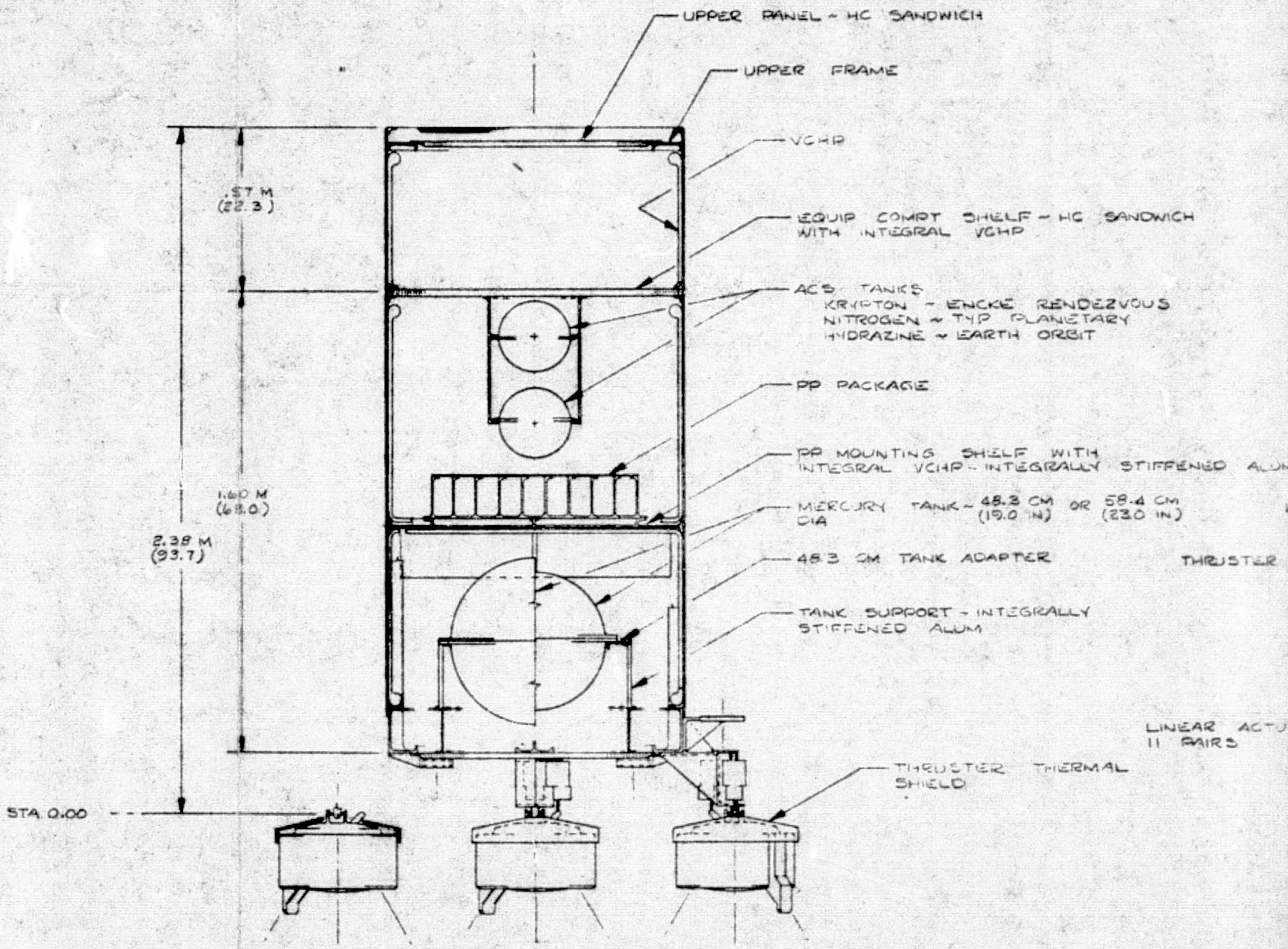

SECTION G-G

FOLDOUT FRAME

FOLD

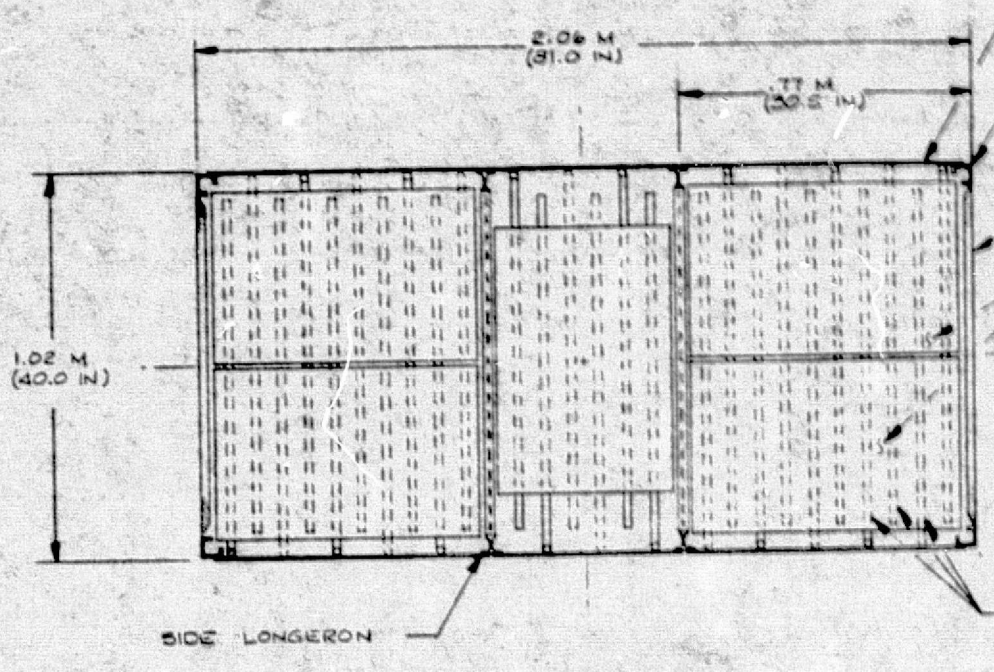

SECTION **F-F**

OUTR

ALUM

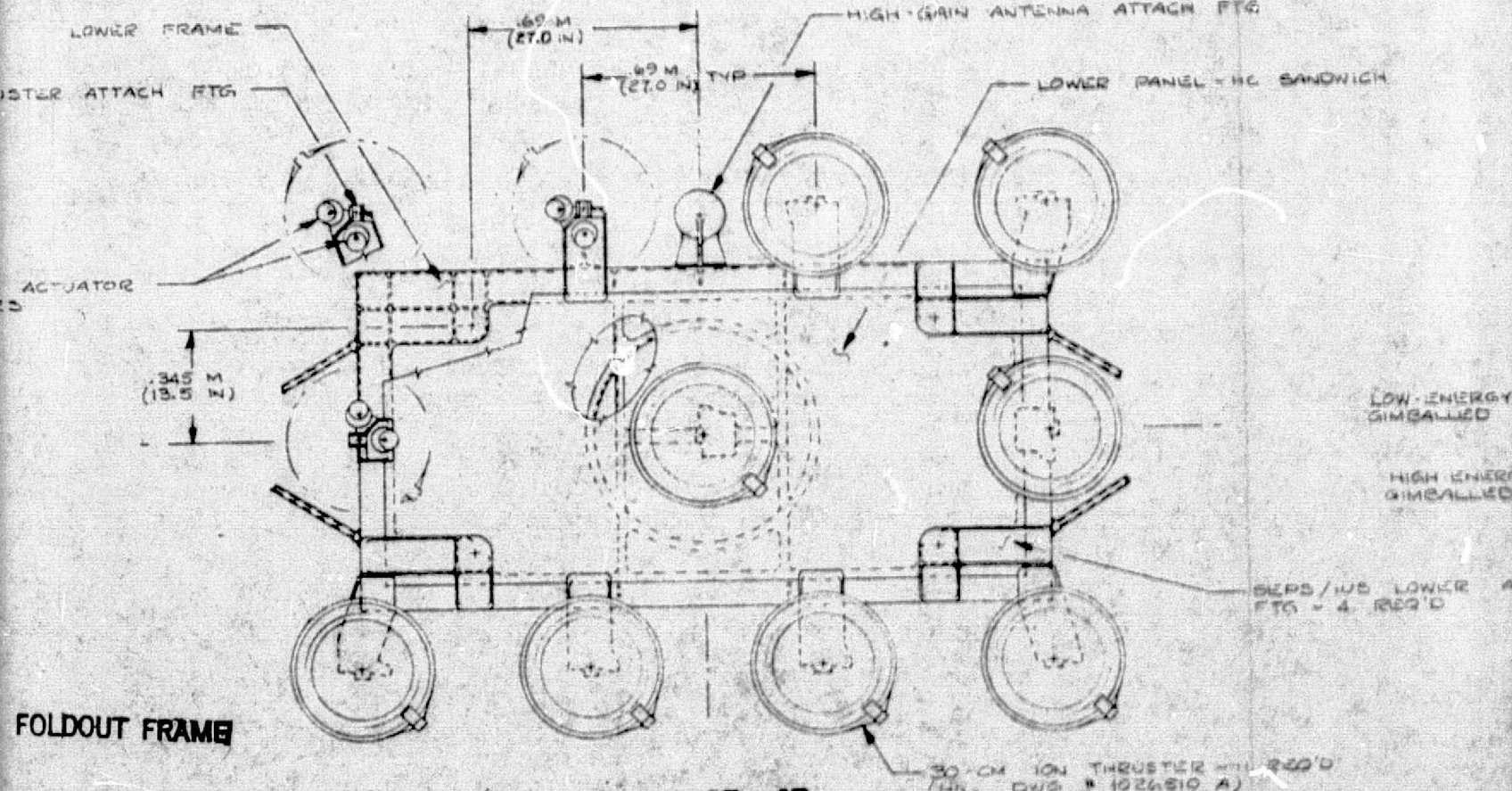

FOLDOUT FRAME

VIEW **E-E**

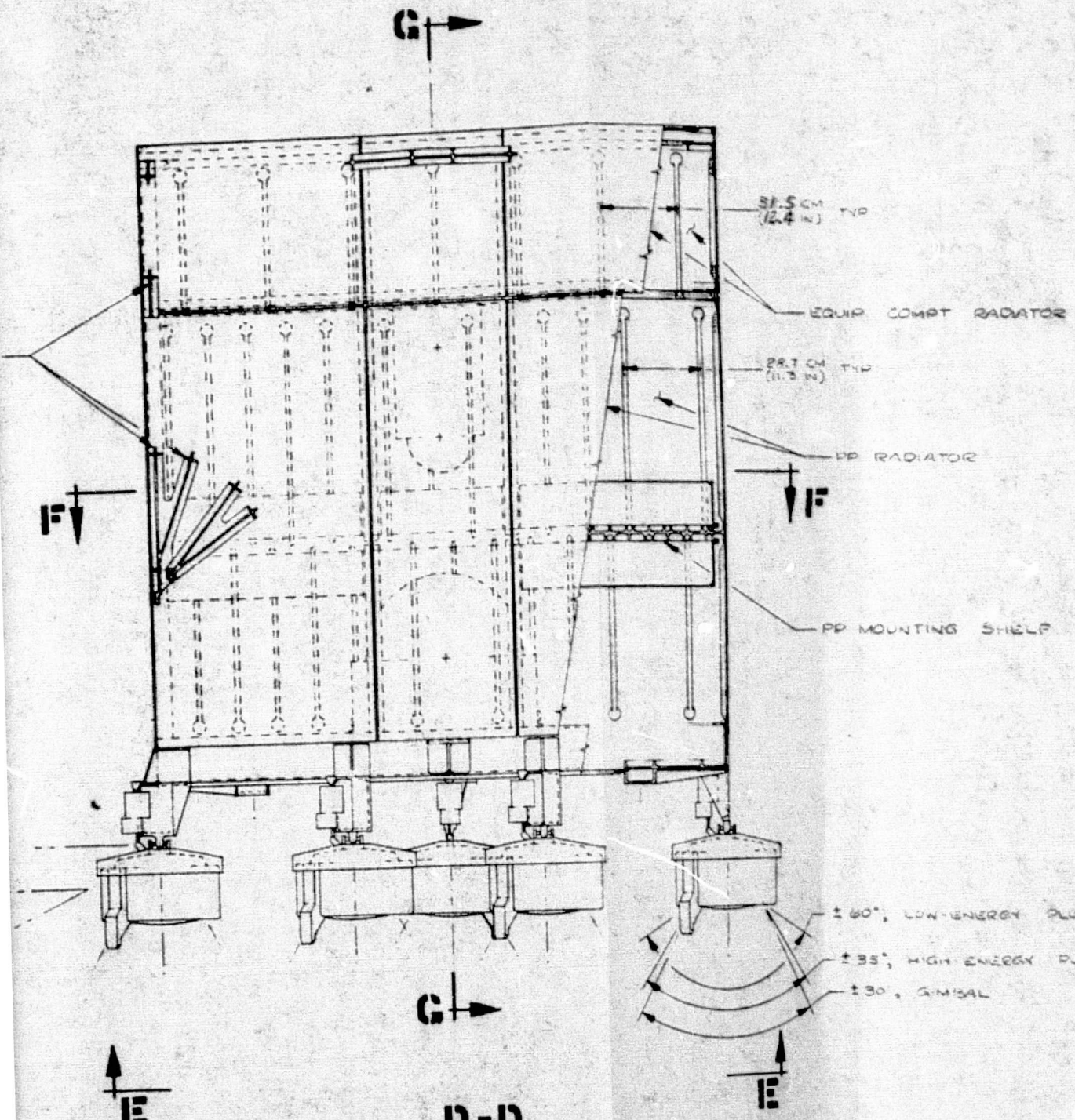

VIEW D-D

FOLDOUT FRAME

3

FOLDOUT FRA

4

FIGU

SCALE 1/10	DR WATKINS	ROCKWELL INTERNATIONAL C
	DATE 12-6-74	SPACE DIVISION
	MODEL	

BASELINE PLANETARY SEPS

EVOLUTIONARY SEPS

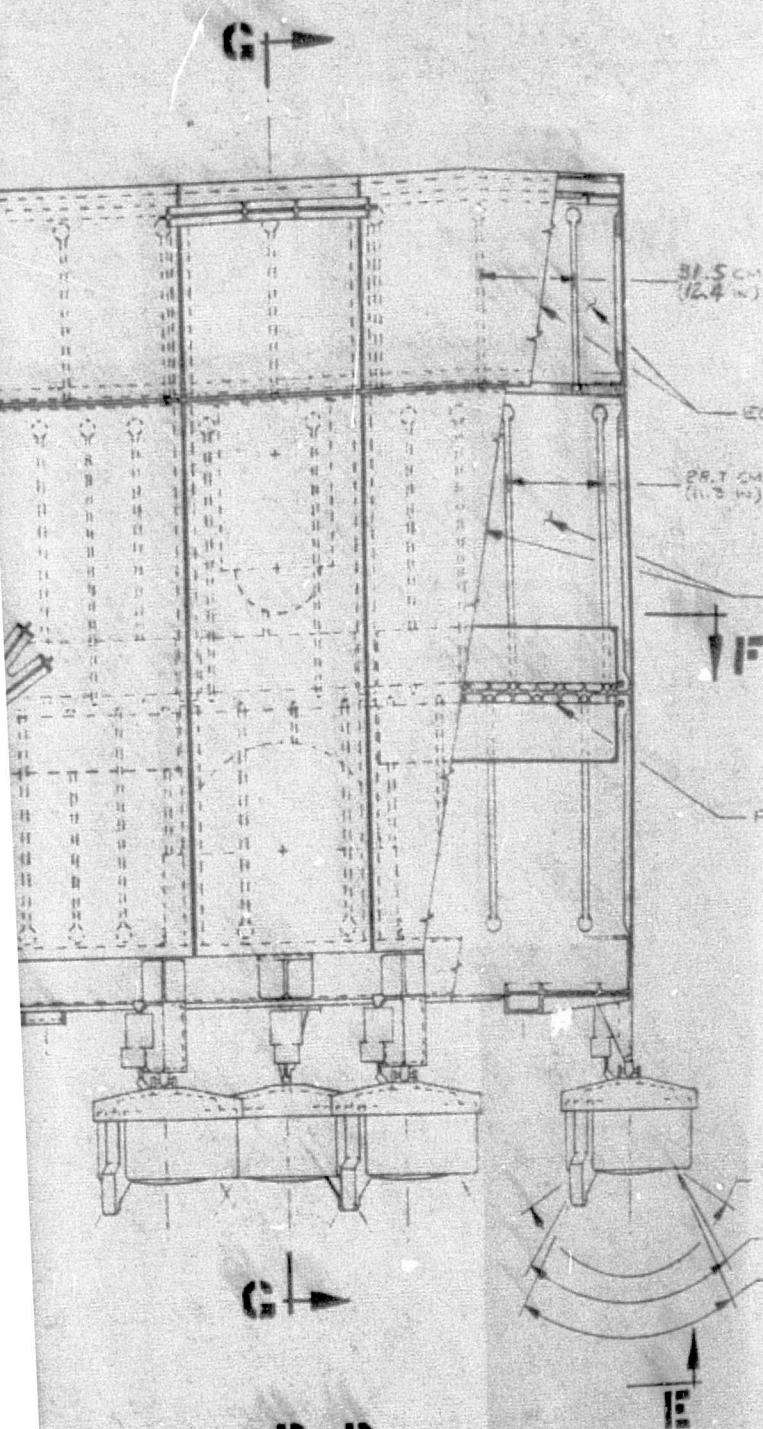

VIEW D-D

FOLDOUT FRAME

4

FIGURE 2-10 SHT 2

1/10	WATKINS	ROCKWELL INTERNATIONAL CORPORATION SPACE DIVISION	2375-13 SHT 2 OF 2
	DATE 12-6-74		
	MODEL		

BASELINE PLANETARY

3.0 THERMAL ANALYSIS

Power Processor Thermal Control Concept Alternatives

The identification of alternative concepts was predicted on a number of key baseline factors:

1. The baseline SEPS configuration provides two opposite surfaces (180° apart) on the SEPS body which are not illuminated by the sun during PP operation.
2. The PP thermal control system is to be basically common for all SEPS missions, planetary and geosynchronous.
3. A total of seven PP's can be operating simultaneously.
4. One PP can be operating with eight PP's not operating. (for example, during a major portion of the Encke Rendezvous mission).
5. The thermal radiator may be integrated with the SEPS structure if practical.
6. Adequate volume is available within the SEPS body to locate the PP electronics internally.

Based on these considerations two tradeoff issues were identified:

1. Thermal control which is an integral part of each 3-kW power processor versus a single common thermal control for all power processors.
2. PP electronics mounted directly to radiator versus PP electronics located internally and connected to the radiator via heat pipes or other heat transfer means.

In the first tradeoff, the integral approach has a weight disadvantage because a separate thermal control system must be provided for each power processor, including the two spares. It is also more difficult to provide thermal control redundancy for each PP without major weight penalty. The common thermal control concept is not affected by the number of spare PP's and, therefore, it is a more flexible design.

In the second tradeoff, the direct mounting to the radiator has the disadvantage of requiring louvers or significant heat power for each power

processor which is not operating. For example, the Encke Rendezvous mission will require louvers or heaters on at least eight power processors.

In summary, five different PP thermal control design concepts have been evaluated. These concepts are briefly described below and are shown on Figure 3-1.

Concept 1 is a Hughes design which was the original baseline. Each power processor is equipped with its own thermal control system consisting of a large thermal radiator covered with louvers. The PP electronics are mounted directly to the inside surface of the radiator. The louvers prevent "freezing" of the power processor when it is not in operation. The combined PP electronics and thermal control packages are installed on the two sides of the SEPS body which are not illuminated by the sun. Therefore, the only major external heat source for Concept 1, as well as for Concepts 2 and 3, is the SEPS solar array.

Concept 2 is basically the LeRC concept in which each PP (including spares) is equipped with its own thermal control system consisting of a variable-conductance heat pipe (VCHP) radiator plus louvers over the PP electronic package. The PP's are installed on the two sides of the SEPS body which are not illuminated by the sun.

Concept 3 also utilizes only the two non-illuminated sides. However, in this concept the louvers are eliminated by locating the PP electronic packages within the insulated SEPS body. Instead of a separate thermal control system for each PP, common thermal control system consisting of VCHP radiators on the two sides is used to accommodate up to 7 PP's operating simultaneously. Therefore, the radiator requirements are not affected by the number of spare PP's carried by the SEPS.

Concepts 4 and 5 utilize all four sides of the SEPS body as common radiators. VCHP radiators are used on the two non-illuminated sides. For the two sides which experience solar illumination. Concept 4 relies on VCHP radiator with very low solar α optical coating (i.e., LMSC Optical

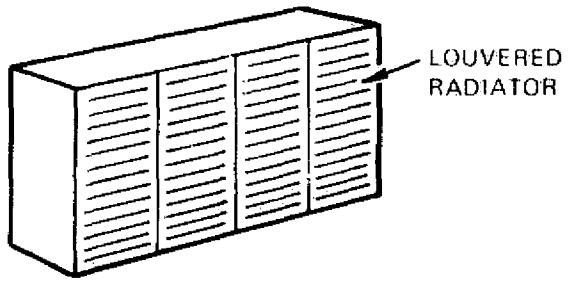

CONCEPT 1. HUGHES TWO SIDE LOUVER

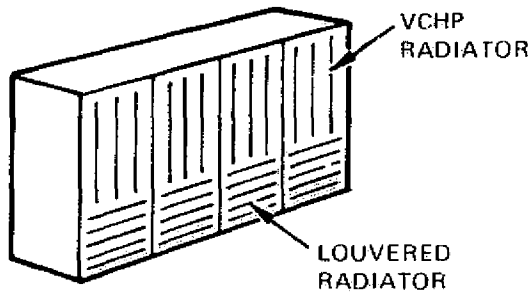

CONCEPT 2. LeRC TWO SIDE VCHP-LOUVER

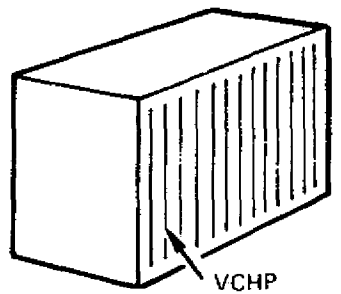

CONCEPT 3. TWO SIDE VCHP

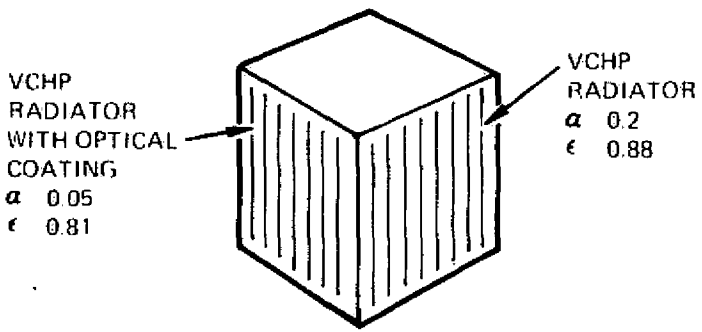

CONCEPT 4. FOUR SIDE VCHP OPTICAL COAT

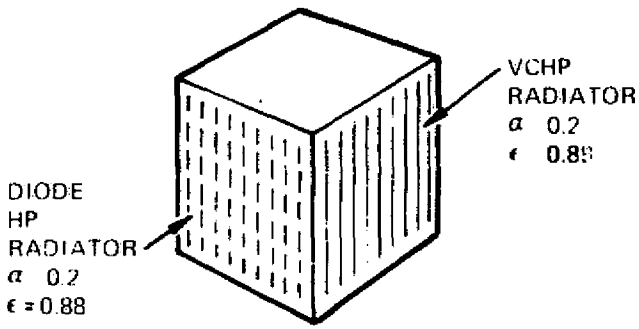

CONCEPT 5. FOUR SIDE VCHP DIODE HP

Figure 3-1. Power Processor Thermal Control Design Concepts

Solar Reflector) to minimize solar heat input, whereas Concept 5 utilizes diode heat pipe radiators to preclude reverse heat flow into the PP electronics.

Analysis Ground Rules and Requirements

Tradeoff analyses of the five concepts were based on a number of key factors, including PP dimensions, temperature limits, heat dissipation, and solar array temperature and view factors. Solar distances ranging from 0.38 AU for the Mercury Orbiter mission to 5 AU for the Jupiter Probe mission were considered.

The dimensions of the power processor are 56.4 x 124 x 20 cm for the original baseline (Hughes) and 45 x 71 x 15 cm for the new baseline (LeRC). The temperature limits of the PP electronics are:

1. Operating 258°K min, 333°K max.
2. Non-operating 223°K min, 373°K max.

The current estimate of PP efficiency is 87 to 92 percent under a full power load of 3-kW input. The thermal analysis was based on a 90 percent efficiency resulting in a 300-W heat dissipation from each operating power processor. An additional power dissipation of 12.5 W per PP was assumed for harness heat load. This totaled 312.5 W per PP or 2187 W (7 x 312.5) for a 21-kW SEPS at full thrust.

For the PP radiators located on the two non-illuminated sides of the SEPS body, the main external heat source is the solar arrays. The variation of the PP louver or radiator to solar array configuration factor as a function of PP to solar array distance and tilt angle is given on Figure 3-2. The effect of the solar array was included in the analysis by assuming that it is approximately 2.50 m from the louver plane, and that the configuration factor, F_L-SA, is 0.12. The temperature of the solar array as a function of solar distance is given in Figure 3-3. The PP heat rejection requirements and the heater power requirements were determined as a function of the solar array temperature. The solar array temperature range used was between 153°K and 423°K in establishing these requirements.

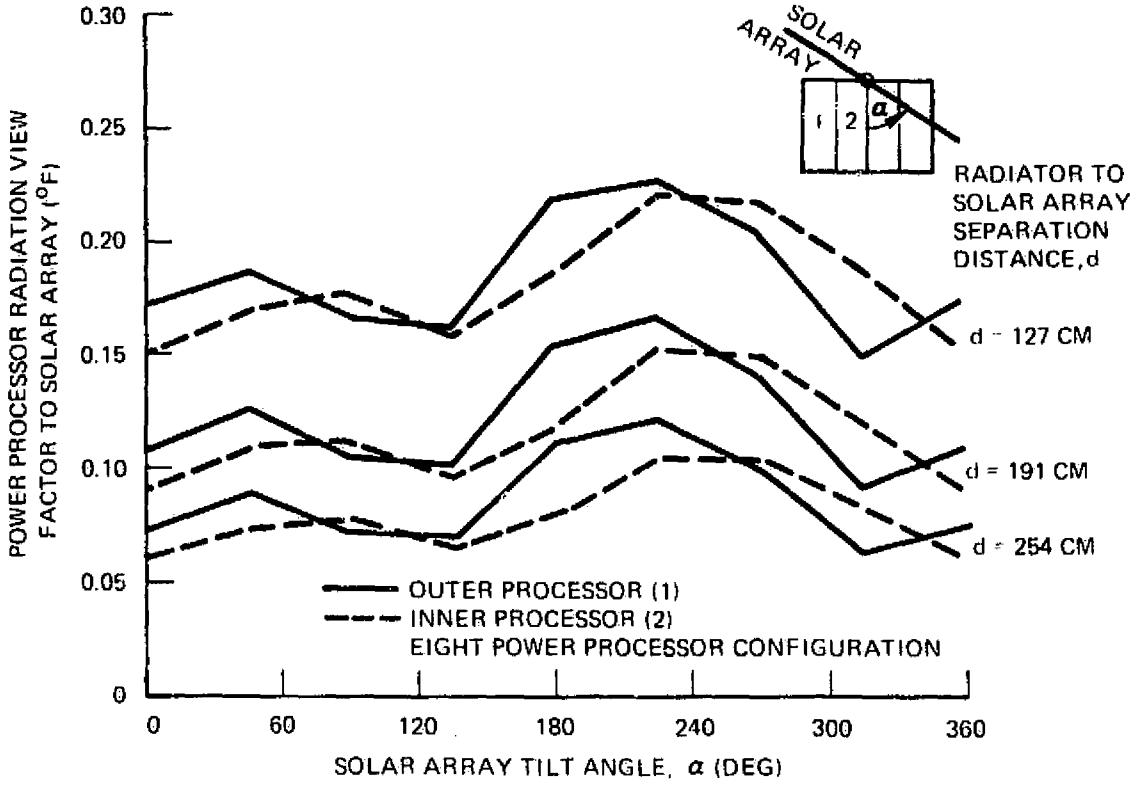

Figure 3-2. PP Radiator to Solar Array Configuration Factor

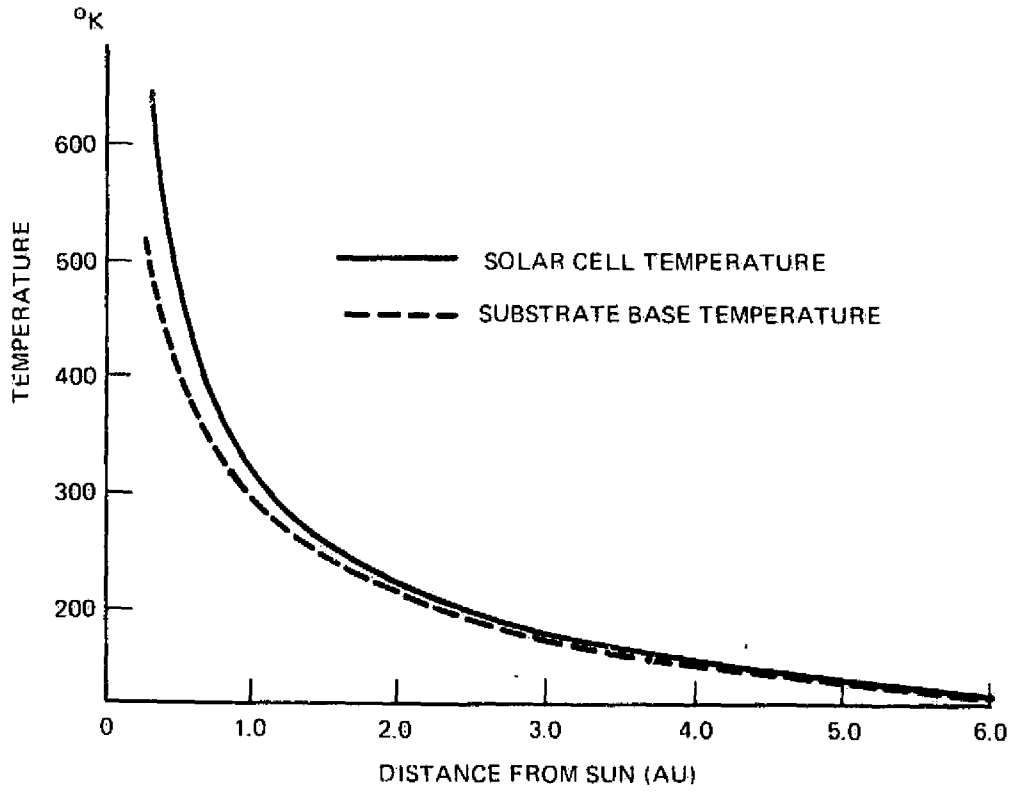

Figure 3-3. Solar Cell/Substrate Temperature

Concept 1 - Hughes Louver

In this concept the electronic modules are mounted on one side of a radiator panel, allowing the other side to radiate directly to space through bimetallic thermostatically controlled louvers. The PP's are mounted side by side on the two surfaces not illuminated by the sun. The other surfaces are covered with multilayer insulation. The basic configuration of the Hughes PP is shown on Figure 3-4. The area of the PP is $0.7M^2$. The baseline power dissipation of each module at full power condition also is indicated on Figure 3-4. It was assumed in the analysis that the multilayer insulation has an effective emittance (ϵ_{eff}) of 0.03 and α_s = 0.05 - 0.12. For missions other than the Mercury Orbiter (0.38 AU) where low α_s/ϵ outside surface is required (α_s/ϵ = .05 - .1), the outside surface properties can be α_s/ϵ = .1 - 0.15 corresponding to back aluminized FEP teflon.

The thermal analysis was performed by using a multinode model of each PP, where each module was represented by a node, combined into a cluster of eight, and solved by Rockwell's digital thermal analyzer program. The thermal network and detail calculations are shown in the Appendix A-1 page 1-13. Initially the analysis was performed using a PP area of $0.7M^2$. Average and hot spot temperatures were determined for the PP's considering 1.0 AU and .38 AU solar distances. The louver characteristics used in the analysis are shown on Figure 3-5. The results on Figure 3-6 indicate that the temperatures for 0.38 AU and 1.0 AU are almost identical due to the different solar array position in respect to the louvers at .38 AU and 1.0 AU. The results also indicate that hot spot temperatures on the PP are well over the 333°K max. temperature limits, while PP average temperatures are only 2°K above that value.

Additional analyses results indicate that a radiating surface area of $1.06M^2$/PP is required to keep temperatures on the panel below 333°K as shown on Figure 3-7. This indicated that the $0.7M^2$ Hughes configuration must be anlarged to satisfy the requirements assumed in the Rockwell analysis.

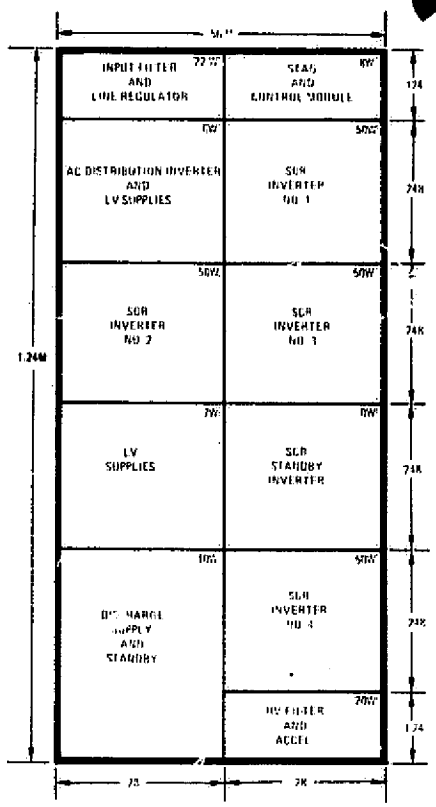

Figure 3-4. HRL Power Processor

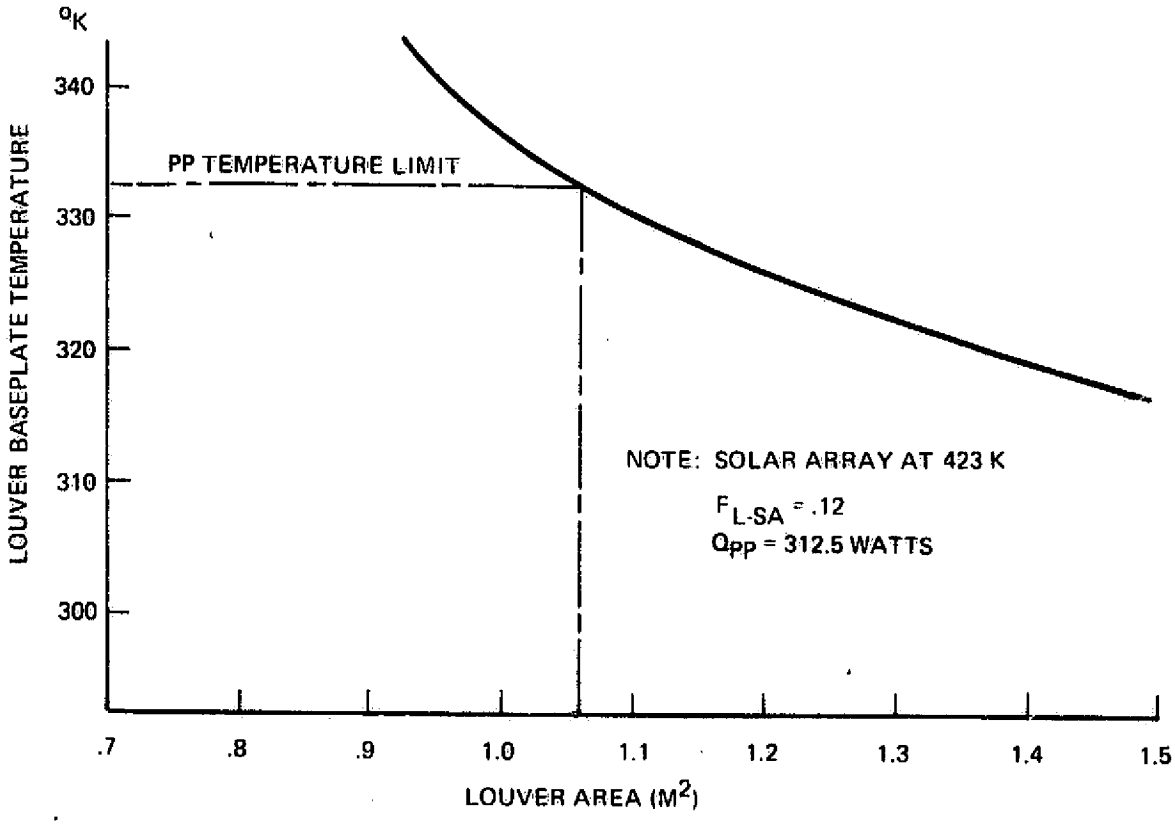

Figure 3-7. Louver Baseplate Temperature

BASE RADIATOR - OSR REF. AIAA 72-268

ϵ_{EFF} =0.15 AT FULL CLOSED

0.73 AT FULL OPEN

α_{EFF} WORST CASE FOR SUN AT EACH SIDE

AT 0° OR 180° SUN ANGLE

10° OR 170° SUN ANGLE

20° OR 160° SUN ANGLE

30° OR 150° SUN ANGLE

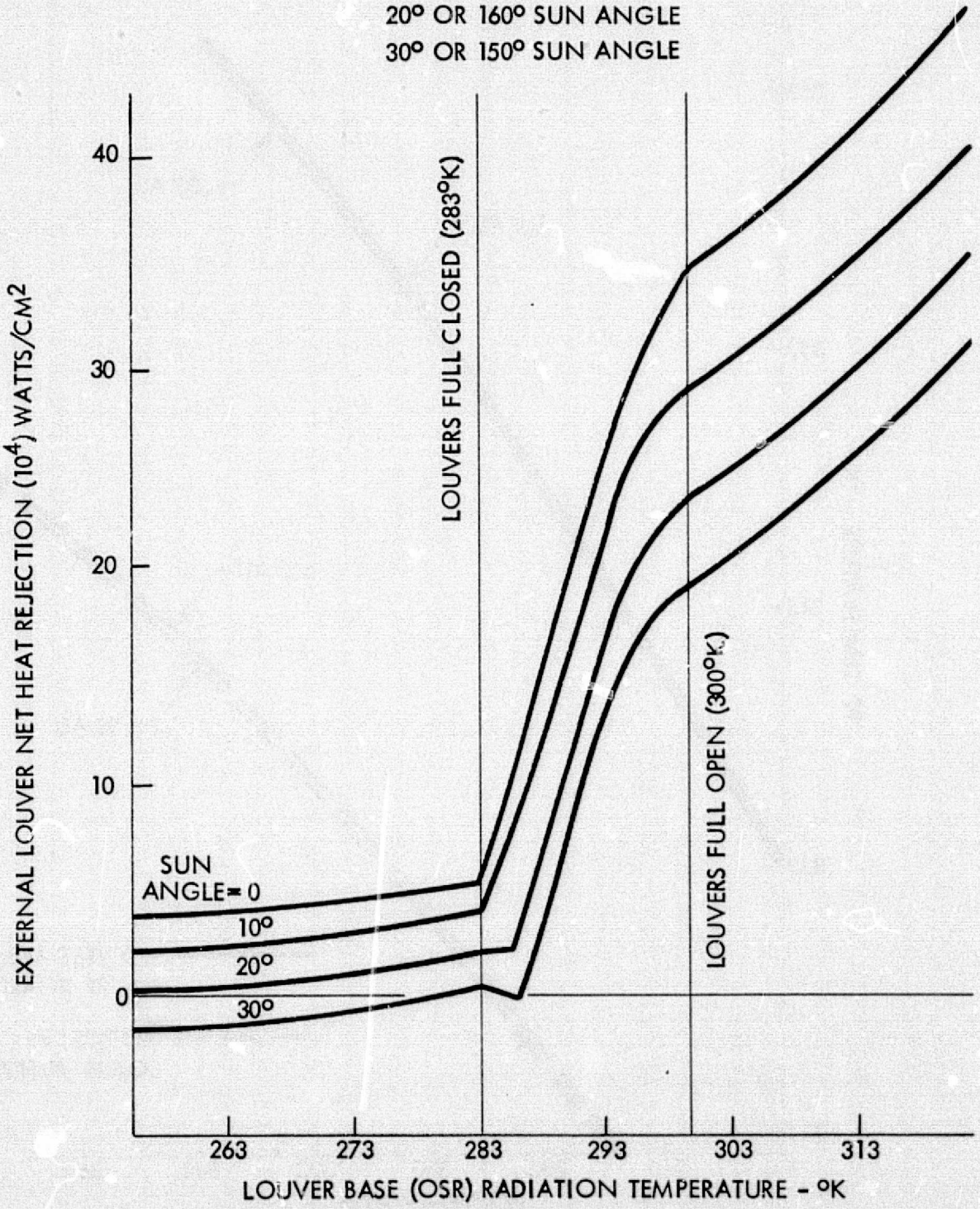

Figure 3-5. Louver Characteristics

NOTE: ALBEDO AND EARTH EMISSION EFFECTS INCLUDED AT 1.0 AU.

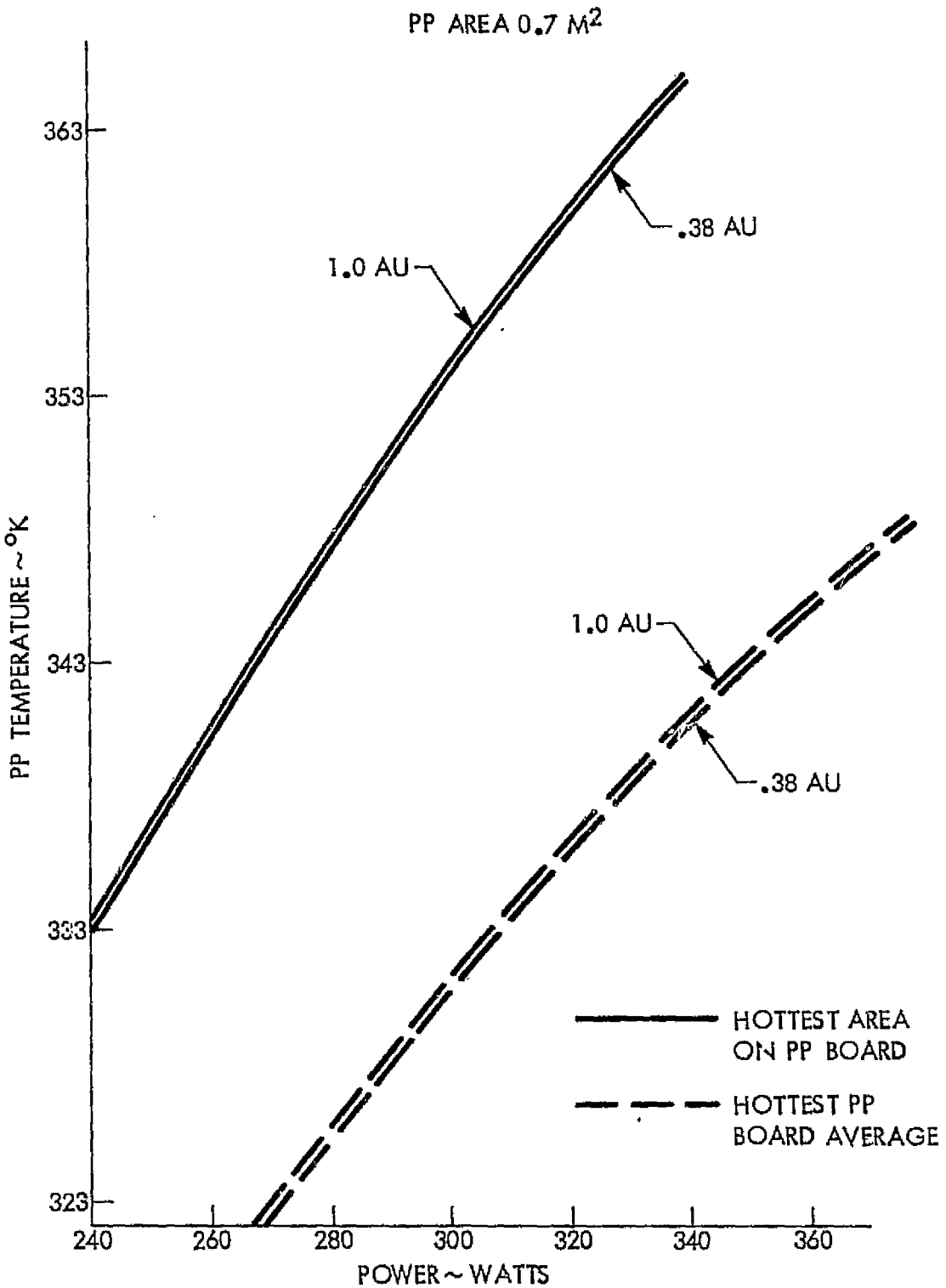

Figure 3-6. Power Processor Temperature - Concept 1

Concept 2 - LeRC Two-Side VCHP - Louver

The thermal control design concept developed by LeRC is illustrated in Figure 3-8. The electronic components are located on "Z" sections held by two shear plates in contrast to the Hughes concept where a single panel served as the electronics mounting plate. The new PP packaging design results in a smaller electronics package and a louver area of 0.327 M^2. Variable conductance heat pipes transport the heat from the PP's to the radiators. In this design, each PP has its own radiator. The heat pipe design details are given in Table 3-1. The same heat pipe design was used on the Communications Technology Satellite (CTS) for the transmitter experiment package thermal control. The radiator panel thickness was assumed to be .10 cm together with radiator emissivity of ε = .88 and solar absorptance of α_s = ?? (S13G Paint)

The analysis of this system for the maximum power condition with louvers fully open, ε_{eff} = 0.7, shows the louver heat rejection to be 122.5 W/PP assuming 328K for the louver baseplate temperature. Assuming a fin efficiency of 86 (η = .86) percent for the radiator sizing resulted in the heat pipe spacing of 0.23 M (0.115 M fin length). The radiator area was then determined to be 0.609 M^2/PP assuming 328°K average radiator temperature. In the thermal design and analysis it was assumed that a narrow light weight sun shield will be deployed around the louvers and radiators and therefore no solar flux is expected on them. Consequently the effective radiator area is a function of the solar array temperature only as shown on Figure 3-9. The variable-conductance heat pipes regulate the effective radiator area depending upon the existing solar array temperature. The calculations performed to derive the indicated results are in the Appendix A-2. The system heater power requirements are shown on Figure 3-10 as a function of the solar array temperature to maintain the PP's at 223°K non-operating survival temperature.

Concept 3 - Two-Side VCHP

This PP thermal control design concept also utilizes the unilluminated sides of the SEPS body to radiate to deep space. However, in this concept the louvers are eliminated by locating the PP electronic packages within the

Table 3-1. LeRC Heat Pipe Design Details

Concept 2

Item	Characteristics
Tubes	304 Stainless Steel, 1.27 cm O.D. x 0.071 cm wall, internally threaded with 100 TPI, 0.0127 cm deep, 40° included angle grooves.
Reservoirs	304 Stainless Steel, spun hemispherical cap with 4.445 cm O.D. cylindrical center section. Reservoir to condenser volume ratio varies from 1.5 to 2.0.
Wicks	Reservoir: 304 stainless steel metal felt, 0.051 cm thick, spot welded to interior walls. Tube: 304 stainless steel metal felt, 0.127 cm thick, interference fit across diameter of tube. Arteries: 150 mesh 316 stainless steel screen formed and welded to 0.16 cm I.D. tubes and spot welded to diametral wick. Priming Foils: 0.00127 cm thick 304 stainless steel foil with 0.025 cm holes, formed and welded to 0.16 cm I.D. tubes and spot welded to ends of arteries and diametral wick.
Saddles	6061 aluminum alloy extrusion soldered to tubes.
Working Fluid	Methanol, spectrophotometric grade.
Control Gas	90% nitrogen, 10% helium, research grade.

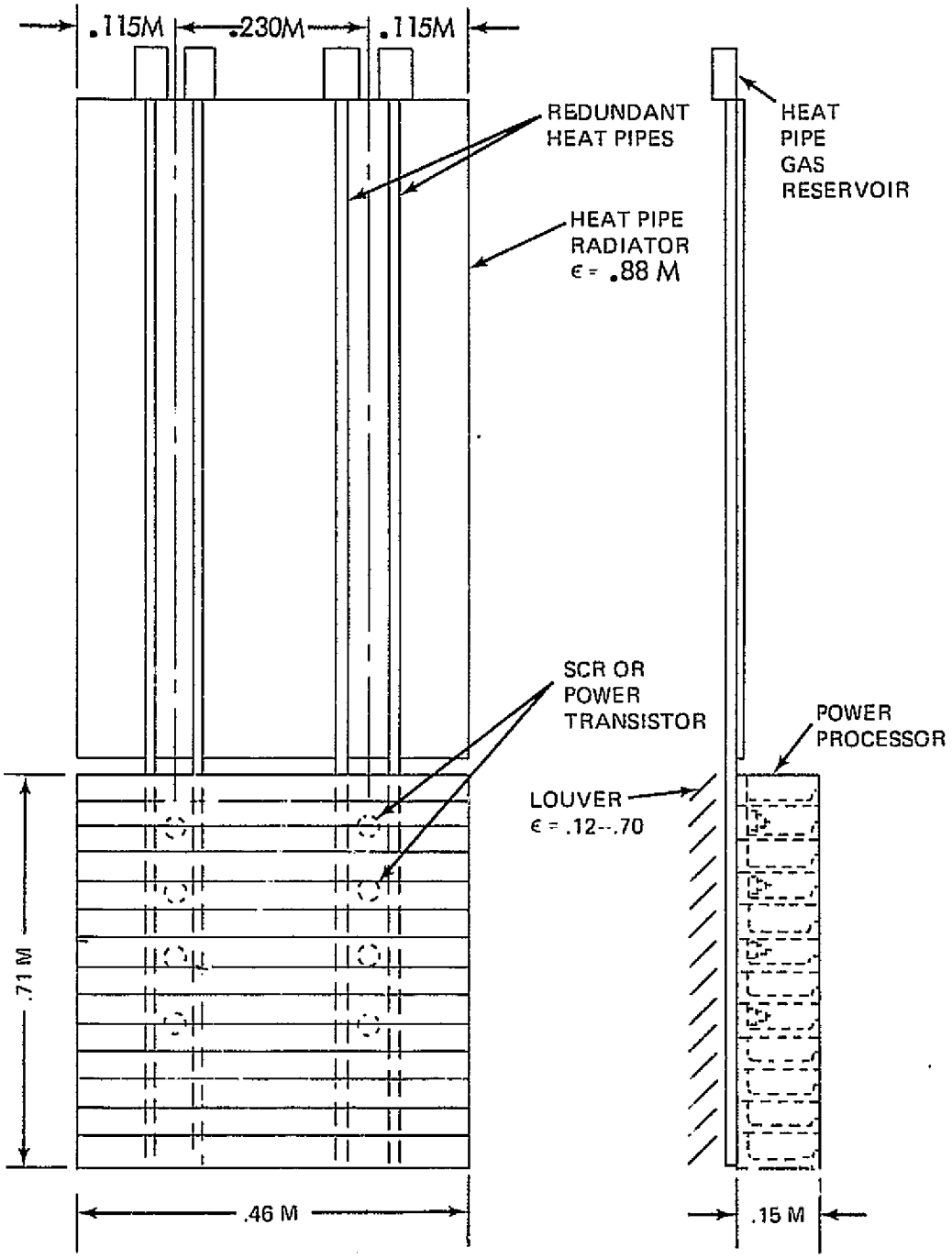

Figure 3-8. LeRC Power Processor - Concept 2

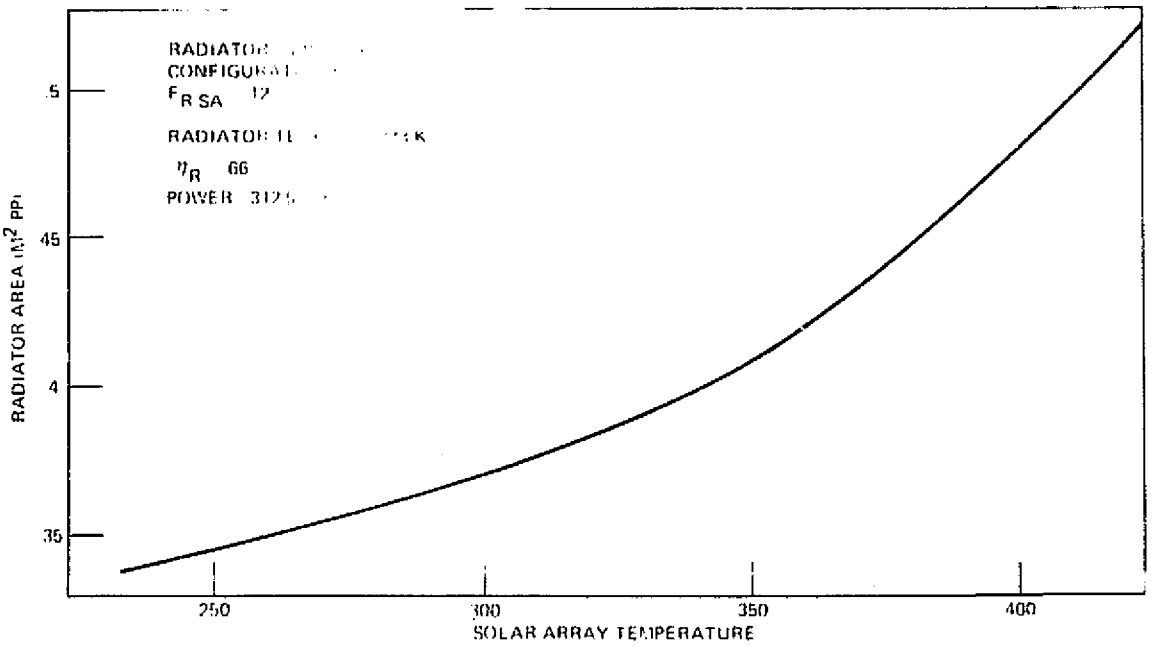

Figure 3.9. Radiator Area vs Solar Array Temperature - Concept 2

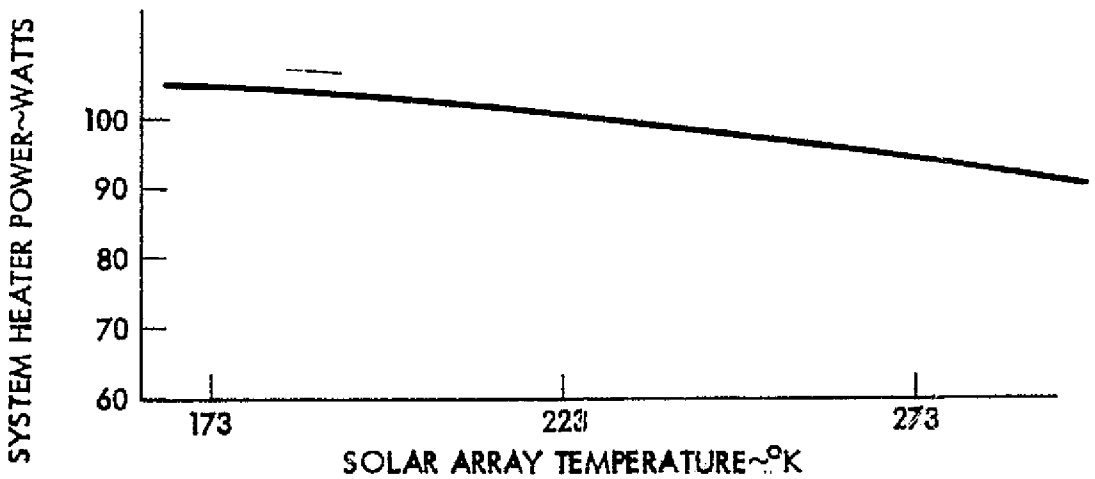

Figure 3-10. LeRC (Concept 2) Heater Power Requirements

Table 3-2 Rockwell Heat Pipe Design Details

Item	Characteristics - Concept 3-5
Tubes	6063-T6 aluminum, 1.27cm O.D. x 0.089cm wall thickness (minimum); 0.419cm inside radius. Heat pipes are one-piece extrusion.
End Caps	6061-T6 aluminum welded to ends. Fill tube is 0.635cm O.D. x 0.016cm I.D.
Grooves	20 grooves, 0.127cm diam. truncated to a 0.025cm wide opening. Grooves are integrally extruded with the tube and welded at ends to prevent intragroove communication.
Saddles	Two flanges, 4.4cm wide x 0.010cm thick, integrally extruded with the tube and groove. Base is flat to 0.001 in./in. and <125μ in. finish.
Reservoirs	1.9cm long x 3.8cm O.D. cylinder with hemispherical ends; 0.016cm wall 6061-T6 aluminum. Reservoir to condenser volume ratio >1.0.
Working Fluid	N-butane, research grade (99.9% pure).
Control Gas	Helium, research grade.

insulated SEPS body, thus isolating them from environmental changes. Instead of a separate thermal control system for each PP, a common thermal control system consisting of VCHP radiators on the two sides are used to accommodate up to 7 PP's operating simultaneously. Therefore, the radiator requirements are not affected by the number of spare PP's carried by the SEPS.

During the analysis several design configurations have been evaluated by considering different radiator temperatures, efficiencies, and thicknesses. For the radiator surface coating S-13G or similar white paint having surface properties of α_s = 0.2 and ϵ = 0.88 was assumed. The nine

PP's are located inside the insulated SEPS body on a common shelf. A total of 26 VCHP's connect the PP's to the radiators. This design configuration is shown on Figure 2-10. The PP electronics package and physical dimensions are identical to the design developed by LeRC (0.46m x 0.71m). Figure 3-11 presents the effective radiator area as a function of radiator temperature and efficiency for the maximum case with total power dissipation of 2187.5W (312.5W/PP). From this figure, at 0.38 AU where the solar array temperature would equal 423°K with a radiator temperature of T_R = 328°K and a radiator efficiency of η_R = 0.785, the effective radiator area is determined to be approximately 0.96M^2/PP. The total radiator area for 7 PP is therefore 7 x 0.96 = 6.72M^2. Because of structural and dynamic considerations, the final design point was selected to have a radiator efficiency of η_R = 0.8 (80%) with a t = 0.1cm radiator thickness. This resulted in a total radiator area of 6.65M^2 (0.95M^2/PP). The preliminary design calculations are shown in Appendix A-3 page 1-20. Detailed computer analysis verified the preliminary calculations.

The PP shear plate temperature derived by digital computer techniques, as a function of the solar array temperature are shown in Figure 3-12. This figure indicated that with a PP heat load of 2187.5W (312.5W/PP) the PP electronics package shear plate will be at 328°K, and the radiator temperature will be about 2°K lower than the design goal of 328°K. The average electronics shear plate temperature of 328°K will allow a 20°K temperature rise to the 348°K electronics junction temperature required by reliability.

The heat pipe design details are shown in Table 3-2. The VCHP geometry is presented in Figure 3-13.

Several methods of attaching the heat pipes to the radiator skin were investigated. Some of the configurations are shown in Figure 3-14.

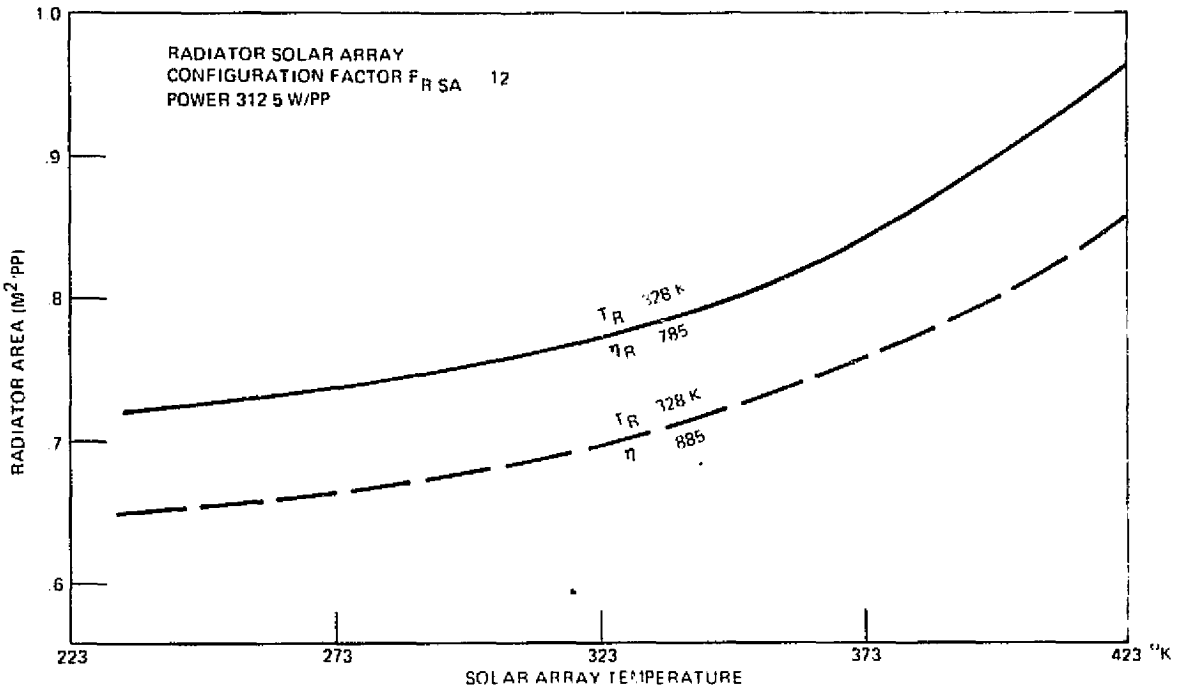

Figure 3-11. Radiator Area/PP - Concept 3

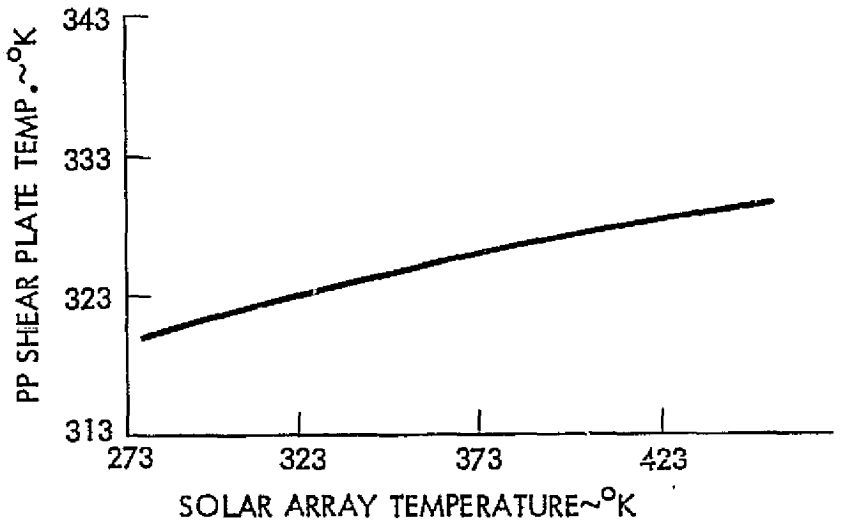

Figure 3-12. PP Shear Plate Temperature Variation - Concept 3

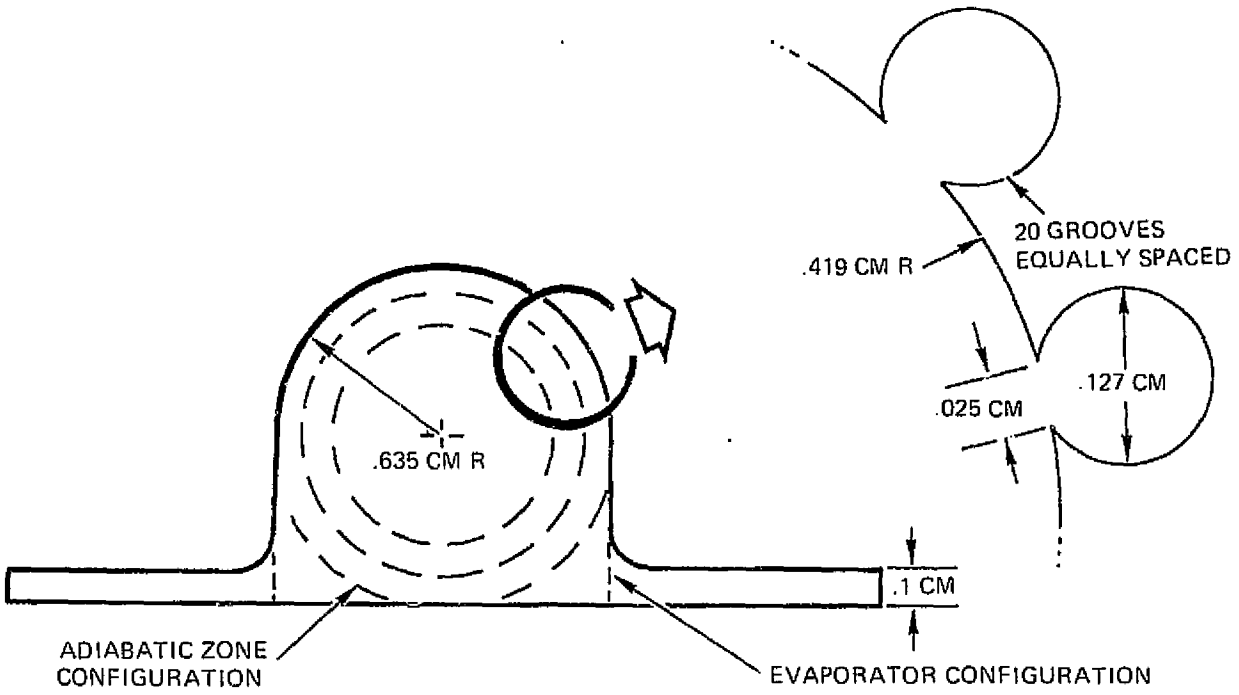

Figure 3-13. VCHP Geometry - Concept 3

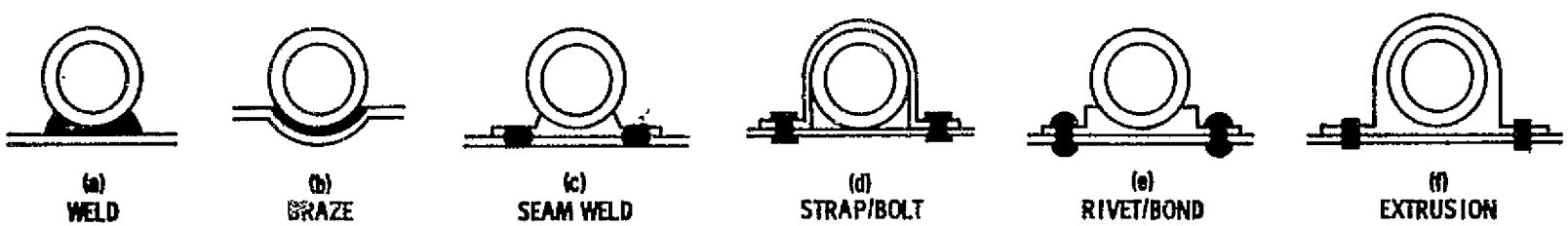

Figure 3-14. Heat Pipe to Radiator Attachment Methods

Brazing or welding, Figures 3-14a and 3-14b was felt thermally to be the best approach, but was undesirable from a fabrication standpoint. The temperatures associated with welding or brazing would require re-heat treatment of the pipes and skin and a reprocessing of the heat pipes after the operation. Quenching the assembly after heat treat would also distort the system considerably. Other methods included seam welding heat pipes with flanges, and riveting or bolting the heat pipes with flanges or flanges made out of extrusion with a thermally conductive grease or adhesive in between. The system finally selected, shown on Figure 3-14f, has an interface heat transfer coefficient of 876 $W/M^2°K$ or better as the design goal. Figure 3-15 shows the effect of the heat transfer coefficient on the interface conductance between the radiator and VCHP saddle. Figure 3-16 demonstrates the effect of the heat transfer coefficient on the PP shear plate temperature. A wicked, cold reservoir heat pipe was selected for the system because it is the simplest, most reliable gas controlled variable conductance system. It is also the least costly to fabricate and integrate into spacecraft design. The broad control range (258°K to 333°K) permits the reservoir to experience large variations in temperature and still provide adequate control with modest storage capacity.

Butane was selected as the working fluid because it has sufficient transport capability in the operating temperature range and has a very low freezing point (135°K). The low freezing point is required to avoid diffusion freeze-out that could occur at the low temperature sink condition. If the effective sink temperature is below the melting point of the working fluid, there is a continuous diffusion of vapor into the sub-freezing zone where the vapor freezes and is lost to the system. This will result in a deficiency of liquid in the active portion heat pipe and can ultimately lead to burn-out and loss of control. By properly coupling the radiator and reservoir to the spacecraft interior, the temperature of the inactive portion of the heat pipe can be kept above the freezing point of butane at the minimum load and sink condition.

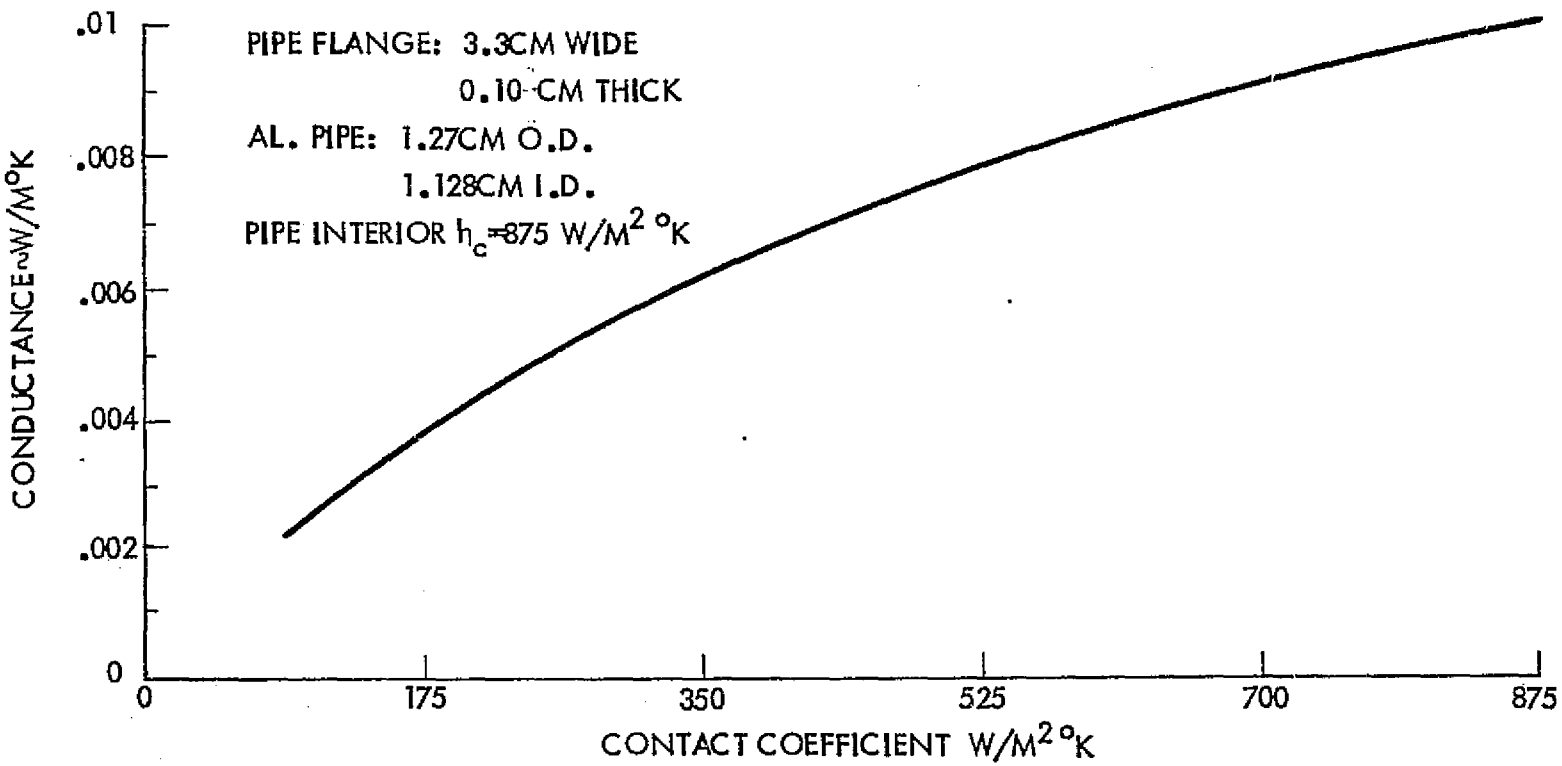

Figure 3-15. Conductance Between Heat Pipe and Radiator

The gas reservoir requirements are shown in Figures 3-17 and 3-18 as a function of source temperature control band for various maximum reservoir temperatures. The operating temperature at the maximum condition was taken as 333°K and the minimum effective sink temperature at 140°K. The reservoir would be thermally coupled in such a way that at minimum condition it would be above the freezing point of butane.

When the PP's are not operating, their temperature must be maintained above 223°K which is the non-operating survival temperature limit. VCHP's were selected for the PP thermal control system (TCS) because they have the ability to shut off the radiators during the cold outbound missions when the PP's are operating at a minimum power level and very little internal heat is being dissipated. This desirable feature reduces the heater power required to maintain the PP's at or above the survival temperature of 223°K. Since the radiators are shut off from the system (cold mode), the only heat leak from the thermal control system is that conducted through the heat pipe walls and saddles. The necessary heater power to maintain the temperature limit condition is shown on Figure 3-19 as a function of the solar array temperature. For example, for a solar array temperature of T_{SA} = 173 K at 3.3 AU, the total required heater power is approximately 63.5 W which corresponds to 7.06 W/PP.

Concept 4 - Four Side VCHP Optical Coat

Preliminary structural and dynamics requirements indicated that a thicker or square cross-section SEPS body was preferred over the narrow rectangular cross-section design. The thicker SEPS body would make four sides available for radiating surfaces as compared to the two sides used for the narrow cross-section design. Of the two added sides, one or the other may be illuminated by the sun during all or part of the mission. This results in a maximum incident heat flux of 9618 W/M^2 at 0.38 AU for the mercury orbiter mission. To minimize the amount of solar radiation absorbed, a second surface mirror coating was selected which

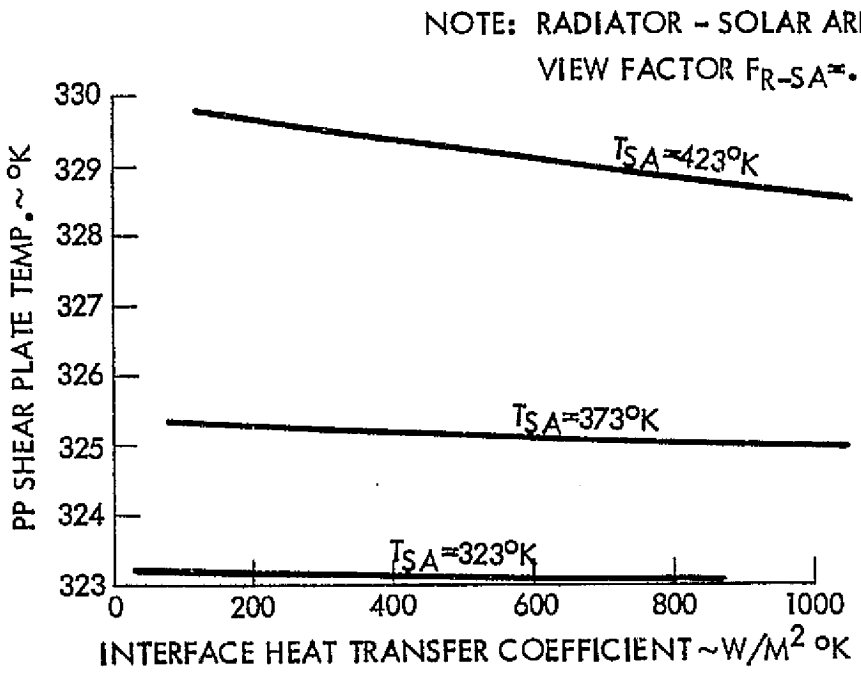

Figure 3-16. PP SHEAR PLATE TEMPERATURE - CONCEPT 3

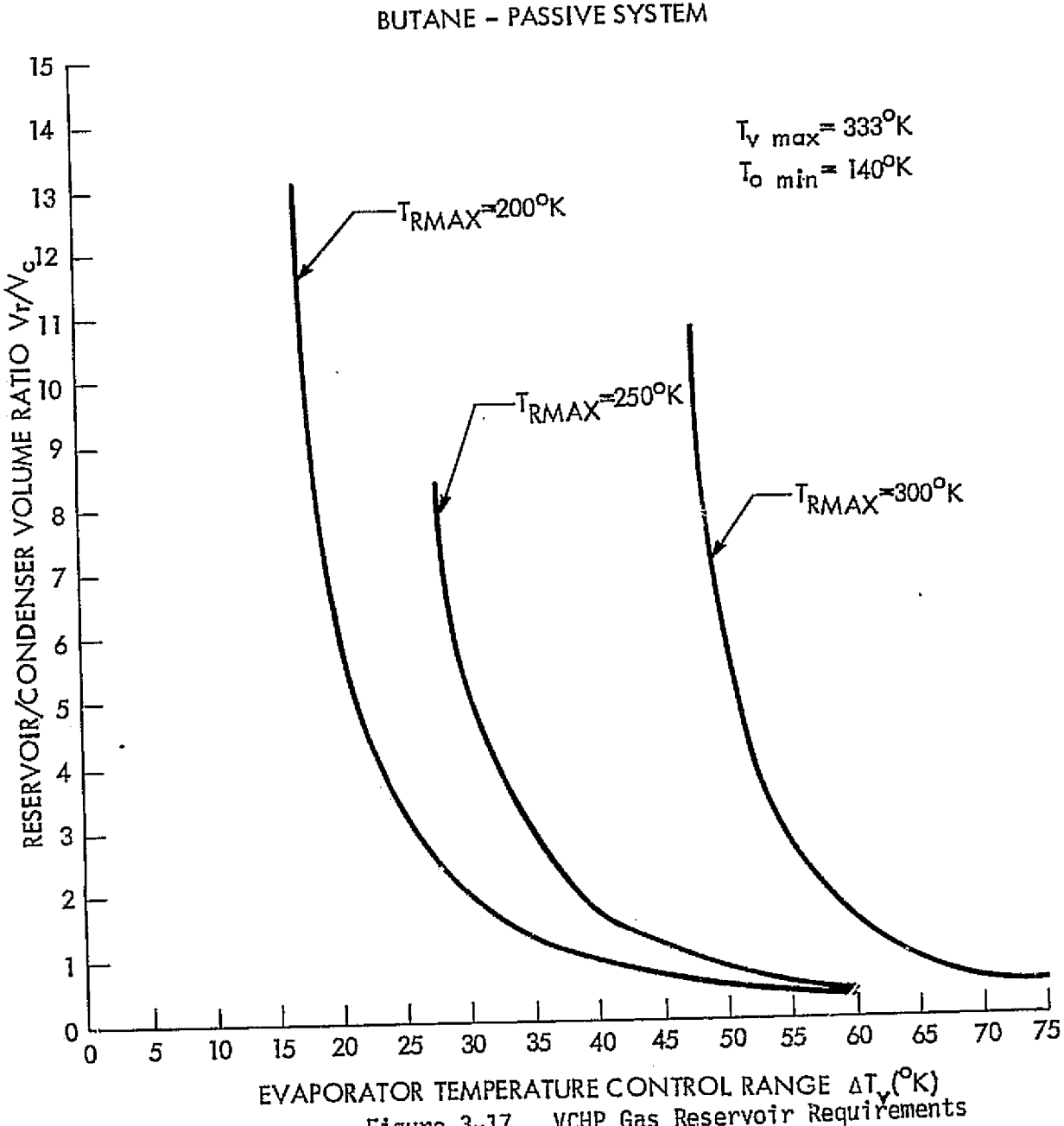

Figure 3-17. VCHP Gas Reservoir Requirements

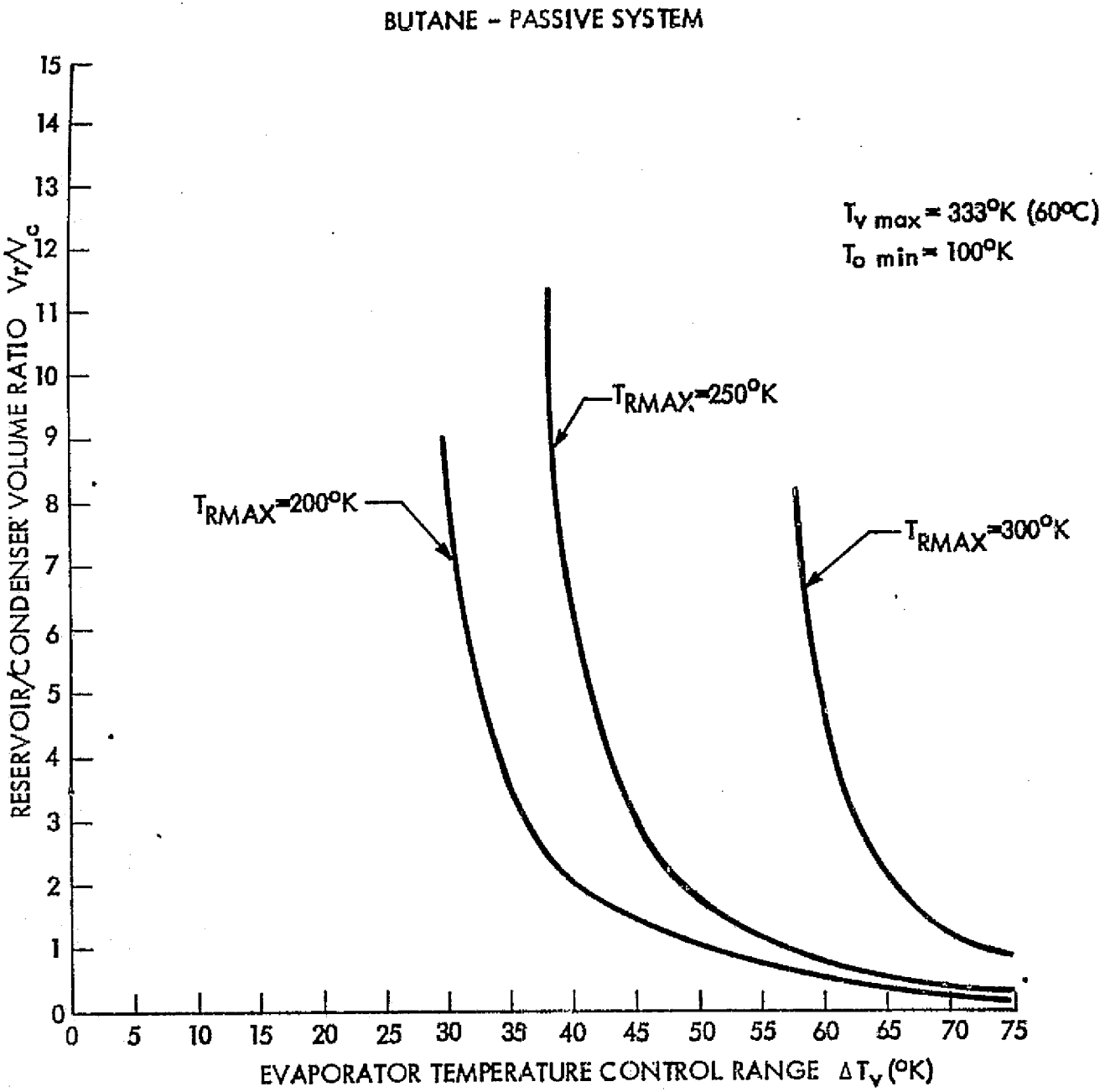

Figure 3-18 VCHP Gas Reservoir Requirements

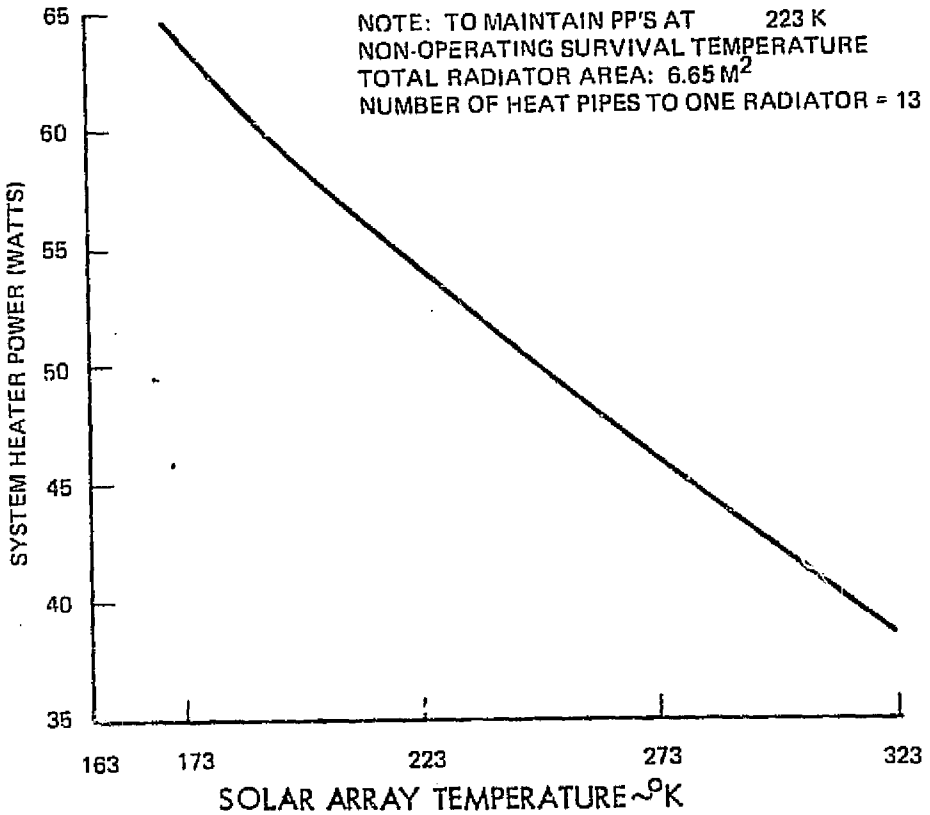

Figure 3-19. System Heater Power Requirements - Concept 3

has optical properties of a very low absorptivity to emissivity ratio $\alpha_s/\varepsilon = 0.06$. A typical coating is the Lockheed Optical Solar Reflector (OSR) which has the above optical properties and also has shown very little degradation over a test period of 10,000 equivalent sun hours. The two surfaces that are not illuminated by the sun would have a coating with an $\alpha_s/\varepsilon = 0.2$.

Dissipated heat from the operating PP's mounted within the SEPS is transported to the radiators by means of ..HP's. The heat pipes are designed to handle the heat dissipated by seven PP's operating simultaneously at full power. Parametric studies were made by varying the external dimensions of the SEPS body to determine the minimum radiator area that

could handle the maximum anticipated heat load. These study results (delineated in Appendix 4) were made available for integration into a structural/solar array optimization analysis to define the SEPS baseline configuration. Figure 3-20 shows the radiator area as a function of PP heat dissipation, and a solar heat load at 0.38 AU, and aspect ratio (L/W). The aspect ratio (L/W) is the ratio of SEPS body thickness (L) to body width (W). The solar array temperature was assumed to be 423°K. The view factor of 0.12 between the solar array and adjacent radiator corresponds to a solar array/radiator distance of 2.5 M. The radiator temperature was maintained at 328°K to allow for a temperature gradient of 20°K between the PP junction and the PP shear plate. Temperature gradients in the system result from interface resistances between the heat pipe evaporator and heat pipe-radiator interfaces. The fin efficiency of 88.5 percent which was used in the analysis corresponds to a radiator thickness of 0.1 cm and fin length of 15.3 cm. Data indicate that with increasing aspect ratio (L/W) of the SEPS body, the required radiator area also increases. For the baseline heat dissipation of 312.5 W/PP, the radiator area required per operating PP is 0.85 M^2 and 1.08 M^2 for aspect ratios of 0 and 1.0 respectively. A zero aspect ratio, which theoretically corresponds to the zero thickness SEPS body, requires 0.2 M^2 less radiator area/PP than the square body design. Therefore, this concept does not optimize for a thick body design.

For out-bound missions, when the variable conductance heat pipes are in the cold operational mode, the radiators are shut off. Thus, the only heat leak from the thermal control system is through the heat pipe walls. Figure 3-21 shows the heater power required as a function of solar array temperature, to maintain the power processors at a non-operating survival temperature of 223°K. The calculations for the heater power requirements are presented in Appendix 4.

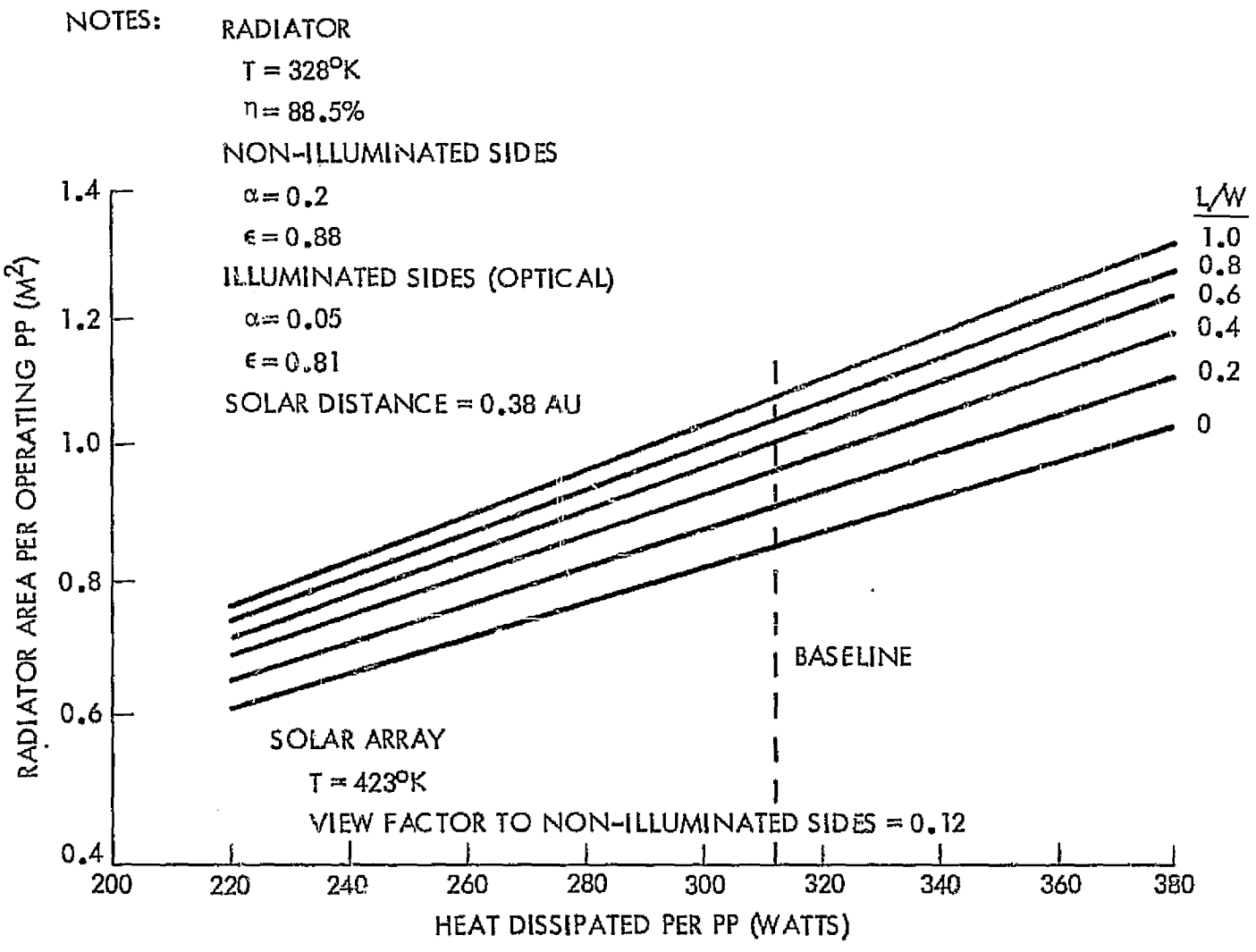

Figure 3-20. Radiator Area Requirements for VCHP/OSR Concept 4

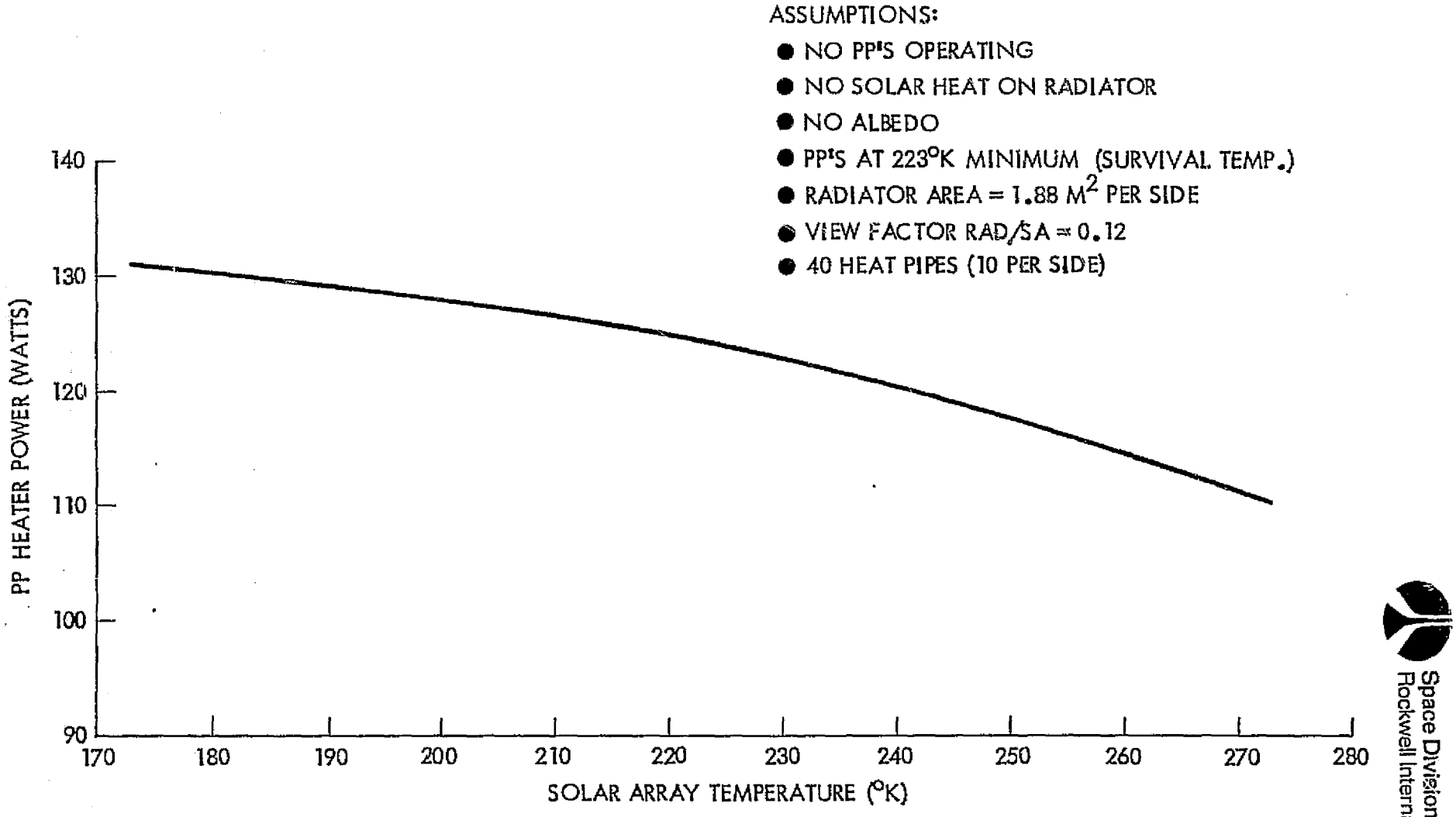

Figure 3-21 Heater Power Requirements for VCHP/OSR Concept 4

Concept 5 - Four Side VCHP Diode HP

Concept 5 also utilizes four sides of the SEPS body as radiators. Rather than using optical coatings as in Concept 4, diode heat pipes are used for the two sides which may experience sun illumination. The diode heat pipe (DHP) is designed to restrict heat flow to one direction only and would preclude reverse flow from the two sun-illuminated radiators into the PP electronics. In the normal mode, heat is absorbed at the PP's and radiated at the condenser. In the reverse mode, when the radiator is illuminated by the sun, the working fluid transfers heat to the PP's. However, this is temporary because the fluid is trapped at the evaporator end of the pipe, thereby stopping the reverse heat flow.

A parametric thermal study was made of Concept 5, and the calculations are presented in Appendix 5. For this analysis, the optical properties of all four radiators were assumed to be α_s = 0.2, ε = 0.88. The results of the study, presented in Figure 3-22 indicate that for the baseline heat dissipation of 312.5 W/PP, the required radiator area decreased from 0.855 to 0.798 M^2 per PP as the aspect ratio increases from 0 to 1.0. This is just the reverse of the Concept 4 Four Side VCHP Optical Coat results, which showed the radiator area to increase with increasing aspect ratio. The radiators were sized to maintain the PP shear plate at 328°K, 20°K below the PP allowable junction temperature of 348°K.

The diode heat pipes have the same cold mode shutoff characteristics as the VCHP systems during the outbound mission when the PP's are non-operational. The heater power requirements for the diode system are presented in Figure 3-23 and indicate less heater power required for this system as compared to Concept 4. The heater power calculations are presented in Appendix 5.

To verify the calculated results for the radiator area requirements, an analytical thermal model was constructed to simulate the VCHP/DHP

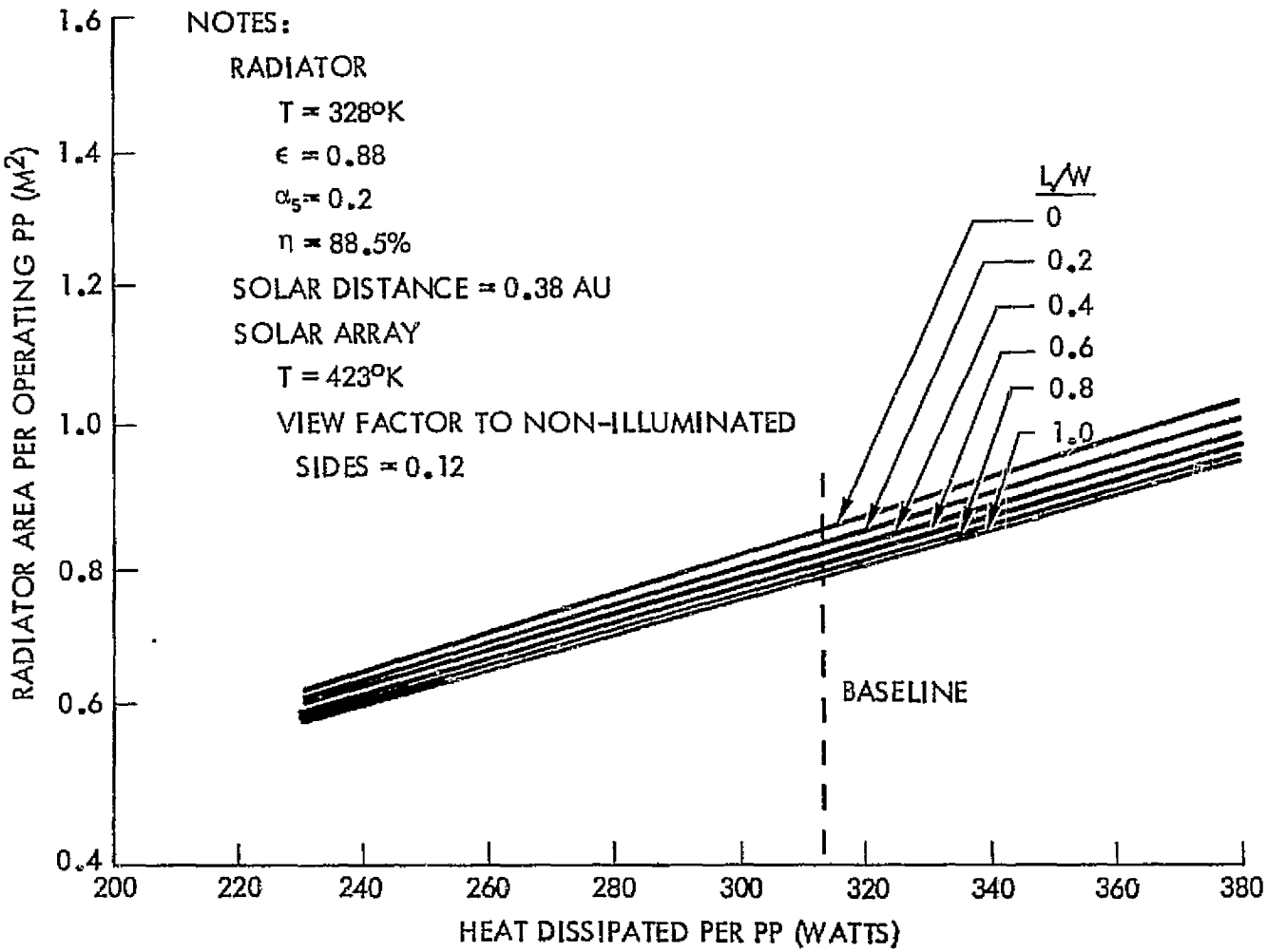

Figure 3-22. Radiator Area Requirements for VCHP/DHP Concept 5

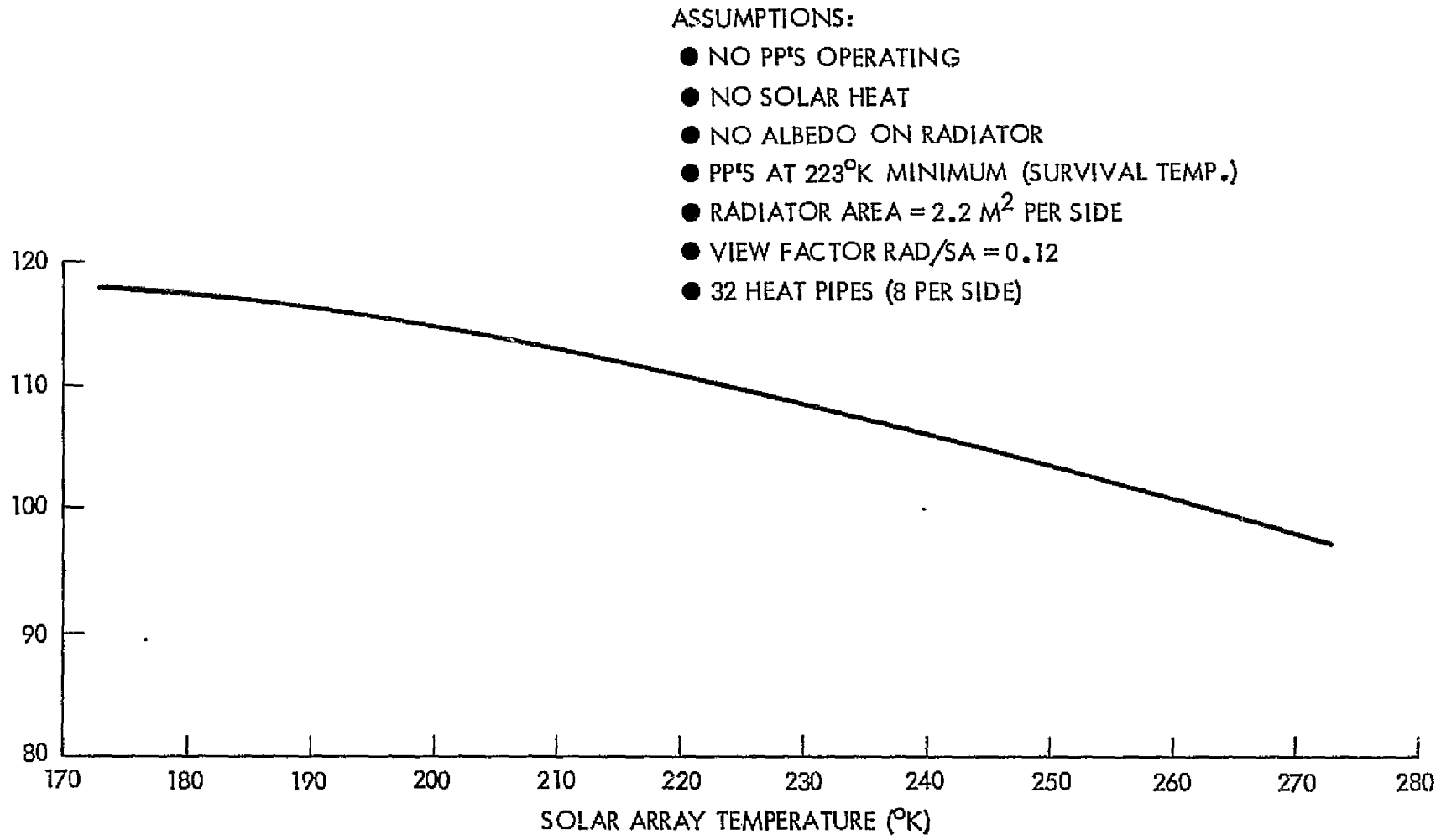

Figure 3-23. Heater Power Requirements for VCHP/DHP Concept 5

thermal control system. The model shown in Appendix 5, consists of one VCHP, one DHP and the associated fin area corresponding to a radiator area with an aspect ratio L/W - 1.0 as defined in the parametric study. The operational characteristics of VCHP and DHP were included in the model, i.e., the conductance of the radiator fin varied as the location of the control gas/vapor interface changed, and the diode radiator section would shut off when the heat flow reversed from PP to radiator to PP from radiator. The resulting shear plate temperature for a 0.38 AU mission, using the thermal model, was 327°K and was within 1°K of the calculated temperature of 328°K. For the cold case, simulating an outbound mission, the model results were again in good agreement with the calculated data and indicated that with a heater power input of 117.9 watts the PP section temperature will be maintained at 232°K. This is above the survival temperature of 223°K.

EQUIPMENT COMPARTMENT THERMAL ANALYSIS

For designing the Equipment Compartment (EC) thermal control system two basic concepts were evaluated: (1) Louver system, (2) VCHP - radiator system. The EC is located at the upper section of the SEPS body above the PP's.

The basic difference between the PP and EC thermal control system is that the latter's louver baseplate or radiator temperature is limited to 298°K. This relatively low radiator temperature is required by the temperature limits of the SEPS components located in the EC (Table 2-1).

In evaluating the EC thermal control system using louvers, the same louver characteristics were used as for the PP's (Concept 1 - Figure 3-5). The louver sizes, positioned 90 degrees to the sun, are indicated on Figure 3-24 for several assumed power levels. The effect of the solar array on the louver is incorporated in the curves. The other EC surfaces are covered with multilayer insulation. The surface properties of the MLI vary depending upon the nature of the mission (inbound, outbound, etc.). For outbound missions FEP back-aluminized teflon (α_s/ε = .1), for inbound missions silverized Kapton or OSR is applicable (α_s/ε = .06).

Another type of thermal control system for the equipment compartment is conceptually identical to the one selected for the power processors. Two variable-conductance heat pipe controlled radiators positioned 90 degrees to the sun provide thermal control for the equipment compartment. The other surfaces are covered with multilayer insulation having surface properties as described previously. The total maximum heat load in the equipment compartment is expected to be between 410 and 450 W. The thermal performance is shown on Figure 3-25 for expected range of heat loads as a function of radiator efficiency. The effect of the solar array having a maximum temperature of 423°K also is included in

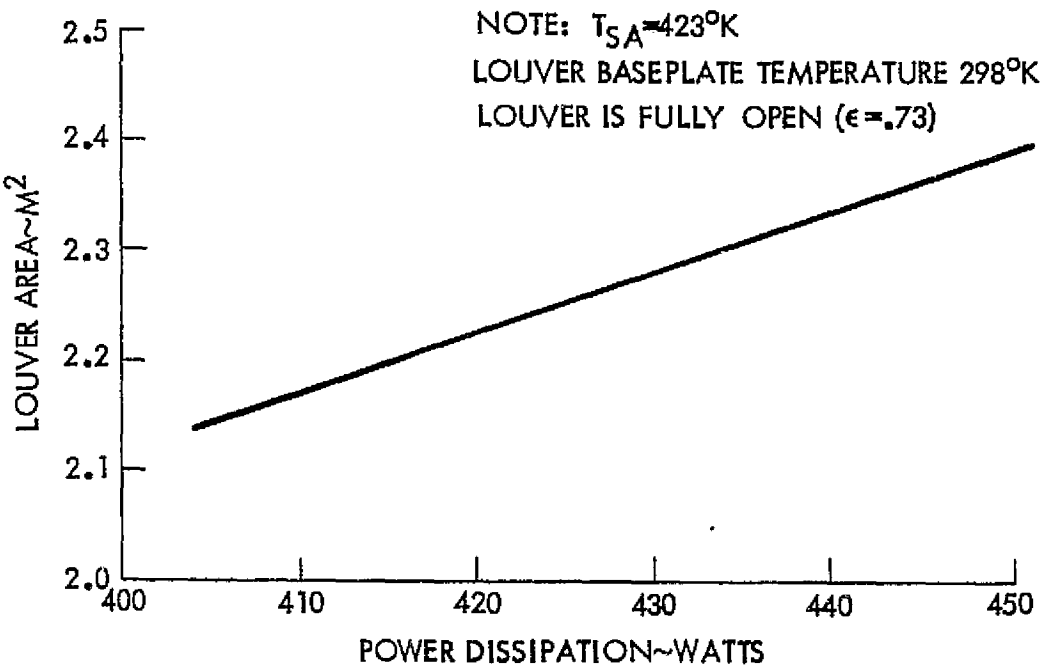

Figure 3-24. Equipment Compartment Louver Area

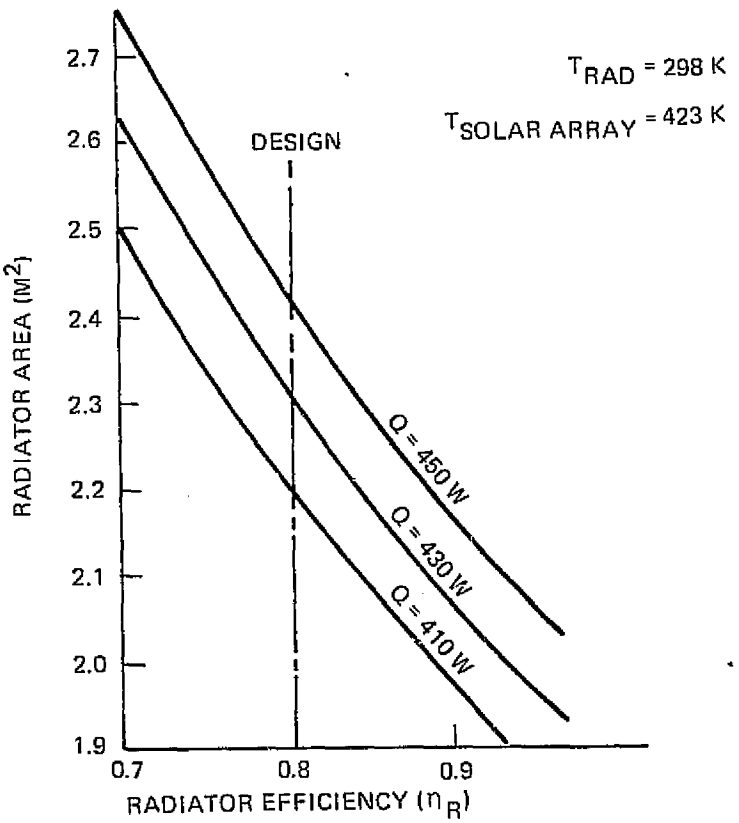

Figure 3-25. Equipment Compartment Radiator Efficiency

the curves. To prevent direct solar load on the radiators, a lightweight sun shield will be positioned around the radiator periphery.

Seven VCHP's corresponding to a radiator efficiency of 0.8 (80%) will transport the heat from the different components of the equipment compartment to each radiator panel. The radiator panel surface properties are identical to the ones used for the PP's (α_s = .2; ε = .88). The VCHP design is identical to that described and shown for the PP's. (Table 3-2, Figure 3-13).

Due to substantial curtailments in the SEPS program ordered by NASA in late 1974, the development of a detailed thermal model for the EC was not possible. No specification control drawings were available for the different units and therefore their positioning within the EC was not possible, thus preventing any detailed configuration studies.

No heater is necessary for the EC because the equipments located in it are operating during each mission. However, feasibility calculations performed for the EC indicate, that during periods where the PP's are not operating and their temperature drops close to or below their survival temperature limit of 223°K, heat from the EC could be used to keep the PP's warm. As Figure 3-19 indicates about 87.0 W heater power is necessary to keep the PP's at their non-operating survival temperature of 223°K. The EC minimum operational temperature limit is 298°K. Assuming 430 W of power dissipated in the EC,the necessary heater power would be 90.5 W to keep the EC temperatures at 298°K. Since 430 W is dissipated, the excess power would be 430 - 90.5 = 339.5 W. This power or any fraction of it could then be used to keep the PP's at their non-operating survival temperature limit of 223°K or at their minimum operating temperature of 258°K. To transport the heat from the EC to the PP's diode heat pipes could be applied. Such a configuration is shown on Figure 3-26.

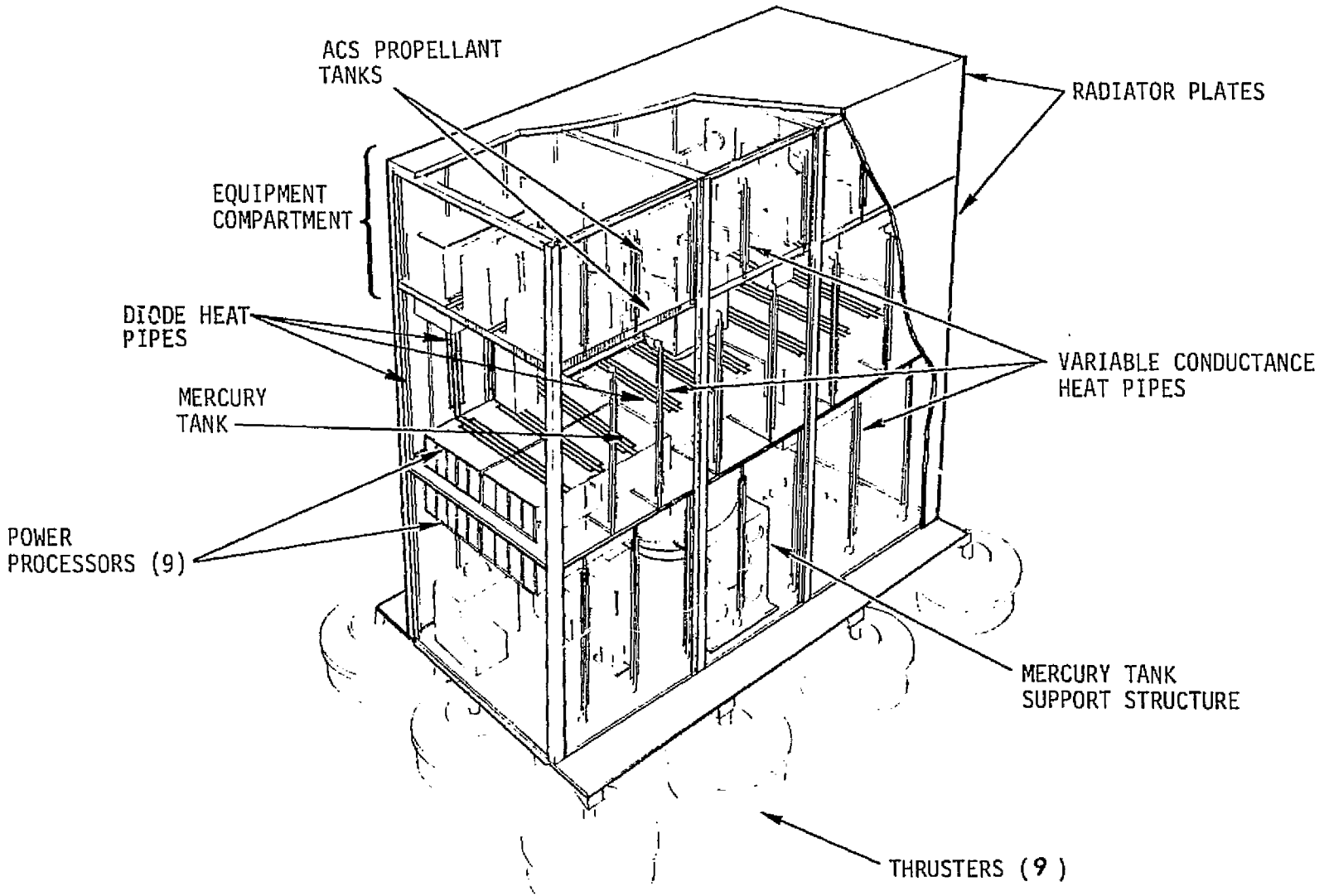

Figure 3-26. Heating of PP's with Diode Heat Pipes from EC

Solar Array

The solar array is one of the major components determining the environmental conditions for the Equipment Compartment (EC) and the Power Processors (PP's). The technology evaluation and preliminary design for a 25 KW Solar Array System for SEPS was completed by the Space Systems Division of Lockheed Missiles and Space Company (LMSC). The results are summarized in LMSC-D384250 document entitled "Solar Array Technology Evaluation" dated September 1, 1974.

From the beginning of the SEPS Thermal Analysis Study Contract constant coordination was maintained between Rockwell International and LMSC regarding solar array development. Because in their studies LMSC developed a thermal model for the solar array, to avoid duplication, Rockwell International did not develop a solar array thermal model but asked and received the thermal data needed from LMSC to perform this study. However, the geometrical relationship (configuration or view factor) between the solar array and the EC and PP's was determined by Rockwell (Figure 3-2). For this study the absolute maximum solar array temperature was taken as 423°K as indicated in LMSC-D384250 Report.

Design Impact of 0.1 AU Operation

A cursory investigation was made to determine the design impact of a 0.1 AU mission on the SEPS thermal design. At this distance the solar intensity is equivalent to 100 suns with an incident heat flux of approximately 139.0 KW/M^2.

One of the basic assumptions in evaluating the different thermal control concepts, was that a light weight sun shield will be deployed around the louver or radiator periphery and these surfaces will be 90 degrees to the sun. The other surfaces will be covered by multilayer insulation. It is therefore the primary concern to protect the MLI from burning up by providing some kind of heat shield or shields with appropriate (low α_s/ε) thermal coating.

In this high energy ultraviolet environment, inorganic coating systems, such as silicone oxides, aluminum oxides, i.e., glass and ceramics, can lose oxygen molecules causing a darkness in the material due to the production of color centers. Loss of less than one percent of the oxygen can produce this condition in some glasses. If in air, the oxygen is quickly recovered and color centers are not noticed, however, in a space environment the color centers persist and cause significant opacity in coatings. Some glass manufacturers have developed glass that resists development of color centers under UV conditions equivalent to several suns, however, no data or literature exists that describes the reaction of these glasses exposed to the intensity of 100 suns.

The same problem exists with ceramics which are used directly as coatings or as pigment in white coatings. Titanium dioxide which is a common pigment used in white paint is very unstable in a space environment and high UV exposure. Currently zinc oxide pigments are used for space applications for white paint thermal applications (S13G/LO used on P72-2 and Z-93 on the Apollo) and are acceptably stable under low UV in space. However, there is no assurance they would survive under

high intensity UV exposure. Ceramics and glass should not be completely eliminated as possible thermal coatings, for they may be acceptable if data were available.

Possible alternatives to the glass and ceramic coatings would be a specially designed system similar to ablative systems or multilayer reflective shieldings.

At present no test data are available for surface properties of coatings which could be applicable in a 100 sun intensity environment. Results from the thermal control coatings experiment obtained from OSO III flight indicate that several coatings which could be considered for SEPS, such as Z-93, OSR and barrier layer anodic, were stable and did not show appreciable degradation over 7500 ESH (Equivalent Sun Hours).

The possibility of .1 AU SEPS flight depends upon the development of adequate thermal coating withstanding the high sun intensity environment. Until that time such a flight seems very remote.

For example, a surface having spectral properties of α_s = 0.2, ε = 0.88 (e.i., S13G paint) at 0.1 AU solar distance the equilibrium temperature would be 866°K. For the same condition Z-93 (α_s = 0.17, ε = 0.9) paint and OSR (α_s = 0.05, ε = 0.76) would have equilibrium temperatures of 833°K and 639°K respectively.

4.0 THERMAL CONTROL SYSTEM EVALUATION

Evaluation and Selection of Thermal Control Concepts

A preliminary comparison and evaluation was made of the concepts investigated for the PP's and EC. Evaluation criteria included weight, reliability, simplicity (relative to cost), heater power requirements and flexibility (mainly with respect to the number of spare PP's).

The weight comparison is given in Table 4-1. As shown, the concepts using heat pipes weigh significantly less than those using louvers alone and the louver-VCHP combination (PP Concept 2). An overall comparison considering the other evaluation factors are given in Table 4-2.

Simplicity was considered more with respect to impact on development and unit costs than in relation to reliability. PP Concept 1 (all louvers) and PP Concept 3 (All VCHP) were considered the simplest designs primarily because they involve only one type of thermal control system. The same is true for the EC.

Heater power requirements are the lowest for PP Concept 3 because the heat leak to the radiators is only through the heat pipe walls (13/radiator). Concepts 1 and 2 heater power requirements are larger because each PP is directly exposed to deep space. Relatively larger heater power is required for PP Concepts 4 and 5 because of the 4 instead of the 2 radiators (Concept 3). Heater power requirements can be practically eliminated by coupling the EC to the PP's by diode heat pipes as described while discussing the EC thermal control system.

Flexibility was considered mainly with respect to requirement for a larger number of spare PP's for reliability. As discussed earlier, Concepts 3, 4 and 5 are independent of the number of spare PP's and, therefore, have an advantage over Concepts 1 and 2.

TABLE 4-1 WEIGHT AND RADIATOR AREA COMPARISON OF THERMAL CONTROL CONCEPTS

Concept	Fin Efficiency (%)	Radiator Area (m^2)	Louver Area (m^2)	Total Area (m^2) (9 PP's)	Radiator Weight (kg)*	Louver Weight (kg)	Total Weight (kg)
PP Concept 1	----	10.44	10.44	10.44	37.12	55.03	92.15
PP Concept 2	86	4.95	2.93	7.88	42.38	15.31	57.69
PP Concept 3	80	6.65	----	6.65	26.54	----	26.54
PP Concept 4**	88.5	7.56	----	7.56	44.44	----	44.44
PP Concept 5**	88.5	5.59	----	5.59	32.46	----	32.46
EC Louver	----	2.39	2.39	2.39	8.49	12.6	21.09
EC VCHP-Radiator	80	2.41	----	2.41	11.0	----	11.0

* Including heat pipe, associated hardware, and OSR coating where applicable

** Data corresponds to square cross-section SEPS Body (W/L = 1.0)

TABLE 4-2. COMPARISON OF THERMAL CONTROL CONCEPTS

CRITERIA / CONCEPT	WEIGHT KG	RELIABILITY	SIMPLICITY	HEATER POWER * WATTS	FLEXIBILITY
PP Concept 1	92	Very Good	Good	152.1	Poor
PP Concept 2	58	Good	Fair	104.9	Poor
PP Concept 3	27	Good	Good	87.3	Good
PP Concept 4	44	Poor	Fair	131.2	Good
PP Concept 5	32	Good	Fair	117.9	Good
EC Louver	21	Very Good	Good	-----	Good
EC VCHP-Rad	11	Good	Good	-----	Good

* For 223°K non-operating survival temperature; solar array temperature 173°K

Based on this evaluation, Concept 3 (two side VCHP) was determined to have the most advantages without any major weakness. A second choice, especially if a very thick SEPS body is required for structural dynamics, is Concept 5 (Four-Side VCHP - Diode HP).

All five PP concepts also were evaluated in the SEPS configuration design and integration analysis. Although structural dynamics preferred a square cross-section SEPS body, an intermediate thickness was selected to accommodate the Advanced System Technology (AST) solar array design. Consequently, Concept 3 (Two-Side VCHP)also was the recommended choice.

For the EC the VCHP-radiator controlled thermal control concept is recommended. It is preferred over the louver controlled system, because employing a VCHP-radiator system for the PP's the application of the same kind of system would lower development and manufacturing costs for both the PP and EC thermal control systems.

5.0 CONCLUSIONS AND RECOMMENDATIONS

The results of the analyses clearly indicate the recommended thermal control concept (two side VCHP-Concept 3) will satisfy SEPS thermal operational requirements. However, the capability of the thermal control system to maintain the required PP and EC temperatures must be demonstrated prior to any mission flight. Therefore it is recommended to undertake a development and test program to build a VCHP with n-butane as the working fluid. The requirements of the VCHP development and test program should be fully satisfied before applying the VCHP to the system testing (i.e., to test it with the radiator). The technology program for the n-butane filled VCHP's could be applied to other thermal control systems using heat pipes.

In addition to the VCHP development program a system test should also be performed. This test is necessary to demonstrate the VCHP-radiator system heat rejection capability. A section of the radiator has to be manufactured and the VCHP attached to it. The test can then be performed under vacuum conditions simulating the environment the system will be exposed to. Within the system test program the interface conductance of the VCHP to the radiator and/or to the PP or EC mounting surface has to be demonstrated also.

Based on the discussion presented under "Design impact of 0.1AU Operation" the development and testing of thermal control coatings is also highly recommended. The implementation of this program will not only enhance the successful operation of the SEPS thermal control system at 0.1 AU solar distance, but will improve the state of the art of thermal control elements used in general.

REFERENCES

1. Stimpson, L. D., and W. Jaworski. Effects of Overlaps, Stitches, and Patches on Multilayer Insulation, AIAA Paper No. 72-285 (1972)

2. Millard, J. P., and B. D. Pearson, Jr., Optical Stability of Coatings Exposed to Four Years Space Environment on OSO-III. AIAA Paper No. 73-734 (1973).

3. "Multilayer Insulation Synopsis", Vol. I of Insulation Commonality Report. Space Division, Rockwell International Corporation, SD73-SA-0831 (1973).

4. Bienert, W. P., and P. J. Brennan. Transient Performance of Electrical Feedback-Controlled Variable-Conductance Heat Pipes. ASMA Paper No. 71-AV-27 (1971).

5. Wright, J. P., and W. R. Pence, Development of a Cryogenic Heat Pipe Radiator for a Detector Cooling System. ASME Paper No. 73-ENAS-47.

6. Mock, P. R., B. D. Marcus and E. A. Edelman. Communication Technology Satellite. A Variable Conductance Heat Pipe Application. AIAA Paper No. 74-749.

7. Marcus, B. D., Theory and Design of Variable Conductance Heat Pipes. NASA CR-2018.

8. Heat Pipe Design Handbook. Dynatherm Co., DRD No. 354 T.

9. Michalek, T. J., E. A. Stipandic and M. J. Coyle, Analytical and Experimental Studies of an All Specular Thermal Control Louver System in a Solar Vacuum Environment, AIAA Paper No. 72-268.

10. Clausen, O. W., and J. P. Kirkpatrick. Thermal Tests of an Improved Louver System for Spacecraft Thermal Control. AIAA Paper No. 69-627 (1969).

11. Williams, R. J., Frictionless Bi-metal Actuated Louvers System. ASME Paper No. 71-AV-39 (1971).

12. Cunnington, G. R., Jr., Thermal Conductance of Filled Aluminum and Magnesium Joints in a Vacuum Environment. ASME Paper No. 64-WA/HT-40 (1964).

13. J. E. S. Venart and V. K. Magapu, Thermal Contact Conductance of Irregular Metallic Surfaces, AIAA Paper No. 74-696.

14. Ruttner, L. E., Thermal Control of the Solar Electric Propulsion Stage, AIAA Paper No. 73-1118 (1973).

15. Extended Definition Feasibility Study for a Solar Electric Propulsion Stage (Final Report). Space Division, Rockwell International Corporation, SD72-SA-0177-2-1, 2 (1972).

16. Extended Definition Feasibility Study for a Solar Electric Propulsion Stage (SEPS) Concept Definition, Volume II, Rockwell International Corporation, SD73-SA-0132-2-1.

17. Solar Array Technology Evaluation. Final Report LMSC-D384250 September 1, 1974, Lockheed Missiles and Space Company.

18. Flight Performance Insulation Development for Complex Surfaces and Heat Pipe Systems, Thermal Isolation Development Test. Rockwell International, Space Division, Laboratory Report LTR 1962-3201, May 1973.

19. Long Life High Reliability Thermal Control Systems Study Data Handbook. Prepared by G. E. for NASA under Contract NAS8-26252 (1971).

20. Concept Definition and Systems Analysis Study for a Solar Electric Propulsion Stage. Volume II-1 SD 74-SA-0176-2-1 (February 3, 1975).

APPENDIX

PREPARED BY:	SPACE DIVISION NORTH AMERICAN ROCKWELL CORPORATION	PAGE NO. 1 OF 13
CHECKED BY:		APPENDIX 1 REPORT NO. A-1
DATE:	HRL PP	MODEL NO. CONCEPT 1.

MODULE ATTACH PLATE MATERIAL 7075 AL. .05IN THICK.

$K = 75$ BTU/HR FT °F $= .31$ CAL/CM SEC °C

$\rho = .101$ LB/IN^3

THE CONDUCTANCE BETWEEN NODES WILL INCLUDE TWO STRUCTURAL AND ONE INTERFACE CONDUCTANCE. THE INTERFACE CONDUCTANCE IN THIS CASE WILL BE A FUNCTION OF THE NO. AND SIZE OF BOLTS (SCREWS). # & SCREWS ARE RECOMMENDED BY THE DESIGNER

$R = 2.5$ HR °F/BTU (FOR ONE SCREW)

$R = \frac{1}{C}$ ∴ $C = \frac{1}{R} = \frac{1}{2.5} = .4$ BTU/HR °F

CONDUCTANCE CALCULATIONS

1(1-2)

$$C = \frac{K A}{L} \quad \left[\frac{BTU}{HR\ FT\ °F}\ \frac{FT^2}{FT}\right]$$

1A.

$$C_A = \frac{75(11.1 \times .05)}{12(2.44)} = 1.42 \text{ BTU/HR °F}$$

1C.

$$C_C = \frac{75(11.1 \times .05)}{12(4.88)} = .71 \text{ BTU/HR °F}$$

1B.

TWICE & # 8 SCREWS PARALLEL

$$C_B = 8(.4) = 3.2 \text{ BTU/HR °F}$$

$$R_T = \frac{1}{1.42} + \frac{1}{.71} + \frac{1}{3.2} + \frac{1}{3.2} = 2.73$$

$$C = \frac{1}{2.73} = .365 \text{ BTU/HR °F}$$

2(2-3)

$C_A = .71$ BTU/HR °F $= C_C$

$C_B = 3.2$ BTU/HR °F

$R_T = \frac{2}{.71} + \frac{1}{3.2} = 3.44$ HR °F/BTU

$C_2 = \frac{1}{3.129} = .29$ BTU/HR °F

$C_2 = C_3 = C_4 = C_7 = C_8 = C_9 = .29$

5(5-6)

$C = \frac{75(11.1 \times .05)}{12(4.88 + 2.44)} = .474$ BTU/HR °F

$C_5 = C_6 = .474$ BTU/HR °F

11(1-12)

$C_A = \frac{75(4.88 \times .05)}{12(11.1)} = .137$ BTU/HR °F

C_B

TWICE 2 # 8 SCREWS

$C = .4$ BTU/HR °F FOR 2 IN PARALLEL

$C = .2$ FOR TWICE 2 IN PARALLEL

$C_C = .137$ BTU/HR °F

$R_T = \frac{1}{.137} + \frac{1}{.137} + \frac{1}{.12} = 19.6$ HR °F/BTU

$C_{11} = \frac{1}{R} = .05$ BTU/HR °F $= C_{16}$

12(2-11)

$$C_A = C_C = \frac{75(9.76 \times .05)}{12(11.1)} = .274 \text{ BTU/HR°F}$$

TWICE 5 # 8 SCREWS IN PARALLEL

$$C = \frac{2.5}{5} = .5$$

$$C_B = \frac{.5}{2} = .25 \text{ BTU/HR°F}$$

$$R_T = \frac{1}{.274} + \frac{1}{.271} + \frac{1}{.25} = 11.3 \text{ HR°F/BTU}$$

$$C_{12} = \frac{1}{R_T} = .089 \text{ BTU/HR°F} = C_{13} = C_{14} = C_{15}$$

89(1-50)

STRUCTURE (NODE 52) EQUIVALENT THICKNESS = .04 IN

CONTACT RESISTANCE: 2 # 8 SCREWS

$$R = \frac{2.5}{5} = .5 \text{ HR°F/BTU}$$

$$R_T = .5 + \frac{12(2.44)}{75(11.1)(.05)} + \frac{12(9.05)}{75(8)(.04)} = .5 + .7 + 4.53 = 5.725 \text{ HR°F/BTU}$$

$$C = \frac{1}{R} = .175 \text{ BTU/HR°F}$$

90(12-50)

$$R_T = .5 + .7 + \frac{12(14.1)}{75(8)(.04)} = .5 + .7 + 7.05 = 8.25 \text{ HR°F/BTU}$$

$$C = \frac{1}{R_T} = .12 \text{ BTU/HR°F}$$

77(1-52)*

CONTACT RESISTANCE -- 2 # 8 SCREWS $R_S = \frac{2.5}{2} = 1.25$ HR°F/BTU

STRUCTURE EQUIVALENT THICKNESS — .05 IN

$$K_T = 1.25 + \frac{12(5.55)}{75(.05)9.88} + \frac{12(4+22.16)}{75(.05)(8)} = 1.25 + 3.64 + 10.64$$

$$= 15.354 \text{ HR°F/BTU}$$

$$C = \frac{1}{R_1} = .065 \text{ BTU/HR°F}$$

78(2-52)*

$$R_S = \frac{2.5}{5} = .5 \text{ HR°F/BTU}$$

$$R_T = .5 + \frac{12(5.55)}{75(.05)9.76} + \frac{12(4+14.84)}{75(.05)(8)} = .5 + 1.82 + 7.94$$

$$= 10.26 \text{ HR°F/BTU}$$

$$C = \frac{1}{R_T} = .098 \text{ BTU/HR°F}$$

79(3-52)*

$$R_S = \frac{2.5}{5} = .5 \text{ HR°F/BTU}$$

$$R_T = .5 + 1.82 + \frac{12(4+5.08)}{75(.05)8} = 2.32 + 3.63 = 5.95 \text{ HR°F/BTU}$$

$$C = \frac{1}{R_T} = .168 \text{ BTU/HR°F}$$

* FOR IDENTICAL CONDUCTORS SEE DATA SHEET.

$281(50-150)$; $282(53-153)$

$L = 22.2 + 36 + 22.2 = 80.4$ IN

$t = .04$ IN

$K = 75$ BTU/HR FT °F

$d = 8$ IN

$A = 8(.04) = .32$ IN^2

$C = \frac{75(.32)}{12(80.4)} = .0248 \sim .025$ BTU/HR °F

PREPARED BY:	SPACE DIVISION NORTH AMERICAN ROCKWELL CORPORATION	PAGE NO. 6 OF 13
CHECKED BY:		REPORT NO. A-1
DATE:		MODEL NO. COMPT 1

CALCULATION OF RADIATION CONFIGURATION FACTORS:

NODES 1 - 25, 6 - 30, 7 - 31, 12 - 36

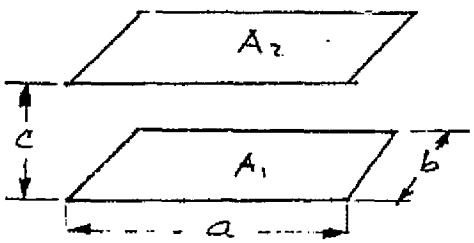

a = 11.1
b = 4.88
c = 8.0

$X = \frac{b}{c}$; $Y = \frac{a}{c}$

$X = \frac{4.88}{8.0} = .61$

$F_{1-25} = .17$

$Y = \frac{11.1}{8.0} = 1.3875$

2 - 26, 3 - 27, 4 - 28, 5 - 29, 8 - 32, 9 - 33, 10 - 34, 11 - 35

a = 11.1
b = 9.76
c = 8.0

$X = \frac{9.76}{8} = 1.22$

$Y = \frac{11.1}{8.0} = 1.3875$

$F_{2-26} = .265$

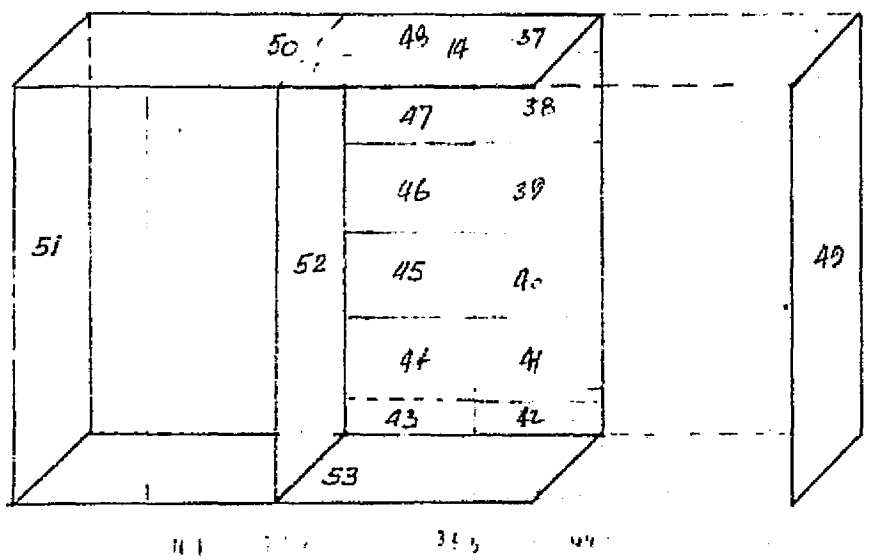

FORM M152-R-2 REV. 11-67

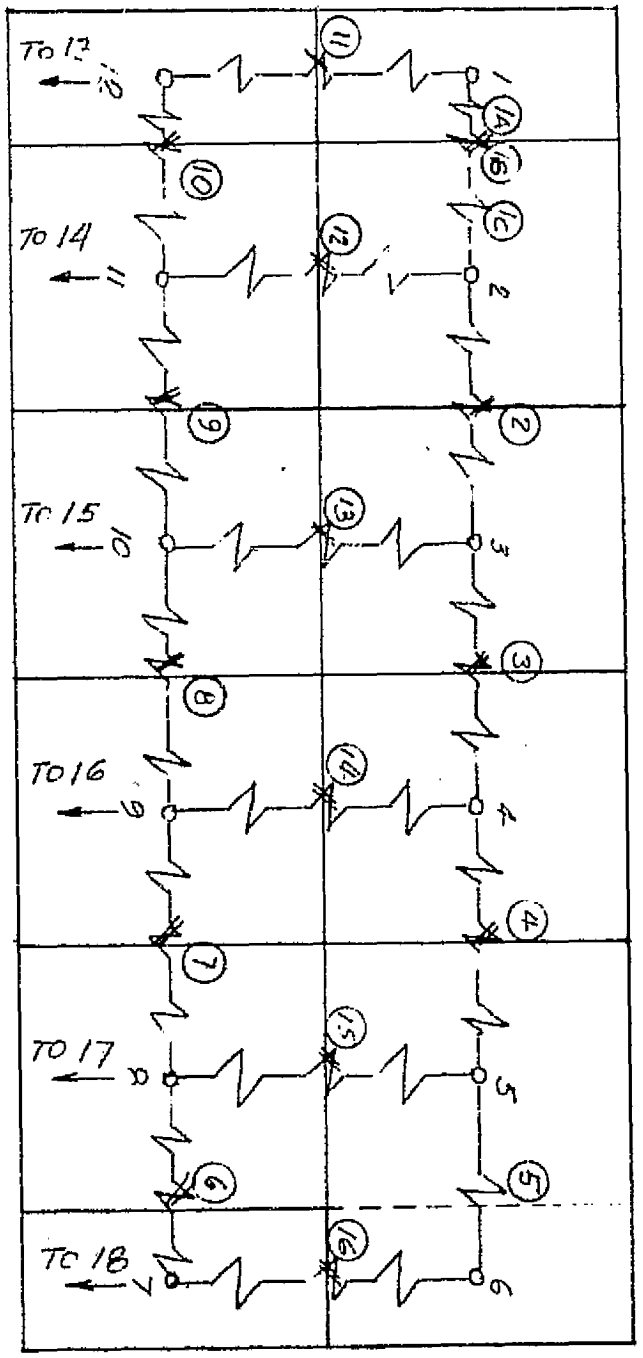

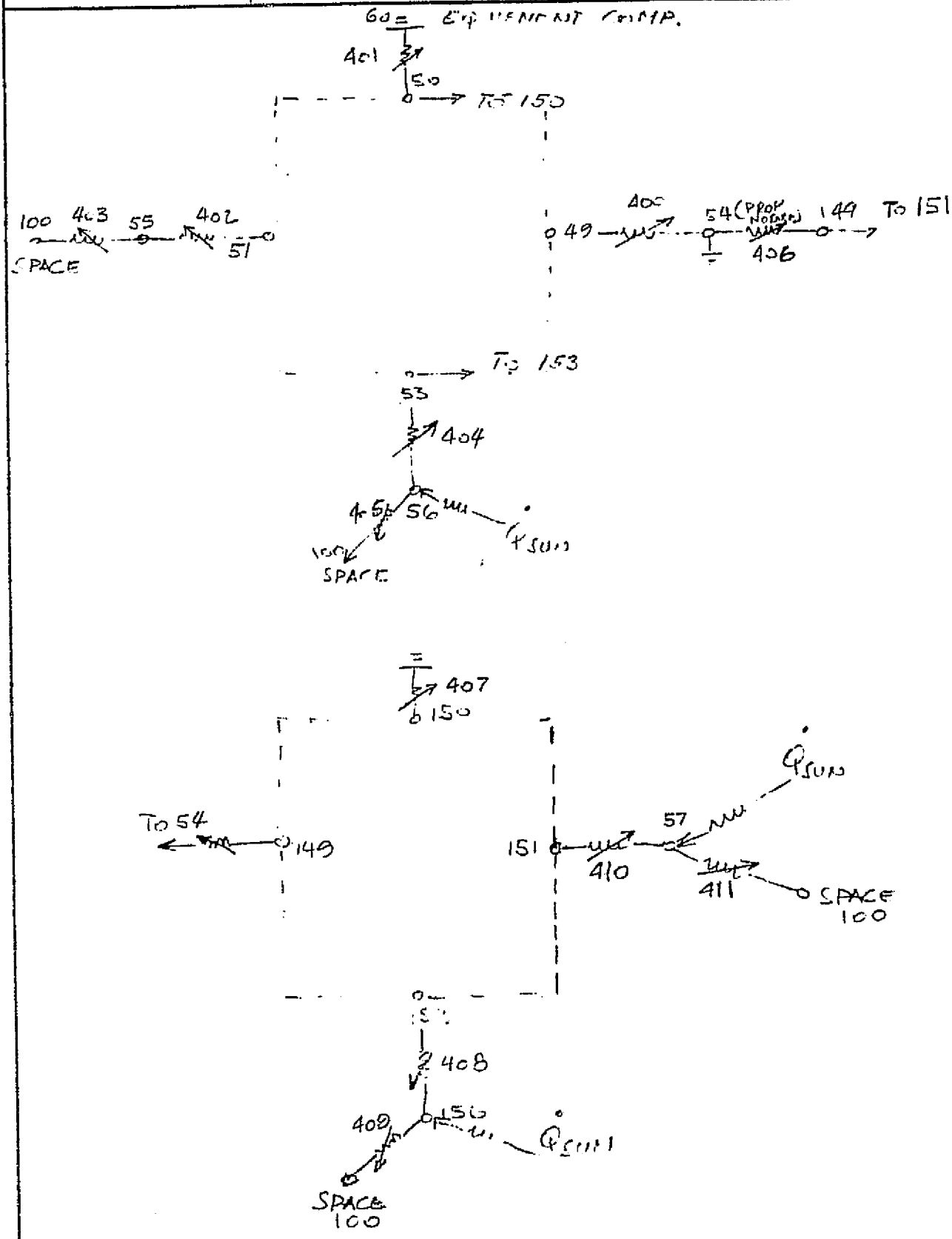

SOLAR LOAD INTO NODE 56

$S = 3050$ BTU/HR FT^2 @ .38 AU

$A = 44.4 \times 11 = 488.4$ IN^2 $= 3.39$ FT^2

$\alpha_s = .05$

$\epsilon = .81$

$\theta = 90 - 10 = 80°$

$\dot{Q} = SA\alpha_s \cos\theta = 3050(3.39)(.05)\cos 80° = 89.77$ BTU/HR

SOLAR LOAD INTO NODE 149 @ .38 AU

$A = 48.8 \times 11 = 536.8$ IN^2 $= 3.73$ FT^2

$\dot{Q} = 3050(3.73)(.05)\cos 10 = 560.18$ BTU/HR

IF $\alpha_s = .1$

SOLAR LOAD INTO NODE 56

$\dot{Q} = 179.54$ BTU/HR

INTO NODE 149

$\dot{Q} = 1120.36$ BTU/HR

BECAUSE $\epsilon_{eff} = .02 - .03$ FOR THE MLE THIS CHANGE OF α_s (.05 TO .1) DOES NOT HAVE SIGNIFICANT EFFECT ON PP TEMPERATURES (ONLY 2-3°F)

PREPARED BY:	SPACE DIVISION NORTH AMERICAN ROCKWELL CORPORATION	PAGE NO. 10 OF 13
CHECKED BY:		REPORT NO. A-1
DATE:		MODEL NO. CONCEPT 1

FORM M192-R-2 REV. 11-67

LOW EARTH ORBIT MISSION (500 NM)

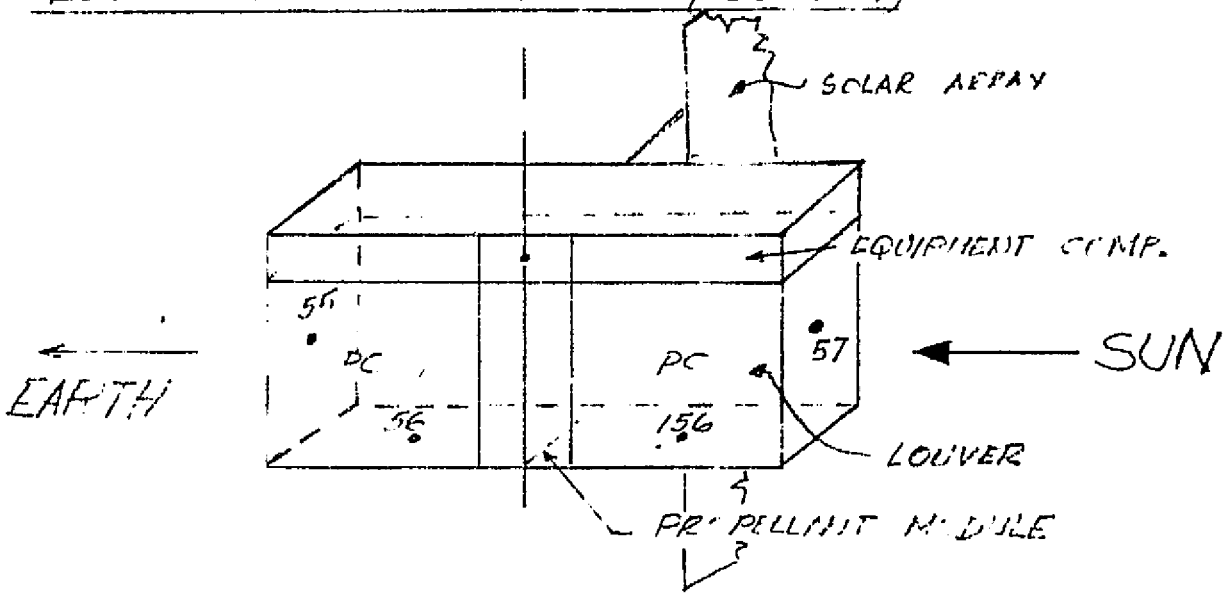

SUN INTENSITY 440 BTU/HR FT²

EARTH EMISSION ON A HORIZONTAL SURFACE FACING EARTH @ 500 NM 52.5 BTU/HR FT²

EARTH EMISSION ON A VERTICAL SURFACE 18 BTU/HR FT²

ALBEDO ON A FLAT SURFACE (HORIZONTAL) 128 BTU/HR FT²
ALBEDO ON A FLAT SURFACE (VERTICAL) 34 — " —

SOLAR LOAD ON NODE 57

$A = 5310.8 IN^2 - 3.73 FT^2$

$\alpha_s = .045$

$\epsilon = .76$

$Q_s = 440(.045)\ 3.73 = 73.85\ BTU/HR$

EARTH EMISSION + ALBEDO LOAD ON NODE 55

$A = 3.39\ FT^2$

$Q_E + Q_A = 128(.76) + 52.5(.76) = 137.1\ BTU/HR\ FT^2$

$Q_E = 137.1(3.73) = 371.67\ BTU/HR$

PREPARED BY:	SPACE DIVISION NORTH AMERICAN ROCKWELL CORPORATION	PAGE NO. 11 OF 13
CHECKED BY:		REPORT NO. A-1
DATE:		MODEL NO. CONCEPT 1

EARTH EMISSIVITY + ALBEDO HEAT (A) ARCS 56 & 156

$A = 3.39\ FT^2$

$G_F + G_A = 341.76 + 18(.045) = 26.65\ BTU/HR\ FT^2$

$G_t = 26.65(3.37) = 90.34\ BTU/HR$

PREPARED BY:	SPACE DIVISION NORTH AMERICAN ROCKWELL CORPORATION	PAGE NO. 12 OF 13
CHECKED BY:		REPORT NO. A-1
DATE:		MODEL NO. CONCEPT 1

48	37	36	25
47	38	35	26
46	39	34	27
45	40	33	28
44	41	32	29
43	42	31	30

24	13	12	1
23	14	11	2
22	15	10	3
21	16	9	4
20	17	8	5
19	18	7	6

148	137	136	125
147	138	135	126
146	139	134	127
145	140	133	128
144	141	132	129
143	142	131	130

124	113	112	101
123	114	111	102
122	115	110	103
121	116	109	104
120	117	108	105
119	118	107	106

DETERMINATION OF HEATER POWER

$A_L = 1.06\ m^2 = 11.4\ FT^2$

$\epsilon_L = .76$

$\epsilon_{SA} = .8$

$F_{L-SA} = .12$ (LOUVERS FULLY CLOSED)

$\epsilon_{L-SP} = .88$

$T_{SA} = -100°C = -148°F = 312°R$

$T_L = -50°C = -58°F = 402°R$ NON-OPERATING SURVIVAL TEMP.

$$Q_H = \epsilon_L \epsilon_{SA} F_{L-SA} A_L \sigma (T_L^4 - T_{SA}^4) + \epsilon_L \epsilon_{SP} F_{L-SP} A_L \sigma (T_L^4)$$

$$= (.12)(.8)(.12)\,11.4\,\sigma (402^4 - 312^4) + (.12)(1)(.88)\,11.4\,\sigma (402^4)$$

$$= 53.87 + 3.75 = 57.62\ BTU/HR = 16.9\ W/PP;$$

$$Q_T = 9(16.9) = 152.1\ W$$

$T_{SA} = -50°C = -58°F = 402°R$

$$Q = 53.87\ BTU/HR = 15.8\ W$$

$$\underline{Q_T = 9(15.8) = 142.2\ W}$$

$T_{SA} = 0°C = 32°F = 492°R$

$$Q_H = 53.87 - (.12)(.8)(.12)\,11.4\,\sigma (492^4 - 402^4)$$

$$= 53.87 - 7.31 = 46.56\ BTU/HR = 13.65\ W$$

ORIGINAL PAGE IS OF POOR QUALITY

$$\underline{Q_T = (9)\,13.65 = 122.89\ W}$$

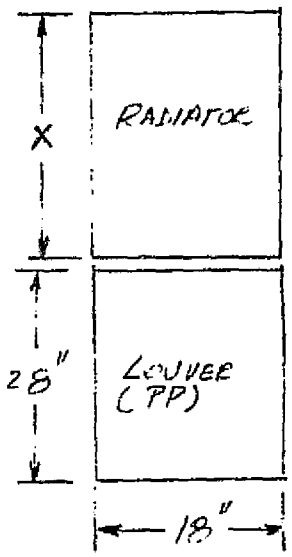

ASSUME: RADIATOR WIDTH TO BE 18 IN

AREA = 18 x X

('X' TO BE DETERMINED)

A_{LOUVER} = 18 x 28 - 504 IN^2 - 3.5 FT^2 = .327 M^2

Q_{PP} = 312.5 W

PRECEDING PAGE BLANK NOT FILMED

LOUVER

ϵ_L = .65 - .70

ϵ_{SA} = .8

α_S = .2 (.2 - .32)

F_{L-SA} = .12 (LOUVER TO SOLAR ARRAY)

$F_{L-SPACE}$ = .88

T_{SA} = 150°C

DESIGN FOR A RADIATOR TEMPERATURE (AVERAGE) OF 55 °C.

NO SOLAR FLUX - Q_{SOLAR} = 0

Q_{SA-L}

ORIGINAL PAGE IS OF POOR QUALITY

T_L = 65 °C

$\epsilon_L \epsilon_{SA} F_{R-SA}$ = (.65)(.8)(.12) = .0624

FROM CURVE A.) (Q/A) = 107.89 W/FT^2

Q = 107.89 (.0624) 3.5 = 23.56 W

Φ_{L-SP}

$\epsilon_L F_{L-SP} = (.65)(.88) = .572$

FROM CURVE "B" $(\Phi/A) = 35\ W/FT^2$

$\Phi = (35)(3.5) = 122.5\ W$

$\Phi_{VCHP} = \Phi_{PP} + \Phi_{SA-L} + \Phi_{VCHP-SA} - \Phi_{SA-L}$

$= 312.5 + 23.56 + \Phi_{VCHP-SA} - 122.5$

$= 213.56 + \Phi_{VCHP-SA}$

$(\Phi/A)_{SA-R}$

$\epsilon_R \epsilon_{SA} F_{R-SP} = (.88)(.8)(.12) = .08448$

FROM CURVE A $(\Phi/A)_{SA-R} = 107.89\ W/FT^2$

$(\Phi/A)_{SA-R} = 107.89/(.08448) = 9.11\ W/FT^2$

$(\Phi/A)_{R-SP}$

$\epsilon_R F_{R-SP} = (.88)(.88) = .774$

FROM CURVE B $(\Phi/A)_{R-SP} = 47.0\ W/FT^2$ @ .774 AND 55°C

$47A = 213.56 + 9.11A$

$A = \frac{213.56}{37.89} = 5.64\ FT^2$

ASSUME A RADIATOR EFFICIENCY OF $\eta_R = .86$

$A = \frac{5.64}{.86} = 6.55\ FT^2 = .609\ M^2$

$X = \frac{6.55 \times 144}{18} = 52.4\ IN = 1.33\ M$

IN THE PREVIOUS CALCULATIONS IT WAS ASSUMED THAT BOTH LOWER BASEPLATE AND RADIATOR WILL BE AT THE SAME TEMPERATURE (55°C). THE RESULTS OBTAINED THIS WAY ARE ABOUT 5% HIGHER IF A LOWER PLATE TEMPERATURE OF $T_L = 60°C$ IS ASUMED LEAVING THE RADIATOR TEMPERATURE AT 55°C, THUS ALLOWING A 5°C TEMPERATURE DROP.

DETERMINATION OF HEATER POWER

LOUVER AREA $A_L = .327\ m^2 = 3.52\ FT^2$

RADIATOR AREA $A_R = .609 m^2 = 6.55\ FT^2$

$\dot{Q}_{PP} =$ ~~Θ~~

$T_{SA} = -100°C = -176°F = 312°R$

$\epsilon_L = .12$ (LOUVERS FULLY CLOSED)

$\epsilon_R = .88$

$F_{L-SA} = F_{R-SA} = .88$

RADIATOR IS CONNECTED TO PP'S (LOUVER BASE PLATE) BY 2 (DOUBLE BARREL) HEAT PIPES (STAINLESS STEEL)

$$A_{VCHP} = \frac{(.5)^2\pi}{4} - \frac{(.484)^2\pi}{4} = .0415\ IN^2$$

$K = 9.4\ BTU/HR\ FT\ °F$

ASSUME 1 IN GAP BETWEEN RADIATOR AND LOUVER BASE PLATE.

$$R = \frac{12L}{KA} = \frac{12(1)}{9.4(.0415)} = 30.76\ HR\ °F/BTU$$

FOR 4 PIPES

$$R_T = \frac{30.76}{4} = 7.69\ HR\ °F/BTU$$

LET $T_L = -50°C = -58°F = 402°R$. NON-OPERATING SURVIVAL TEMP.

$$\dot{Q}_1 = \epsilon_L \epsilon_{SA} F_{L-SA} A \sigma (T_L^4 - T_{SA})$$

$$\dot{Q}_2 = \epsilon_L \epsilon_{SP} F_{L-SP} A \sigma (T_L^4)$$

$q_1 = (.12)(.12)(.8)\, 3.52\, \sigma (402^4 - 312^4) = 1.156$ BTU/HR

$q_2 = (.12)(.3^2)(1)\, 3.52\, \sigma (402^4) = 16.63$ " "

$q_1 + q_2 = 18.19$ BTU/HR $= 5.33$ W

HEAT BALANCE FOR RADIATOR

$q_{IN} = q_{OUT}$

$$q_{IN} = \frac{\Delta T}{R_T} + \epsilon_R \epsilon_{SA} F_{R-SA} A_R \sigma (T_{SA}^4 - T_R^4),$$

$\Delta T = T_L - T_R$

$$q_{OUT} = \epsilon_R \epsilon_{SP} F_{R-SP} A_R \sigma (T_R^4)$$

$$q_{IN} = \frac{402 - T_R}{7.69} + (.86)(.8)(.12)\, 6.55\, \sigma (312^4 - T_R^4)$$

$$q_{OUT} = (.88)\,1\,(.88)\, 6.55\, \sigma (T_R^4) = 8.694 \times 10^{-9} T_R^4$$

$$\frac{402 - T_R}{7.69} + 8.98 - 9.484 \times 10^{-10} T_R^4 = 8.964 \times 10^{-9} T_R^4$$

$$402 - T_R + 69.11 - 7.293 \times 10^{-9} T_R^4 = 6.893 \times 10^{-8} T_R^4$$

$$471.11 = 7.623 \times 10^{-8} T_R^4 + T_R$$

LET $T_R = 250\,^\circ R$

$471.11 = 198 + 250$

$471 > 7\,548$

$T_R = 240$

$253 + 240 > 471$

T_R = 237°R

240 + 237 = 477 ≈ 471

T_R = 236°R

236 + 236 = 472 ≈ 471

T_D = 236°R = −224°F

$Q_{VCHP} = \frac{402-236}{7.69} = \frac{166}{7.69}$ = 21.58 BTU/HR = 6.33 W

Q_{HEATER} = 5.33 + 6.33 = 11.66 W/PP

FOR 9 PP Q_{H_T} = (9) 11.66 = 104.94 W

LET T_{SA} = −50°C = −58°F = 402°R

$Q_1 = 0$

Q_2 = 16.63 BTU/HR = 4.88 W

Q_{VCH_2} = 6.33 W

Q_H = 6.33 + 4.88 = 11.21 W

Q_{H_T} = (9) 11.21 = 100.89 W

T_{SA} = 0°C = 32°F = 492°R

$Q_1 = (.12)(.12)(.8)\,3.52\,(492^4 - 402^4)\,6$ = 2.26 BTU/HR

$Q = Q_2 - Q_1$ = 16.63 − 2.26 = 14.37 BTU/HR = 4.21 W

Q_H = 6.33 + 4.21 = 10.54 W

Q_{H_T} = (9) 10.54 = 94.86 W

ORIGINAL PAGE IS
OF POOR QUALITY

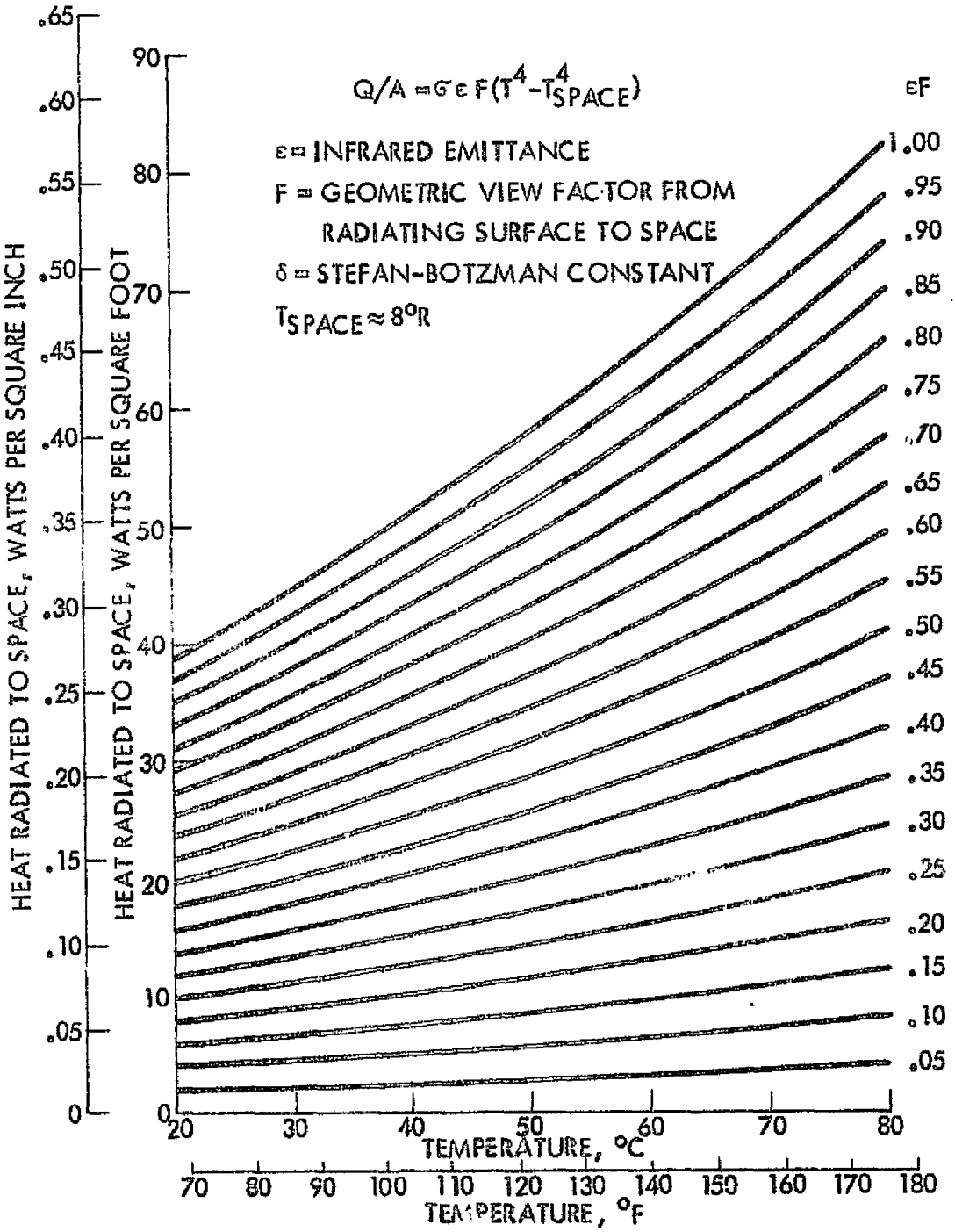

FIGURE A-2-1

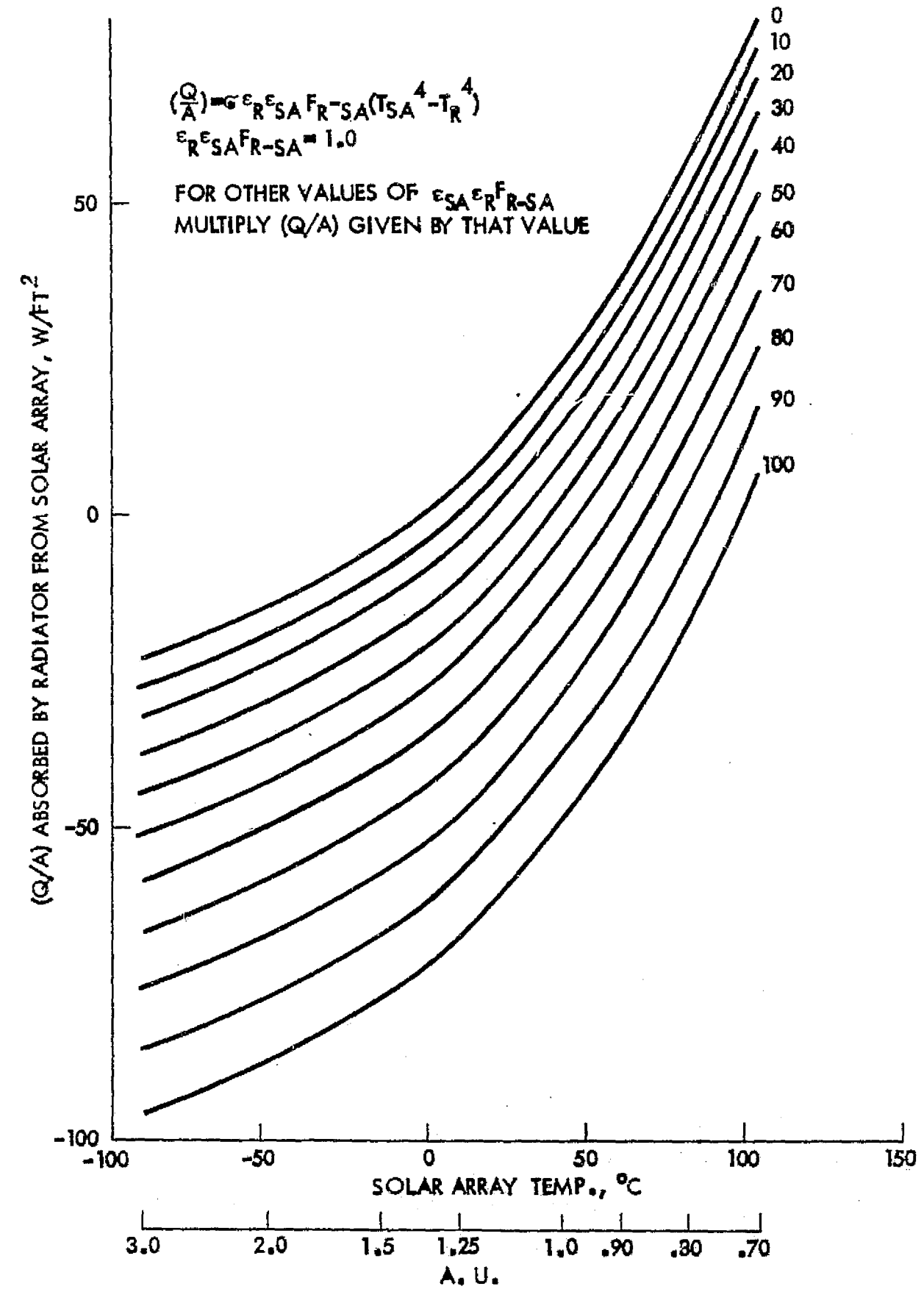
$(\frac{Q}{A}) = \sigma \varepsilon_R \varepsilon_{SA} F_{R-SA} (T_{SA}^4 - T_R^4)$
$\varepsilon_R \varepsilon_{SA} F_{R-SA} = 1.0$
FOR OTHER VALUES OF $\varepsilon_{SA} \varepsilon_R F_{R-SA}$
MULTIPLY (Q/A) GIVEN BY THAT VALUE
(Q/A) ABSORBED BY RADIATOR FROM SOLAR ARRAY, W/FT^2
50
0
-50
-100
0
10
20
30
40
50
60
70
80
90
100
-100
-50
0
50
100
150
SOLAR ARRAY TEMP., °C
3.0
2.0
1.5
1.25
1.0
.90
.80
.70
A. U.

FIGURE A-2-2

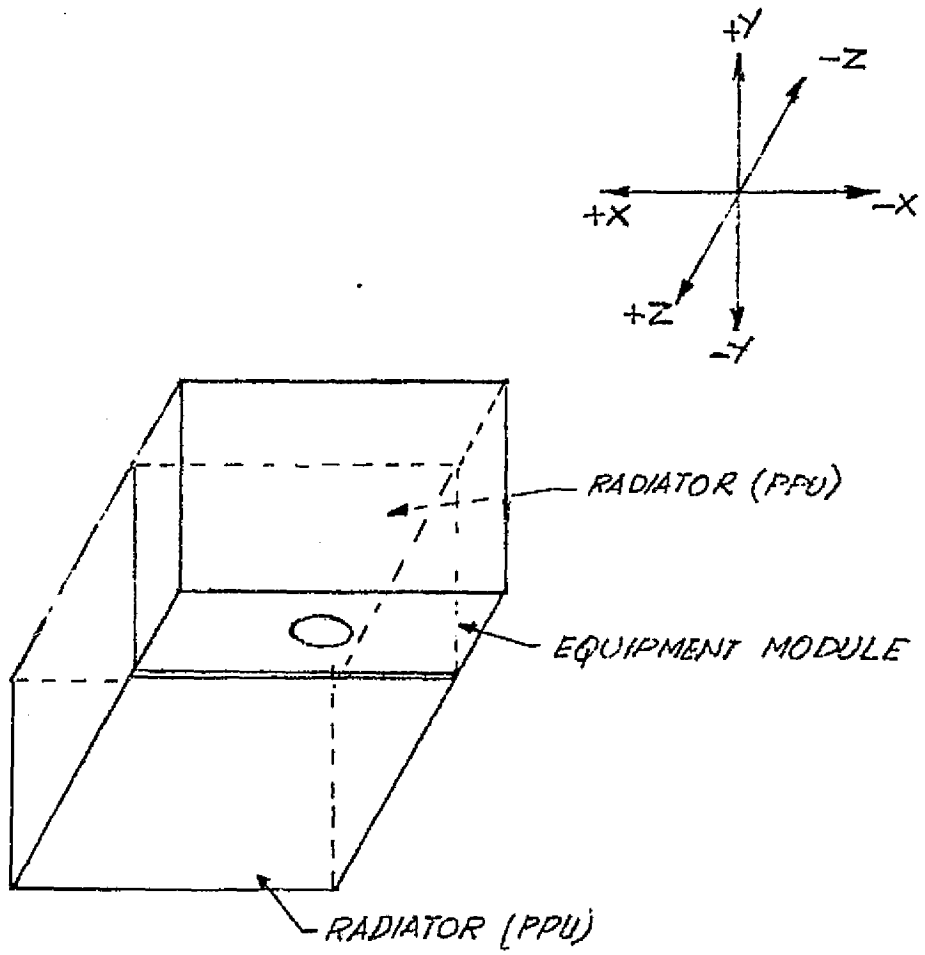

FIGURE A-3-1

PREPARED BY: LER	SPACE DIVISION NORTH AMERICAN ROCKWELL CORPORATION	PAGE NO. 2 OF 20
CHECKED BY:		REPORT NO. A 3
DATE: 11/74	2 SIDE VCHP	MODEL NO. CONCEPT 3.

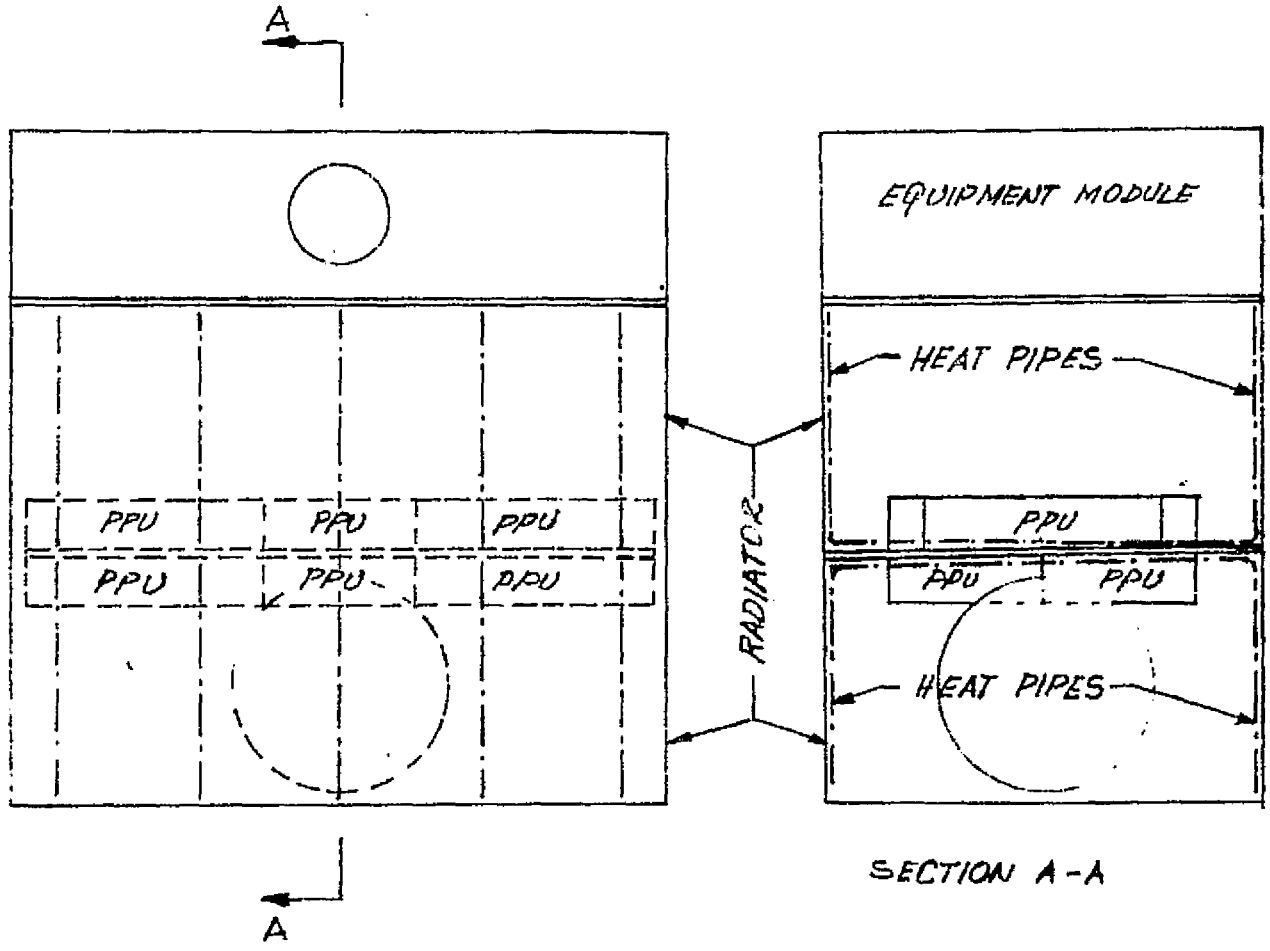

SECTION A-A

FIGURE A-3-2

PREPARED BY: LEE	SPACE DIVISION NORTH AMERICAN ROCKWELL CORPORATION	PAGE NO. 3 OF 20
CHECKED BY:		REPORT NO. A-3
DATE:	2 SIDE VENT	MODEL NO. CONCEPT 3.

ASSUMPTION: RADIATOR $\alpha_s = .2$

$\epsilon = .88$

$q_{PP} = 312.5$ W/FT

AT ONE TIME MAX. OF 7 OUT OF 9 CAN BE ON.

$\therefore Q = 312.5(7) = 2187.5$ W

$T_{SA} = 150°C$

$T_R = 55°C$ (5.5°C)

$F_{R-SA} = .12$ $\epsilon_{SA} = .8$

$F_{R-SP} = .88$

FROM CURVE A

$(q/A)_{SA-R}$ @ $T_{SA} = 150°C$

$\epsilon_R \epsilon_{SA} F_{R-SA} = (.88)(.8)(.12) = .08448$

$(q/A)_{SA-R} = (.08448)(111.53) = 9.42$ W/FT^2 (9.11 W/FT^2)

$(q/A)_{R-SP}$ @ $\epsilon_R F_{R-SP}$ & $T_R = 55°C$

$\epsilon_R F_{R-SP} = (.88)(.88) = .774$

$(q/A)_{R-SP} = 44.5$ W/FT^2 (47.5 W/FT^2) FROM CURVE E

$(q/A)_{R-R}(A) = q + (q/A)_{SA-R}(A)$

$44.5A = 2187.5 + 9.42A$

$A = 62.357 \sim 62.36$ FT^2 (56.77 FT^2)

DETERMINATION OF RADIATOR EFFICIENCY

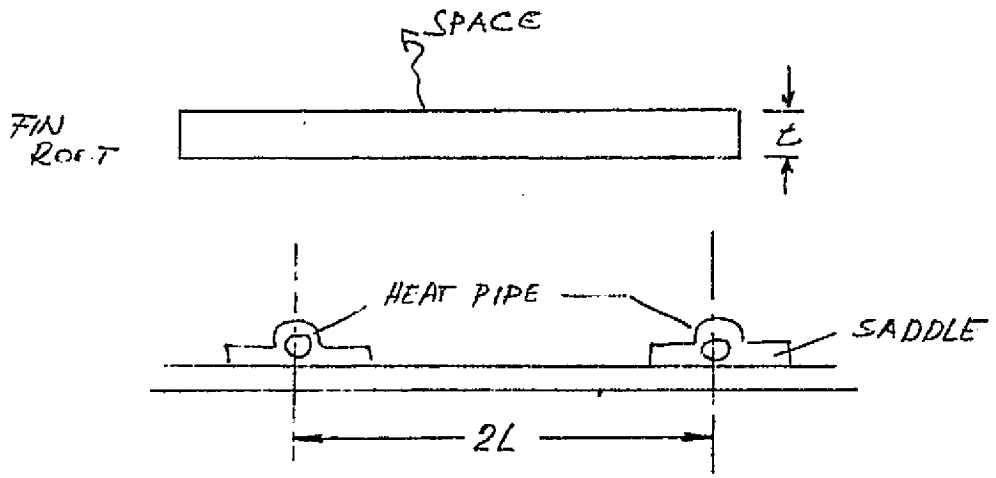

THE FIN PARAMETER $N = \dfrac{\epsilon_R \sigma L^2 T_R^3}{k t}$ (1)

THE EQUATION FOR FIN EFFICIENCY

$$\left(\frac{2N\theta_e^5}{5}\right)^{1/2} = -\frac{\theta_e}{5}\int_{\theta_e}^{\cdot} z^{-7/10}(1-z)^{-1/2}\,dz \quad (2)\ *$$

THE SOLUTION OF EQ. (2) FOR θ_e AND FIN EFFICIENCY (η) IS TABULATED ON PG. 5 FOR DIFFERENT VALUES OF "N"

ASSUME: FIN MATERIAL 6061-T6 AL

$K = 95$ BTU/HR FT °F

$T_R = 55°C = 131°F.$

$\epsilon_R = .88$

* T.J. KUO: RADIATIVE HEAT TRANSFER C.E. MERRILL 1968.

N	ϵ_e	η
∞	0	0
3.147	.631	.335
1.567	.724	.451
.938	.786	.545
.611	.833	.626
.407	.871	.7
.272	.903	.765
.174	.931	.831
.101	.956	.89
.045	.979	.944
0	1.0	1.0

$$N = \frac{(.88)\,\bar{\epsilon}\,L^2/591)^3}{95(t)} = 3.26 \times 10^{-3}\left(\frac{L^2}{t}\right)$$

FIN PARAMETER (N) vs. EFFICIENCY

FIG. A-3-3

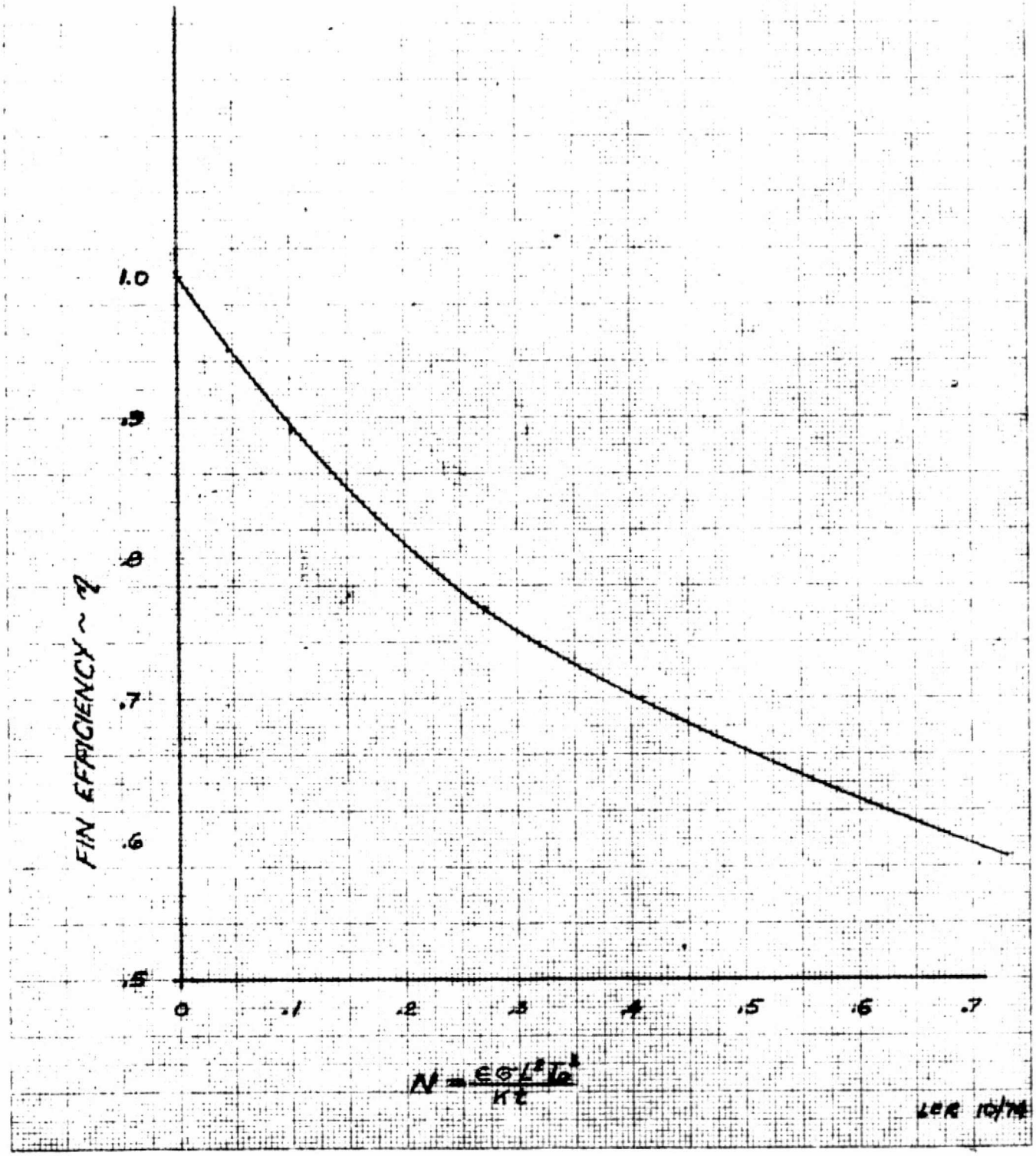

FIN LENGTH VS. FIN EFFICIENCY

FIG. A-3-4

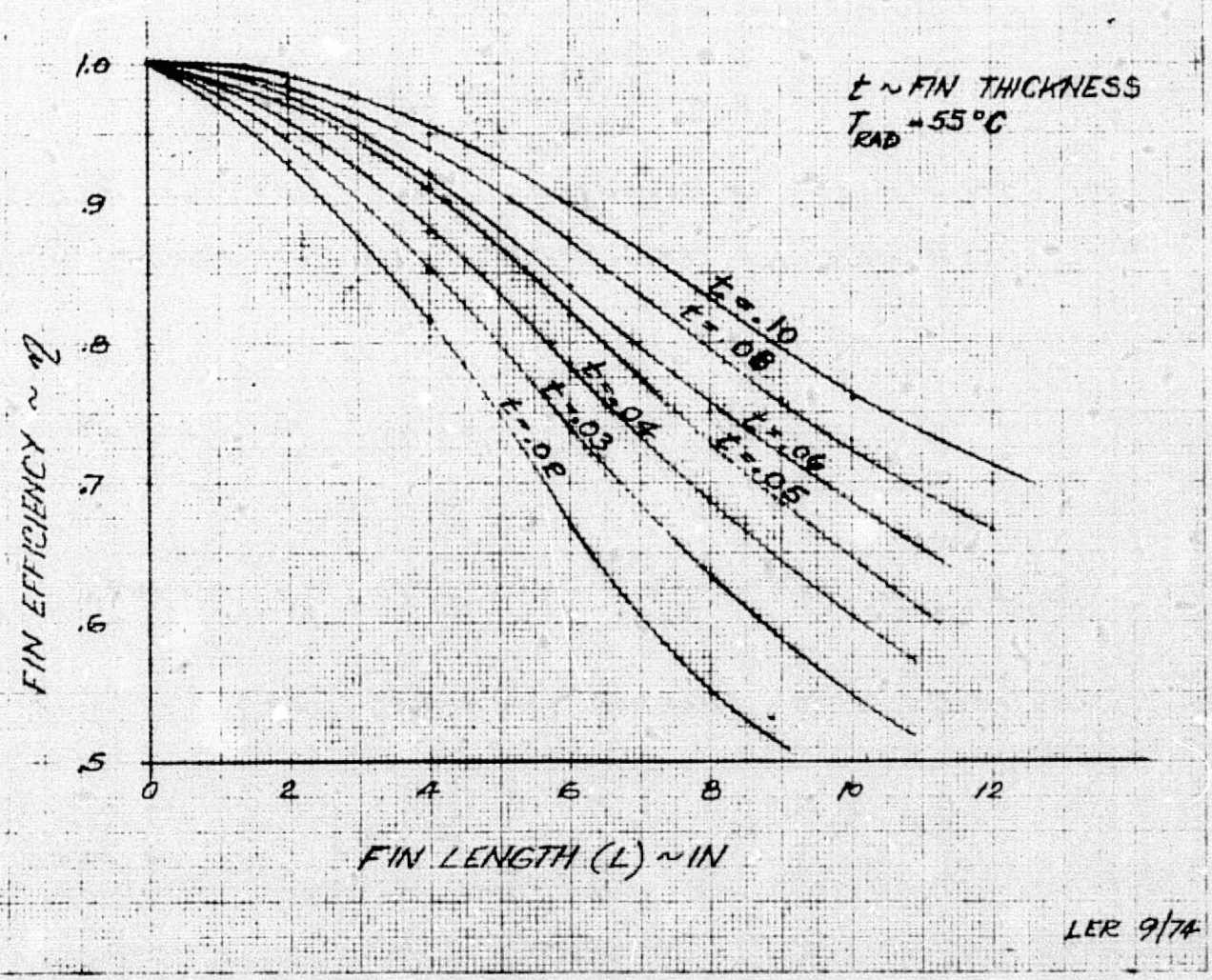

LER 9/74

FROM CURVE "D"

@ $\eta = .785$ $L = 6$ IN
$\eta = .885$ $L = 4$ IN
} @ $t = .04$ IN (RADIATOR THICKNESS)

$$A_F = \frac{A}{\eta} = \frac{62.36}{.785} = 79.44 \text{ FT}^2 \ (72.6 \text{ FT}^2)$$

ONE SIDE OF RADIATOR $A = \frac{79.44}{2} = 39.72 \text{ FT}^2 \ (36.3 \text{ FT}^2)$

DUE TO THE TEMP. DROP EXPECTED IN THE ELECTRONICS PACKAGE DESIGN FOR $T_R = 55°C$ $(T_{DO} = 60°C)$

USING $\eta = .885$

$$A_F = \frac{56.99}{.885} = 64.395 \sim 64.4 \text{ FT}^2$$

STRUCTURAL & DYNAMICS CONSIDERATION REQUIRE TO KEEP ONE RADIATOR DIMENSION AT APPROX. 80 IN.

$\therefore A_F = 8C(W)$

$$W = \frac{36.3 \times 144}{80} = 65.34 \text{ IN} \quad @ \ \eta = .785$$

$$W = \frac{32.4 \times 144}{80} = 57.96 \text{ IN} \quad @ \ \eta = .885$$

HEAT PIPE SPACING ($\eta = .785$) $L = 6.0$ IN

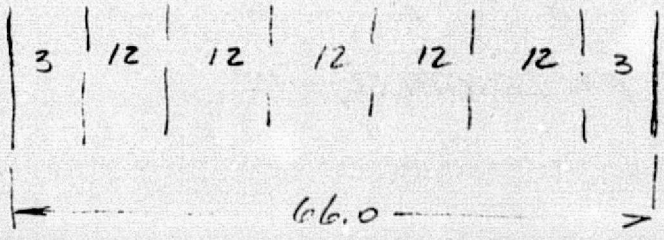

NO. OF PIPES 6

HEAT PIPE SPACING ($\eta = .885$) $L = 4.0$ IN.

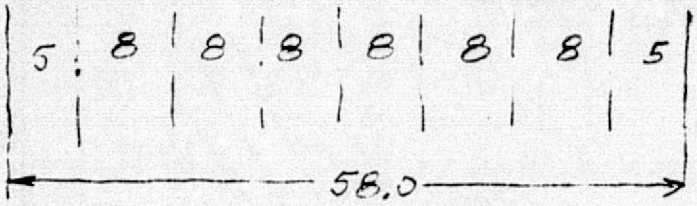

NO. OF PIPES 7

ON PAGE 10-12 CURVES ARE SHOWN SUCH AS

RADIATOR HEAT REJECTION VS. RADIATOR EMISSIVITY @ .7 AU $T_{SA} = 100°C$

RADIATOR AREA VS. HEAT REJECTION @ .7 AU $T_{SA} = 100°C$

RADIATOR AREA VS. HEAT REJECTION @ 1.0 AU $T_{SA} = 50°C$

RADIATOR HEAT REJECTION VS. EMISSIVITY

.7AU
$T_{SA} = 100°C$
$\alpha_{RAD} = .2$
——— $T_{RAD} = 55°C$
— — $T_{RAD} = 50°C$

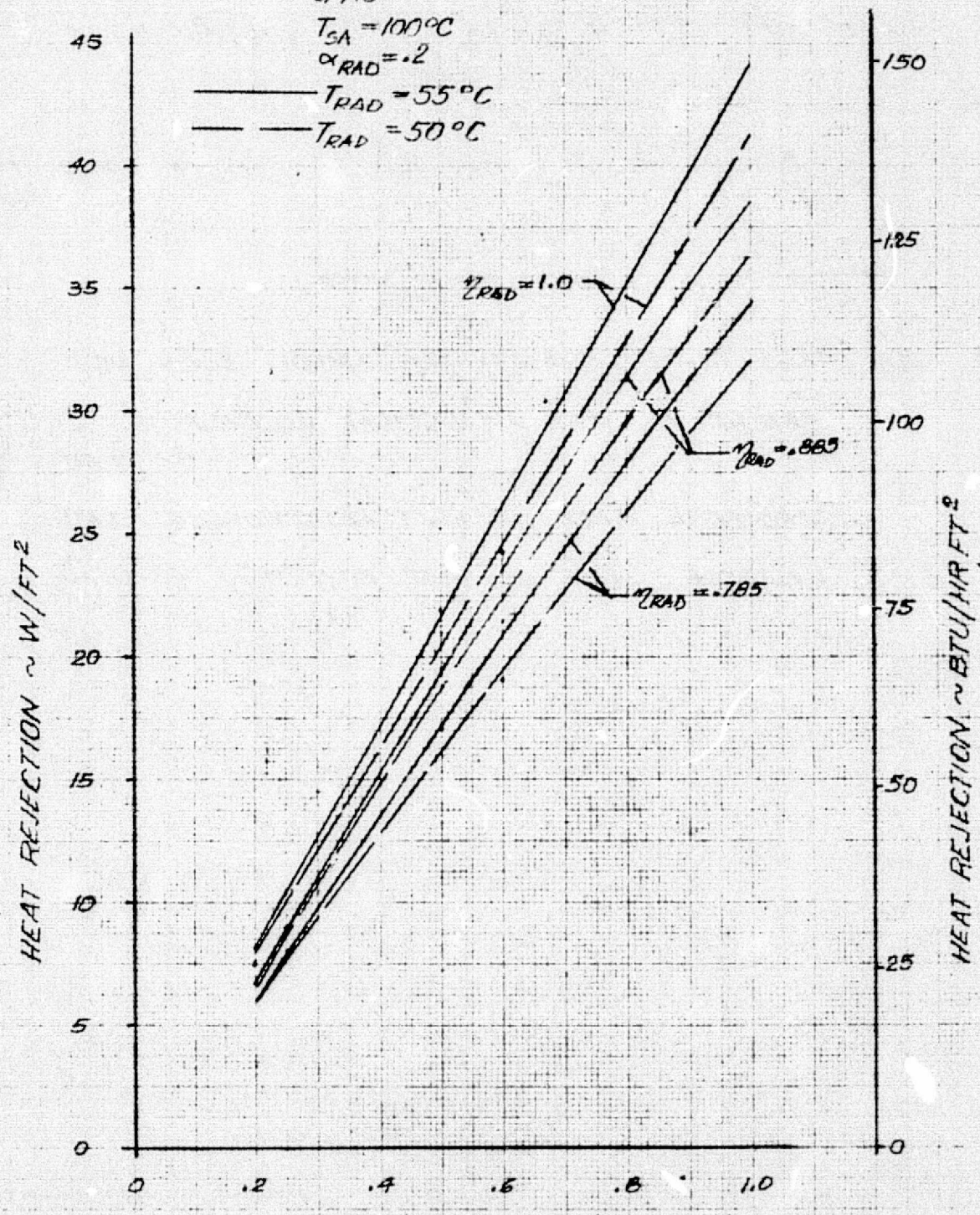

FIG. M-3-5

RADIATOR AREA vs HEAT REJECTION
.7 AU

$T_{SOLAR\ ARRAY} = 100°C$
$\epsilon_{RAD} = .88$
$\alpha_{RAD} = .2$

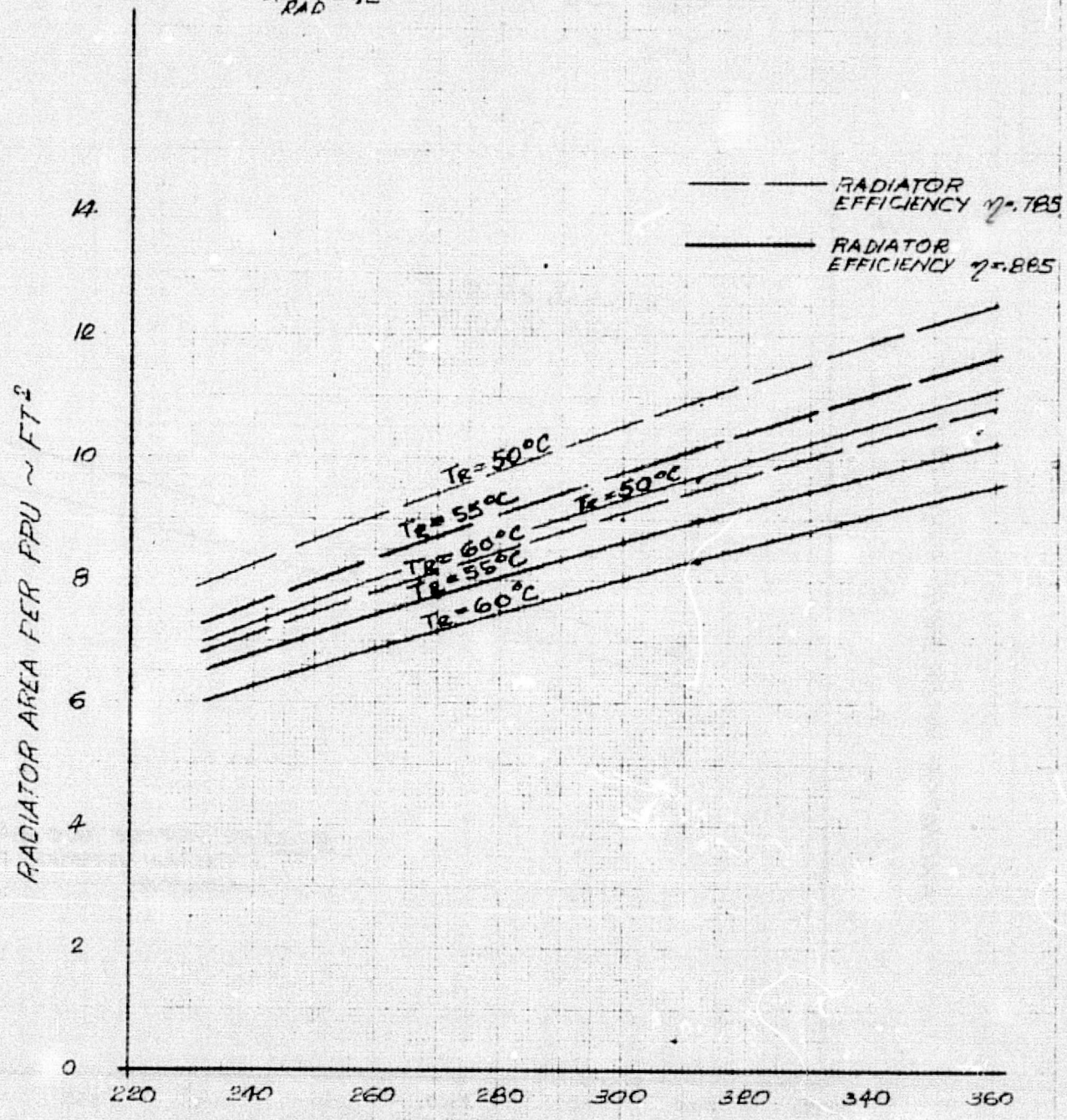

FIG. A-2-6

LER 9/74

RADIATOR AREA vs. HEAT REJECTION
1.0 AU

$T_{SOLAR\ ARRAY} = 50°C$

RADIATOR EFFICIENCY $\eta = .885$

$\epsilon_{RAD} = .88$

$\alpha_{RAD} = .2$

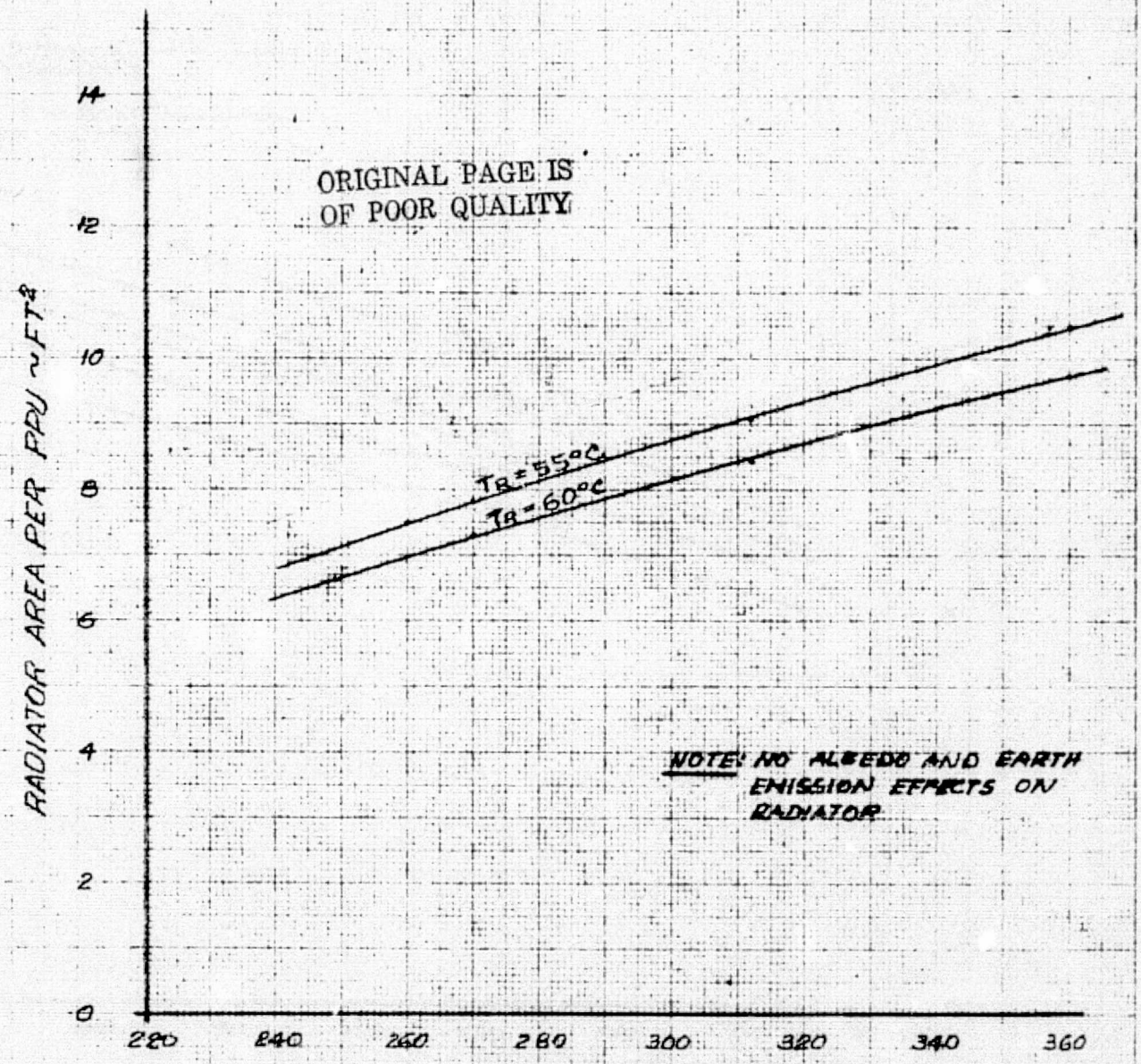

FIG. A-3-7

LER 10/74

PREPARED BY:	SPACE DIVISION NORTH AMERICAN ROCKWELL CORPORATION	PAGE NO. 13 OF 21
CHECKED BY:		REPORT NO. A 3
DATE:		MODEL NO. "C" PART 3

HEAT PIPE MOUNTING
& TEMP. DROP.

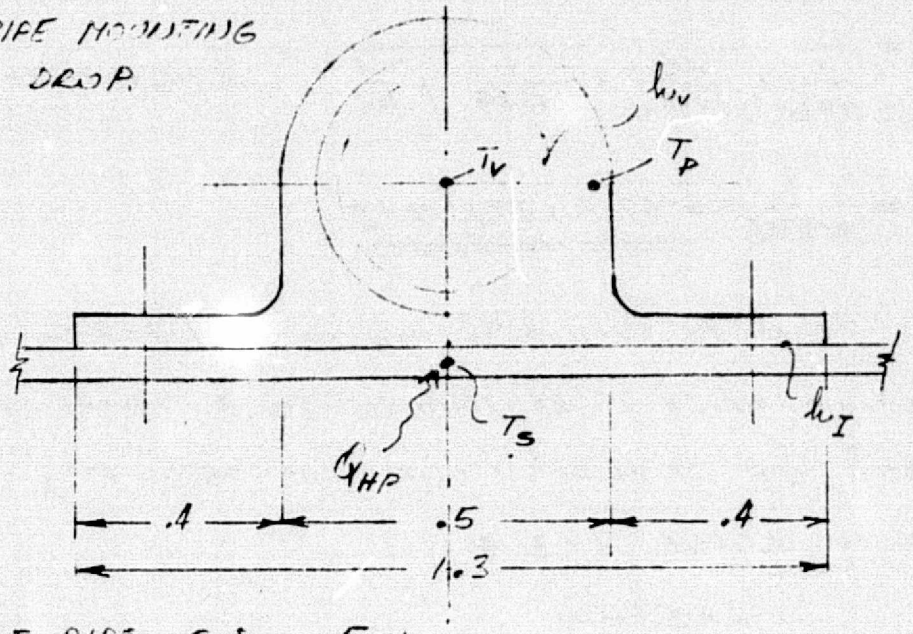

HEAT PIPE O.D .5 IN

I.D .33 IN

EVAPORATOR LENGTH 36 IN

ASSUME:

$h_V = 500$ BTU/HR FT^2 °F

$h_I = 500$ — " —

$K_{AL} = 100$ BTU/HR FT °F

TO BE CALCULATED ΔT_{V-S} FOR 1.3 IN SADDLE

$$\Delta T_{V-S} = \Delta T_{V-P} + \Delta T_{P-I} + \Delta T_{I-S}$$

$$K_T = \frac{1}{\frac{1}{K_{V-P}} + \frac{1}{K_P} + \frac{1}{K_b + K_F} + \frac{1}{K_I}}$$

$$K_T = \frac{1}{\frac{1}{\frac{500(\pi)(.33)36}{144}} + \frac{\ln(.5/.33)}{2\pi\frac{100}{12}36} + \frac{1}{\frac{(100/12)(.5)(36)}{.1014}} + \frac{1}{\frac{(100/12)(.08)(36)}{.4}} + \frac{1}{(500/144)36(1.3)}}$$

$$K_T = \frac{1}{\frac{1}{129.6} + \frac{.415}{1229.2} + \frac{1}{1539} + \frac{1}{162.5}} = \frac{1}{.007716 + .000622 + .000646 + .00615} =$$

$$= \frac{1}{.014736} = \underline{67.86 \text{ BTU/HR°F}}$$

THE FINAL DESIGN ASSUMED A RADIATOR EFFICIENCY $\eta = .8$ WHICH CORRESPONDS TO A TOTAL RADIATOR AREA OF $71.24 FT^2$ (ONE SIDE $35.62 FT^2$)

FROM CURVE A-3-4

$L = 5.68$ IN

THE DIMENSIONS OF THE RADIATORS 63IN × 81 IN

A TOTAL OF 26 VCHP'S (13 TO EACH RADIATOR) WILL TRANSPORT THE HEAT FROM THE PP ELECTRONICS TO THE RADIATORS.

$$\Phi_{VCHP} = \frac{2187.5}{26} = 84.13 \text{ W/VCHP}$$

$$\Phi = \frac{\Delta T}{R}$$

$$\therefore \Delta T = R\Phi = \frac{\Phi}{K_T} = \frac{84.13(3.41)}{67.86} = 4.227 \sim 4.23°F$$

ASSUME .9 IN SADDLE

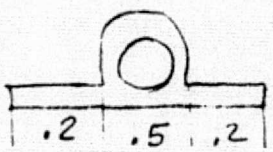

$$K_T = \frac{1}{.007936 + \frac{1}{1479.29 + \frac{(100/12)(.08)36}{.2}} + \frac{1}{(500/144)36(.9)}} =$$

$$K_T = \frac{1}{.007936 + .00625 + .0089} = 57.27 \text{ BTU/HR °F}$$

$$\Delta T = \frac{84.13\,(3.41)}{57.27} = 5.009\ ^\circ F$$

IF SADDLE .5 IN

$$A = \frac{.5^2\pi}{4} - \left(\frac{.33^2\pi}{4} + 20\,\frac{.05^2\pi}{4}\right) = .0715\ IN^2$$

$$K_T = \frac{1}{.007936 + .016676} = 40.63 \text{ BTU/HR °F}$$

$$\Delta T = \frac{84.13\,(3.41)}{40.63} = 7.06\ ^\circ F$$

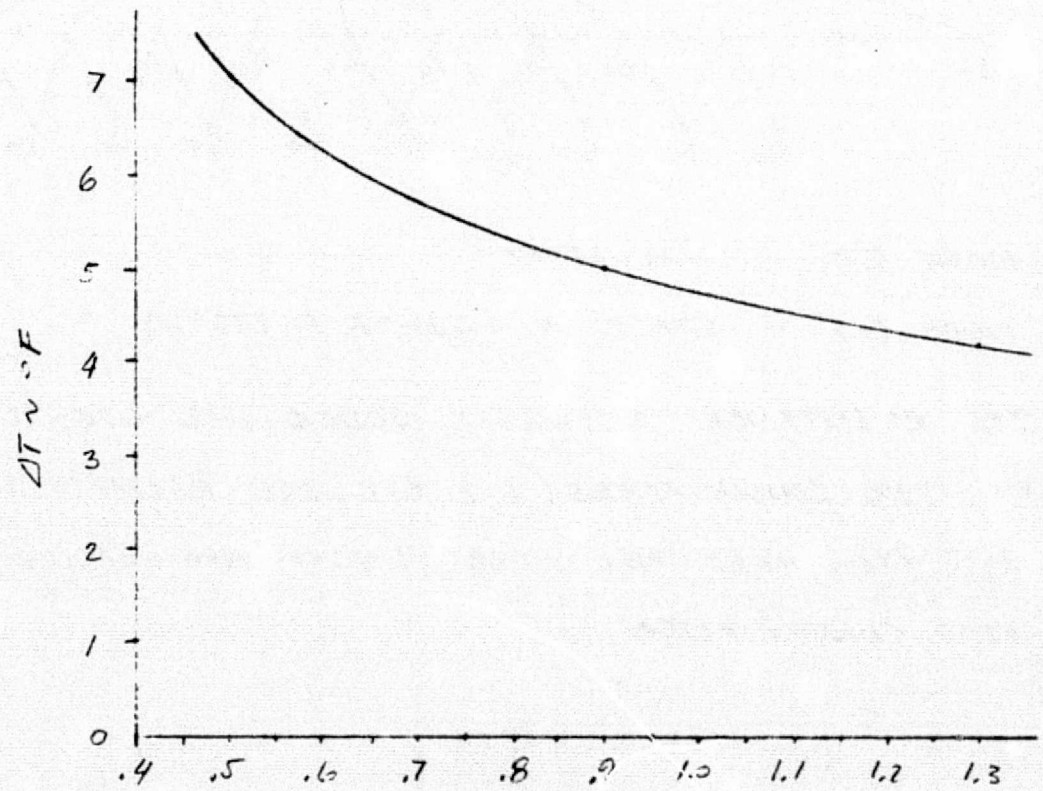

TO VERIFY PRELIMINARY ANALYTICAL RESULTS (HAND CALCULATIONS) A THERMAL NETWORK FOR ONE FIN SEGMENT OF THE RADIATOR WILL BE DEVELOPED AND SOLVED BY THE THERMAL ANALYZER (XF0014)

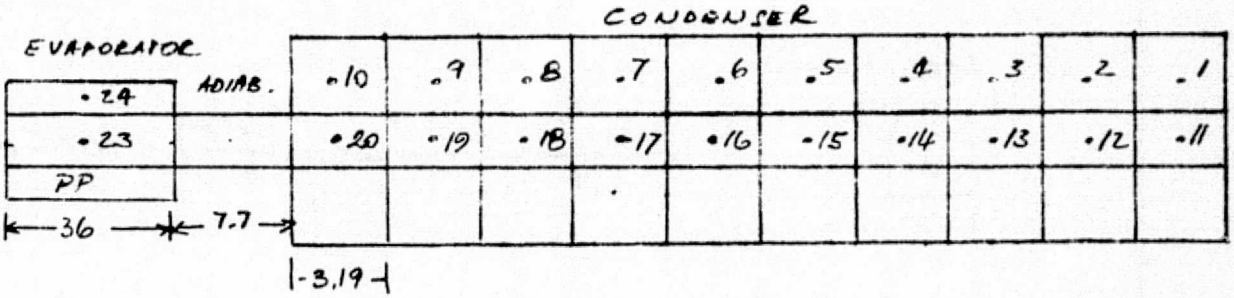

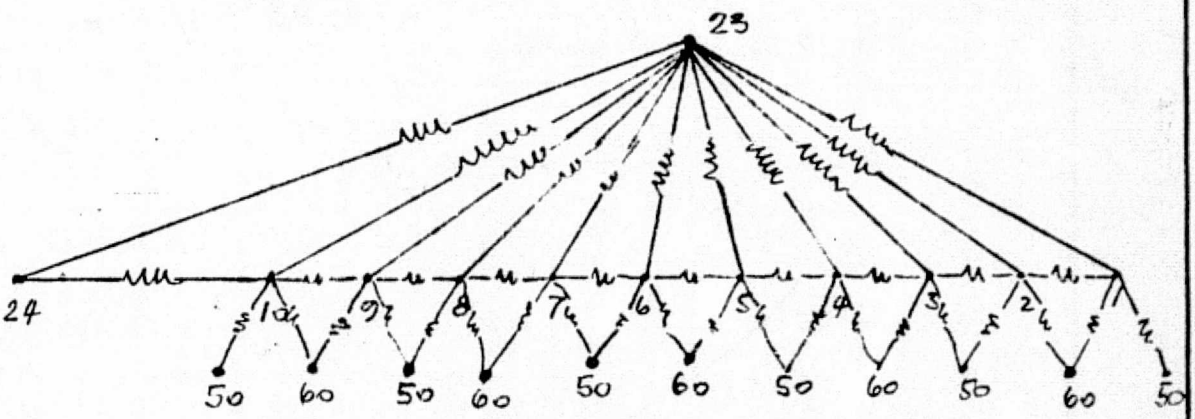

NODE 50 - SOLAR ARRAY

NODE 60 - SPACE @ -460°F (-273°K)

THE RESISTANCE BETWEEN NODES 1-2 ETC. IS COMPOSED OF TWO CONDUCTANCES (1, 2 ETC. ARE RADIATOR NODES; 11, 12 ETC. HEAT PIPE NODES): VCHP PIPE + SADDLE + RADIATOR CONDUCTANCE

CONDUCTANCE ALONG RADIATOR PLATE

$$K = \frac{KA}{12L} = \frac{100(11.36)(.04)}{12(3.19)} = 1.187 \text{ BTU/HR °F}$$

CONDUCTANCE ALONG HEAT PIPE & FLANGE (CONDENSER SECTION)

$$K = \frac{100(.13037)}{12(3.19)} = .341 \text{ BTU/HR °F}$$

CONDUCTANCE ALONG PIPE (COND & ADIABATIC)

$$R_T = R_1 + R_2 = \frac{12(1.59)}{100(.13037)} + \frac{12(3.85)}{100(.0715)} = 1.464 + 6.46 = 7.93 \text{ HR °F/BTU}$$

$$K = \frac{1}{R_T} = \frac{1}{7.93} = .126 \frac{\text{BTU}}{\text{HR °F}}$$

CONDUCTANCE ALONG PIPE (EVAP. & ADIABATIC)

$$R_T = R_1 + R_2 = \frac{12(3.85)}{100 \times .0715} + \frac{12(18)}{100 \times .1307} = 6.46 + 16.568 = 23.028 \frac{\text{HR °F}}{\text{BTU}}$$

$$K = \frac{1}{R_T} = .0434 \frac{\text{BTU}}{\text{HR °F}}$$

DETERMINATION OF HEATER POWER

$q_{PP} = 0$

$T_{SA} = -100°C = 312°R$

HEAT LEAK FROM THE PP'S TO THE RADIATORS WILL BE THROUGH THE VCHP WALLS. THE DISTANCE BETWEEN PP'S AND RADIATORS WILL BE APPROX. 7.5 IN

$A_{VCHP} = .0715\ in^2$ (ADIABAITC SECTION)

$$R = \frac{12L}{KA} = \frac{12(7.5)}{100(.0715)} = 12.923\ HR°F/BTU$$

13 VCHP'S TO ONE RADIATOR

$$\therefore R_T = \frac{12.923}{13} = .994\ HR°F/BTU$$

$T_{PP} = -50°C = -58°F = 402°R$ NON-OPERATING SURVIVAL TEMP.

HEAT BALANCE FOR RADIATOR

$q_{IN} = q_{OUT}$

$$q_{IN} = \frac{T_{PP} - T_R}{R_T} + \sigma \epsilon_R \epsilon_{SA} F_{R-SA} A_R (T_{SA}^4 - T_R^4)$$

$$q_{OUT} = \sigma \epsilon_R \epsilon_{SP} F_{R-SP} A_R (T_R^4)$$

$$\frac{402 - T_R}{.994} + \sigma(.88)(.8)(.2)\,35.62\,(312^4 - T_R^4) = \sigma(.88)1(.88)35.62(T_R^4)$$

$$402 - T_R + 48.93 = 4.73 \times 10^{-8} T_R^4$$

$$450.93 = 4.73 \times 10^{-8} T_R^4 + T_R$$

LET $T_R = 300°R$

$383 + 300 = 683 > 451$

LET $T_R = 250°R$

$184 + 250 = 434 < 451$

LET $T_R = 255°R$

$200 + 255 = 455 > 451$

LET $T_R = 254°R$

$196 + 254 = 450 \sim 451$

$T_R = 254°R$

$$q_H = \frac{402 - 254}{.994} = 148.89 \text{ BTU/AR} = 43.66 \text{ W}$$

FOR TWO RADIATORS

$$\underline{q_T} = 2(43.66) = \underline{87.32 \text{ W}}$$

$T_{SA} = -50°C = -58°F = 402°R$

$402 - T_R + 134.86 = 4.73 \times 10^{-8} T_R^4$

$536.86 = 4.73 \times 10^{-8} T_R^4 + T_R$

LET $T_R = 270°R$

$251 + 270 = 521 < 537$

LET $T_R = 273°R$

$263 + 273 = 536 \sim 537$

$T_R = 273°R$

$$Q_H = \frac{402 - 273}{.994} = 129.78 \text{ BTU/HR} = 38.06 \text{ W}$$

$$Q_{H_T} = 38.06(2) = 76.12 \text{ W}$$

$T_A = 0°C = 32°F = 492°R$

$$402 + 302.58 - T_R = 4.73 \times 10^{-8} T_R^4$$

$$704.58 = 4.73 \times 10^{-8} T_R^4 + T_R$$

LET $T_R = 300°R$

$383 + 300 = 683 < 704$

LET $T_R = 302°R$

$393 + 302 = 695 < 704$

LET $T_R = 307°R$

$399 + 303 = 702 < 704.6$

$T_R = 304°R$

$$Q_H = \frac{402 - 304}{.994} = 98.59 \text{ BTU/HR} = 28.91 \text{ W}$$

$$Q_T = (2)\,28.91 = 57.82 \text{ W}$$

PREPARED BY: ALS	SPACE DIVISION NORTH AMERICAN ROCKWELL CORPORATION	PAGE NO. 1 OF 4
CHECKED BY:		REPORT NO. APPENDIX 4
DATE: 11 74	4 SIDE VCHP/OSR	MODEL NO. CONCEPT 4

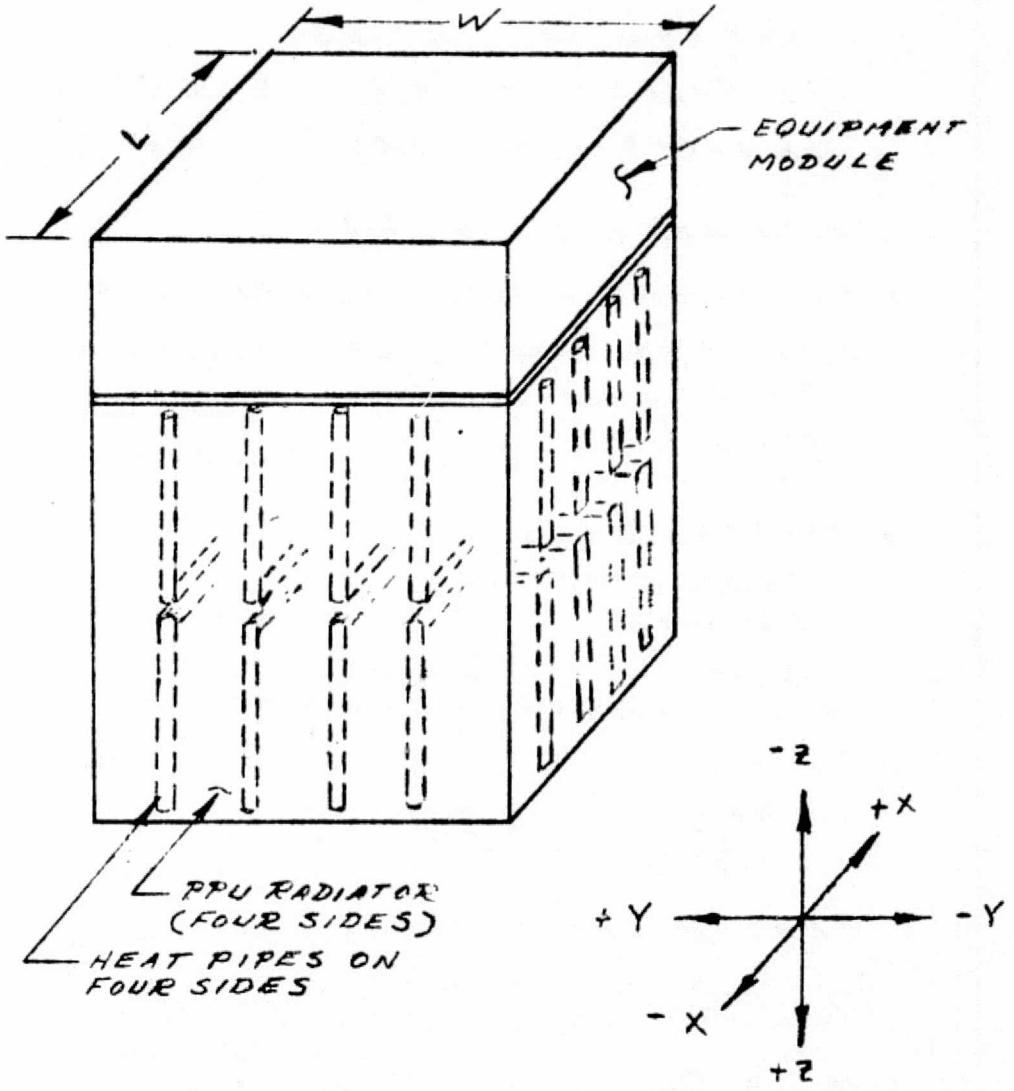

OPTICAL SOLAR REFLECTOR (OSR) SURFACES ON RADIATORS EXPOSED TO SUN (YZ FACES).

LOW α/ϵ ($\frac{0.2}{0.88}$) FOR XZ FACES.

PRECEDING PAGE BLANK NOT FILMED

FIGURE 1

PREPARED BY: RLS	SPACE DIVISION NORTH AMERICAN ROCKWELL CORPORATION	PAGE NO. 2 OF 4
CHECKED BY:		REPORT NO. APPENDIX 4
DATE: 11/74	4 SIDE VCHP/OSR	MODEL NO. CONCEPT 4

CALCULATIONS FOR RADIATOR SIZING:

- OPTICAL PROPERTIES.

  XZ FACES - $\alpha_s = 0.2$, $\epsilon = 0.88$ } RADIATORS *

  YZ FACES - $\alpha_s = 0.05$, $\epsilon = 0.81$ }

  SOLAR ARRAY - $\epsilon = 0.8$

- RADIATION CONFIGURATION FACTORS

  RADIATOR/SOLAR ARRAY - $F_{R-SA} = 0.12$ (XZ FACES)

  RADIATOR/SPACE $F_{R-SP} = 0.88$ (XZ FACES)

  RADIATOR/SPACE $F_{R-SP} = 1.0$ (YZ FACES)

- TEMPERATURES

  SOLAR ARRAY 150°C

  RADIATOR 55°C

  SINK -273.2°C

- FIN EFICIENCY - η - REFER TO APPENDIX 3, PGS. 4 THRU 9.

- INCIDENT SOLAR HEAT FLUX @ 0.38 AU

$$S = \frac{440}{.38^2} \approx 3047 \frac{BTU}{HR\ FT^2}$$

HEAT BALANCE CALCULATIONS:

$$Q_{OUT} = Q_{IN}$$

$$Q_{OUT} = Q_{SP}$$

$$Q_{IN} = Q_{SOLAR} + Q_{R-SA}$$

$$Q_{REJ.} = Q_{OUT} - Q_{IN} \quad \text{(REPRESENTS TOTAL HEAT DISSIPATED BY HP'S)}$$

$$Q_{REJ.} = \sigma \epsilon_R \times F_{R-SP}\, \eta\, 2A_{XZ} \times T_R^4 + \sigma \epsilon_R \times F_{R-SP}\, T_R^4\, 2A_{YZ} - \alpha S A_{YZ} - \sigma \epsilon_{SA} \epsilon_R \times F_{R/SA} \left(T_{SA}^4 - T_R^4\right) 2A_{XZ}\, \eta$$

$$Q_{REJ.} = .1714 \times 10^{-8} \times .88 \times .88 \times \eta \times \frac{2 \times L \times 80}{144} T_R^4 + .1714 \times 10^{-8} \times .88 \times .81 \times \eta \times \frac{2 \times W \times 80}{144} \times T_R^4 - 0.5 \times 3047 \times \frac{2 \times W \times 80}{144} - .1714 \times 10^{-8} \times .8 \times .88 \times .12 \left(T_{SA}^4 - T_R^4\right) \frac{2 \times L \times 80}{144} \eta$$

* SEE FIG. 1 FOR RADIATOR ORIENTATION

PREPARED BY: RLS	SPACE DIVISION NORTH AMERICAN ROCKWELL CORPORATION	PAGE NO. 3 OF 4
CHECKED BY:		REPORT NO. APPENDIX 4
DATE: 11/74	4 SIDE VCHP/OSR	MODEL NO. CONCEPT 4

HEATER POWER REQUIREMENTS.

ASSUMPIONS: $L/W = 1.0$

$\eta = 0.885$ FIN EFFICIENCY 40 HEAT PIPES (10 PER SIDE)

RADIATOR HEIGHT - 80"

$L = W = 36.5"$ RAD. LENGTH = RAD. WIDTH

HEAT LEAK THRU PIPE WALL ONLY

PIPE CROSS SECTION AREA = $0.0715\ IN^2$

PIPE LENGTH $\ell = 7.7"$ ADIABATIC SECTION BETWEEN EVAPORATOR AND RADIATOR

CONDUCTANCE OF PIPE *

$$C = \frac{KA}{12\ell} = \frac{100\ \frac{BTU}{FT\,^\circ F} \times .0715\ IN^2}{12\ \frac{IN}{FT} \times 7.7\ IN} = 0.0773\ \frac{BTU}{HR\,^\circ F}$$

$$R = \frac{1}{C} = \frac{1}{.0773} = 12,937\ \frac{HR\,^\circ F}{BTU}$$

$$R_T = \frac{1}{\frac{1}{R_1} + \frac{1}{R_2} + \frac{1}{R_3} + \ldots \frac{1}{R_{40}}} = \frac{1}{\frac{40}{12.937}} = 0.323\ \frac{HR\,^\circ F}{BTU}$$

HEAT BALANCE:

PP @ SURVIVAL TEMP = $-50^\circ C$

SOLAR ARRAY TEMP = $-100^\circ C$

$Q_{OUT} = Q_{R-SP}$

$Q_{IN} = Q_{SA-R} + Q_{HEATER}$

$Q_{OUT} = Q_{IN}$

$$\sigma \epsilon_R \times F_{R-SP} \times T_R^4 (2A_{XZ}) + \sigma \epsilon_R \times F_{R-SP} \times T_R^4 (2A_{YZ}) =$$

$$\sigma \epsilon_R^4 \times \epsilon_{SA} F_{R-SA} (T_{SA}^4 - T_R^4) \times 2A_{XZ} + \frac{T_{PP} - T_R}{R}$$

$$.1714 \times 10^{-8} \times .88 \times .88 \times T_R^4 \left(\frac{2 \times 36.5 \times 80}{144}\right) + .1714 \times 10^{-8} \times .81 \times 1.0 \times T_R^4 \left(\frac{2 \times 36.5 \times 80}{144}\right) =$$

$$.1714 \times 10^{-8} \times .88 \times .8 \times 0.12 (312^4 - T_R^4) + \frac{402 - T_R}{R}$$

* SEE APPENDIX 3 FOR HEAT PIPE DETAILS PGS. 13-15

(CONT. NEXT PAGE)

HEATER POWER REQ. (CONT.):

$$5.38\times10^{-8}T_{RAD}^4 + 5.63\times10^{-8}T_R^4 = 5.87\times10^{-9}(312^4 - T_R^4) + \frac{402 - T_R}{.323}$$

$$11.01\times10^{-8}T_{RAD}^4 = 5.87\times10^{-9}(312^4 - T_{RAD}^4) + \frac{402 - T_{RAD}}{.323}$$

$$3.556\times10^{-8}T_R^4 = 1.896\times10^{-9}(312^4 - T_R^4) + 402 - T_R$$

$$3.746\times10^{-8}T_R^4 + T_R = 419.97$$

TRY $T_R = 250°R$

$146.33 + 250 = 396 < 419.97$

TRY $255°R$

$158.14 + 255 = 413.14 < 419.97$

TRY $257°R$

$155.67 + 257 = 412.67$

TRY 257.5

$164.43 + 257.5 = 421.93 \approx 419.97$

$$Q_{HEATER} = \frac{T_{PP} - T_{RAD}}{R} = \frac{402 - 257.5}{.323} = 447.37\ \frac{BTU}{HR} = 131.2\ WATTS$$

POWER REQ. IF SOLAR ARRAY TEMP. $= -50°C = 402°R$:

$$3.746\times10^{-8}T_R^4 + T_R = 451.52$$

TRY $T_R = 265°R$

$184.74 + 265 = 449.74 \approx 451.52$

$$Q_{HEATER} = \frac{T_{PP} - T_R}{.323} = \frac{402 - 265}{.323} = 424\ \frac{BTU}{HR} = 124.4\ WATTS$$

IF SOLAR ARRAY $= 0°C = 492°R$

$3.746\times10^{-8}T_R^4 + T_R = 513.1$ TRY $T_R = 280.5$

$231.9 + 280.5 = 512.4 \approx 513.1$

$$Q_{HEATER} = \frac{402 - 280.5}{.323} = 376 = 110.3\ W$$

PREPARED BY: R L S	SPACE DIVISION NORTH AMERICAN ROCKWELL CORPORATION	PAGE NO. 1 OF 6
CHECKED BY:		REPORT NO. APPENDIX 5
DATE: 11/72	4 SIDE VCHP/DHP	MODEL NO. CONCEPT 5

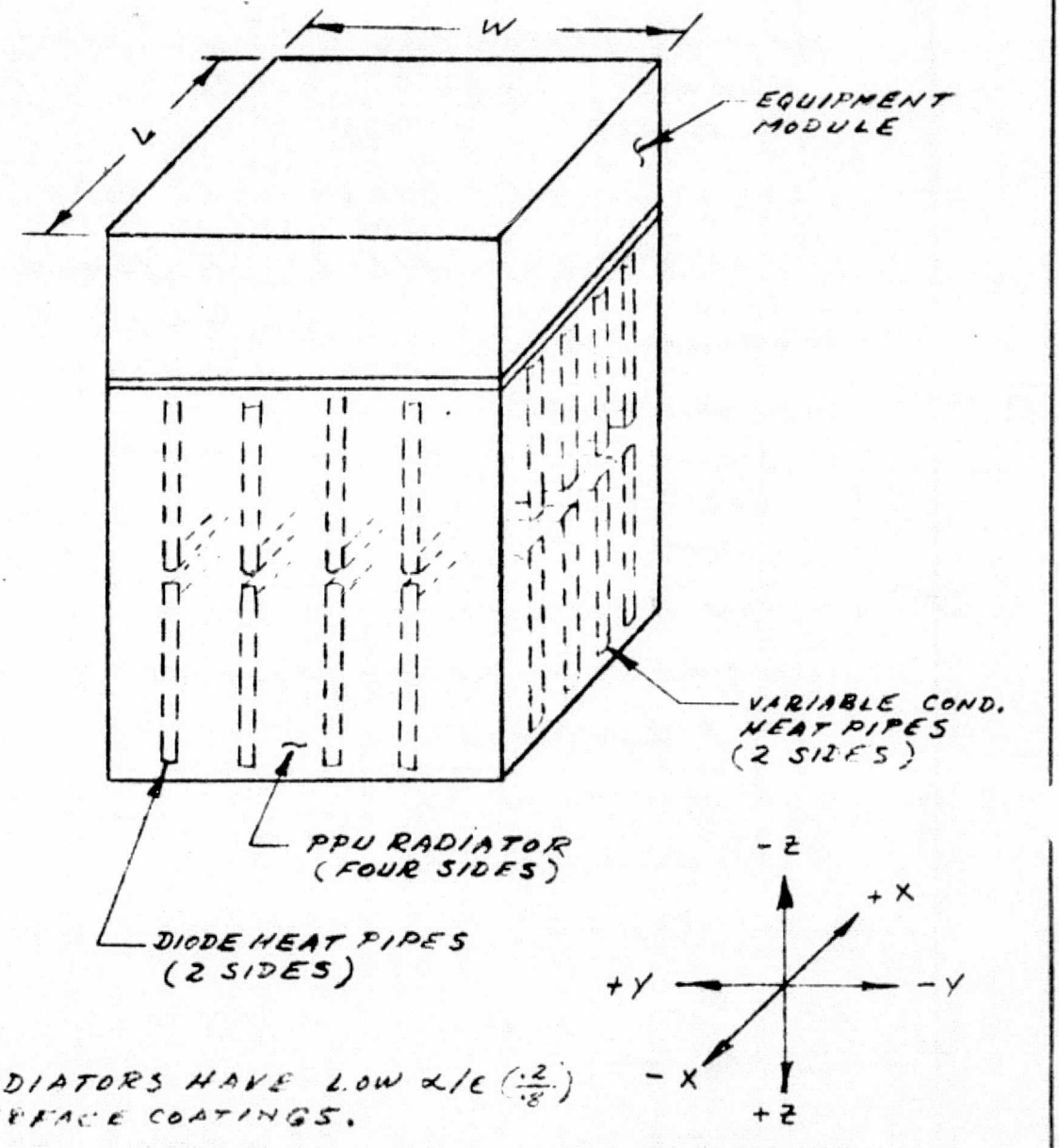

RADIATORS HAVE LOW α/ε $\left(\frac{.2}{.8}\right)$ SURFACE COATINGS.

FIGURE 1

PREPARED BY: [illegible]	SPACE DIVISION NORTH AMERICAN ROCKWELL CORPORATION	PAGE NO. 2 OF 10
CHECKED BY:		REPORT NO. [illegible]
DATE: 11/24	4 SIDE VCHP/DHP	MODEL NO. CONCEPT 5

CALCULATIONS FOR RADIATOR SIZING:

- OPTICAL PROPERTIES

  RADIATOR $\alpha_s = 0.2$, $\epsilon = 0.85$

  SOLAR ARRAY $\epsilon = 0.8$

- RADIATION CONFIGURATION FACTORS *

  RADIATOR / SOLAR ARRAY $F_{R\text{-}SA} = 0.12$ (X2 FACES)

  RADIATOR / SPACE $F_{R\text{-}SP} = 0.88$ (X2 FACES)

  RADIATOR / SPACE $F_{R\text{-}SP} = 1.0$ (Y2 FACES)

- TEMPERATURES

  SOLAR ARRAY 150 °C

  RADIATOR 55 °C

  SINK -273.2 °C

- FIN EFFICIENCY η; REFER TO APPENDIX 3, PGS. 4-9

- INCIDENT SOLAR HEAT FLUX @ 0.38 AU

$$S = \frac{440}{0.38^2} = 3047 \frac{BTU}{HR\,FT^2}$$

HEAT BALANCE:

$Q_{REJ} = Q_{OUT} - Q_{IN}$ (REPRESENTS TOTAL HEAT DISSIPATED BY RAD.)

$Q_{OUT} = Q_{SP}$

$Q_{IN} = Q_{SA\text{-}R}$

$$Q_{REJ} = \sigma \epsilon_R X F_{R\text{-}SP} \eta\, 2A_{XZ} T_R^4 + \sigma \epsilon_R X F_{R\text{-}SP} \eta\, 2A_{YZ} - \sigma \epsilon_{SA} \epsilon_R X F_{R\text{-}SA} \eta\, 2A_{XZ}$$

$$Q_{REJ} = .1714 \times 10^{-8} \times .88 \times .88 \times \eta \frac{2 \times L \times 60.5}{144} T_R^4 + .1714 \times 10^{-8} \times .81 \times 1.0 \times \eta \frac{2 \times W \times 60.5}{144} T_R^4 - .1714 \times 10^{-8} \times .8 \times .88 \times .12\, \eta \frac{2 \times L \times 60.5}{144} T_R^4$$

* SEE FIG. 1 FOR RADIATOR ORIENTATION

HEATER POWER REQUIREMENTS

ASSUMPTIONS:

L/W = 1.0 32 HEAT PIPES (8 PER SIDE)

η = 0.735 FIN EFFICIENCY

RAD. HEIGHT = 60.54" L = W = 56.62"

HEAT LEAK THRU PIPEWALL ONLY

HEAT PIPE CROSS SECTIONAL AREA = 0.0715 IN^2

PIPE LENGTH ℓ = 7.7" ADIABATIC SECTION BETWEEN EVAPORATOR AND RADIATOR

CONDUCTANCE OF PIPE

$$C = \frac{KA}{12\ell} = \frac{100 \times 0.0715}{12 \times 7.7} = 0.0773 \frac{Btu}{HR\ ^\circ F} \quad *$$

$$R = \frac{1}{C} = \frac{1}{.0773} = 12.937 \frac{HR\ ^\circ F}{Btu}$$

$$R_T = \frac{1}{\frac{1}{R_1} + \frac{1}{R_2} + \cdots \frac{1}{R_{32}}} = \frac{1}{\frac{32}{12.937}} = 0.4043 \frac{HR\ ^\circ F}{Btu}$$

HEAT BALANCE WITH PP @ -50°C SOLAR ARRAY @ -100°C

$Q_{OUT} = Q_{R-SP}$

$Q_{IN} = Q_{SA-R} + Q_{HEATER}$

$Q_{OUT} = Q_{IN}$

$$\sigma \epsilon_R \times F_{R-SP} \times T_R^4 \left(\frac{2 \times 56.62 \times 60.54}{144}\right) + \sigma \epsilon_R F_{R-S} T_{R-S}^4 \left(\frac{2 \times 56.62 \times 60.54}{144}\right)$$

$$= \sigma \epsilon_R \times \epsilon_{SA} F_{R-SP} \left(T_{SA}^4 - T_R^4\right)\left(\frac{2 \times 56.62 \times 60.54}{144}\right) + \frac{T_{PP} - T_R}{R}$$

$$.1714 \times 10^{-8} \times .88 \times .88 \times T_R^4 \ (47.61) + .1714 \times 10^{-8} \times .88 \times 1.0\ T_R^4 \ (47.61) =$$

$$.1714 \times 10^{-8} \times .88 \times .8 \times .12 \left(312^4 - T_R^4\right)(47.61) + \frac{T_{PP} - T_R}{.4043}$$

* SEE APPENDIX 3, (PGS. 13-15) FOR HEAT PIPE DETAILS

(CONT.)

HEATER POWER REQ. (CONT.)

$$6.32\times10^{-8}T_R^4 + 7.18\times10^{-8}T_R^4 = 6.89\times10^{-9}(312^4 - T_R^4) + \frac{402 - T_R}{.4043}$$

$$13.5\times10^{-8}T_R^4 = 6.89\times10^{-9}(312^4 - T_R^4) + \frac{402 - T_R}{.4043}$$

$$5.458\times10^{-8}T_R^4 = 2.786\times10^{-9}(312^4 - T_R^4) + 402 - T_R$$

$$5.737\times10^{-8}T_R^4 + T_R = 428.4$$

TRY $T_R = 230°R$

THEN $160.54 + 230 = 390.54 < 428.4$

TRY $240°R$

THEN $190.34 + 240 = 430.83 > 428.4$

TRY 239.5

$188.76 + 239.5 = 428.3 \approx 428.4$

$$Q_{HEATER} = \frac{402 - 239.5}{.4043} = 401.93 \frac{Btu}{HR} = \underline{117.9 \text{ WATTS}}$$

HEATER POWER REQ. IF SOLAR ARRAY TEMP. = $-50°C = 402°R$

$$5.737\times10^{-8}T_R^4 + T_R = 2.786\times10^{-9}(402^4 - T_R^4) + 402$$

$$5.737\times10^{-8}T_R^4 + T_R = 474.67$$

TRY $T_R = 240°R$

$190 + 240 = 430°R < 474.67$

TRY $250°R$

$224.10 + 250 = 474.1 \approx 474.67$

$T_R = 250°R$

$$Q_{HEATER} = \frac{402 - 250}{.4043} = 375.96 \frac{Btu}{HR} = \underline{110.25 \text{ WATTS}}$$

HEATER POWER REQ. IF SOLAR ARRAY TEMP. = $0°F = 492°R$

$$5.737\times10^{-8}T_R^4 + T_R = 2.786\times10^{-9}(492^4 - T_R^4) + 402$$

$$5.737\times10^{-8}T_R^4 + T_R = 163.25 + 402 = 565.25$$

TRY $T_R = 268°R$ $\quad 268 + 296 = 564 \approx 565.25$

$$Q_{HEATER} \quad \frac{402 - 268}{.4043} = 331.43 \frac{Btu}{HR} = \underline{97.20 \text{ WATTS}}$$

PREPARED BY:	SPACE DIVISION NORTH AMERICAN ROCKWELL CORPORATION	PAGE NO. 5 OF 6
CHECKED BY:		REPORT NO. APPENDIX 5
DATE:	THERMAL MODEL	MODEL NO. SNAPSHOT 5

CALCULATIONS AND ASSUMPTIONS USED TO DEVELOPE THERMAL MODEL:

CONDUCTANCE BETWEEN HEAT PIPE AND EVAPORATOR

$C = 67.86 \frac{BTU}{HR\ ^\circ F}$ REFERE TO APPENDIX 3, PGS. 13-15. FOR CALCULATION.

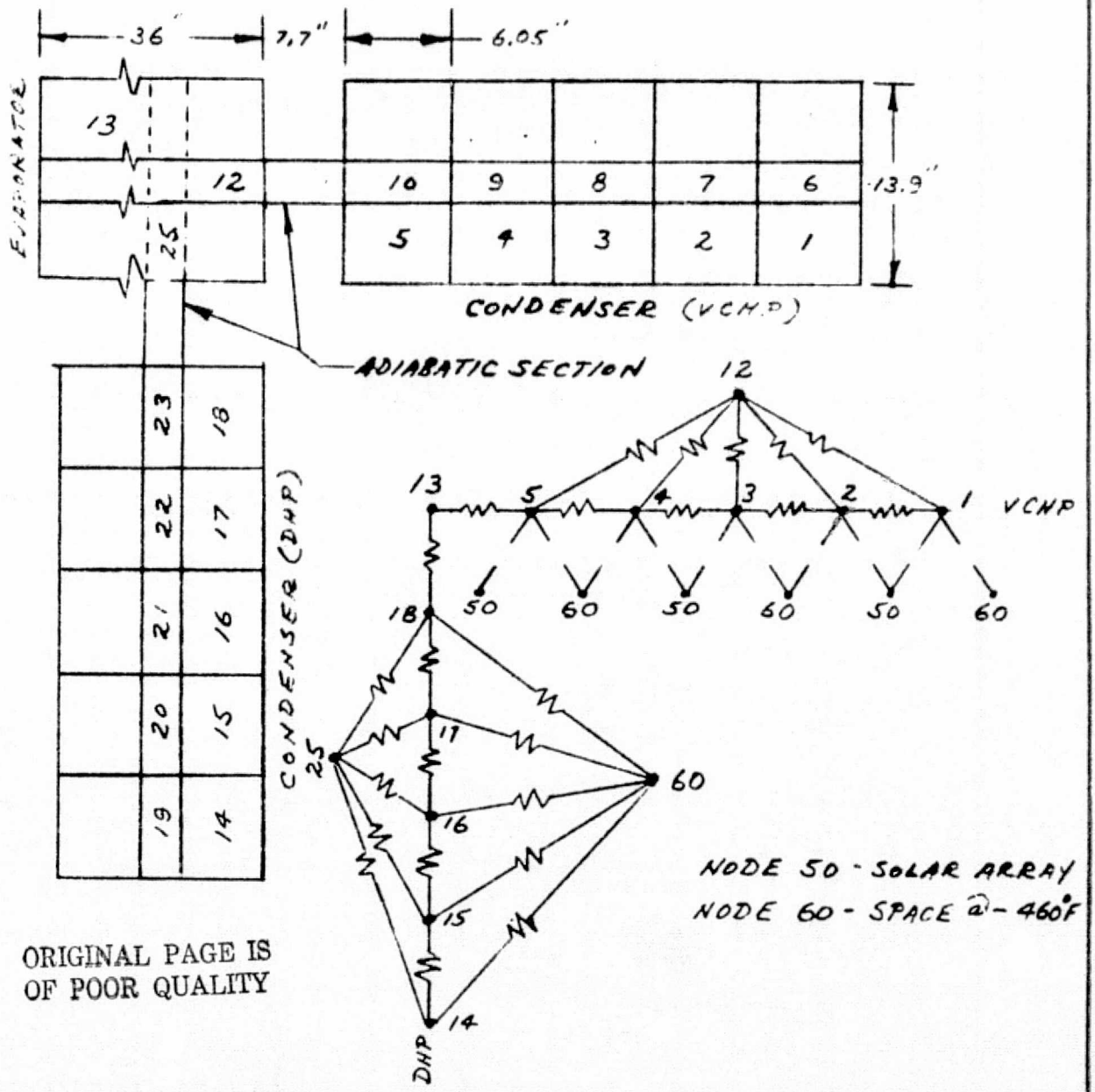

NODE 50 - SOLAR ARRAY
NODE 60 - SPACE @ - 460°F

ORIGINAL PAGE IS
OF POOR QUALITY

NOTE: THE RESISTANCES BETWEEN NODES 1-2 ETC ARE EQUIVALENT TO RESISTANCES BETWEEN 1 AND 2 + 6 AND 7 ADDED IN PARALLEL. ALSO TRUE OF 14-15 AND 19-20 ETC.

CONDUCTANCE BETWEEN HP AND RADIATOR NODES:

$$C = K_{HP/EVAP} \times \frac{\ell_{NODE}}{\ell_{EVAP.}} = 67.86 \times \frac{6.05}{36} = 11.404 \frac{BTU}{HR\,^\circ F}$$

• CONDUCTANCE ALONG RADIATOR.

$$C_1 = \frac{KA}{12\ell} = 100 \frac{BTU}{HR\,^\circ F} \times \frac{13.9 \times .04\ IN^2}{\frac{12\ IN}{FT} \times 6.05\ IN} = 0.7658 \frac{BTU}{HR\,^\circ F}$$

• CONDUCTANCE ALONG HEAT PIPE AND FLANGE.

$$C_2 = \frac{KA}{12\ell} = \frac{100 \times .13037}{12 \times 6.05} = 0.1796$$

• $C_{PLATE+PIPE} = C_1 + C_2 = 0.7658 + .1796 = 0.9454 \frac{BTU}{HR\,^\circ F}$

• CONDUCTANCE ALONG PIPE (COND.- ADIABATIC SECTION)

$$R_T = R_1 + R_2 = \frac{12 \times 3.025}{100 \times .13037} + \frac{12 \times 3.85}{100 \times .0715} = 2.784 + 6.462$$

$$R_T = 9.246$$

$$C = \frac{1}{R_T} = 0.1082 \frac{BTU}{HR\,^\circ F}$$

• CONDUCTANCE ALONG PIPE (ADIABATIC – EVAP. SECTION)

$$R_T = R_1 + R_2 = \frac{12 \times 3.85}{100 \times .0715} + \frac{12 \times 18}{100 \times .13037} = 6.462 + 16.568$$

$$R_T = 23.03 \frac{HR\,^\circ F}{BTU}$$

$$C = \frac{1}{R_T} = 0.0434 \frac{BTU}{HR\,^\circ F}$$

• CONDUCTANCE ALONG PIPE (ADIABATIC SECTION)

$$C = \frac{KA}{12\ell} = \frac{100 \times .0715}{12 \times 7.7} = 0.0773 \frac{BTU}{HR\,^\circ F}$$

PREPARED BY: LER	SPACE DIVISION NORTH AMERICAN ROCKWELL CORPORATION	PAGE NO. 1 OF 7
CHECKED BY:		APPENDIX 6 REPORT NO. A-6
DATE:	EQUIPMENT COMPARTMENT	MODEL NO. EC-LOUVER

THE EQUIPMENT COMPARTMENT IS LOCATED ON TOP OF THE PP BAY (FIGURE A-3-1 & A-3-2)

$Q = 450$ W

$T_{SA} = 150°C$

ASSUME LOUVER GOVERNED THERMAL CONTROL SYST.

$\epsilon_L = .73$ (100% OPEN)

$\epsilon_L = .15$ (100% CLOSED)

FROM CURVE A-2-2

$$\epsilon_L \epsilon_{SA} F_{L-SA} = (.73)(.8)(.12) = .07008$$

$(Q/A)_{SA}$ @ $T_{SA} = 150°C$

$$\therefore (Q/A)_{SA} = 127.98(.07008) = 8.97 \text{ W/FT}^2$$

$(Q/A)_{L-SD}$ FROM CURVE A-2-1

@ $T_R = 25°C$

$$\epsilon_L F_{L-SP} = (.73)(.88) = .6424$$

$$(Q/A)_{L-SD} = 26.5 \text{ W/FT}^2 \quad @ .6424$$

$$26.5A = 450 + 8.97$$

$$17.53A = 450$$

$$A = \frac{450}{17.53} = 25.67 \text{ FT}^2 = 2.39 \text{ m}^2$$

$Q = 430$ W

$$\therefore A = \frac{430}{17.53} = 24.53 \text{ FT}^2 = 2.28 \text{ m}^2$$

$Q = 410$ W

$$A = \frac{410}{17.53} = 23.39 \text{ FT}^2 = 2.17 \text{ m}^2$$

DETERMINATION OF RADIATOR EFFICIENCY

ASSUMPTIONS:

MAT'L AL 6061-T6

$K = 95$ BTU/HR FT °F

$T_R = 25°C = 77°F = 537°R$

$\epsilon_R = .88$

$\alpha_R = .2$

FIN PARAMETER $N = \dfrac{\epsilon \sigma L^2 T_R^3}{Kt}$

$$N = \frac{.88\sigma(L^2)(537)^3}{95\,t} = 2.459 \times 10^{-3}\left(\frac{L}{t}\right)^2$$

FROM PG. 5 OF A-3 DEVELOPED FIGURES A-6-1 AND A-6-2.

$Q = 450$ W

$T_{SA} = 150°C$

$F_{R-SA} = .12$

$F_{R-SP} = .88$

$T_R = 25°C$

$(Q/A)_{R-SA}$ @ 150 °C

FROM FIG. A-2-2

$\epsilon_R \epsilon_{SA} F_{R-SA} = (.88)(.8)(.12) = .08448$

$(Q/A)_{R-SA} = 10.81$ W/FT^2

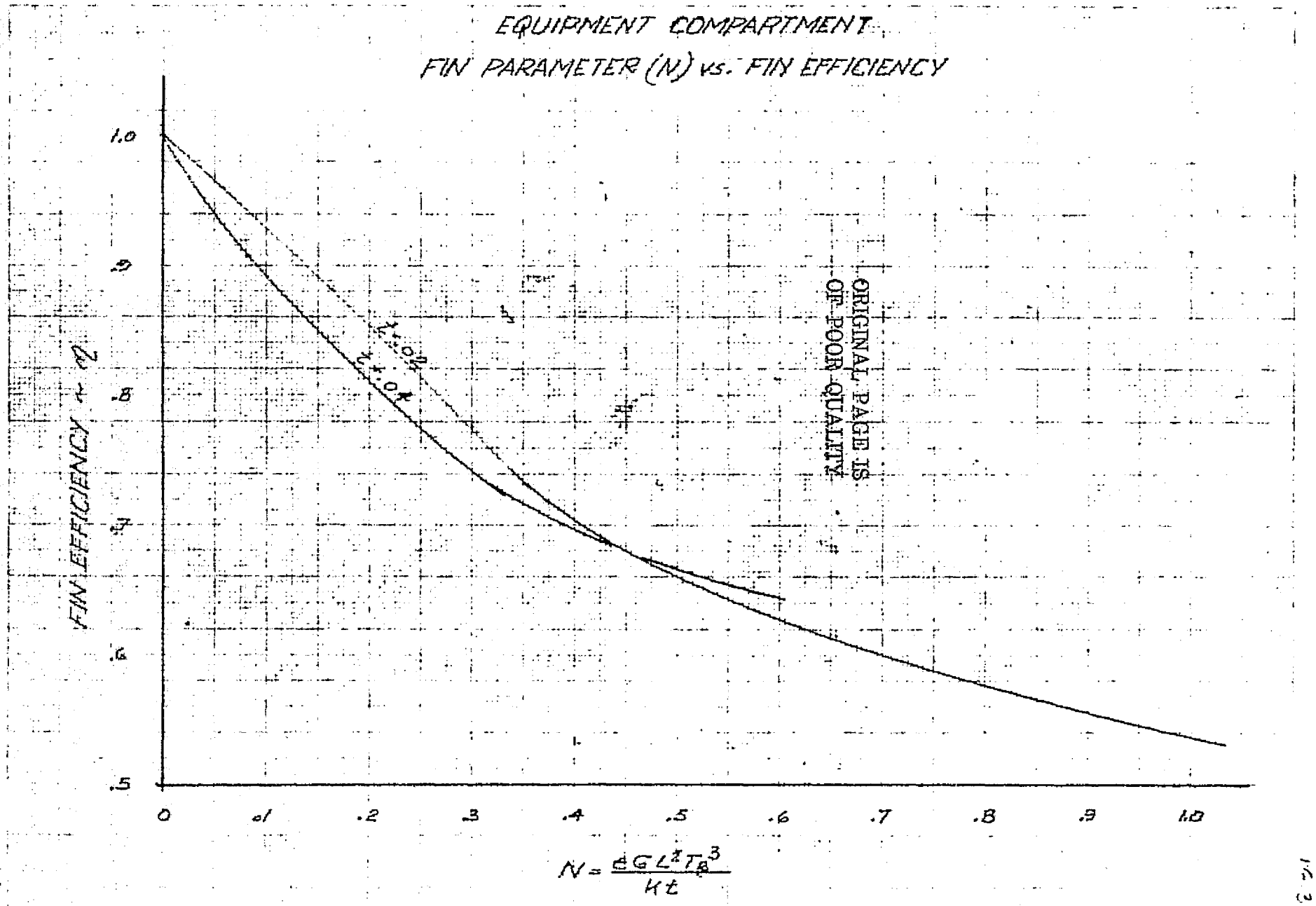

FIG. A-6-1

EQUIPMENT COMPARTMENT

FIN LENGTH vs. FIN EFFICIENCY

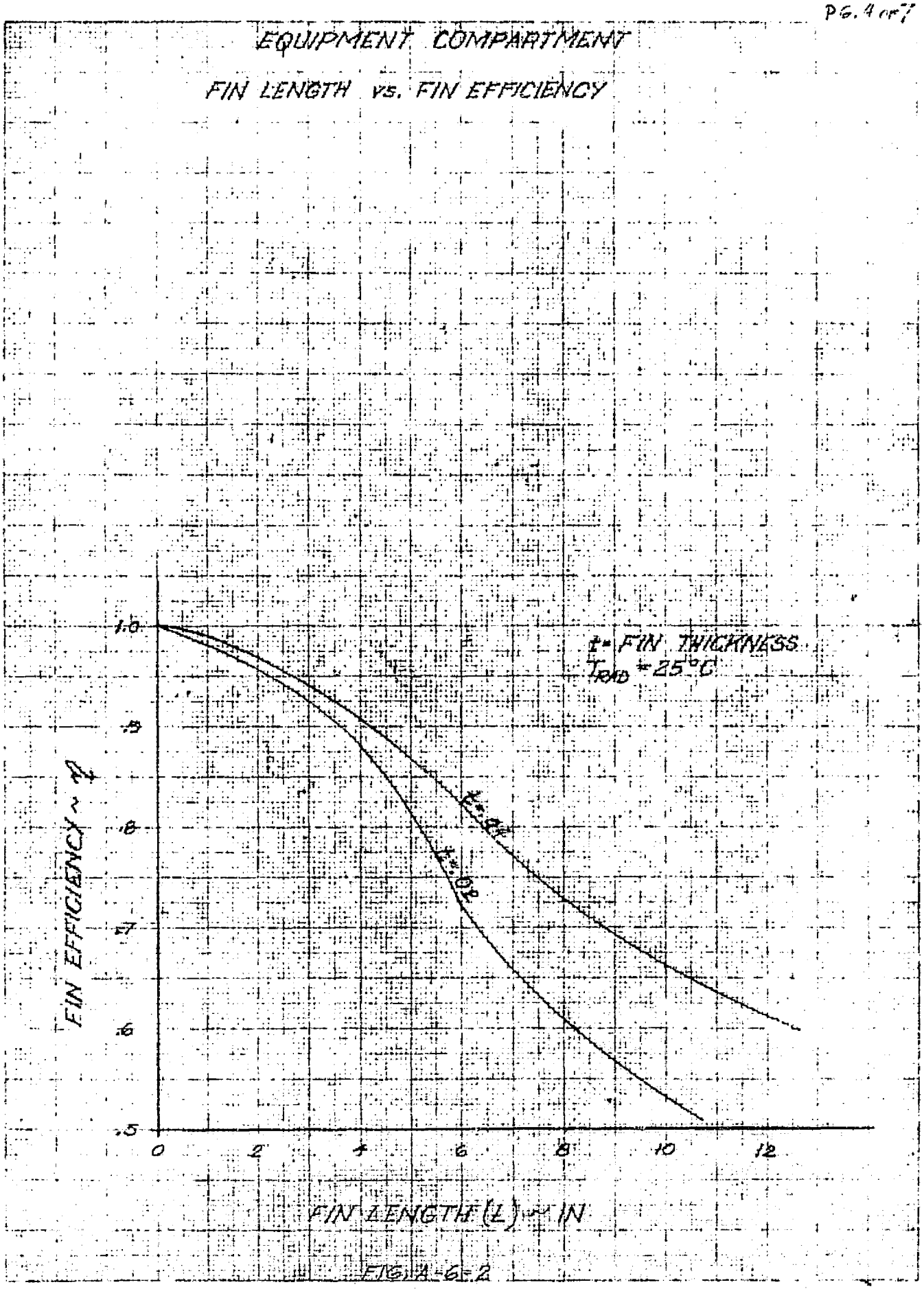

FIG A-6-2

$(q/A)_{R-SP}$ @ $\epsilon_R F_{R-SP}$

$\epsilon_R F_{R-SP} = (.88)(.88) = .774$

$(q/A)_{R-SP}$ FROM CURVE A-2-1

$(q/A)_{R-SP} = 32.5\ W/ft^2$ @ $.774$

$32.5A = 450 + 10.81A$

$21.69A = 450$

$A = \frac{450}{21.69} = 20.75\ ft^2$

$\eta_R = .9$

$A = \frac{20.75}{.9} = 23.05\ ft^2 = 2.14\ m^2$

$\eta_R = .8$ $\quad A = \frac{20.75}{.8} = 25.93\ ft^2 = 2.41\ m^2$

$\eta_R = .7$

$A = \frac{20.75}{.7} = 29.64\ ft^2 = 2.75\ m^2$

SELECTING $\eta_R = .8$ FROM CURVE A-6-2

@ $t = .04$ IN RADIATOR THICKNESS

$L = 6.4$ IN

1 VCHP'S (SAME DESIGN AS FOR PP'S)

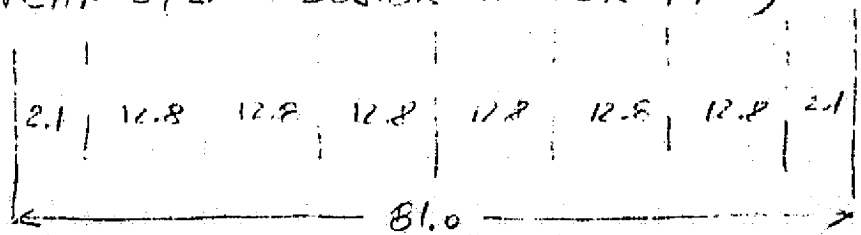

PREPARED BY:	SPACE DIVISION NORTH AMERICAN ROCKWELL CORPORATION	PAGE NO. 6 OF 7
CHECKED BY:		REPORT NO. A-C
DATE:		MODEL NO. EC-VCHP

DETERMINATION OF EXCESS POWER IN EC TO USE FOR CP HEATING.

ASSUME: $A = 25\ FT^2$

$T_{EC} = 25°C = 77°F = 537°R$ MINIMUM OPERATING TEMP. LIMIT OF A COMPONENT LOCATED IN EC.

$T_{SA} = -100°C = -148°F = 312°R$

$q = 430\ W$

$A_{VCHP} = .1715\ IN^2$

ASSUME 6 IN LENGTH BETWEEN RADIATOR AND EC HEAT SOURCE (ADIABATIC LENGTH)

$$L_1 = \frac{12\,L}{V} = \frac{12(6)}{100(.0715)} = 10.07\ HR°F/BTU$$

FOR 7 VCHP'S

$$R_T = \frac{10.07}{7} = 1.438\ HR°F/BTU$$

HEAT BALANCE FOR RADIATOR

$$q_{IN} = q_{OUT}$$

$$q_{IN} = \frac{T_{DD} - T_R}{1.438} + \sigma \epsilon_R \epsilon_{SA} F_{R-SA} A (T_{SA}^4 - T_R^4)$$

$$q_{OUT} = \sigma \epsilon_R \epsilon_{SP} F_{R-SP} A (T_R^4)$$

$$\frac{537 - T_R}{1.438} + \sigma (.88)(.8)(.12) 25 (312^4 - T_R^4) = \sigma (.88)(1)(25)(T_R^4)$$

$537 + 24.66 = 2.509 \times 10^{-8} T_R^4 + T_R$

$561.66 = 2.509 \times 10^{-8} T_R^4 + T_R$

LET $T_R = 310°K$

$231 + 310 = 541 < 562$

LET $T_R = 315°R$

$247 + 315 = 562 \sim 561.66$

$\therefore T_R = 315°R$

$Q_{INCIDENT} = \frac{537 - 315}{1.436} = \frac{222}{1.43R} = 154.34 \text{ BTU/HR} = 45.27 W$

$Q_{NEEDED_T} = 2(45.27) = 90.54 W$

EXCESS POWER $430 - 90.54 = 339.46 W$

236.5 W IS AVAILABLE FROM FC TO USE FOR THE PP'S HEATING.

ORIGINAL PAGE IS
OF POOR QUALITY